Electrochemical Society

GLC Anodes Are CUSTOM MADE for JEFFERSON CHEMICALS

The Jefferson Chemical Company Inc., chlor-alkali cell room at Port Neches, Texas

ACCELERATE your cost reduction program by putting GLC custom made anodes to work in your electrolytic cells.

OUR TECHNICAL PERSONNEL can help gear GLC anode characteristics to the goals of longer anode life, longer diaphragm life, reduced power and labor costs.

PRODUCTS ELECTRODE GLC DIVISION YOU CAN TRUST ®

GREAT LAKES CARBON CORPORATION

18 EAST 48TH STREET, NEW YORK 17, N.Y. OFFICES IN PRINCIPAL CITIES

EDITORIAL STAFF

C. L. Faust, Chairman, Publication Committee
Cecil V. King, Editor
Norman Hackerman, Technical Editor
Ruth G. Sterns, Managing Editor
U. B. Thomas, News Editor
H. W. Salzberg, Book Review Editor
Natalie Michalski, Assistant Editor

DIVISIONAL EDITORS

W. C. Vosburgh, Battery
Milton Stern, Corrosion
R. T. Foley, Corrosion
Louis J. Frisco, Electric Insulation
Seymour Senderoff, Electrodeposition
H. C. Froelich, Electronics
Ephraim Banks, Electronics
Ernest Paskell, Electronics—Semiconductors
D. R. Frankl, Electronics—Semiconductors
Sherlock Swann, Jr., Electro-Organic
Stanley Wawzonek, Electro-Organic
John M. Blocher, Jr., Electrothermics and Metallurgy
J. H. Westbrook, Electrothermics and Metallurgy
N. J. Johnson, Industrial Electrolytic
C. W. Tobias, Theoretical Electrochemistry
A. J. deBethune, Theoretical Electrochemistry
R. M. Hurd, Theoretical Electrochemistry

ADVERTISING OFFICE

ECS
1860 Broadway, New York 23, N. Y.

ECS OFFICERS

Henry B. Linford, President
Columbia University, New York, N. Y.

F. L. LaQue, Vice-President
International Nickel Co., Inc.,
New York, N. Y.

W. J. Hamer, Vice-President
National Bureau of Standards,
Washington, D. C.

Lyle I. Gilbertson, Vice-President
Air Reduction Co., Murray Hill, N. J.

Ernest G. Enck, Treasurer
Felicity Farm,
Gwynedd Valley, Pa.

Ivor E. Campbell, Secretary
National Steel Corp., Weirton, W. Va.

Robert K. Shannon, Executive Secretary
National Headquarters, The ECS,
1860 Broadway, New York 23, N. Y.

Manuscripts submitted to the Journal should be sent, in triplicate, to the Editorial Office at 1860 Broadway, New York 23, N. Y. They should conform to the revised Instructions to Authors, last published on pp. 145C-146C of the July 1961 issue. Manuscripts so submitted become the property of The Electrochemical Society and may not be published elsewhere, in whole or in part, unless permission is requested of and granted by the Editor.

The Electrochemical Society does not maintain a supply of reprints of papers appearing in its Journal. A photoprint copy of any particular paper, however, may be obtained by corresponding direct with the Engineering Societies Library, 29 W. 39 St., New York 18, N. Y.

Inquiries re positive microfilm copies of volumes should be addressed to University Microfilms, Inc., 313 N. First St., Ann Arbor, Mich.

Walter J. Johnson, Inc., 111 Fifth Ave., New York 3, N. Y., have reprint rights to out-of-print volumes of the Journal, and also have available for sale back volumes and single issues, with the exception of the current calendar year. Anyone interested in securing back copies should correspond direct with them.

Journal of the

Electrochemical Society

SEPTEMBER 1961 **VOL. 108 • NO. 9**

CONTENTS

Editorial

A Bell for St. Michael's 205C

Technical Papers

Solubility and Stability of Silver Oxides in Alkaline Electrolytes. *R. F. Amlie and P. Rüetschi* 813

The Structure of Silver Oxide Determined by Means of Neutron Diffraction. *V. Scatturin, P. L. Bellon, and A. J. Salkind* 819

The Reaction between Anodic Aluminum Oxide and Water. *W. J. Bernard and J. J. Randall, Jr.* 822

A Study of the Formation of Anodic Oxide Films on Titanium. *W. Mizushima* 825

Oxidation of Iron in the Temperature Range of 260°-470°C. *E. J. Caule, K. H. Buob, and M. Cohen* 829

The Annealing of Oxide Films on Iron. *E. J. Caule and M. Cohen* 834

Corrosion and Electrochemical Behavior of Chromium-Noble Metal Alloys. *N. D. Greene, C. R. Bishop, and M. Stern* 836

Some Observations of Copper Deposits on Single Crystals of Copper. *I. Giron and F. Ogburn* 842

Studies of Color Centers Produced in Apatite Halophosphates by Shortwave Ultraviolet Radiation. *L. Suchow* 847

Microsecond Response of Electroluminescent Cells. *J. E. Johnson* 852

Germanium Dendrite Studies, I. Studies of Twin Structures and the Seeding Mechanism. *J. W. Faust, Jr., and H. F. John* 855

Germanium Dendrite Studies, II. Lateral Growth Processes. *J. W. Faust, Jr., and H. F. John* 860

Germanium Dendrite Studies, III. Dislocations. *J. W. Faust, Jr., and H. F. John* 864

Scribe-Plating and -Etching. *W. Rindner and J. M. Lavine* 869

Some Properties of In_2Te_3 and Ga_2Te_3. *J. C. Woolley and B. R. Pamplin* 874

Single Crystal Silicon Overgrowths. *A. Mark* 880

Oxidation-Resistant Silicide Coatings for Columbium and Tantalum Alloys by Vapor Phase Reaction. *R. H. Lorenz and A. B. Michael* 885

Influence of Some Factors on Cathodic Formation of Hydrogen in the Mercury Cell. *J. H. Entwisle and W. E. Cowley* 893

"Electrocapillary" Studies on Solid Metals. *D. N. Staicopolus* 900

Technical Notes

Investigation on the Silver-Zinc Storage Battery with Radioactive Ag^{110} Isotope *T. Z. Palágyi* 904

Variation of Composition with Thickness in Thin Electrodeposited Films of Nickel-Iron Alloys. *G. H. Cockett and E. S. Spencer-Timms* 906

Current Affairs 209C-222C

Published monthly by The Electrochemical Society, Inc., from Manchester, N. H., **Executive Offices, Editorial Office** and **Circulation Dept.**, and **Advertising Office** at 1860 Broadway, New York 23, N. Y., combining the JOURNAL and TRANSACTIONS OF THE ELECTROCHEMICAL SOCIETY. Statements and opinions given in articles and papers in the JOURNAL OF THE ELECTROCHEMICAL SOCIETY are those of the contributors, and The Electrochemical Society assumes no responsibility for them. Subscription to members as part of membership service; subscription to nonmembers $24.00. Single copies $1.70 to members, $2.25 to nonmembers.

Copyright 1961 by The Electrochemical Society, Inc.

Entered as second-class matter at the Post Office at Manchester, N. H., under the act of August 24, 1912.

Polyelectrolyte Solutions: *A Theoretical Introduction*

By STUART A. RICE, *University of Chicago, and* MITSURU NAGASAWA, *Nagoya University*
With a contribution by H. MORAWETZ, *Brooklyn Polytechnic Institute*

October 1961, 568 pp.

This is the first monograph to deal exclusively with the study of the properties of solutions of polyelectrolytes. Emphasis is consistently placed on the interrelation of theory and experiment, on the construction of simple models for the interpretation, correlation, and prediction of both molecular and thermodynamic properties, and on the information derivable from the general theory of solutions without specific reference to models. The current status of knowledge of the properties of polyelectrolyte solutions is illustrated with carefully selected experimental data.

Electrolytic Dissociation

By C. B. MONK, *University College of Wales*

1961, 320 pp., $10.00

This book is intended for those who require detailed introductory accounts of the numerous methods and theoretical treatments used in studying the dissociation of electrolytes in solution, together with a broad, up-to-date review of the main conclusions that have been drawn. The second half of the book is devoted to the interpretation of experimental information in terms of incomplete dissociation, especially important in light of recent findings.

Interfacial Phenomena

By J. T. DAVIES, *University of Birmingham and* E. K. RIDEAL, *University of Cambridge*

1961, 474 pp., $14.00

This book satisfies the need for a unified, comprehensive account of the properties of surfaces and interfaces, including adsorption. It gives an up-to-date presentation of the fundamentals of the subject and a systematic account of recent research, including more than one thousand references. Many of the results and treatments presented have not been published before. The systematic manner of presentation makes the work suitable as a text in advanced courses, and the extensive coverage of recent results makes it highly useful for all engaged in research in this field.

The Electrochemistry of Semiconductors

Edited by P. J. HOLMES, *Associated Electrical Industries Ltd., Aldermaston, England*

September 1961, about 450 pp.

DEFINITIONS OF ELECTROCHEMICAL AND THERMODYNAMIC TERMS, AND THEIR RELATION TO SEMICONDUCTOR PARAMETERS
By H. F. GOHR

THE SEMICONDUCTOR-GAS AND SEMICONDUCTOR-METAL SYSTEMS
By A. R. PLUMMER

SEMICONDUCTOR ASPECTS OF A SEMICONDUCTOR ELECTRODE
By C. G. B. GARRETT

EXPERIMENTAL INFORMATION ON ELECTROCHEMICAL REACTION AT GERMANIUM AND SILICON SURFACES
By D. R. TURNER

OXIDATION REACTIONS AND POTENTIALS OF GERMANIUM AND SILICON
By J. I. CARASSO *and* M. M. FAKTOR

CHEMICAL ETCHING OF SEMICONDUCTORS
By B. A. IRVING

PRACTICAL APPLICATIONS OF ELECTROLYTIC TREATMENT TO SEMICONDUCTORS
By J. I. PANKOVE

PRACTICAL APPLICATIONS OF CHEMICAL ETCHING
By P. J. HOLMES

REFERENCES

Reference Electrodes: *Theory and Practice*

Edited by DAVID J. G. IVES, *Birkbeck College, London, and* GEORGE J. JANZ, *Rensselaer Polytechnic Institute*

1961, 651 pp., $20.00

GENERAL AND THEORETICAL INTRODUCTION
By D. J. G. IVES *and* G. J. JANZ

THE HYDROGEN ELECTRODE
By G. J. HILLS *and* D. J. G. IVES

THE CALOMEL ELECTRODE AND OTHER MERCURY—MERCUROUS SALT ELECTRODES
By G. J. HILLS *and* D. J. G. IVES

SILVER—SILVER HALIDE ELECTRODES
By G. J. JANZ

THE GLASS ELECTRODE
By R. G. BATES

THE QUINHYDRONE ELECTRODE
By G. J. JANZ *and* D. J. G. IVES

OXIDE, OXYGEN, AND SULFIDE ELECTRODES
By D. J. G. IVES

ELECTRODE REVERSIBLE TO SULFATE IONS
By D. J. IVES *and* F. R. SMITH

MEMBRANE ELECTRODES
By G. J. HILLS

REFERENCE ELECTRODES IN NONAQUEOUS SOLUTIONS
By G. J. HILLS

MICROELECTRODES AND ELECTRODES USED IN BIOLOGY
By D. B. CATER *and* I. A. SILVER

ELECTRODES IN FUSED SALT SYSTEMS
By R. W. LAITY

AUTHOR INDEX—SUBJECT INDEX.

ACADEMIC PRESS

111 Fifth Avenue, New York 3, New York

New York and London

17 Old Queen Street, London, S.W. 1

Editorial

A Bell for St. Michael's

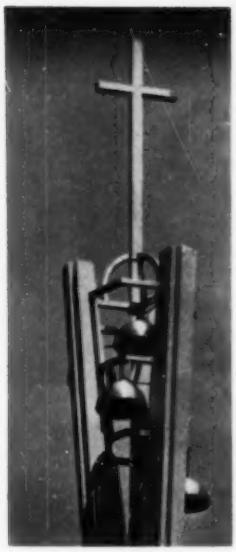

ST. MICHAEL AND ALL ANGELS' is a small Episcopal Mission which stands beside the campus of the University of California at Santa Barbara. Came the day when it needed a bell—

Arcturus Manufacturing Corp. makes, among other things, gas pressure vessels for Atlas missiles. Titanium billets are forged and hammered into hemispheres which are then welded together into spherical vessels. One day a hemisphere had to be rejected because of a dimensional imperfection; Mr. R. B. McCormick of Arcturus happened to give it a kick and was impressed by the resulting pure ringing tone. He quickly secured the services of experts who, after exhaustive tests, pronounced the titanium hemisphere ideal for a church bell. A new bell for St. Michael's, the first of its kind in the world!

This particular hemisphere was about 24 inches in diameter, ½ inch in thickness, and weighed a little under 50 pounds. After forging, it had been machined and polished to a beautiful silvery luster. As a bell, its fundamental tone is near E-flat above middle C, and it has well-balanced overtones covering the entire piano range. It was fitted with a clapper made of a phenolic resin-wood flour mixture, about as large as a croquet ball and covered with thin leather.

Several similar "rejects" have been converted to church bells, and Arcturus now manufactures titanium hemispherical bells to order; they are sold by Judson Stained Glass Studio of Pasadena. Their shape and appearance are a delight to the designers of modern architecture, and their light weight is amazing to everyone. The accompanying photograph shows an installation of four titanium bells at Peace Lutheran Church, Pico Rivera, Los Angeles.

Should Mr. McCormick's discovery be called a case of serendipity? Conversion of part of a potentially deadly missile into a church bell of course calls to mind "beating swords into plowshares."

Most of the above information was supplied by Oliver W. Storey, who has been a member of the ECS (and also of ACS) since 1911. Mr. Storey was active in ECS affairs for many years, holding various offices and serving as Chairman of the Publication Committee for five years during the 1940's and at the time when the JOURNAL replaced the PREPRINTS and the TRANSACTIONS. Mr. Storey suggests that there may be electrochemical overtones associated with the titanium bells.

The original story of St. Michael's bell was written for *Trinity News* of Trinity Episcopal Church, Santa Barbara, by Sidney V. Petertyl, research engineer in a Santa Barbara laboratory. An article about the new bells appeared in *Space Age News* early in June 1961.

—CVK

Photograph courtesy of Richard B. McCormick, Arcturus Manufacturing Corp., Venice, Calif.

WILEY BOOKS

Latest in the Electrochemical Society Series . . .

TRANSACTIONS OF THE SYMPOSIUM ON ELECTRODE PROCESSES

Edited by ERNEST YEAGER, *Morley Chemical Laboratory, Western Reserve University*

Under the sponsorship of The Electrochemical Society, Inc., and the Office of Scientific Research of the United States Air Force, scientists from ten nations report here on virtually all phases of basic research into electrode processes. This is the only work in recent years to include the contributions of so many internationally recognized experts.

Although the fundamentals are presented fully and past work is reviewed, stress in this volume is concentrated on the newer areas of research. Specifically these are:

Hydrogen discharge kinetics
Electrodeposition and dissolution of metals
The electrical double layer
Adsorption phenomena
Kinetics of fast electrode processes

1961 374 pages $20.00

Four other new works of importance . . .

METAL IODIDES AND IODIDE METALS

By ROBERT F. ROLSTEN, *Design Specialist, Convair Division of General Dynamics Corp.*

An important reference for the chemist, metallurgist, and engineer, with a threefold purpose: 1) to present the information necessary to design and operate an iodide cell; 2) to explain details of the preparation and properties of the metal iodides (including boron, germanium, and silicon iodides); and 3) to show how the various iodide compounds can be utilized to prepare high-purity elements and alloys. In addition, the literature has been most thoroughly surveyed and reported, indicating where data are lacking and where anomalies exist.

Sixty-one elements are covered in *Metal Iodides and Iodide Metals.* They are grouped according to the periodic system, and each chapter deals with one sub- or main-group.

Pertinent theoretical aspects of iodide process are given for each section, wherever such data have been obtained. Then, a condensation of all these theoretical considerations is presented and discussed in a separate chapter.

1961 Approx. 496 pages Prob. $17.50

INDUSTRIAL FURNACES, Volume I

FIFTH EDITION

By W. TRINKS *and* M. MAWHINNEY, *Consulting Engineers.* Greatly revised and modernized. Added: calculating heat transfer in furnaces; capacity of forced-convection and axial heating furnaces; charts of adiabatic flame temperatures; new furnace types. Answers three questions: how to design, build, and operate furnaces with given specifications.

1961. 486 pages $17.00

MINERALS FOR THE CHEMICAL AND ALLIED INDUSTRIES

SECOND EDITION

By SYDNEY J. JOHNSTONE *and* MARGERY G. JOHNSTONE. Gives about 250 specifications for various minerals, showing the needs of the chemical industry for purity, size, composition, etc. Also stimulates ideas on when substitutes may be used. Each chapter covers one metal or mineral, and bibliography for further reference. 1961. In Press.

TEMPERATURE MEASUREMENT IN ENGINEERING, Volume II

By H. DEAN BAKER, *Columbia University,* E. A. RYDER, *United Aircraft Corp., and* N. H. BAKER, *Columbia University.* Gives directions for measuring temperature in laboratory, shop and field. Part I develops basic methods, resistance thermometry and radiation pyrometry techniques. Part II covers specific problems and methods most useful for solving them. Throughout, special techniques are presented and fully described in terms of their greatest adaptability, in conjunction with the specific problems for which they may offer solutions. *1961. 510 pages. $13.00. VOL. I: 1953. 179 pages. $4.95.*

SEND NOW FOR YOUR ON-APPROVAL COPIES

JOHN WILEY & SONS, Inc.
440 PARK AVENUE SOUTH,
NEW YORK 16, N. Y.

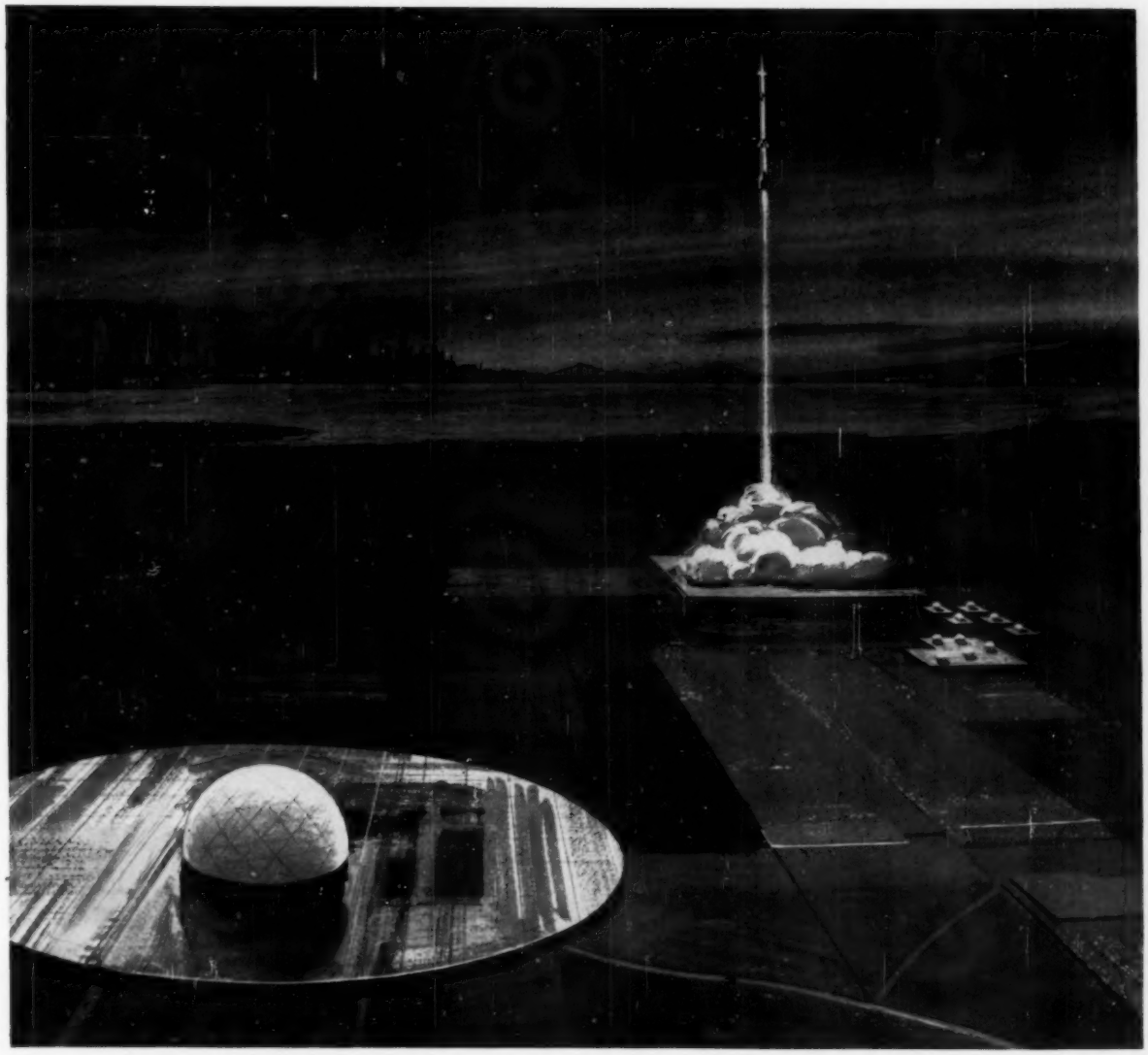

More than 450,000 pounds of thrust lifts the U. S. Army's Nike Zeus missile skyward in a cloud of vapor. The Nike Zeus missile being developed for the project by the Douglas Aircraft Company will be designed to intercept ballistic missiles traveling over 15,000 miles per hour, and destroy them at a safe distance from the defended area.

How do you stop an ICBM?

How do you detect, track, intercept—and destroy within minutes—an ICBM that is moving through outer space ten times faster than a bullet?

Bell Telephone Laboratories may have designed the answer: Nike Zeus, a fully automated system designed to intercept and destroy all types of ballistic missiles—not only ICBM's but also IRBM's launched from land, sea or air. The system is now under development for the Army Ordnance Missile Command.

Radically new radar techniques are being developed for Nike Zeus. There will be an acquisition radar designed to detect the invading missile at great distances. And a discrimination radar designed to distinguish actual warheads from harmless decoys that may be included to confuse our defenses.

The system tracks the ICBM or IRBM, then launches and tracks the Nike Zeus missile and automatically steers it all the way to intercept the target. The entire engagement, from detection to destruction, would take place within minutes and would span hundreds of miles.

Under a prime Army Ordnance contract with the Western Electric Company, Bell Laboratories is charged with the development of the entire Nike Zeus system, with assistance from many subcontractors. It is another example of the cooperation between Bell Laboratories and Western Electric for the defense of America.

BELL TELEPHONE LABORATORIES

World center of communications research and development

How "Plus-4®" Anodes cut electroplating costs

Tank sludge, build-up of copper sulfate in solution, and cathode roughness due to the sludging off of tiny copper particles from the anode are costly problems in acid-copper electroplating. "Plus-4" (phosphorized copper) wrought anodes solve these problems effectively.

Take anode sludge, for example. "Plus-4" anodes *eliminate* sludge formation. The phosphorized copper in "Plus-4's" develops an adherent dark brown film during electrolysis. This in no way interferes with plating, nor does it increase the electrical resistance of the bath.

For further details, write for your copy of Publication C-5 which describes Anaconda Wrought Anodes in greater detail. Address: Anaconda American Brass Co., Waterbury 20, Conn. In Canada: Anaconda American Brass Ltd., New Toronto, Ontario.

61-929

New low price anode—Electranodes® are pure Anaconda copper anodes a full 1 inch thick. If you need an "economy type" anode, Electranodes are the best for the least.

ANACONDA®
AMERICAN BRASS COMPANY

Solubility and Stability of Silver Oxides in Alkaline Electrolytes

R. F. Amlie and P. Rüetschi

The Carl F. Norberg Research Center, The Electric Storage Battery Company, Yardley, Pennsylvania

ABSTRACT

The solubility of Ag_2O and AgO in alkaline electrolytes has been studied with a polarographic technique, using a rotating platinum electrode. Only a monovalent (and no divalent) silver species could be detected in solutions which had been in intimate contact with AgO powder over prolonged periods of time.

Quantitative measurements of the solubility of Ag_2O in KOH solutions ranging from 1-14 moles per liter, were carried out utilizing a potentiometric titration method. The solubility has a maximum at about 6*N* KOH where it reaches a value of $4.8 \cdot 10^{-4} N$.

The rate of the decomposition reaction $2AgO \rightarrow Ag_2O + \frac{1}{2} O_2$ in alkaline electrolytes was investigated with a very sensitive microvolumetric method. The reaction rate increases with increasing hydroxyl ion concentration and is sensitive to day-light. The decomposition appears to proceed at the solid-liquid interface. Any divalent silver dissolving in minute amounts into the electrolyte is decomposed rapidly due to its instability. The decomposition proceeds at a rate of about 16% in 1 year at 30°C and 49% in 1 year at 45°C. This reaction can contribute significantly to the self-discharge of AgO-Zn batteries.

Anodic oxidation of silver in alkaline solutions is a two-step process. First, a layer of monovalent Ag_2O is produced on the metal. Subsequently, when this layer has reached a critical thickness and mass transport through the layer becomes slow, Ag_2O is oxidized to AgO. Further anodization leads to evolution of oxygen. Simultaneously, the oxidation of metallic silver continues at a very low rate. There is also evidence of the formation of highly unstable "higher oxides" than AgO during prolonged anodization.

The standard potential of the Ag/Ag_2O couple in alkaline solutions is 0.342 v (1) and the potential of the Ag_2O/AgO couple, 0.604 v (2). If an electrode contains both metallic silver and AgO, a local action mechanism must proceed (3, 4) with a driving force of 0.262 v or −6.05 kcal, according to

$$2Ag + 2(OH)^- \rightleftarrows Ag_2O + H_2O + 2e \quad E_o = 0.342$$

$$Ag_2O + 2(OH)^- \rightleftarrows 2AgO + H_2O + 2e \quad E_o = 0.604$$

with the first reaction proceeding in the forward direction, and the second reaction in the backward direction, resulting in

$$Ag + AgO \rightarrow Ag_2O \qquad \Delta G = -6.05 \text{ kcal}$$

This local action mechanism should be a fast process, because the individual component electrode reactions are known to have high exchange currents.

Measurements of the double layer capacity and the interface resistance during anodic formation of Ag_2O films (3, 5, 6) give an insight into the mechanism of oxidation. The double layer capacity decreases during build-up of the Ag_2O layer, apparently due to increased separation of the charge layers in the solution and on the metal. At the same time, the interface resistance increases sharply, indicating restriction of mass transfer. The resistance decreases again when the formation of AgO begins. This decrease in resistance must be correlated with the breakdown of the Ag_2O layer, and with the high electric conductivity of the divalent oxide. The conductivity is in the order of $7 \cdot 10^{-2}$ ohm^{-1} cm^{-1} and increases with increasing temperature (7). AgO has been shown to be diamagnetic (7), a fact which is best explained on the basis of monovalent and trivalent states of silver in the lattice and the formation of covalent or metallic bonds. This is supported by crystallographic studies including x-ray diffraction (8) and neutron diffraction (9). It is possible to prove that the silver atoms in the AgO lattice are *not* equivalent, and have two different Ag-O distances, namely 2.18 and 2.03Å, corresponding to monovalent and trivalent silver atoms. In view of these results, the analysis of Stehlik and Weidenthaler (10) which suggests a cubic lattice for AgO with an average Ag-O bond length of 2.08Å is doubtful, since it cannot explain the diamagnetic behavior. In any case, AgO is a true oxide, like CuO, and not a peroxide.

The crystallographic data on oxides higher than AgO are quite uncertain. Some authors (11) have suggested a cubic structure for Ag_2O_3, but the extreme instability renders the study very difficult.

The stability of silver oxide electrodes in alkaline solution is of considerable importance to the technology of manufacturing silver-zinc batteries. One factor determining battery performance and life is the solubility of the oxides. Dissolved silver species will diffuse across and around the separators or membranes and will be plated out as metallic silver at the negative electrode. If the battery is on open-circuit stand, it suffers an equivalent self-discharge by conversion of a corresponding amount of Zn to ZnO in the negative plates. On charge, silver deposits can cause shorting through the separators.

Very precise work on the solubility of Ag_2O in alkaline solutions has been done by Johnston *et al.* (12). These authors showed that the solubility of Ag_2O increases linearly with the concentration of $(OH)^-$ ions in dilute alkaline solutions. At concentrations above 1*N*, the solubility starts to deviate from linearity to increasing lower values. Unfortunately, the measurements of Johnston *et al.* were only taken up to a concentration of 6*N* OH^- ions, which covers only part of that range of interest in the silver-zinc battery system.

Johnston *et al.* assumed that in alkaline solution Ag_2O produces a soluble anion in the following manner:

$$Ag_2O + 2\,OH^- \rightarrow 2AgO^- + H_2O \qquad [1]$$

That a negative silver species is formed, follows clearly from the linear increase of solubility with OH^- concentration in dilute solution. However, the postulate of AgO^- species has been questioned (13). Pleskov and Kabanov (13) have given evidence that the ions of monovalent silver form in alkaline solution a tri-nuclear, uni-negative complex:

$$3Ag_2O + 2\,OH^- + H_2O \rightarrow 2(Ag_3O(OH)_2)^- \qquad [2]$$

This result was arrived at by potentiometric and polarographic techniques. The solubility of monovalent silver has been shown to increase with temperature (14). While the solubility of Ag_2O in alkaline solutions has been measured precisely in the more dilute range, more uncertainty exists with regard to the solubility of AgO.

Dirkse *et al.* (15) have reported solubilities of AgO in alkaline solution which nearly coincide with the solubility values of Johnston *et al.* for Ag_2O. However, Dirkse *et al.* did not show that the silver species in solution was divalent, which renders the coincidence rather suspicious. Pleskov (16) has studied the instability of divalent silver ions in solution, using a rotating gold disk electrode; he found that the cathodic polarization curve of a KOH solution in contact with solid AgO only showed the diffusion current of Ag_2O. He found only indirect evidence for the presence of dissolved divalent silver in trace amounts, not polarographically measurable.

Solid divalent silver oxide is thermodynamically unstable in contact with alkaline solutions. Because its electrode potential is above the potential of the oxygen electrode in this environment, it decomposes to Ag_2O with evolution of oxygen:

$$Ag_2O + 2(OH)^- \rightleftarrows 2AgO + H_2O + 2e \quad E = 0.604$$

$$2(OH)^- \rightleftarrows H_2O + \tfrac{1}{2}\,O_2 + 2e \quad E = 0.401$$

with the first reaction proceeding in the backward direction and the second reaction in the forward direction, resulting in

$$2AgO \rightarrow Ag_2O + \tfrac{1}{2}\,O_2 \qquad \Delta G = -9360 \text{ cal or } -9512 \text{ cal} \qquad [3]$$

The best values for the free energy of formation of Ag_2O and AgO are −2586 cal (17) and +3463 cal (2), respectively, leading to a free energy of the decomposition reaction of −9512 cal, whereas from Latimer's value of the oxygen electrode potential and the value of Bonk and Garrett for AgO, one arrives at a free energy of −9360 cal.

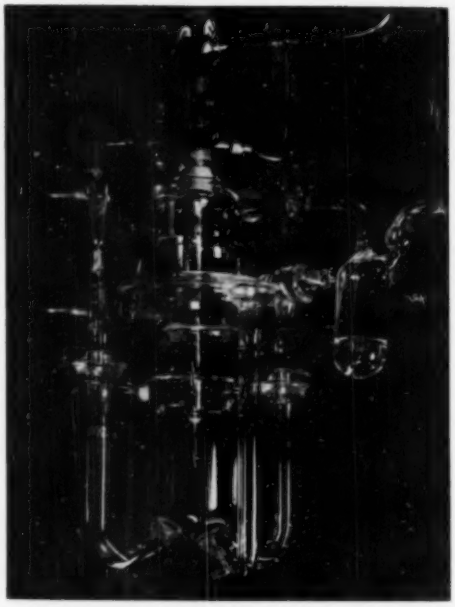

Fig. 1. Polarographic cell equipped with rotating platinum microelectrode.

Because of the decomposition reaction, solutions in contact with AgO will contain Ag_2O (14), and the differentiation between divalent and monovalent silver species in solution is quite difficult. In spite of the thermodynamic instability, solid AgO has a reasonable degree of metastability in contact with alkaline solutions and can be used as a practical electrode. The reason for this relative stability is probably connected with oxygen overvoltage slowing down the anodic part of the local action mechanism [3] and with the protection of AgO by formation of an Ag_2O film.

Experimental

In the first part of the present study, a special polarographic arrangement was used to investigate both the nature and concentration of the various soluble silver species in KOH solutions. A rotating platinum microelectrode was used instead of a dropping mercury electrode because potentials positive to the Hg/HgO oxidation potential were encountered. Figure 1 shows a photograph of the glass cell with the Pt microelectrode sealed axially into the rotating glass tube at the lower end. The exposed wire electrode was 0.6 mm in diameter and 5 mm long. Electric contact to the rotating Pt electrode was made by mercury, which filled the inner rotating tube and the enlarged section of the surrounding bearing sleeve, and which was retained in the latter by a lubricated ground glass bearing. A small hole through the glass tube wall served to make electrical contact between the mercury in the rotating tube and the mercury in the outer jacket.

Side arms on the cell were provided for inlet and outlet of purified nitrogen or oxygen, for a reference electrode, and for auxiliary counter electrodes. The glass cell assembly was thermostated at 25°C. The

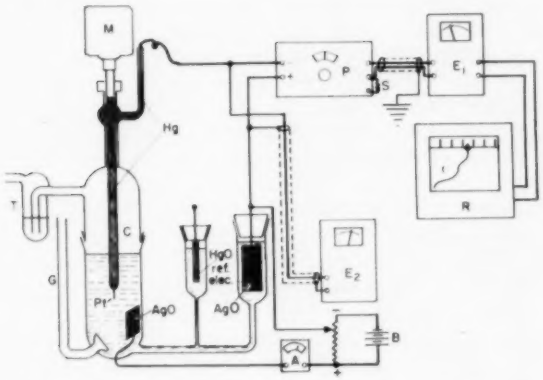

Fig. 2. Schematic of polarographic apparatus including polarographic cell C, gas inlet tube with porous diffuser disk G, gas outlet and trap T, electrode rotating motor M, L&N No. 7669 polarizing unit P, shunt resistor S, General Radio type 1230-A d-c amplifiers and electrometers E_1 and E_2, recorder R, microammeter A, and anodizing current supply B.

rotating Pt electrode was cleaned in 1:1 nitric acid and thoroughly washed with triple distilled water, prior to taking each polarogram. The platinum microelectrode was rotated at 1950 rpm.

Figure 2 shows a schematic diagram of the experimental setup. Polarograms were taken using a L&N polarizing unit, No. 7669, shown at P, which applied a potential increasing linearly with time between the rotating electrode and the side arm electrode. The diffusion current was determined by means of an electrometer-input amplifier E_1, which measured the voltage drop across a precision resistor, and which drove the high speed recorder R. A second electrometer-input amplifier E_2 was used to check the voltages of the rotating electrode and auxiliary electrodes *vs.* each other, and *vs.* the HgO reference electrode. Shown are also the gas inlet G, gas outlet trap T, and rotating motor M.

In a second phase of the present investigation, the solubility of Ag_2O in KOH solutions was studied with a high-precision potentiometric method. The technique followed the one developed by Johnston *et al.* (12) and involved neutralization of the Ag_2O saturated KOH solution and subsequent potentiometric titration, using standardized dilute solutions of KI as the precipitant and a small silver foil as the indicator electrode.

Fisher certified KOH pellets were used to prepare the KOH solutions. The solutions were shaken with an excess of Mallinckrodt purified Ag_2O on a Burrell wrist-action shaker for 3 to 4 weeks. After removal from the shaker, the solutions were allowed to stand for 1 to 2 hr and were then filtered through a fine Pyrex fritted glass filter with a maximum pore size of 5μ.

Pipetted 100 ml samples of the filtrate were neutralized with concentrated nitric acid to the acidic endpoint of the meta-cresol-purple indicator (pH 2). This made it possible to remove all traces of carbonate by subsequent boiling for several hours.

The potential of the Ag electrode during titration of the sample with 1/100*N* standardized KI solution was followed with an electrometer—d-c amplifier,

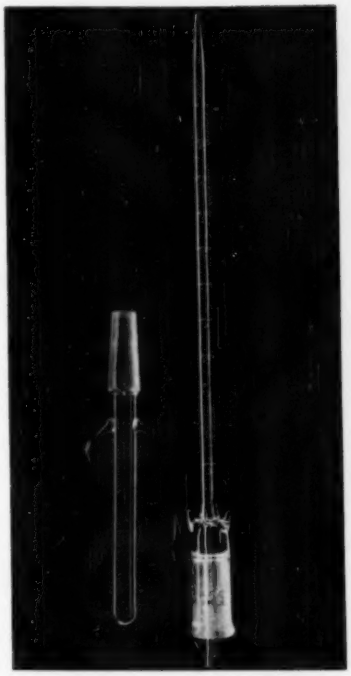

Fig. 3. Microvolumetric apparatus for measuring O_2 evolved from AgO samples in alkaline electrolytes.

driving a recorder. The attainment of a steady potential value was realized before proceeding with the next incremental addition of KI solution. During titration the solution was held at 45°C in a "low actinic" Pyrex beaker. The beaker was stoppered to prevent photochemical reaction by room light. Each titration was completed within 1-2 hr. Prior to each titration, the silver electrodes were etched in dilute nitric acid and washed with triple distilled water. Potentials were measured with a saturated calomel reference electrode, separated from the sample solution by a 1 mm capillary, filled with saturated KNO_3, leading to a KNO_3 reservoir, from which a second capillary led to the calomel electrode.

The third part of the present investigation was a study of the decomposition reaction $AgO \rightarrow Ag_2O + \frac{1}{2} O_2$ in alkaline solution. The microvolumetric apparatus used is shown in Fig. 3. Samples of loose or pelletized AgO were weighed out into the 10 cc test tube. The tube was completely filled with alkaline electrolyte. The capillary tube section was equipped with an extension which was ring-sealed above the joint and which had a tiny hole through the side wall near the lower end. The electrolyte was displaced to about the zero mark of the capillary when the capillary section was put in place. During the test periods oxygen was evolved by decomposition of AgO and displaced an equivalent volume of electrolyte, causing the electrolyte level in the capillary to rise. Volume changes of 1/100 of a cc were easily detectable. This volume corresponds to 4.10^{-7} moles or about 1.10^{-5} g of oxygen. With AgO samples of 1 g, a decomposition of 0.01% was therefore readily detectable. The test tube was carefully thermostated to ±0.02°C using a water bath heated by an infrared lamp, and a mercury contact thermometer, which

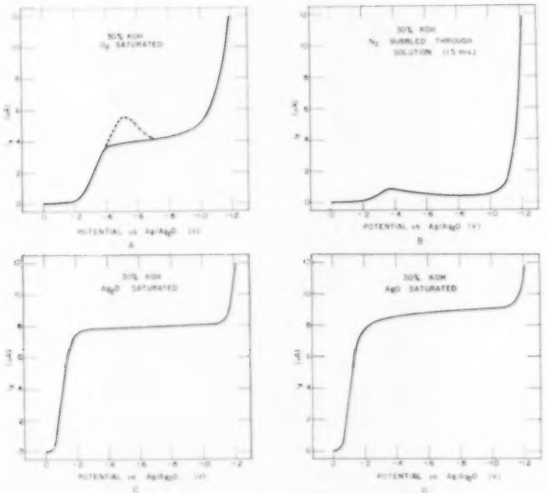

Fig. 4. Polarograms in 30% KOH electrolytes at 25°C. A, O_2 polarogram; B, O_2 polarogram after N_2 flushing; C, polarogram of nitrogen flushed KOH saturated with Ag_2O; D, polarogram of nitrogen flushed KOH equilibrated with AgO.

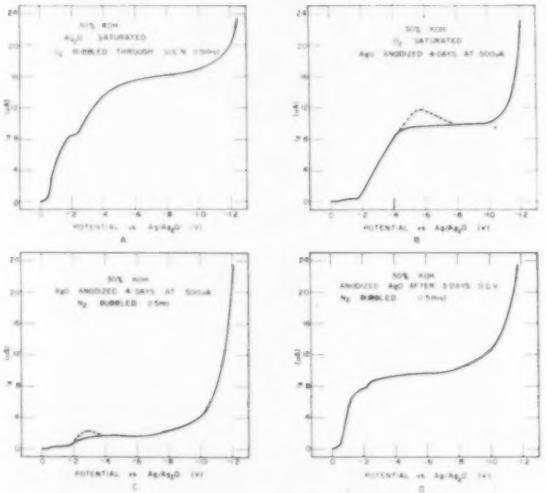

Fig. 5. Polarograms in 30% KOH solutions at 25°C. A, polarogram of a solution saturated with Ag_2O and O_2; B, polarogram of same solution after 4-day anodization of AgO electrode in the cell (silver wave eliminated); C, polarogram of same solution after N_2 flushing; D, polarogram of solution after 3-day open-circuit stand of AgO electrode in the cell and after N_2 flushing.

switched the infrared lamp through an electronic relay. Volume readings were corrected for atmospheric pressure changes using a blank tube without AgO.

Results and Discussion

Results obtained from the polarographic studies are shown in Fig. 4 and 5. The data in Fig. 4 were obtained with a modification of the experimental arrangement shown in Fig. 2. The AgO electrode in the compartment of the rotating electrode was omitted, and the AgO electrode in the side arm was replaced by an Ag_2O electrode. The latter was prepared by electrolytic oxidation of a porous sintered Ag plate, 4 x 1 x 0.1 cm under controlled potential.

The polarograms were started at a potential of 0 v *vs.* the Ag_2O electrode in the side-arm, and the potential of the rotating microelectrode was varied in a negative (cathodic) direction, at a constant speed of 2 mv/sec. All polarograms were taken in a 30% KOH (387 g/liter) supporting electrolyte.

Curve A of Fig. 4 shows the polarogram of the oxygen-saturated supporting electrolyte solution. The limiting diffusion current for O_2 reduction was in the order of 4 μa. Very often a nonreproducible maximum was apparent with the oxygen wave. Only one step was observed, in agreement with Kolthoff (18), whereas on a dropping mercury electrode oxygen is reduced in two steps (oxygen and peroxide wave).

Curve B demonstrates the effect of removal of oxygen by nitrogen flushing. As shown below, oxygen removal is essential because its wave occurs in the vicinity of the silver wave.

Curves C and D show polarograms of 30% KOH solutions which were previously in intimate contact with Ag_2O and AgO powder, respectively. Oxygen was substantially removed by nitrogen bubbling. It is evident that the two polarograms have identical half-wave potentials, indicating that the same soluble species is produced in each instance. The mono- and divalent silver oxides used to saturate the KOH solution were Mallinckrodt purified Ag_2O and Merck "Divasil" AgO, respectively. Both materials had a purity of better than 96%. Apparently the AgO sample either contained enough Ag_2O, or produced enough Ag_2O in contact with KOH by decomposition, to saturate substantially the solution with Ag_2O.

The polarograms in Fig. 4 give no indication of the presence of dissolved divalent silver. The diffusion current at the Ag/Ag_2O potential is zero. It should also be noted that the oxygen half-wave potential is at about −0.3 v vs. Ag/Ag_2O, while the monovalent silver half-wave potential is at about −0.1 v. This allows a clear separation of the two waves.

In order to further characterize the dissolved silver species, additional experiments, as represented in Fig. 5, were carried out. For this series of experiments an AgO electrode was inserted into the compartment of the rotating electrode as shown in Fig. 2. In addition, the side arm electrode was now an AgO electrode. Both AgO electrodes were prepared by prolonged electrochemical oxidation of porous sintered silver at controlled potential. Polarograms were started at −0.25 v *vs.* the potential of the AgO side arm electrode, which corresponds to 0 v *vs.* the potential of an Ag_2O electrode.

Polarogram 5A was taken in a 30% KOH solution saturated with Ag_2O and with oxygen. Clearly visible are both the silver and the oxygen wave. The height and the half-wave potential of the silver wave are about the same as in Fig. 4C and 4D.

Figure 5B shows a polarogram of the same solution after the AgO electrode in the rotating electrode compartment had been anodized for 4 days at 500 μa against the AgO electrode in the side arm. During this anodization, the AgO electrode in the side arm remained at 20 mv below its reversible open-circuit potential (0.50 v *vs.* Hg/HgO) and returned to this

open-circuit value after interruption of current, subsequent to the 4-day discharge. This eliminated the possibility of removal of dissolved monovalent silver at the side arm electrode by reduction to metallic Ag. The potential of the AgO electrode in the rotating electrode compartment was about 90 mv positive to its open-circuit value during the anodization period, and was evolving oxygen.

The polarogram 5B shows that the soluble silver had disappeared completely from the solution after the 4-day anodization period, and this occurred inspite of the fact that some monovalent dissolved silver might have diffused into the rotating electrode compartment from the side arm containing the discharging AgO electrode. Only the oxygen wave is visible in the polarogram 5B with a half-wave potential of −0.3 v *vs.* Ag/Ag_2O.

This result suggests that the monovalent silver in solution was oxidized at the AgO electrode in the rotating electrode compartment and was precipitated on this electrode in the form of insoluble AgO, or possibly higher oxides. The disappearance of the silver from the solution indicated that AgO is not dissolved in alkaline solutions in measurable quantities.

Any divalent silver species dissolving into the electrolyte are apparently decomposed rapidly since even a minute amount (*e.g.*, 10^{-4} moles per liter) would have been indicated by the very sensitive polarographic techniques used here. In addition, the dissolution step of the decomposition reaction must be quite slow since AgO is relatively stable in contact with alkaline electrolytes over long periods of time. It is probable that AgO is always protected from the electrolyte by a film of Ag_2O, rendering the dissolution and decomposition relatively slow.

In Fig. 5C it is demonstrated that the wave of Fig. 5B is indeed due to oxygen only, since it can be reduced by flushing with N_2. Finally, Fig. 5D shows a polarogram of the same solution after the anodizing current had been interrupted for 3 days. The silver wave is again apparent, together with a minor oxygen wave, which had been reduced by nitrogen flushing. The AgO electrode had again produced enough Ag_2O by decomposition to saturate substantially the solution with the monovalent silver species.

The experimental data relating to the second phase of the present investigation, the precise determination of the solubility of Ag_2O in concentrated alkaline electrolytes by potentiometric titration, are summarized in Fig. 6. Here, the solubility of Ag_2O in KOH solutions at 25°C is expressed in terms of normality of dissolved silver. The solubility shows a maximum at about 6*N* KOH, coinciding with the maximum in conductivity. At higher KOH concentrations the solubility decreases, possibly because of a shortage of water of hydration and corresponding electrostatic effects between the ions. The present data are in agreement with the results of Johnston *et al.* (12), shown in Fig. 6 by the dotted line, except at concentrations above 5*N*, where our data are somewhat lower. It should be mentioned that all the saturated Ag_2O solutions showed a small Tyndall-effect, indicating the presence of colloidal matter. The Tyndall-effect was not reduced materially by centrifuging at 3000 rpm (600 G). The Tyndall-effect was also present in solutions below 5*N* KOH where our data coincided with the results of Johnston *et al.* It is suggested that colloidal Ag_2O could be responsible for only a minute fraction of the total solubility obtained with the present method.

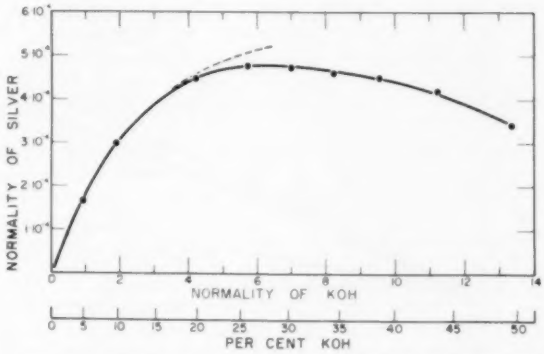

Fig. 6. Solubility of Ag_2O in KOH electrolyte as determined by potentiometric titration.

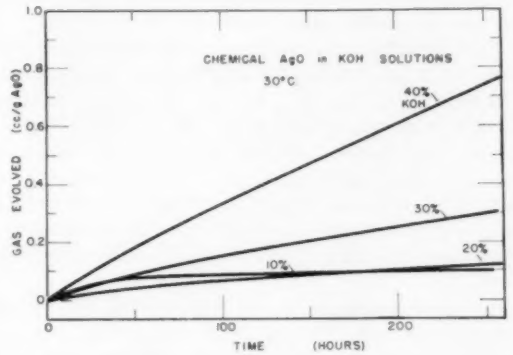

Fig. 7. Effect of KOH concentration on gassing of Merck Divasil AgO at 30°C.

Some measurements of the Ag_2O solubility were also obtained in KOH solutions containing zincate. These solutions were prepared by adding ZnO to KOH solutions. For each molecule of ZnO added, two $(OH)^-$ ions were thus removed, according to $ZnO + 2KOH + H_2O \rightarrow K_2[Zn(OH)_4]$. In a solution of 7.0*N* KOH and 1.9*N* potassium zincate, the solubility of Ag_2O was found to be 4.05 $10^{-4}N$, whereas in 7.0*N* KOH without zincate the concentration of dissolved silver was found to be 4.8 $10^{-4}N$. In another solution, containing 5.04*N* KOH and 1.52*N* potassium zincate, the solubility of Ag_2O was 4.3 $10^{-4}N$, whereas in 5.04*N* KOH without zincate, solubility was 4.7 $10^{-4}N$. Therefore the presence of zincate in the electrolyte has only a slight influence on the solubility of Ag_2O.

The results of the third phase of the present investigation relating to the study of the decomposition reaction

$$AgO \rightarrow Ag_2O + \tfrac{1}{2} O_2$$

are illustrated in Fig. 7 through 10. The evolution of oxygen from AgO in KOH solutions of various concentrations is given in Fig. 7. These results were obtained at 30° ± 0.02°C. The AgO samples were Merck Divasil. The decomposition rate increased with in-

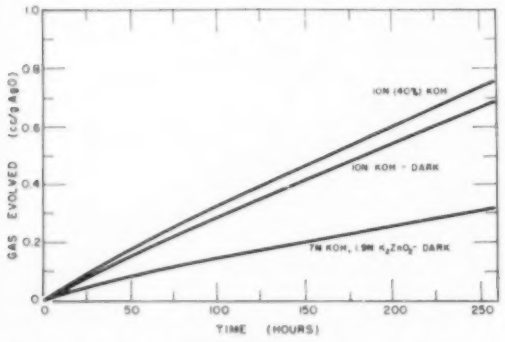

Fig. 8. Influence of light and ZnO addition on gassing of Merck Divasil in KOH.

creasing KOH concentration, even at high concentrations up to 40% KOH.

The solubility of Ag_2O, on the other hand, was somewhat smaller in 40% KOH that in 30% KOH, as shown above. There is no direct relation between solubility of Ag_2O and the gassing rate of AgO. *A priori*, no relation should be expected, since one quantity is an equilibrium value and the other a rate value. The decomposition rate must depend on oxygen overvoltage and the structure and porosity of the protecting Ag_2O film which can limit mass transport.

The decomposition of AgO in alkaline electrolytes is light-sensitive. This is illustrated in Fig. 8, showing gas evolution rates at 30° ± 0.02°C in 40% KOH in the presence and absence of daylight.

Adding ZnO to a KOH electrolyte effectively lowers the $(OH)^-$ concentation by formation of zincate ions. To an electrolyte containing 8.9*N* KOH, ZnO was added to lower the $(OH)^-$ concentration to 7.0*N* and to produce a zincate concentration of 1.9*N*. The decomposition rate in this solution was practically identical to the one observed in 7*N* (30%) KOH solution without zincate. This can be seen by comparing the corresponding curves for 7*N* or 30% KOH in Fig. 7 and 8. It is therefore predominantly the $(OH)^-$ ion activity which governs the decomposition rate of AgO, while additions of zincate ions have little influence.

Figure 9 shows decomposition rates in NaOH solutions at 30° ± 0.02°C. The decomposition rate is smaller in 13.8*N* (40%) NaOH than in 10*N* (40%)

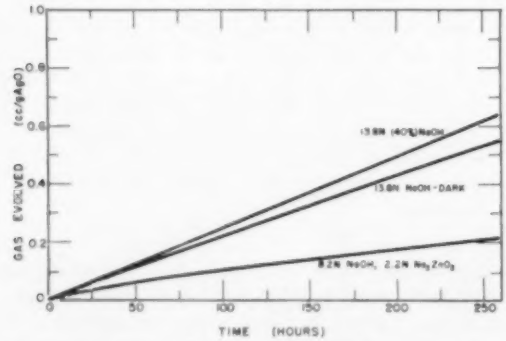

Fig. 9. Influence of light and ZnO addition on gassing of Merck Divasil AgO in NaOH.

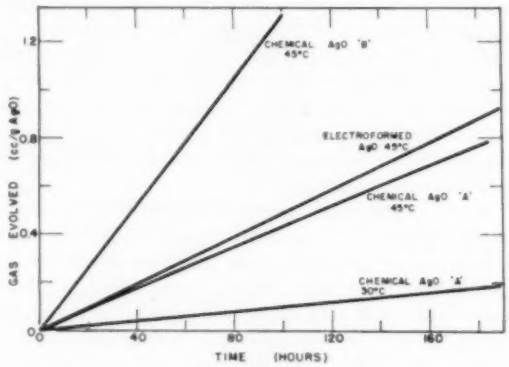

Fig. 10. Gassing of electroformed and chemically prepared AgO samples.

KOH. The influence of daylight is again apparent. In an electrolyte containing 8.2*N* NaOH and 2.2*N* potassium zincate, the gassing is much lower than in 13.8*N* NaOH, due to the lower $(OH)^-$ ion concentration.

The decomposition of AgO in alkaline electrolytes was also studied with samples other than Merck Divasil. Figure 10 shows results for different AgO samples which were tested in a solution of 8.2*N* NaOH + 2.2*N* potassium zincate. The two chemically prepared AgO samples shown are Merck Divasil, designated as chemical AgO "A," and a sample prepared by oxidation with potassium persulfate in alkaline medium (19), designated chemical AgO "B." An electroformed AgO sample, formed by the anodic oxidation of porous silver at controlled potentials, is also included. The samples have widely different decomposition rates. There is a slight correlation between surface area and crystal shape of the individual AgO particles on one hand, and decomposition rate on the other. Figure 10 also illustrates that the decomposition increases rapidly with temperature.

If the decomposition is written as a first order reaction, one obtains

$$-\frac{dc}{dt} = K \cdot c \qquad \text{or} \qquad c = e^{-kt}$$

if $c = 1$ when $t = 0$. The initial rates of decomposition for Merck Divasil, as shown in Fig. 10, at 30° and at 45°C, are 0.10 cc and 0.40 cc/100 hr/g, respectively. This is 8.75 cc and 35 cc/year, respectively. Since 0.0646 of O_2 is generated per gram of AgO decomposed completely into Ag_2O, corresponding to a volume of 50.2 cc at 30°C and 52.7 cc/year at 45°C, respectively, one obtains for the rate constants

$k = 0.17$/year at 30°C and $k = 0.66$/year at 45°C

These rate constants are characteristic for Merck Divasil. Other materials have been found to decompose at different rates.

If a 1-g sample of AgO is in contact with a solution of 8.2*N* NaOH and 2.2*N* potassium zincate, for a period of 1 year, only 0.84 g and 0.51 g of AgO will remain at 30° and 45°C, respectively. This indicates that the decomposition reaction can contribute significantly to the self-discharge of silver-zinc batteries. In sealed cells it might cause excess oxygen pressure and rupture.

Acknowledgment

Part of this work was supported by the US Army Signal Research and Development Laboratory. The authors wish to thank the management of The Electric Storage Battery Company for permission to publish this investigation. The authors are also indebted to Messrs. B. D. Cahan and R. T. Angstadt for contributions to the experimental part of this study.

Manuscript received March 24, 1961. This paper was prepared for delivery before the Houston Meeting, Oct. 9-13, 1961.

Any discussion of this paper will appear in a Discussion Section to be published in the June 1962 JOURNAL.

REFERENCES

1. W. J. Hamer and D. N. Craig, *This Journal*, **104**, 206 (1957).
2. J. F. Bonk and A. B. Garrett, *ibid.*, **106**, 612 (1959).
3. B. D. Cahan, J. B. Ockerman, R. F. Amlie, and P. Ruetschi, *ibid.*, **107**, 725 (1960).
4. R. W. Ohse, *Z. Elektrochem.*, **63**, 1063 (1959).
5. B. Kabanov and D. Leikis, *ibid.*, **62**, 660 (1958).
6. D. I. Leikis, G. L. Vidovitsh, L. L. Knoz, and B. N. Kabanov, *Z. physik. Chem.* (Leipzig), **214**, 334 (1960).
7. A. B. Neiding and I. A. Kazarnovski, *Doklady Akad Nauk SSSR*, **78**, 713 (1951).
8. V. Scatturin, P. Bellon, and R. Zannetti, *Ricerca sci.*, **7**, 2163 (1959).
9. A. Salkind and V. Scatturin, *Ricerca sci.*, to be published.
10. B. Stehlik and P. Weidenthaler, *Collection Czeckoslov. Chem. Communs.*, **24**, 1416 (1959).
11. B. Stehlik, P. Weidenthaler, and J. Vlach, *ibid.*, **24**, 1581 (1959).
12. H. L. Johnston, F. Cuta, and A. Garrett, *J. Am. Chem. Soc.*, **55**, 2311 (1933).
13. Y. V. Pleskov and B. N. Kabanov, *Zhur. Neorg. Khim.*, **2**, 1807 (1957).
14. L. D. Kovba and N. A. Balashova, *ibid.*, **4**, 225 (1959).
15. T. P. Dirkse and B. Wiers, *This Journal*, **106**, 284 (1959).
16. Y. V. Pleskov, *Doklady Akad. Nauk. SSSR.*, **117**, 645 (1957).
17. W. M. Latimer, "Oxidation Potentials," 2nd ed., Prentice Hall, Inc., New York (1933).
18. I. M. Kolthoff and J. J. Lingane, "Polarography," p. 441, Interscience Publishers, Inc., New York (1941).
19. J. C. Bailar, Jr., Editor, "Inorganic Synthesis IV," p. 4, McGraw-Hill Book Co., New York (1953).

The Structure of Silver Oxide Determined by Means of Neutron Diffraction*

Vladimiro Scatturin and Pier Luigi Bellon

Brookhaven National Laboratory, Department of Chemistry, Upton, New York, and Istituto di Chimica generale e inorganica, Universita di Bari, Bari, Italy

and Alvin J. Salkind

The Carl F. Norberg Research Center, The Electric Storage Battery Company, Yardley, Pennsylvania

ABSTRACT

The crystal structure of AgO has been determined by means of neutron diffraction. The nuclear scattering of Ag and O atoms has made it possible to determine the positions of the oxygen atoms and to modify the space group which was reported for this compound from x-ray data. No magnetic diffractions were observed even at liquid helium temperature; the absence of magnetic scattering confirms the diamagnetism of the compound. The lattice was found to be monoclinic, space group $P\ 2_1/c$, with four formula weights of AgO in the unit cell. The silver atoms are not equivalent, and in the structure there are two Ag-O distances of 2.18Å and 2.03Å; the first one corresponds to colinear Ag(I)-O bonds, the second distance corresponds to square planar Ag(III)-O bonds.

The recent interest in the electrochemical properties of the silver oxide AgO (1) has led us to reexamine and refine the crystal structure of this compound.

Previous x-ray investigations (2) indicated that the oxide was monoclinic, space group C 2/c, with four atoms of silver and oxygen in the unit cell. The silver atoms formed a face-centered lattice while the oxygen occupied the special position ± 0, y, ¼; (+ 0, 0, 0; ½, ½, 0). On the basis of the intensities of the powder diffraction lines the most probable value of y = 0.086 was assigned to the variable parameter, taking into account the limitations due to the difference in atomic number of the two species present in the structure.

These x-ray results showed that the silver atoms were equivalent, with square planar coordination to the oxygen, having two different Ag-O distances, 2.04 and 2.35Å. Therefore it was deduced that the AgO structure was similar to CuO structure, but the type of hybridization and bonding used by silver was uncertain.

These conclusions appeared to agree with the magnetic data of Klemm (3), Noyes *et al.* (4), and

* Research performed in part under the auspices of the U.S. Atomic Energy Commission.

with the work of Denison (5) and Barbieri (6) on the chemical behavior of AgO. The rather low AgO magnetic susceptibility ($X_M = +40 \times 10^{-6}$) measured by Klemm could have been due to a possible antiferromagnetism of the compound.

To solve this latter problem and at the same time to define the oxygen positions more precisely, the crystal structure of AgO was reexamined using neutron diffraction. The amplitudes of nuclear scattering of Ag and O ($b_{Ag} = 0.61 \times 10^{-12}$ cm and $b_o = 0.58 \times 10^{-12}$ cm (7)) make the two atomic species almost equal in scattering. Moreover neutron diffraction is the only technique available at this time which can be used to determine the magnetic structure of crystalline solids.

During the course of our research we learned of the magnetic measurements of Neiding and Kazarnovskii (8), who, in disagreement with Klemm, found AgO to be diamagnetic, excluding the presence of Ag^{++} with an unpaired electron. This result is confirmed by the magnetic measurements and by the neutron diffraction results to which we will refer in this work.

Experimental

Powder diagrams with x-rays and neutrons were obtained from samples of Merck Divasil (AgO) which contained ($Ag_2O_{1.88}$) by analysis. Magnetic measurements on these samples made with Gouy's method show that the compound is diamagnetic, confirming the results of the Russian authors (8).

X-ray analysis.—Before going to neutron analysis we redetermined the x-ray diffraction pattern partly to correlate its identity with those previously obtained (2), partly to enable us to compare our results with the diverging ones of other authors (9, 10).

These authors claim that the crystalline powders obtained by oxidation of $AgNO_3$ by persulfate are mixtures of AgO, Ag_2O_3, Ag_2O, and a sub-oxide of Ag with an uncertain formula. The most intense x-ray lines of the patterns of these powders are claimed to correspond to AgO, the weaker ones to the other compounds. All the substances are reported as cubic, and AgO in particular is assigned a ZnS type of structure (10).

Our patterns obtained using Divasil samples and CrKα, FeKα, CuKα radiations have reconfirmed our earlier results. All the lines can be indexed on the basis of a monoclinic lattice having the parameters: $a_o = 5.85_2$Å, $b_o = 3.47_4$Å, $c_o = 5.49_2$Å; $\beta = 107° 30'$.

Table I presents our results for CuKα radiation and those of other authors (10). From it one can see that it is not possible to assign cubic indices to the lines present in our patterns and not reported in other papers. Moreover the lines reported with the cubic indices (111), (200), (420) for Ag_2O_3 and (200), (331) for Ag_2O would be resolved and not overlapping the corresponding AgO lines. Finally the intensities obtained are in agreement with the multiplicities of the monoclinic system. Therefore it can be considered established that the oxide of silver corresponding to the formula AgO is a well determined compound and not a mixture of oxides. In particular the x-ray analysis confirmed

Table I. Comparison of x-ray reflections from AgO (radiation = 1.5418Å)

Monoclinic indices, hkl	$\sin^2\theta$, calc	$\sin^2\theta$, obs	$\sin^2\theta$, S.W.	Cubic index assigned by S.W. (10) AgO	Ag_2O_3*	Ag_2O*	Silver sub-oxide
110	0.0680	0.0687					
200	0.0762	0.0770	0.077	111	111(k)		
11$\bar{1}$	0.0776	0.0782	0.080			111	
002	0.0865	0.0870	0.086				111
111	0.1020	0.1026	0.103	200	200(k)	200(k)	
20$\bar{2}$	0.1139	0.1142	0.115				200
020	0.1963	0.1963	0.198		220		
31$\bar{1}$	0.2056	0.2059	0.205	220			
202	0.2117	0.2118	0.214			220	
11$\bar{3}$	0.2261	0.2260	0.230				220
220	0.2725	0.2725	0.273		311		
311	0.2790	0.2792					
022	0.2828	0.2824	0.282	311			
40$\bar{2}$	0.2936	0.2941	0.295		222	311	
113	0.2996	0.2995					
31$\bar{3}$	0.3053	0.3052	0.308	222			
22$\bar{2}$	0.3102	0.3100	0.315				311
204	0.3246	0.3248	0.322			222	
004	0.3462	0.3466	0.346				222
222	0.4080	0.4074	0.410	400			
40$\bar{4}$	0.4554	0.4559	0.427			400	
13$\bar{1}$	0.4701	0.4696	0.470		331		
51$\bar{1}$	0.4861	0.4864	0.487	331		331(k)	
42$\bar{2}$	0.4899	0.4899					
131	0.4946	0.4843					
420	0.5012	0.5012	0.511	420	420(k)		
22$\bar{4}$	0.5202	0.5205					
313	0.5254	0.5253					
51$\bar{3}$	0.5368	0.5369	0.537				
024	0.5425	0.5423					
11$\bar{5}$	0.5479	0.5478					
31$\bar{5}$	0.5781	0.5782					
33$\bar{1}$	0.5981	0.5978	0.594				
511	0.6084	0.6084					
13$\bar{3}$	0.6187	0.6185	0.614	422			
60$\bar{2}$	0.6258	0.6260					

* The lines indicated with (k) are the ones considered by Stehlik and Weidenthaler to be coincident with the corresponding lines of AgO.

that the most probable space group was C 2/c with the heavier atoms arranged in a face-centered monoclinic lattice.

Neutron analysis.—Neutron diffraction data were obtained with Corliss and Hastings spectrometer of the Brookhaven National Laboratory, Upton, New York. We used powder samples in aluminum containers at the temperature of liquid nitrogen and helium. A monochromatic neutron beam, of 1.064Å wavelength, was obtained from the spectrum of the Brookhaven reactor by diffraction from a lead single crystal.

A BF_3 counter was used to determine the intensity of the diffracted rays. The incident neutron beam was monitored during the continuous scanning of the spectrum, and the counts of the incident and diffracted beams were recorded at each tenth of degree 2θ.

Magnetic reflections were absent even at liquid helium temperature. Figure 1 shows both the liquid nitrogen neutron pattern and the CuKα x-ray

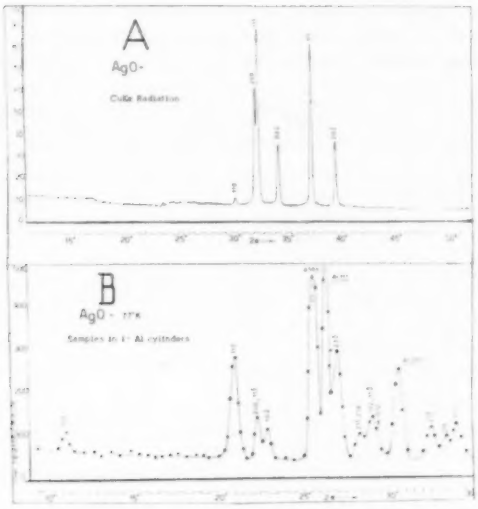

Fig. 1. Diffraction patterns of AgO: A, x-ray; B, neutron

pattern, the latter obtained with the Norelco diffractometer.

It was possible to assign indices to all the nuclear lines on the basis of the monoclinic cell arrived at with x-rays. As can be seen the indexing shows that the cell is primitive and not C centered; the hol reflections, occur only with 1 even, showing the presence of a c-glide plane of symmetry. The intensities of all the lines with either all even or all odd indices are stronger than those with mixed indices except the (200) (020) (002) lines.

This confirms that the silver atoms form a face-centered lattice and that the oxygen must be located in positions close to those determined by x-rays which make the contributions of the silver and oxygen to the (200) (020) and (002) reflections opposite in phase. With x-rays the silver scattering makes the phase difference practically inoperative, but it is detectable with neutrons, given the almost equal scattering amplitudes of the Ag and O nuclei.

These results make most probable in AgO, packing in the primitive space groups of the monoclinic system, and among these P $2_1/c$ permits silver to form a face-centered lattice, and satisfies the hol extinctions. We therefore chose this space group for AgO with the metal occupying the special positions (a) 000; 0, ½, ½ and (d) ½, 0, ½; ½, ½, 0 and the oxygen in the general position (c) ± (x_o, y_o, z_o; x_o, ½ − y_o, ½ + z_o).

The position of the oxygen now depends on three parameters rather than only one, as appeared from the x-ray study.

The best position for oxygen was found minimizing the reliability index $R = \frac{\Sigma|I_{obs} - I_{calc}|}{\Sigma I_{obs}}$ while the parameters are varied. To compute R, the integrated observed and calculated intensities were used after corrections for scale and Lorentz factors. The final results are shown in Fig. 2, in which R is represented at $y_o = 0.350$ and various values of x_o and z_o. The y_o level is the best one to make R a minimum.

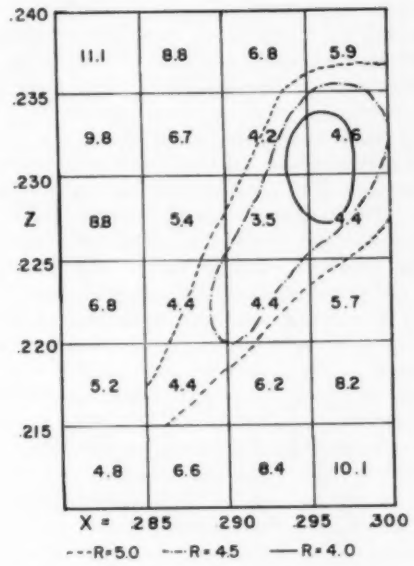

Fig. 2. Reliability index variation with Xo,Zo

Table II contains the observed and calculated intensities with the following parameters:

	x/a	y/b	z/c
Ag_1	0	0	0
Ag_2	½	0	½
O	0.295	0.350	0.230

Discussion of the Structure

The results obtained with neutron diffraction have shown that in AgO there are two types of crystallographicaliy different silver atoms which could not be differentiated with x-rays. Both occupy centers of symmetry and while Ag, at 000 has two oxygen atoms at a distance of 2.18Å, Ag_2 at ½, 0, ½, has four oxygens at a distance of 2.01Å and 2.05Å with an O-Ag_2-O angle of 91° 30′. This second group of atoms forms a square, with silver at the center and oxygen at the corners at an average distance of 2.03Å.

Table II. AgO observed and calculated intensities

hkl monoclinic	j F^2 calc	Σj F^2 calc	obs j F^2
100	0.84	0.84	0.68
110	12.96	12.96	12.00
200	0.38		
11$\bar{1}$	5.32	8.48	9.70
10$\bar{2}$	2.78		
111	56.00	56.00	55.14
20$\bar{2}$	31.84	31.84	30.96
211	3.04		
210	4.08	17.60	17.63
102	0.00		
11$\bar{2}$	10.48		
21$\bar{2}$	7.52		
211	1.36	22.96	21.92
112	14.08		

These experimental results confirm those of McMillan (11), based on the AgO diamagnetism, which is confirmed, at least to the liquid helium temperature, by the absence of any kind of magnetic scattering in the neutron pattern.

The bond lengths and stereochemistry of the two silver atoms in the AgO unit cell, correspond to the covalent bonding properties of Ag^{+} ($4\ d^{10}$) and Ag^{+++} ($4\ d^{8}$). The measured bond distances agree, in fact with the values 2.19Å and 1.97Å calculated as sum of the covalent radii of Ag(I) and Ag(III) (12) with the covalent radius of oxygen atom (12).

The two types of silver contained in the lattice explain the AgO diamagnetism and exclude the presence in the lattice of Ag^{++} ($4\ d^{9}$) with an unpaired electron. The AgO nonstoichiometry can probably be attributed to Schottky type crystal defects (unoccupied lattice sites) which would contribute to the electrical conductivity. However, some of the unusually high conductivity (8, 13) may be due to the dual-valency coordination of AgO, similar to what is proposed by de Boer and Verwey (14) for other metallic oxides.

Acknowledgment

The experimental part of this work was made possible by a grant to Vladimiro Scatturin from the National Academy of Sciences, Washington, D. C., and from International Cooperation Administration. The authors also wish to thank Dr. R. Dodson for his help and warm hospitality at B.N.L.: to Drs. L. Corliss and J. Hastings for the use of the neutron spectrometer of the Brookhaven National Laboratory, Dr. N. Elliot for the Apparatus for magnetic measurements. The assistance of Mr. C. J. Venuto of the Electric Storage Battery Company in obtaining x-ray patterns is also greatly appreciated.

Manuscript received Dec. 9, 1960; revised manuscript received April 27, 1961. This paper was prepared for delivery before the Houston Meeting, Oct. 9-13, 1960.

Any discussion of this paper will appear in a Discussion Section to be published in the June 1962 JOURNAL.

REFERENCES

1. T. P. Dirkse, *This Journal*, **106**, 453 (1959).
   J. A. Mc Millan, *Acta Cryst.*, **7**, 640 (1954); Publicaciones C.E.A. Argentina, Fisice. No. 4 (1954).
2. V. Scatturin, P. L. Bellon, and R. Zannetti, *Ric. Sci.*, **27**, 2163 (1957).
   V. Scatturin, P. L. Bellon, and R. Zannetti, *J. Inorg. Nucl. Chem.*, **8**, 462 (1958).
3. W. Klemm, *Z. Anorg. Chem.*, **201**, 32 (1931).
4. A. A. Noyes, K. S. Pitzer, and E. L. Dunn, *J. Am. Chem. Soc.*, **57**, 1229 (1935).
5. I. A. Denison, *Trans. Electrochem. Soc.*, **90**, 387 (1946).
6. G. A. Barbieri, *Atti. Acc. Lincei*, **13**, 882 (1931).
7. D. J. Hughes and R. B. Schwartz, "Neutron Cross Sections," 2nd ed., Brookhaven Nat. Lab., Upton, N. Y., July 1958.
8. A. B. Neiding and I. A. K. Kazarnovski, *Dokl. Akad. Nauk. SSSR*, **78**, 713 (1951).
9. P. Jones and H. H. Thirsk, *Trans. Faraday Soc.*, **50**, 732 (1954).
10. B. Stehlik and P. Weidenthaler, *Collection Czechoslov. Chem. Commun.*, **24**, 1416 (1959).
11. J. A. Mc Millan, *J. Inorg. Nucl. Chem.*, **13**, 28 (1960).
12. Landolt-Bornstein, Atom und Molecularphysik Tabellen—Teil 4 Kristalle 527 (1955).
13. B. D. Cahan, J. B. Ockerman, R. F. Amlie, and P. Ruetschi, *This Journal*, **107**, 725 (1960).
14. E. J. W. Verwey and J. H. de Boer, *Rec. trav. chim.*, **55**, 531 (1936).

The Reaction between Anodic Aluminum Oxide and Water

Walter J. Bernard and John J. Randall, Jr.

Sprague Electric Company, North Adams, Massachusetts

ABSTRACT

The action of water at 100°C on barrier anodic aluminum oxide has been studied for reaction times up to 30 min. The hydrated product is essentially the same as that formed when aluminum metal reacts with water under the same conditions. Furthermore, the rate of hydration of anodic oxide is remarkably similar to the rate of aqueous oxidation of the metal, suggesting that the same mechanism produces the hydrated film in each case.

The electrolyte used to form anodic films leaves a tenacious layer on the surface of the oxide. This layer must be penetrated or removed by the boiling water before hydration of the oxide can begin. This process gives rise to an "inhibition period" which is distinguished from a similar time lapse which occurs in the direct reaction of water with aluminum. The latter effect is due to the presence of the natural oxide film on the metal.

It is well known that porous anodic oxide films on aluminum react with boiling water to form a hydrated aluminum oxide (1-4). More recently it has been shown (5, 6) that when barrier oxide films (those formed in aqueous boric acid, tartaric acid, etc.) are so treated a similar reaction occurs, and the barrier properties of the oxide are lost, either partially or completely, depending on the time of reaction. In a previous communication (5) we presented evidence that the hydrated oxide which is formed in this reaction is identical to the final product of the direct chemical reaction between aluminum and water, that is, a substance giving an x-ray diffraction pattern corresponding closely to that of

boehmite (α-$Al_2O_3 \cdot H_2O$), but containing considerably more water than stoichiometric monohydrate. Hunter *et al.* (6) have reported an investigation of this reaction, in particular the measurement of the thickness of barrier oxide as a function of reaction time and the thickness of the hydrated oxide formed.

The present investigation was undertaken as an extension of our earlier work which touched only lightly on the hydration of anodic films. In that work it was assumed that the transitory oxide, which we postulated is formed as the first step in the reaction between aluminum and water at 100°C, is identical to the barrier type of anodic aluminum oxide. The basis of this assumption was the observation of the physical similarity of the final hydrated products obtained from both processes. If this assumption is valid, then a study of the rate of hydration of anodic films should also cast some light on the mechanism of oxidation of aluminum by water.

Experimental

The electropolishing procedure and the techniques used in carrying out the hydration reaction have already been described (5). The aluminum for the experiments was Alcoa 0.003 in. foil of 99.986% purity. Specimens had a surface area of 100 cm².

Anodic oxidations were carried out using a constant current generator[1] designed to maintain a preselected current (from 10^{-5} to 0.5 amp) constant to within 0.2% for voltages from zero to 600 v.

Oxidation experiments were made on electropolished aluminum foil in a solution of 30% ammonium pentaborate in ethylene glycol at 25°C, at a final current density of 0.1 ma/cm². For convenience the major part of the oxidation was carried out at 1.0 ma/cm² and the current was then reduced to 0.1 ma/cm² and was held constant until the final desired voltage was attained. Under these conditions the oxide thickness is 11.9Å/v (7). Capacities were allowed to stabilize by measuring 2 min after removal of voltage. A standard electrolytic capacitor bridge was used at a measuring frequency of 120 cps.

The rate of hydration of anodic films was followed by two methods: measurement of the capacity of the film after reaction, and determination of the thickness of the remaining barrier by voltage measurements. This latter method is similar to the procedure used by Hunter *et al.* (6). Our measurements were made by applying a constant current (equivalent to the final current used to form the original film, usually 0.1 ma/cm²) to the sample and measuring the voltage periodically for about 2 min. The extrapolated value of voltage at zero time then gives a measure of the barrier thickness. This method eliminates error due to film formation occurring by passage of current during the process of measuring the thickness.

The water content of the hydrated portion of the anodic film was calculated from the measured weight gain of the film on hydration, the original weight of barrier film (based on coulometric data, assuming 100% current efficiency of oxide formation), and the barrier voltages before and after hydration. The fraction of the hydrated portion of the film which is water is then:

$$\frac{\Delta W}{\left(\frac{V_o - V}{V_o}\right) W + \Delta W}$$

where W is the original weight of anodic oxide, ΔW the weight change on hydration (assumed to be due entirely to absorption of water), V_o the original barrier voltage, and V the barrier voltage after hydration.

[1] Designed by the Sprague Electric Company, Test Equipment Department.

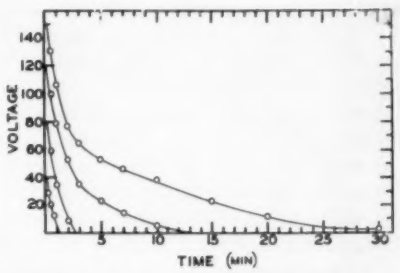

Fig. 1. Remaining barrier voltage vs. hydration time for films originally formed to 40, 80, 120, and 150 v by anodic oxidation.

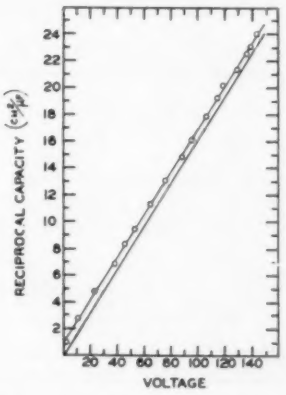

Fig. 2. Reciprocal capacity vs. remaining barrier voltage after hydration for films formed to 150 v. Solid line indicates reciprocal capacity values for nonhydrated specimens.

Results and Discussion

Rate of reaction.—It was reported earlier (5) that when aluminum is treated with water at 100°C an inhibition period exists before the onset of the reaction between the metal and water. This has been attributed to the presence on the metal of a very thin film of oxide which must be penetrated before reaction with the underlying metal can begin. Part of the evidence for this belief stems from measurements of the inhibition period on electropolished aluminum which had been anodically oxidized to voltages up to 25 v. It was found that the time, t_i, necessary to penetrate the anodic oxide was linearly related to the thickness of the film. However, the maximum thickness of anodic films studied was only of the order of 240Å, and later work has shown that the apparent linear rate of oxide hydration does not extend to films of substantially greater thickness. This is shown in Fig. 1 for specimens formed to various

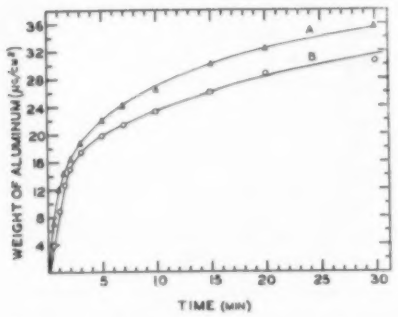

Fig. 3. Weight of aluminum in the hydrated layer vs. hydration time. Curve A, direct reaction between electropolished aluminum foil and water; curve B, hydration of 150 v oxide films.

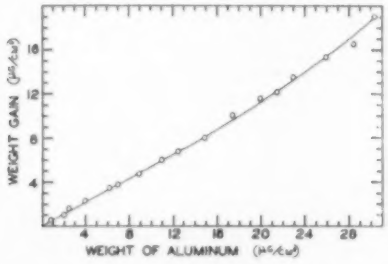

Fig. 4. Weight gain on hydration vs. weight of aluminum in the hydrated portion of 150 v anodic oxide films.

voltages, where the remaining barrier voltage is plotted against hydration time. This plot clearly shows the nearly linear rate of hydration which occurs for the first minute. The shape of these curves is similar to that of Hunter's (6) except for the fact that Hunter finds a longer delay before reaction occurs. (This "inhibition period," which differs from t_A, is discussed below.)

In Fig. 2 reciprocal capacity *vs.* the remaining barrier voltage is plotted for specimens originally formed to 150 v. The linear correspondence shows that capacity data also give a valid measurement of the rate of hydration. The solid line, which represents the reciprocal capacity of nonhydrated films, is slightly displaced from the capacity values for the hydrated samples. This decrease in capacity for comparable barrier voltages is due to the presence of the hydrated film; specimens formed originally to lower voltages give capacities intermediate between these extremes.

By means of coulometric data from anodic oxidation, which gives the total amount of aluminum in the anodic film, and from the fraction, $(V_o - V)/V_o$, of the barrier film destroyed during the hydration reaction, the weight of aluminum in the hydrated portion of the film may be calculated. Data in this form then permit a direct comparison of this reaction with the rate of aqueous oxidation of electropolished aluminum under the same conditions. Plots of these are shown in Fig. 3.[2] There is a striking similarity between the two curves suggesting that the same mechanism gives rise to the hydrated layer in each case. Furthermore, the available evidence indicates that the final hydrated product in each case is the same. Thermogravimetric and x-ray diffraction data (5) showed no difference in the two products. The calculated water content of the hydrated anodic films varied between 20% and 27% (corresponding to 1.6-2.1 moles of H_2O per mole of Al_2O_3), somewhat lower than that observed for films formed in the direct reaction between water and aluminum, with the higher values being found for the longer hydration times. In Fig. 4 the weight gain on hydration is plotted against the weight of aluminum contained in the hydrated portion of the film. It can be seen that there is a nearly constant water content for the first 2 min of reaction followed by a slow increase thereafter.

The rate data for the reaction of anodic aluminum oxide with water have important implications with respect to the mechanism of the reaction of aluminum with water. It was argued earlier by us that the transitory oxide formed during the oxidation of aluminum by water is identical to the amorphous barrier oxide formed by anodic oxidation. The similar appearance of the curves in Fig. 3 is further evidence for this conclusion. The data are plotted on a linear scale because of their failure to fit either the linear, parabolic, cubic, or logarithmic rate laws for film growth.

If the curves in Fig. 3 were identical, it could be reasonably concluded that the rate-determining step in the formation of hydrated oxide from the aluminum-water reaction is the hydration of the transitory anhydrous oxide, since this is the only process common to both reactions. The fact that the rate shown by curve B is somewhat slower than curve A[3] does not necessarily deny this possibility since the slower rate of hydration can be explained by the observation that the anodic film contained a small amount of borate. Spectrographic analysis indicated that the oxide film occluded as much as 0.7% boron (equivalent to about 2% B_2O_3). Since it is known (8) that very small concentrations of boric acid, and presumably borates, may inhibit the growth of hydrated oxide on aluminum, it is reasonable to expect that the presence of borates within an oxide film would reduce the rate of hydration of that film. Therefore, in the absence of borate or other inhibitor curves A and B might coincide. It would then be concluded that the rate-determining step in the formation of hydrated film on aluminum is the hydration of the transitory oxide which was earlier assumed to be identical to the oxide formed by anodic oxidation.

Inhibition period.—Figure 5 shows the early part of the two curves of Fig. 3, emphasizing the difference in inhibition periods for the two reactions. The inhibition time, t_A, for curve A has been discussed before; the time, t_B, required before hydration of anodic films begins is attributed to a different process. It is believed to be due to the presence of a thin film of inhibiting material from the anodizing electrolyte on the surface of the oxide film. This film

[2] The absolute data for the oxidation of electropolished aluminum are somewhat higher than previously reported (5) for degreased aluminum of the same purity. This is partially due to the shorter t_A for electropolished metal.

[3] It was stated erroneously in the previous paper (5) that the rate of hydration of anodic films is greater than the rate of hydrated oxide formation on the metal. This conclusion had been drawn from the incomplete data of hydration of very thin oxide films.

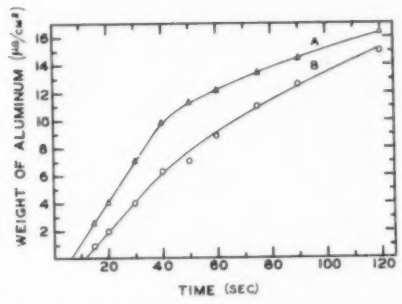

Fig. 5. Weight of aluminum in the hydrated layer vs. hydration time. Curve A, direct reaction between electropolished aluminum foil and water; curve B, hydration of 150 v oxide films.

persists on the surface of the oxide even after continued and vigorous washing in distilled water and must either be removed or penetrated by boiling water before reaction with the oxide may begin. As would be expected, the value of t_s is dependent on the composition of the electrolyte used to form the anodic film. For films formed in the electrolyte used here we find t_s to be about 12 sec (extrapolated data) whereas Hunter (6) presents data from which we estimate a t_s of between 30 and 60 sec for films formed in dilute ammonium tartrate (with a subsequent hydration rate nearly the same as for our borate experiments).

We have also measured t_s for films formed in 3% di-ammonium hydrogen citrate and obtained a value of about 2 min. These observations indicate that t_s is indeed a function of the electrolyte and is not related to t_A, which is due to the pre-existing film on the metal. For the pre-existing film to be responsible for t_s it would be necessary that the anodic oxide be formed between the pre-existing oxide and the metal. Evidence opposing this view has been presented earlier (5) and, furthermore, we have shown that for different pre-existing films which result in different t_A, no effect is observed on t_s. For example, electropolished foil, which had been heated to 200°C in air for several hours, gave a t_A of about 45 sec as compared to 7 sec for nonheat treated foil and a t_s of about 12 sec, the same as for foil not so treated.

Manuscript received April 7, 1961.

Any discussion of this paper will appear in a Discussion Section to be published in the June 1962 JOURNAL.

REFERENCES

1. R. C. Spooner, *Nature*, **178**, 1113 (1956).
2. D. F. MacLennan, *Corrosion*, **15**, 283t (1959).
3. R. K. Hart, *Trans. Faraday Soc.*, **50**, 269 (1954).
4. R. A. Harrington and H. R. Nelson, *Am. Inst. Mining Met. Engrs.*, Inst. Metals Div., Tech. Publ. No. 1158, 14 pp. (1940).
5. W. J. Bernard and J. J. Randall, Jr., *This Journal*, **107**, 483 (1960).
6. M. S. Hunter, P. F. Towner, and D. L. Robinson, *Tech. Proc. Am. Electroplaters Soc.*, 46th Ann. Con., **1959**, 3.
7. W. J. Bernard and J. W. Cook, *This Journal*, **106**, 643 (1959).
8. D. Altenpohl, *Aluminium*, **33**, 78 (1957).

A Study of the Formation of Anodic Oxide Films on Titanium

W. Mizushima

Technical Research Department, Wireless Division, Matsushita Electric Industrial Company, Osaka, Japan

ABSTRACT

The relation between current and field at the formation of anodic oxide films on titanium was studied using nonaqueous electrolyte. The results obtained are consistent with the following relationship between ion current i_+ and electrostatic field across the film: $i_+ = A \exp BE$, where A and B are constant at a fixed temperature. From the temperature dependences of A and B, it was found that the rate-determining mode at high temperature approaches the Cabrera-Mott model, and low temperature favors the effects of space charge. The half width of potential barrier opposing the ionic flow varies from 1.2Å to 1.6Å with the space charge contribution.

The electrochemical behavior of titanium has been studied largely with respect to anodic and cathodic polarization processes (1, 2), and it is generally pointed out that anodic deposition of titanium oxide films are observed under some experimental conditions. However, there have been few investigations on the forming process of thick titanium oxide films at high potentials.

The growth of anodic oxide films on metals has been assumed to depend on the kinetics of the movement of ions into and through the oxide film under the influence of an electrostatic field. Many of the phenomena were established quasi-quantitatively by the classical researches of Guntherschulze and Betz (3), especially for aluminum and tantalum. They showed that, in a forming film, the ionic current density is represented by an exponential function of the field E for very high fields, i.e., $i_+ = A \exp BE$ where A and B are the constants at a given temperature.

Johansen, Adams, and Van Rysselberghe (4) examined the above relation for a number of metals, including titanium, and evaluated the electrolytic parameters in the potential regions below oxygen evolution.

However, by anodizing titanium in suitable electrolytes, it is found that the thick oxide films can be formed at fairly high voltages without oxygen evolved.

In the present paper, the relations between the current and the field during the anodic oxidation of titanium in the nonaqueous electrolyte were studied at constant current densities, and the electrolytic parameters at several temperatures were obtained. Results were not entirely consistent with the rate-determining picture which was established by Mott and Cabrera (5).

The effects of temperature on the kinetic mode will be considered according to Dewald's theory which extends the theory of Mott and Cabrera to include the effects of space charge in the oxide bulk.

Experimental

Titanium sheet KS-50, manufactured by the Kobe Steel Works Ltd., of at least 99.5% purity and 0.12 mm thickness, was used. Each specimen has the nominal surface area of 8 cm^2, and the tab was coated with insulating resin so that the area could be kept constant during a run. The specimen was cleaned by anodic polishing in an electrolyte consisting of 16 parts of 95% H_2SO_4, 3 parts 46% HF, and 1 part H_2O. This procedure removed all scratches and foreign materials and left a smooth surface. Finally the specimen was cleaned in distilled water and then dried.

It has been found that in aqueous electrolytes the current efficiency during formation of titanium oxide was rather small due to oxygen evolution at the anode surface. On the other hand, when water is replaced by organic solvent (*e.g.*, ethylene glycol), any oxygen liberated as bubbles is not observed, and ion conduction becomes the predominant mode of charge transport. Therefore a nonaqueous electrolyte, i.e., 10% ammonium borate solution in ethylene glycol, was used for all of the rate studies.

The formation was carried out, using a platinum cathode, at constant anodic current density, and the applied voltage was increased manually. A series circuit of a variable resistance and a d-c supply was used.

The rate of increase of voltage with time at the constant current density and temperature was measured and dV/idt was calculated, where V is applied voltage, t forming time, and i the current per unit area of the specimen. The above process was applied to five specimens at the same current density and temperature, and the average of data was taken. Values of dV/idt were obtained over the current and the temperature range used, i.e., from 12.5 ma/dm^2 to 200 ma/dm^2 and from 12° to 85°C, respectively.

The reductions in the current efficiency at the higher temperatures were roughly estimated as follows. Titanium specimens were anodized at the several temperatures, from 12° to 85°C, at 100 ma/dm^2 for 100 sec, and V_{12} (the maximum voltage at the oxidation of 12°C) was measured.

Table I. Relative efficiencies of oxidation

Temp. °C	Relative efficiency
12	1
30	1
50	0.96
70	0.91
85	0.85

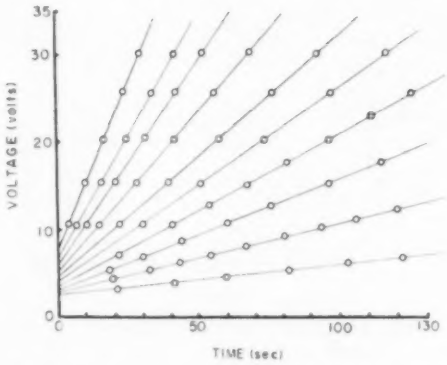

Fig. 1. Voltage-time curves obtained during the formation of anodic films on titanium at constant currents at 12°C.

The interference colors of the specimens were slightly different from each other, so that some differences of the film thicknesses were indicated.

In order to compare the thicknesses, the other specimens were anodized at 12°C and 100 ma/dm^2 until the specimens exhibited interference colors indistinguishable from the colors which were previously obtained at the higher temperatures, and the maximum voltages V_h were measured.

The relative efficiencies of oxidation at the higher temperatures were estimated approximately by V_h/V_{12} assuming that the film thickness is proportional to the efficiency and the color thickness relation remains unchanged with temperature. Results are shown in Table I.

Results

Figure 1 shows typical plots, obtained at 12°C, of applied voltage *vs.* time at several current densities from 12.5 ma/dm^2 to 200 ma/dm^2. The applied voltage, which usually involves an ohmic fall in the electrolyte and a potential drop on the cathode surface, has been customarily used instead of the anodic potential at a fairly high voltage (6). These potential drops could be shown in Fig. 1 if the curves were extrapolated to zero time. The intersections at zero time vary with current densities.

It seems, however, that these potential drops are not changed during the formations because of constant current experiments, and have little influence on the values of dV/dt. Therefore, the changing rate of applied voltage may be satisfactorily used instead of the changing rate of anodic potential.

The average field E across the oxide film may be expressed in terms of dV/dt and the current density, assuming that E is independent of film thickness in a constant current.[1]

That is

$$E = (\sigma\rho F/M\eta)\ dV/idt \qquad [1]$$

where i is the apparent current density, σ roughness factor, ρ density of the oxide, F 96500 coulomb, M

[1] Vermilyea (7) pointed out that the accumulation of a space charge in the oxide film results in the shift of average field at constant current density with film thickness, whereas experimentally it is very nearly constant.

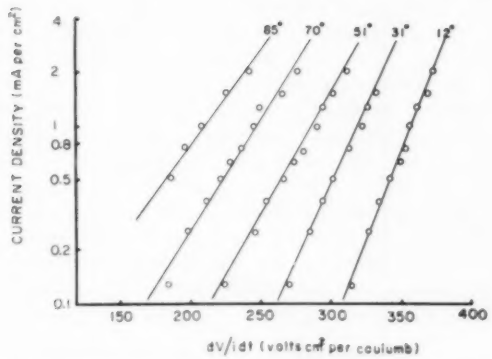

Fig. 2. Current density as a function of dV/idt at the five temperatures.

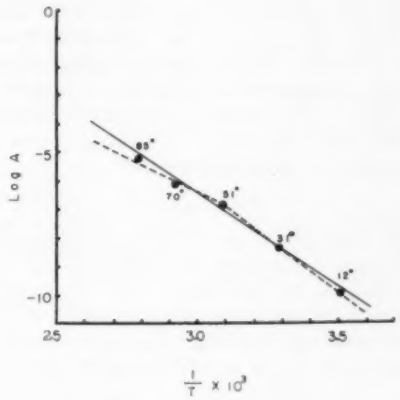

Fig. 3. Temperature dependence of log A

gram equivalent of the oxide, and η current efficiency.

Similarly, ionic current density i_o is related to the apparent current density by

$$i_o = \eta i/\sigma \qquad [2]$$

It has been shown by Guntherschulze and Betz that, when the field is extremely strong such as in the anodic oxide film, the ionic current density may be expressed by

$$i_o = A \exp BE \qquad [3]$$

where A and B are constant for a given temperature. Therefore, substitutions of the assumed relations [1] and [2] into Eq. [3] give the following formula:

$$\log i = \log \sigma A/\eta + 0.4343\, B(\sigma\rho F/M\eta)\, dV/idt \qquad [4]$$

Figure 2 shows a plot of the logarithm of the apparent current density versus dV/idt for the five temperatures. In the figure, it is found that the plots exhibit the linear relations of log i with dV/idt, so that Eq. [4] is fairly well fulfilled in the anodic process of titanium.

The factor $B(\sigma\rho F/M\eta)$ can be estimated by the method of least squares at each temperature. However, the slightly convexed curves may be observed at the higher temperatures. The curvatures arise from the reduction in η at the lower current densities, so that the data in the upper current region were preferred at the higher temperatures. Unfortunately, there is little accurate information with respect to σ, ρ, M, and η.

Therefore, the numerical evaluations of A and B in Eq. [3] were based on tentative assumptions as follows: $\sigma = 1$, if the surface of specimen was completely smooth; $\rho = 3.84$, that is the density of the crystalline anatase TiO_2;[2] $M = 20$, if the oxide film was composed of stoichiometric TiO_2; $\eta = 1.1$,[3] which was obtained, in a preliminary test, assuming TiO_2 formed and comparing weight changes with Faraday's low at the current densities more than 10 ma/dm² at 25°C.

From these assumptions, the factor $\sigma\rho F/M\eta$ at room temperature is found to be 0.0168×10^8 coulomb/cm³, which implies a film growth of about 20Å/v. In addition, the value of 1.1 for η was corrected by the relative efficiencies in Table I at each temperature.

The data are given in Table II, where the values for Ta and Al were calculated from the data obtained by Young (6) and Charlesby (8), respectively. The dimensionless parameter BE_{100} and the field across the oxide film E_{100} are also shown (where E_{100} is the formation field for a current of 100 μa/cm²).

Figure 3 shows a plot of log A *vs.* the reciprocal of the absolute temperature, and the activation energy calculated from the slope of the straight line is 1.3 e.v. However, it is observed that the slope at the higher temperature is somewhat less than that at the lower temperature, and the values of 1.02 e.v. and 1.47 e.v., respectively, can be obtained, if the dotted curves were adopted.

The value of B is decreased with temperature, but no proportional relation between B and $1/T$ can be derived from Table II, even though a few scatterings may be neglected. If B is proportional to $1/T$, values of B at high temperatures should be much larger

[2] The electron diffraction measurement suggests that the anodic oxide film on titanium consists mainly of amorphous TiO_2, and the density will be somewhat different from 3.84.

[3] The efficiency greater than 100% suggests that the composition of oxide film is rather different from TiO_2, but the detail is not at all clear.

Table II. Electrolytic parameters at the formation of anodic oxide films

Metal	Temp, °C	A, amp/cm²	B, cm/v	BE_{100}	E_{100}, v/cm	Film thickness per volt, Å/v	Half-width of barrier (λ), Å
Ti	12	0.994×10^{-10}	2.68×10^{-8}	13.8	5.15×10^{8}	19.4	1.63
	31	0.404×10^{-9}	2.31×10^{-8}	10.1	4.38×10^{8}	22.8	1.51
	51	0.130×10^{-8}	1.78×10^{-8}	6.6	3.71×10^{8}	27.0	1.24
	70	0.711×10^{-8}	1.58×10^{-8}	4.9	3.12×10^{8}	32.0	1.17
	85	0.608×10^{-7}	1.21×10^{-8}	2.8	2.31×10^{8}	43.3	0.94
Ta	20	0.5×10^{-13}	5×10^{-8}	32.9	6.58×10^{8}	15.2	2.5
Al	20	10^{-13}	3×10^{-8}	32.2	10.73×10^{8}	9.3	2.5

than those in Table II, *e.g.*, 2.23×10^{-6} at 70°C. These high values cannot be evaluated from the curves in Fig. 2 unless the relative efficiencies (Table I) at high temperatures are greater than 1.0, *e.g.*, $0.91 \times 2.23/1.58 = 1.2$ at 70°C. Therefore, the extreme reduction of B at high temperatures is not attributed to the uncertainties in η.

Discussion

Cabrera and Mott postulated a single rate-controlling system which was characterized with potential barrier ϕ against the passage of metal ions from metal to interstitial positions in the oxide. According to their theory, the electrolytic parameters A and B in the expression $i = A \exp BE$ are given by

$$A = N\nu q \exp(-\phi/kT) \quad [5]$$

$$B = q\lambda/kT \quad [6]$$

where N is the concentration of atoms in position to jump into the film, ν the vibration frequency of metal ions, q the charge of the ion, ϕ the zero-field activation energy, λ the distance from the equilibrium position of an ion in the metal to the top of the energy barrier, and k Boltzmann constant.

The zero-field activation energy in the Cabrera-Mott picture (5) was evaluated from the slope of log A *vs.* $1/T$ shown in Fig. 3, and the value of 1.3 e.v. (*i.e.*, 30 kcal/mole) was obtained by a linear approximation (solid curve).

It seems that a fairly high field should be required to induce ionic conduction, since the activation energy is over 40 kT which is the criterion of the high field case defined by Dewald (9). However, the value of $BE_{i=0}$ is no more than 14 even though at 12°C, and the values of A are found to be much larger than those in Ta or Al.

Johansen, Adams, and Van Rysselberghe (4) investigated Ti in the low potential range by use of an aqueous electrolyte and obtained the values of $BE_{i=0}$ as large as 20, which is still insufficient to affirm a high field process.

In titanium oxide film, therefore, the influence of field strength on the ionic flow is much less than those in tantalum and aluminum oxide, and the thermal diffusive motion of the ions may be more predominant. Accordingly, the value of 1.3 e.v. (which is 53 and 42 kT at 12° and 85°C, respectively) seems to be too large to expect the large thermal progress of ions, especially at high temperatures.

With $\phi = 1.3$ e.v., the extrapolation of the Fig. 3 to $1/T = 0$ gave a value of 2×10^{21} for $N\nu$, and this value of $N\nu$ is unreasonably greater than that considered by Cabrera and Mott.

On the other hand, assuming that the plot in Fig. 3 curves along the dotted line, the activation energies of 1.02 and 1.47 e.v. may be obtained at the high and low temperature regions, respectively. With $\phi = 1.02$ e.v., $N\nu$ is estimated as of the order of 10^{27} which is in good agreement with the Mott prediction. It seems, therefore, that the high temperature favors the Cabrera-Mott system, and at the low temperature, the rate of oxidation should be determined by the ionic motion through the oxide. More data at the higher temperatures[4] should be required to affirm the dotted curves in Fig. 3.

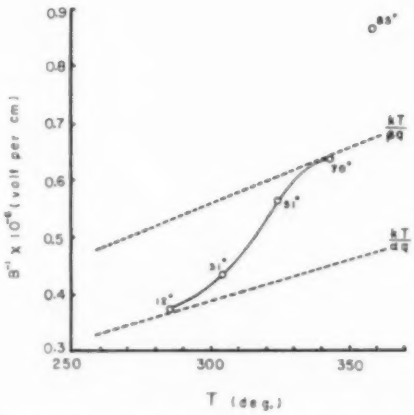

Fig. 4. Variation of Tafel slope (1/B) with temperature for the anodic oxidation of titanium.

However, as shown in Table II, values of B are not proportional to $1/T$, so that the half width of the potential barrier, calculated by Eq. [6], decreases steadily with temperature.

The above fact suggests that the rate-determining mode is shifted from one to another model with temperature, and then supports the dotted feature in Fig. 3.

According to Dewald (9), the field at any point in the film is composed of two parts, a metal-oxide surface charge contribution and a space charge term which arises from the excess charge of the interstitial ions in the oxide bulk. These interstitial ions cannot be compensated electrically under the high field case.

In the present study, the conditions of high field formation were found at the lower temperature, since the activation energy is as large as 1.47 e.v., so that low temperature favors large space charge.

On the other hand, at the higher temperatures, the ion conduction may be achieved by large thermal diffusion of ions and little influence of field. In addition, electronic current neutralizes the excess charge of the interstitial ions under the conditions of reduced efficiency, so that the higher the temperature, the lower the space charge.

Figure 4 shows the temperature dependence of $1/B$ (that is Tafel slope) in the anodic oxidation of titanium. The curve may be considered by Dewald's theory (9) as follows, except the value obtained at 85°C.

In the research on Ta (9), the effect of space charge on the Tafel slope was derived theoretically as

$$\frac{\partial E}{\partial \ln i} = \frac{kT}{\beta q}\frac{\ln(1+\delta)}{\delta} + \frac{kT}{\alpha q}\left\{1 - \frac{\ln(1+\delta)}{\delta}\right\} \quad [7]$$

where α is the half distance between the interstitial positions in the oxide bulk, β the jumping distance of ions at the metal-oxide surface, and δ the dimensionless factor determining the importance of space charge.

[4] The reproducibilities of experimental results at the temperatures over 80°C are very poor because of low current efficiencies and extremely small dV/dt.

When $\delta << 1$, the Tafel slope approaches $kT/\beta q$ and the parameters of the metal-oxide interface are the rate-determining ones. While, if $\delta >> 1$, the rate of oxidation is determined almost entirely by the bulk properties of the film, and the space charge contributions are all important. Therefore, the half width, given in Table II, should be intermediate ones between α and β.

However, when the rate-determining mode approaches the Cabrera and Mott picture at the high temperature, a condition of $U - \alpha/\beta\phi > 0$, pointed out by Dewald, should hold, where U is the activation energy for diffusion through the film, and ϕ the energy for entrance into the film.

Assuming $\phi = 1.02$ e.v. and $U = 1.47$ e.v., the terminal values of half width which are consistent with $U - \alpha/\beta\phi > 0$ are nearly equal to 1.6 and 1.2Å, so that $kT/\beta q$ was expressed, in Fig. 4, by a dotted line nearly passing the plot of 70°C and another dotted line was assigned to $kT/\alpha q$. Thus, with the data obtained from 12° to 70°C, the energy parameters, U, ϕ, α, and β of Dewald's model have the values 1.47 e.v., 1.02 e.v., 1.6Å, and 1.2Å, respectively.

The data at 85°C seem to be rather anomalous, since the resulting value of λ is about 0.9Å, which is too small to visualize. The reason for deviation at 85°C is not entirely clear, but probably attributed to disturbances by side reactions and erroneous measurement.

In general, the ionic conduction in the titanium oxide film is much greater than those of Ta and Al at the same temperature, so that the large film thickness would result.

Therefore, further experiments at the much lower temperatures are desirable to investigate the kinetics of the film growth at high fields.

Acknowledgments

The author wishes to express thanks to Dr. S. Minami and Dr. C. Okazaki for their helpful advice and encouragement. Thanks are also due to Mr. S. Kisaka, the head of this laboratory, for supporting this research.

Manuscript received Nov. 21, 1960; revised manuscript received May 22, 1961.

Any discussion of this paper will appear in a Discussion Section to be published in the June 1962 JOURNAL.

REFERENCES

1. M. Stern and H. Wissenberg, *This Journal*, **106**, 755 (1959).
2. C. D. Hall and N. Hackerman, *J. Phys. Chem.*, **57**, 262 (1953).
3. A. Guntherschulze and H. Betz, *Elektrolytekondensatoren, Krayn, Berlin* (1937).
4. H. A. Johansen, G. B. Adams, and P. Van Ryssselberghe, *This Journal*, **104**, 339 (1957).
5. N. Cabrera and N. F. Mott, *Rep. Prog. Phys.*, **12**, 163 (1948).
6. L. Young, *Trans. Faraday Soc.*, **50**, 159 (1954).
7. D. A. Vermilyea, *This Journal*, **102**, 655 (1955).
8. A. Charlesby, *Proc. Phys. Soc.*, **B66**, 317 (1953).
9. J. F. Dewald, *This Journal*, **102**, 1 (1955).

Oxidation of Iron in the Temperature Range of 260°-470°C

E. J. Caule, K. H. Buob,[1] and M. Cohen

Division of Applied Chemistry, National Research Council, Ottawa, Canada

ABSTRACT

The kinetics of the oxidation of ingot iron in 19 mm O_2 has been studied over the temperature range of 260°-470°C. Both Fe_3O_4 and α-Fe_2O_3 were observed to be present at all temperatures and times. Initially Fe_3O_4 grows to reach a value which becomes constant for some time and then starts to increase again. When the Fe_3O_4 layer recommences growth there is also an increase in the over-all oxidation rate. The rate constant for the early part of the oxidation is about half that of the latter part. In all cases the total oxidation rate is essentially parabolic.

The rate of thickening of oxide films on iron at a given temperature appears to be limited by the thickness of film already present. Typical papers, such as those of Gulbransen (1) and Davies, Simnad, and Birchenall (2), show the oxidation rate decreasing with time and consequently with thickness. The ideal behavior of this form is summarized in the "Parabolic Law" of Pilling and Bedworth (3) which is based on the assumption that rate is inversely proportional to thickness and states that the square of the thickness is proportional to time. As in the papers mentioned, most other data on oxidation of metals are treated as tending under ideal conditions to agree with the parabolic law.

Because iron, even in the range of very thin oxide films, can form several layers of different oxides, difficulty is to be expected, first, in finding a suitable law to express the rate of growth and, second, in interpreting the law. Below 570°C the films consist of magnetite and hematite, and above that temperature of wustite, magnetite, and hematite (2), the oxides being named in the order of their position in the film from the metal outwards. In spite of the voluminous literature on the oxidation of iron, very

[1] N.R.C. Post Doctorate Research Fellow. Present address: Reactor Ltd. of Switzerland, Zurich, Switzerland.

few studies have been reported previously which attempted to measure the growth not only of the whole film but also of the separate constituent layers.

Paidassi (4) cross-sectioned specimens covered by thick oxides and measured the thicknesses with the optical microscope. The curves of growth as a function of time were obtained only for oxides so thick that they must be considered as scales rather than as films. A method suitable for thin films was developed by Davies, Evans, and Agar (5); in their work the outer oxide, hematite, was measured after oxidation by the number of coulombs necessary to remove it in an electrolytic reduction cell, and the inner oxide, magnetite, which was relatively non-reducible, was then determined as the difference between total and outer oxides. Their results were not extensive enough to provide a mechanism, and in addition the electrolytic solution used was later shown not to be ideally suited from the point of view of current efficiency to this system (6).

The data reported here were obtained by a method similar in principle to that of Davies, Evans, and Agar, but employing higher accuracy and a more detailed investigation of oxidation curves. The temperatures of oxidation were in the range from 269° to 463°C, so that only magnetite and hematite were formed (7). Three curves were obtained at each of eight temperatures to show, as a function of time, the weight of oxygen in the whole film, in the hematite, and in the magnetite. The results have enabled some definite conclusions about the course of the reaction to be drawn, in particular as to the validity of the generally accepted parabolic law.

Because the data are new and because it is desired to plot them in a manner involving no preconceived views, this paper displays the results in the most direct and easily handled form and includes a minimum of theoretical treatment.

Experimental

The main type of experiment performed was as follows: at a constant temperature a specimen previously weighed on an analytical microbalance was heated for a measured time, then cooled, reweighed, and analyzed for hematite. The weight of magnetite was obtained by difference. Repetition of this experiment at different times built up curves for the growths of total oxide and constituent layers. The exact procedure is described below.

An oxidation was begun sharply by sudden admission of oxygen to a definite pressure over a specimen already heated to a fixed temperature and from which the air-formed film had already been removed by reduction in hydrogen. Thus the standard initial state of a specimen was that it be hot, film-free, and hanging in a vacuum. By rigid standardization of procedure the standard state and the process of admitting oxygen were made as reproducible as possible. The relatively low scatter of the oxidation results is a consequence of this care.

Measurements of the curve of total gain in weight were also done on single specimens by means of a vacuum microbalance as described and used by Gulbransen (1).

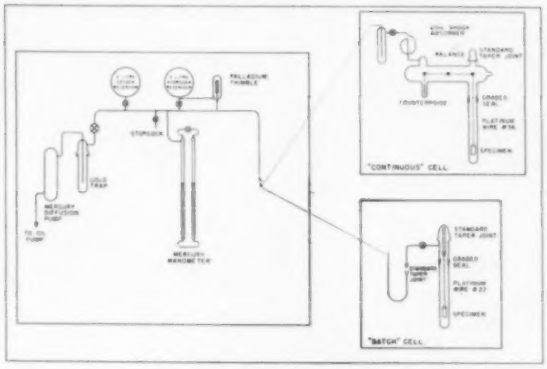

Fig. 1. Diagram of apparatus

Apparatus.—Figure 1 shows the vacuum apparatus and reaction cell, as well as the Gulbransen balance. The tube in which the specimens were hung was of quartz and about 1 in. in diameter externally. The furnace had a tubular core wound with Nichrome wire. The temperature was controlled by a chromel-alumel thermocouple connected to a commercial electronic controller, and a separate removable probe thermocouple showed that the plateau of temperature at which the specimens hung was maintained to better than ± 1½°C.

The analytical microbalance, used in an air-conditioned room, gave an average deviation from the mean of ± 1½μg; since the area of a specimen was about 15 cm^2, the deviation was thus 1/10 μg/cm^2. The reproducibility from day to day was ± 2 μg on the whole specimen.

Materials.—Specimens were cut to follow a template from a sheet of cold-rolled Armco iron of thickness 0.17 mm. After being degreased in benzene their usual weight was 0.94 g. The analysis of the iron was made in the Analytical Section of these laboratories and gave the following for percentage of each impurity: Ni, 0.170; Cr, 0.0045; Mn, 0.0120; Al, 0.0032; P, 0.028; N, 0.0015; C, 0.039; Si, 0.0030; S, 0.0052.

Oxygen and hydrogen were taken from commercial cylinders. The hydrogen was purified by diffusion into the cell through a heated palladium tube, but the oxygen was used without purification. Drying the oxygen by passing it through a trap immersed in liquid nitrogen did not change the rate of oxidation of the iron.

Method.—The sequence of steps in an experiment was as follows: (i) evacuation of cell containing the weighed specimen; (ii) admission of hydrogen to a pressure of 1 cm/Hg; (iii) placing of closed cell in furnace; (iv) after 1 hr, removal of hydrogen by pumping for 40 min; (v) release of a definite amount of oxygen suddenly into cell to bring pressure to 1.9 cm/Hg; (vi) after desired time of oxidation, sudden chilling by plunging closed cell into cold water; (vii) reweighing and analysis of oxide layers.

Reductions with hydrogen were always performed at 417°C or above; consequently for oxidation at

lower temperatures an adjustment of the temperature during step (iv) was necessary.

The rapid cooling during step (vi) prevented "annealing" effects which might have led to changes in the form and relative amounts of the oxides (8). It also reduced the uncertainty in the time of oxidation to perhaps 5 sec.

Analysis of the oxide layer was done by the method of Oswin and Cohen (6), which is an electrolytic reduction and dissolution of the hematite layer. The amount of hematite is measured by the loss in weight of the specimen. By a gravimetric factor this is converted to weight of oxygen in the hematite layer, and subtraction of this quantity from the total gain in weight during oxidation gives the weight of oxygen in the magnetite layer.

In performing oxidations, times and, to a lesser extent, temperatures were taken in a random sequence in order to avoid the appearance of trends due to drifts in instruments.

Results

The results are presented in Fig. 2 to 9 as graphs of gain in weight *vs.* time. Every value for both total oxide and magnetite is low by an amount equal to the weight of oxygen already on the specimen when it was first weighed. Gulbransen's measurement gives the average thickness of this "air-formed" film as about 40Å, and measurements here of the loss in weight of a fresh specimen on reduction by hydrogen while suspended from the vacuum microbalance give the same figure. In terms of weight the error amounts to about 0.7 $\mu g/cm^2$. The graphs have not been corrected for this effect as the correction would have no effect on the shapes of the curves, but would merely increase all values for magnetite and total oxide by a constant amount.

The results obtained by use of the "vacuum" microbalance were designed to confirm the shapes of curves obtained from the "batch" experiments

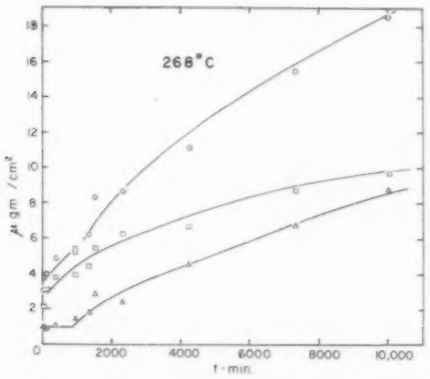

Fig. 2. Weight of oxygen vs. time at pressure of 1.9 cm O_2 and 268°C. O, total oxygen; □, oxygen in hematite; △, oxygen in magnetite.

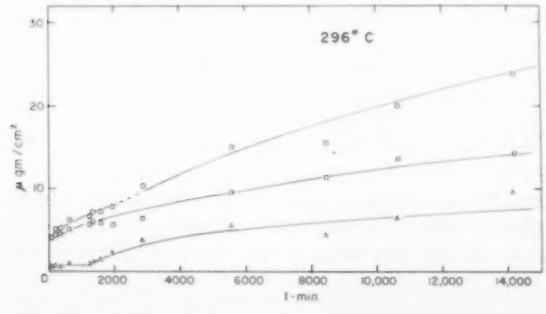

Fig. 3. Weight of oxygen vs. time at pressure of 1.9 cm O_2 and 296°C. O, total oxygen; □, oxygen in hematite; △, oxygen in magnetite.

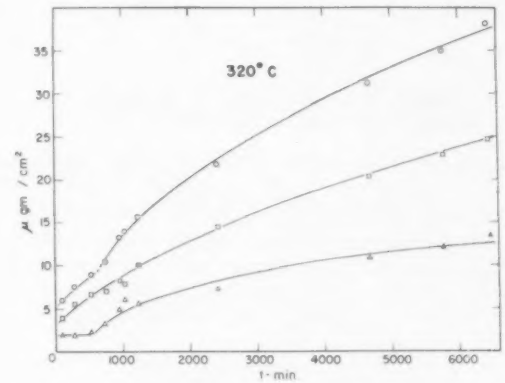

Fig. 4. Weight of oxygen vs. time at 1.9 cm O_2 and 320°C. O, total oxygen; □, oxygen in hematite; △, oxygen in magnetite.

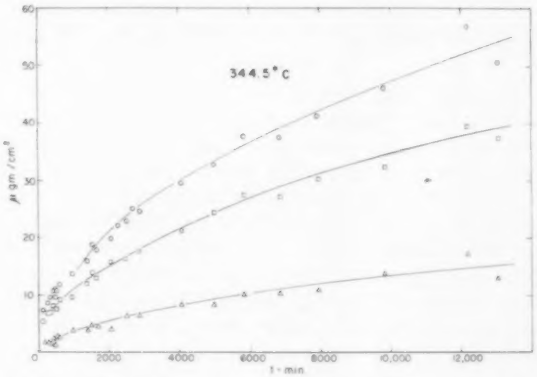

Fig. 5. Weight of oxygen vs. time at 1.9 cm O_2 and 344°C. O, total oxygen; □, oxygen in hematite; △, oxygen in magnetite.

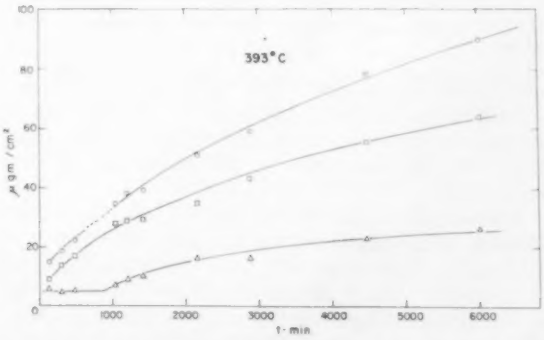

Fig. 6. Weight of oxygen vs. time at 1.9 cm O_2 and 393°C. O, total oxygen; □, oxygen in hematite; △, oxygen in magnetite.

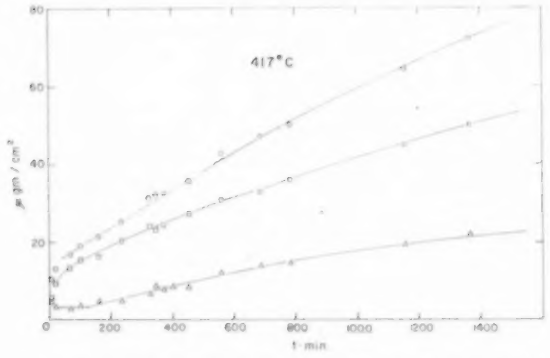

Fig. 7. Weight of oxygen vs. time at 1.9 cm O_2 and 417°C. O, total oxygen; □, oxygen in hematite; △, oxygen in magnetite.

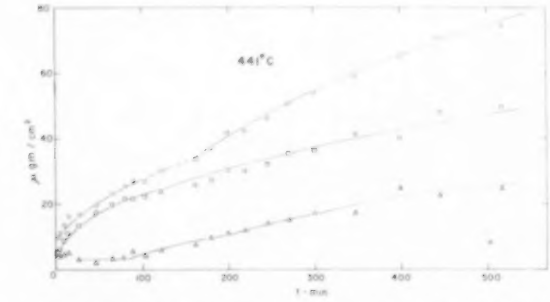

Fig. 8. Weight of oxygen vs. time at 1.9 cm O_2 and 441°C. O, total oxygen; □, oxygen in hematite; △, oxygen in magnetite.

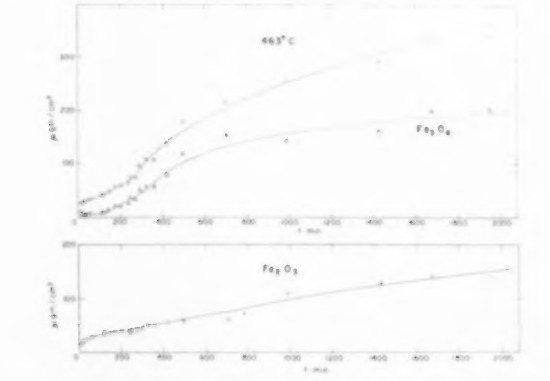

Fig. 9. Weight of oxygen vs. time at 1.9 cm O_2 and 463°C. O, total oxygen; □, oxygen in hematite; △, oxygen in magnetite.

and to provide a correlation with previously published curves of the same type. Since they did so without adding anything significant to the data, they will be mentioned in the discussion without being shown.

Microscopic examination showed that the films formed were relatively smooth and uniform. The cathodic reduction curves were quite normal and indicated a fairly sharp boundary between the hematite and magnetite. In view of these observations the film is treated as consisting of two distinct layers without discontinuities such as whiskers or platelets. Similar results were also obtained with an iron whose main impurity was iron oxide inclusion.

Treatment of Data

The lines shown on the graphs are drawn smoothly through the points. The only discontinuity included is that one which occurs in every graph for magnetite in the first part of the curve with an accompanying discontinuity in the curve for total oxygen. After a short flat section the amount of magnetite rises with time. Consequently each graph can be considered as consisting of two parts, (*a*) an early section with little growth of magnetite beyond an initial quick formation, and (*b*) a later section with simultaneous growth of both magnetite and hematite.

The shape of the graph of total growth does not conform to a simple curve at any temperature. At the highest temperatures, 463° and 441°C, the curve is very clearly sigmoid in shape, which implies that the rate increases after a certain amount of oxide has been formed. A similar acceleration can be seen in the other graphs. Clearly, from inspection, there is very little reason to assume that a single simple parabolic law governs the growth of oxide at all times under the conditions of experiment used here.

If attention is paid to the later parts of the graph without attempting to include in the same law the early points, it is found that parabolas can be fitted at all temperatures. Thus the smooth curves of the latter part of each graph for total oxide are actually fitted parabolic sections. The fit is very definite for some temperatures and is satisfactory for all.

The method of calculating the parabolas is as follows. It is not necessary for the data to cover the parabola from the vertex in order to calculate the constant. The initial statement of the law is that the derivative of thickness with respect to time is inversely proportional to the thickness, *i.e.*,

$$\frac{dW}{dt} = \frac{k}{W}$$

From the rate and the thickness at a given point, a value of k can then be calculated whose accuracy is dependent on there being no additive constant associated with W. At long times, the risk is slight in assuming that this constant is unimportant or zero.

For the eight temperatures of experiment the constant was calculated as shown in Table I.

Table I. Constant calculations

Temp. °C	Time, min	Slope, μg/min = rate	W, μg	k = W (rate), μg²/min	$\log_{10}k$	$\frac{1}{T}$ °K
268	7,000	0.00116	15.3	0.0177	$\bar{2}.248$	0.00185
296	10,600	0.00110	20.0	0.0220	$\bar{2}.342$	0.00176
320	4,000	0.00373	28.7	0.107	$\bar{1}.029$	0.00169
344	11,000	0.00222	51.0	0.113	$\bar{1}.053$	0.00162
393	5,000	0.00843	83.0	0.700	$\bar{1}.845$	0.00150
417	1,200	0.0381	67.0	2.55	0.406	0.00145
441	450	0.0900	72.0	6.48	0.812	0.00140
463	1,600	0.1039	310.0	32.2	1.508	0.00136

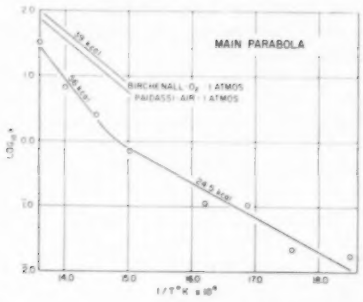

Fig. 10. Plot of logarithm of rate constant in $(\mu g/cm^2)^2/min$ vs. reciprocal of absolute temperature for main parabola.

From the constant the whole parabola could be calculated, plotted on the same scale as the data, applied as an overlay to the original graph, and moved about until a fit was obtained. The method is simpler than, and avoids some of the difficulties of, the more usual way of finding the constant from the slope of a plot of weight *vs.* square root of the time. The latter method is accurate when the position of the vertex of the parabola is known.

The logarithm of the rate constant was then plotted in the usual fashion against the inverse of the absolute temperature to obtain Fig. 10. The values of the activation energies are drawn in on the two slopes as 56 and 24.5 kcal. For comparison, plots of log k from two other studies, with different iron are included in the same graph.

As well as these later, more certain parabolas, short parabolic sections were fitted to the initial points of the total weight gain curves. [It is known from the published work of, *e.g.*, Gulbransen (1) that the first 100 min of the curves should be parabolic and the microbalance curves here confirmed it.] The relative accuracy of the points at short times is low and the fit is very loose. The same procedure of calculation was used as above. In each graph the sections of parabolas are joined by dotted lines to indicate the transition intervals.

The results of the calculation are shown in Table II. The values for W, as read from the graphs of weight against time, have been increased by 0.7 μg to correct for the thickness of the air-formed film. As mentioned previously, this has an effect only for the thinnest films.

The values of the rate constants are obviously inexact, but are useful. In general they tend to be one half or less of the later parabolic constants,

Table II. Results of calculations

Temp, °C	Time, min	Slope = rate	W, μg	k = W (rate), $\mu g^2/min$	$\log_{10} k$	$\frac{1}{T}$ °K
268	500	0.00197	5.4	0.0106	$\bar{2}.025$	0.00185
296	500	0.0020	6.3	0.0126	$\bar{2}.065$	0.00176
320	250	0.0064	8.0	0.0512	$\bar{2}.71$	0.00169
344						
393	400	0.0225	21.2	0.477	$\bar{1}.69$	0.00150
417	100	0.0465	19.7	0.916	$\bar{1}.962$	0.00145
441	50	0.162	21.2	3.43	0.536	0.00140
463	100	0.13	40.7	5.29	0.732	0.00136

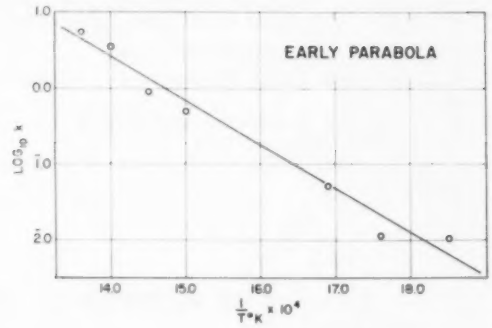

Fig. 11. Plot of logarithm of rate constant in $(\mu g/cm^2)^2/min$ vs. reciprocal of absolute temperature for early parabola.

except for those at 463°C, where the ratio is about 1:6.

When plotted as log k *vs.* $1/T$, they give much the same course as the previous such graph. Figure 11 shows the curve; the slope is the same as the slope of the low temperature region of Fig. 10 and thus corresponds to about 25 kcal.

Discussion

The results for total gain in weight for extended periods of oxidation have been fitted to parabolic curves by using the whole thickness of the oxide as the barrier layer. The analyses show that both magnetite (as an inner layer) and α-Fe_2O_3 (as an outer layer) are present over the whole temperature range.

In the initial period of the oxidation the magnetite layer grows rapidly to a value which is then constant for a time which, in general, decreases with an increase in the temperature of oxidation. When the magnetite starts to grow again there is an increase by a factor of about two in the over-all rate, although this final rate is still parabolic. There is also an increase in activation energy for total growth above a temperature of 410°C. During this second period of growth there is a tendency for the growths of hematite and of magnetite to decrease in rate with time.

The low activation energy indicates that the controlling transport process is probably not the diffusion of metal ions; it is more probable that the critical transport is that of oxygen. The partition of oxygen between the two layers is guided by some unknown function of thickness, temperature, and oxygen pressure. Oxygen can be transported either as molecules through cracks or as ions through the lattice, probably as the latter.

In conclusion it can be stated that the oxidation of iron in the temperature range of 270°-460°C leads to the formation of a two layer film containing magnetite next to the metal and hematite in the outer layer. At short times the magnetite thickness is constant, and the over-all growth rate is parabolic. At longer times both layers grow and the over-all rate is still parabolic.

Manuscript received Feb. 17, 1961; revised manuscript received May 22, 1961.

Any discussion of this paper will appear in a Discussion Section to be published in the June 1962 JOURNAL.

REFERENCES

1. E. A. Gulbransen, *Trans. Electrochem. Soc.*, **81**, 327 (1942).
2. M. H. Davies, M. T. Simnad, and C. E Birchenall, *J. Metals*, **889**, October (1951).
3. N. B. Pilling and R. E. Bedworth, *J. Inst. Met.*, **29**, 259 (1923).
4. J. Paidassi, *J. Metals*, **4**, 536 (1952).
5. D. E. Davies, U. R. Evans, and J. V. Agar, *Proc. Roy. Soc.*, **A225**, 443 (1954).
6. H. G. Oswin and M. Cohen, *This Journal*, **104**, 9 (1957).
7. U. R. Evans, "The Corrosion and Oxidation of Metals," p. 26, Edward Arnold, Ltd., London (1960).
8. E. J. Caule and M. Cohen, *This Journal*, **108**, 834 (1961).

The Annealing of Oxide Films on Iron

E. J. Caule and M. Cohen

Division of Applied Chemistry, National Research Council, Ottawa, Canada

ABSTRACT

The annealing reaction in vacuum of thin films of magnetite and hematite on iron has been studied at 463°C. The gravimetric curves obtained for growth of magnetite and decay of hematite have been compared with the curves of growth of both during oxidation at 5.75 cm pressure of oxygen. The flow of iron through the magnetite during annealing is one fourth its value during the oxidation.

A preceding paper (1) has described a technique of measuring curves of gain in weight as a function of time for the growth of magnetite and hematite on iron heated in oxygen at temperatures between 268° and 463°C. The sensitivity was such that studies could be made on thin films ranging in thickness from 100 to 20,000Å. The resulting data were displayed as three curves at any one given temperature, one each for total oxide, hematite and magnetite. It was obvious from the results that the reactions of growth were complex, with the major product changing with time from hematite to magnetite and back again.

In the oxidation there is a flow of both oxygen and metal to the site of reaction. If, after an oxide layer has been established, the flow of oxygen is shut off by pumping the gas from the reaction vessel, then the iron may continue to flow to the reaction zone. A possible result is the following reaction

$$Fe + 4Fe_2O_3 \rightarrow 3Fe_3O_4$$

This may be a complex reaction in itself but for the present purposes can be considered elementary. There is strong evidence (2, 3, 4) in the literature for the occurrence of the reaction and some measurement of its rate, but the technique used here of measuring the splitting of the whole film into its component layers offers a unique opportunity to study the annealing action directly and to measure its rate and compare it with the over-all rate.

Experimental Procedure

The method and materials for experiments of this type have been fully described in (1). It is sufficient to say here that weighed specimens of pure iron are heated in oxygen after reduction in hydrogen; after definite times of oxidation they are "quenched" rapidly to "freeze" the ratio of the oxides and reweighed. The gain in weight is the weight of the whole film; subsequent analysis for hematite by a method of electrolytic reduction enables the weights of the component layers of the duplex films to be determined.

In the particular set of experiments described here a group of oxidations at 463°C and 5.75 cm pressure of oxygen were each stopped at the same time, 100 min, by rapidly pumping out the oxygen; they were then kept at that same temperature in the vacuum for different specified times of annealing before being rapidly quenched to room temperature by immersion of the quartz reaction cell in cold water. Subsequent analysis showed the change caused by the annealing in the ratio of the thicknesses of the layers while similar oxidations with-

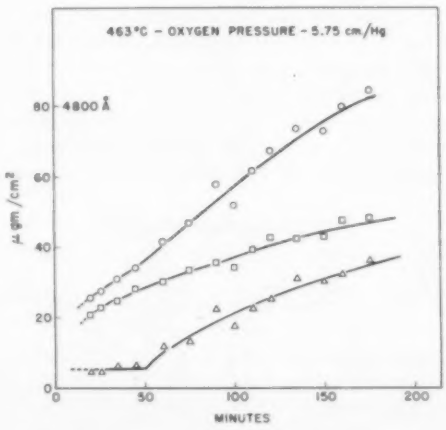

Fig. 1. Weight of oxygen vs. time for oxidation at 463°C and 5.75 cm/Hg pressure of oxygen. Upper curve, total oxygen; middle curve, oxygen as hematite; lower curve, oxygen as magnetite.

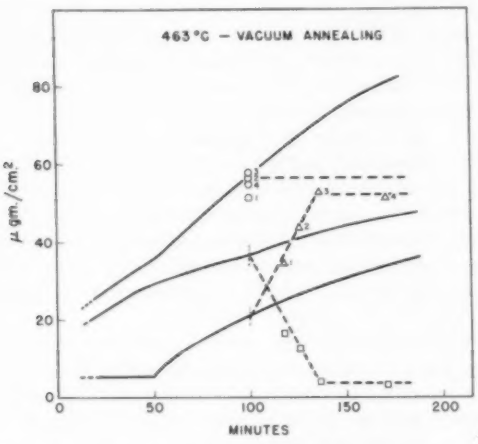

Fig. 2. Weight of oxygen vs. time for annealing at 463°C in vacuum. Pumping begun after 100 min of oxidation.

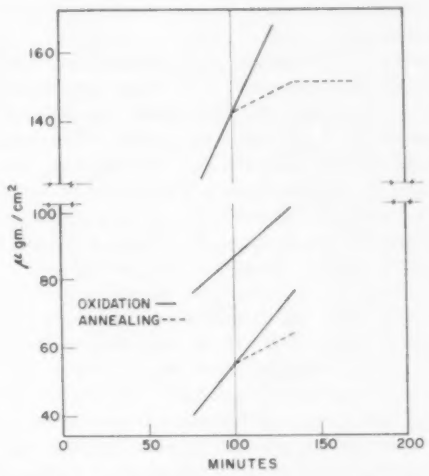

Fig. 3. Rate curves for oxidation and annealing in terms of weight of iron; top, total film; middle, hematite; bottom, magnetite.

out the annealing period were used to show the normal course of the reaction. Several annealings were performed on specimens suspended from a vacuum microbalance as described by Gulbransen; the purpose of these experiments was to confirm precisely that the change in total weight was zero during the annealing, *i.e.*, that oxidation had ceased.

Results

Figure 1 shows the set of experiments which involved no annealing and followed the normal course of the reaction. Smooth curves have been drawn through the points to fit the data without expressing any particular law. Figure 2 shows the results of experiments in which the specimen was annealed. After 100 min of oxidation the system was opened to the pumps and the oxygen removed. Zero time in drawing the annealing curves was taken as 100 min, although obviously the vacuum pumps required some time to produce a vacuum; however since a "nonspark" vacuum (as tested with a Tesla coil) was produced in less than 30 sec, indicating less than 10^{-2} mm pressure, a higher vacuum of the order of 10^{-4} to 10^{-5} mm pressure must have been produced within minutes. The pumps were operating throughout the whole period of the annealing, and the final pressure produced in the period was between 10^{-5} and 10^{-6} mm/Hg.

It can be seen that the magnetite grows at the expense of the hematite, and, as far as can be shown here, in a linear fashion. Also the hematite does not disappear completely, but assumes a constant or slowly decaying value. The lower, nearly constant or constant, level of hematite is probably not due to an experimental deviation about the value zero, because the weight of the hematite layer is measured directly in the analysis to a fairly high precision; the final low level corresponds to a measured weight loss in the analysis of about 150 μg, and the normal precision measure on this weight is about 3 μg. Accordingly the curve for the annealing has been drawn as shown by the dotted line.

That the vacuum for the annealing was essentially nonoxidizing is shown by the fact that the final gains in weight of the annealed specimens clustered about the value for 100 min of oxidation time and did not rise about it as they would have done if appreciable oxidation had continued during the annealing. The vacuum microbalance confirmed this result.

Discussion of Results

The reaction of annealing consumes hematite and produces magnetite and the only other reagent available to it is iron. Consequently it is reasonable to write the reaction as

$$4Fe_2O_3 + Fe \rightarrow 3Fe_3O_4$$

Since the interface between the two oxides is some distance from the metal and moves outward, there must be a flow of iron to the site of reaction.

The first two figures have shown the flow of oxygen rather than iron into the two layers, since the abscissas are graduated in micrograms of oxygen per square centimeter. Accordingly Fig. 3 was drawn to show the flow of iron in both annealing and oxidation. The solid lines refer to oxidation; the dashed lines refer to annealing. For the oxidation curves the change from weight of oxygen to weight of iron was made simply by multiplying the figures for oxygen by the ratio of weight of iron to weight of oxygen in the formula of the oxide concerned. For the annealing curve the change was a little more complex; reference was made to the equation written above which shows that the introduction of 1 g-atom of iron causes the transfer of 12 g-atoms of oxygen from one layer to the other. The ratio calculated from this relationship was applied to the annealing curve for magnetite to give the dashed line for "Total" after 100 min.

It is seen that the rate of flow of iron which causes the annealing is equal to neither of the rates of flow of iron which cause the growth of the oxides in oxidation. In other words the annealing reaction uses iron at one fourth the rate that the oxidation does, at least at this particular time in the oxidation; it is a slower reaction than oxidation rather

than faster, although Fig. 2 would give the latter impression.

The total amount of annealing, which consumed nearly all the hematite, is so large and required so great an amount of iron that the only possible source of the latter was the underlying metal. The linearity of the annealing curve suggests that here the rate of flow of iron is limited by its acceptance at the interface between the oxides and not by the thickness of magnetite. The data are not precise enough to permit insistence on this point.

The course of reduction shown above is quite different from that published by Davies, Evans, and Agar (3). Their curve for thickness of Fe_2O_3 resembles an exponential decay curve becoming asymptotic to zero. The disagreement is probably due to the great difference in the thicknesses of films used in the two groups of experiments; those used by Davies *et al.* are thinner by a factor greater than ten than those of the present set of measurements.

The amount of hematite left unreduced corresponds to about 3.3 μg of oxygen per square centimeter corresponding to $< 10\%$ of the α-Fe_2O_3. The easiest explanation of the nonreduction of this layer is that the upper part of the hematite is a loose rubble of needles and plates and that contact of these with the body of the oxide is so poor that iron can penetrate only with difficulty. The total amount of this loose material would be a function of the time of oxidation and for thin films would be very small. There are other possible explanations such as that the annealing reaction itself produces voids at the interface which eventually shut off the transport of iron.

For application to oxidation mechanisms, the most interesting feature is that the rate of flow of iron in annealing is less than the rate of flow during oxidation under the conditions used here. This implies either that oxidation removes the mechanism of control at the interface or that it supplies an increased driving force to transport iron through the magnetite.

The annealing effect must be taken into account in any measurement of layer thicknesses. It can be seen from the above that, although slow cooling in vacuum will prevent further oxidation of iron, the ratio of oxides will change.

Manuscript received Feb. 17, 1961; revised manuscript received May 19, 1961.

Any discussion of this paper will appear in a Discussion Section to be published in the June 1962 JOURNAL.

REFERENCES

1. E. J. Caule, K. H. Buob, and M. Cohen, *This Journal*, **108**, 829 (1961).
2. E. A. Gulbransen and Roswell Ruka, *Ind. Eng. Chem.*, **43**, 697 (1951).
3. D. E. Davies, U. R. Evans, and J. N. Agar, *Proc. Roy. Soc.*, **A225**, 443 (1954).
4. K. H. Buob, A. F. Beck, and M. Cohen, *This Journal*, **105**, 74 (1958).

Corrosion and Electrochemical Behavior of Chromium-Noble Metal Alloys

N. D. Greene,[1] C. R. Bishop, and M. Stern[2]

Metals Research Laboratories, Union Carbide Metals Company, Division of Union Carbide Corporation, Niagara Falls, New York

ABSTRACT

Alloying chromium with small amounts of platinum, palladium, iridium, rhodium, ruthenium, or osmium markedly improves its corrosion resistance to nonoxidizing acids such as sulfuric or hydrochloric acid. The presence of rhodium, palladium, or osmium has little influence on the resistance of chromium to an oxidizing acid such as nitric acid, while platinum, iridium, or ruthenium greatly increases corrosion rates in this medium. These phenomena can be explained in terms of the electrochemical and corrosion behavior of the metals involved and are related to the passive and transpassive behavior exhibited by chromium.

Passivation of a metal or alloy is achieved by establishing a potential within its particular passive potential region (1-6). This can be accomplished by application of suitable anodic current (7, 8) or the addition of oxidizers (1-3, 9). Further, if the passive region extends to potentials more active than the redox potential of the medium, passivity can be induced by alloying (10-12) with, or galvanically coupling (12-14) to a noble metal having a high cathodic exchange current density. Metals and alloys which demonstrate stable passivity at potentials more active than the reversible hydrogen potential are of particular interest. In these cases, it is possible to cause spontaneous passivation in the complete absence of any substance more oxidizing than hydrogen

[1] Present address: Department of Metallurgical Engineering, Rensselaer Polytechnic Institute, Troy, New York.
[2] Present address: Speedway Laboratories, Linde Company, Division of Union Carbide Corporation, 1500 Polco Street, Indianapolis 24, Indiana.

ions by coupling to or alloying with, low-hydrogen overvoltage elements.

Tomashov and Chernova (10) and Stern and Wissenberg (12) have shown that noble metal alloying functions in the same manner as galvanic coupling. If the noble metal is attacked negligibly by an environment, and the alloy base is attacked, the alloy surface is enriched with the noble metal and a galvanic couple is created. Spontaneous passivation results if there is sufficient surface enrichment of the low overvoltage component. Based on the above concept, the effectiveness of noble metals has been shown to vary with their alloy concentration and specific hydrogen overvoltage characteristics (12).

Chromium and high chromium-iron alloys demonstrate stable passive states at potentials more active than reversible hydrogen (4, 15); thus, the passivating tendency of chromium should be improved by noble metal alloying. In these respects chromium is similar to titanium (12, 16-18). As described above, such materials should passivate in the complete absence of oxygen or oxidizers and would be desirable as corrosion-resistant materials. It was of interest, therefore, to study the effect of noble metal alloying on the corrosion resistance and electrochemical characteristics of chromium. As described elsewhere (19), chromium-base alloys show similar characteristics.

Experimental

Chromium alloy buttons. weighing 100 g, were prepared by arc melting and remelting three times with a tungsten electrode in an argon atmosphere. The buttons were sectioned into specimens for corrosion testing and electrochemical studies. All measurements were performed with specimens in the as-cast condition.

Corrosion tests in boiling acid solutions were conducted by conventional techniques. Three 40- to 60-hr test periods were used to determine the average corrosion rates of all specimens with rates less than 200 mpy (mils per year). Only one test period was used for specimens demonstrating corrosion rates greater than 200 mpy. The accuracy of these measurements was approximately ±1 mpy.

Polarization measurements were performed using a classical potentiostat with a potential control of ±1 mv (20). All potentials were measured relative to a saturated calomel electrode with a Luggin probe and a high impedance potentiometer circuit. Room temperature was 25° ± 1°C.

Results

Corrosion tests.—The corrosion rates of chromium and 10 chromium-noble metal alloys determined in boiling H_2SO_4, HCl, and HNO_3 are listed in Table I. Table II shows the influence of varying platinum and palladium contents on corrosion rates. The beneficial effect of noble metal additions in the nonoxidizing acids is particularly striking. Comparison of Tables I and II shows that an addition of only 0.1% platinum decreases the corrosion rate of chromium by a factor of 10^5 or more. It should be emphasized that these are average corrosion rates. It was generally observed that the corrosion rates of alloys showing good resistance toward H_2SO_4 and HCl decreased during the three test periods. Frequently, no weight loss was observed during the third period. However, because of the strong tendency for the high-chromium alloys to become passive, they sometimes exhibit metastable passivity even in nonoxidizing environments. Under these conditions, passivity is usually removed readily by a cathodic treatment, for example, contacting the specimen with an iron wire while in test. In order to determine whether the passivity obtained by the addition of noble metals to chromium is stable rather than metastable, most of the specimens were "activated" by contact with an iron wire while in the boiling solutions. The activation tests were confined to those solutions where

Table I. Effect of alloy additions on the corrosion resistance of chromium corrosion rate in mils/year

Nominal composition	Boiling H_2SO_4											Boiling HCl			Boiling 65% HNO_3
	5%	10%	20%	30%	40%	50%	60%	70%	80%	90%	Conc.	5%	10%	15%	
Cr	D	D[a]	D	D	D	D	D	D	D	2400	300	D[b]	D	D	3
Cr + 0.5% Ir	—	1	2	13 (49)	43	100	D	—	—	—	—	<1	2 (20)	D	34
Cr + 0.5% Rh	—	—	3	16 (23)	68	66	970	—	—	—	—	<1 (11)	3 (45)	D	5
Cr + 0.5% Ru	—	2	11	17 (48)	83	7100	—	—	—	—	—	<1 (11)	<1 (D)	D	110
Cr + 0.5% Pt	<1	3	12 (16)	28	175	120	36	D	D	D	185	<1	8 (25)	D	200
Cr + 0.5% Pd	—	2	8 (14)	22	180	1500	1300	—	—	—	—	<1 (56)	D	D	15
Cr + 0.5% Os	<1	1 (18)	67	560	—	—	—	—	—	—	—	5 (2800)	D	D	8
Cr + 0.5% Au	<1 (300)	690	1900	—	—	—	—	—	—	—	—	D	—	—	120
Cr + 0.5% Re	<1 (D)	D	D	—	—	—	—	—	—	—	—	D	—	—	5
Cr + 2% Cu	780	2700	D	D	D	—	—	—	—	—	—	D	D	D	70
Cr + 0.5% Ag	2600	—	D	—	—	—	—	—	—	—	—	D	—	—	4

D Dissolved during test.
( ) Sample activated with an iron wire for at least 1 min.
[a] Corrosion rate = 100,000 mpy (0.5 hr test).
[b] Corrosion rate = 240,000 mpy (0.5 hr test).

Table II. Effect of platinum and palladium alloy content on the corrosion resistance of chromium corrosion rate in mils/year

Nominal composition	Boiling H_2SO_4								Boiling HCl			Boiling 65% HNO_3
	5%	10%	20%	30%	40%	50%	60%	70%	5%	10%	15%	
Cr	D	D	D	D	D	D	D	D	D	D	D	3
Cr + 0.1% Pt	2	1	5 (11)	22	100	840	D	D	<1	9 (1400)	D	9
Cr + 0.5% Pt	<1	3	12 (16)	28	175	120	36	D	<1	8 (25)	D	200
Cr + 1.0% Pt	—	—	6 (3)	22	210	68	21	1260	<1 (5)	140	D	500
Cr + 2.0% Pt	—	—	6 (18)	18	130	28	9	56	<1	3 (51)	D	300
Cr + 5.0% Pt	—	—	1 (4)	18	51	12	—	55	<1 (1)	170 (280)	D	490
Cr + 0.05% Pd	—	—	0-22 (56)	57	—	D	D	—	D	D	—	6
Cr + 0.1% Pd	—	—	0-20 (20)	31	130	1600	D	—	0-40 (915)	D	—	5
Cr + 0.2% Pd	—	—	0-13 (13)	23	150	1400	D	—	0-36 (94)	D	—	7
Cr + 0.3% Pd	—	—	1-12 (13)	21	370	1400	300	—	<1 (48)	D	—	5
Cr + 0.5% Pd	—	2	8 (14)	22	180	1500	1300	—	<1 (56)	D	D	15
Cr + 1.0% Pd	—	—	2 (16)	56	2800	725	400	—	2 (12)	D	D	23

D Dissolved during test.
( ) Sample activated with an iron wire for at least 1 min.

corrosion rates were relatively low. Results of the activation tests are shown in Table I and II.

It will be noted that the activation treatment generally increased the corrosion rates of the noble metal-bearing specimens. In most cases the increases were moderate, indicating a rapid return to the passive condition. As shown in Table I, iridium, rhodium, ruthenium, platinum, and palladium were more effective than osmium, gold, or rhenium in maintaining stable passivity. The data in Table II show that, in general, increasing percentages of platinum or palladium tend to increase corrosion resistance.

In summary, the results of the "activation" tests indicate that the presence of certain noble metals greatly enhances the probability of passivation and continued low corrosion rates of chromium in non-oxidizing environments.

Qualitatively, these corrosion tests support the noble metal alloy concept. The effectiveness of the various alloy additions in H_2SO_4 and HCl generally decreases in the order: iridium, rhodium, ruthenium, platinum, palladium, osmium, gold, rhenium, copper, and silver. This order parallels almost exactly the hydrogen overvoltage behaviors of these elements.[3] Elements with low hydrogen overvoltages (*e.g.*, iridium, rhodium, platinum, palladium) are very effective, whereas those with relatively high overvoltages (*e.g.*, gold, silver, copper) are not.

It is of interest to note the detrimental effect of noble metal alloying on the corrosion resistance in HNO_3 as shown in Tables I and II. Several of the alloying elements accelerate corrosion in this medium, and the effect becomes more pronounced with increasing alloy content. Platinum, gold, and ruthenium are especially detrimental to HNO_3 corrosion resistance. However, small amounts of rhodium, palladium, and osmium improve corrosion resistance in H_2SO_4 and HCl without significantly affecting HNO_3 resistance. These aspects are considered further below.

Electrochemical studies.—High chromium contents are usually detrimental to the corrosion resistance of alloys in chloride media and HCl. However, the corrosion tests suggest, surprisingly, that chromium metal can be passivated in HCl. To verify this, potentiostatic anodic polarization measurements were performed with chromium in normal HCl at room temperature. The polarization curve is shown in Fig. 1. The active state corrosion potential is indicated on the ordinate. In general, the curve shape is characteristic of the active-passive behavior of chromium in H_2SO_4 (4, 15). As the potential is made more noble, the current density corresponding to the dissolution of chromium increases. Current density increases to a maximum of 24 ma/cm^2 at a point designated as the critical anodic current density, I_c. The corresponding potential, the primary passive potential, E_{pp}, is −0.520 v. E_{pp} may be considered to indicate the beginning of the passive region. At potentials more noble than E_{pp}, current and dissolution rate decrease, eventually to very small values between −0.400 and 0.900 v.[4] At 0.900 v the transpassive region begins. Here, current and dissolution rate again increase and gas evolution occurs (oxygen and/or chlorine). Comparison of the E_{pp} and I_c

[3] Exchange current densities for the hydrogen reduction process may be used as a measure of hydrogen overvoltage since all these elements have approximately the same Tafel constant. As exchange current density increases, hydrogen overvoltage decreases. Reported exchange densities in dilute sulfuric and hydrochloric acids are (21-24) : Ir, Rh, Pt (10^{-3} to 10^{-4}); Pd (10^{-4}); Au, Ag (10^{-5} to 10^{-6}); Cu (10^{-7}) amp/cm^2.

[4] In this region, as with some other passive systems (4, 20), current decreases with time. However, this is not pertinent to the present discussion.

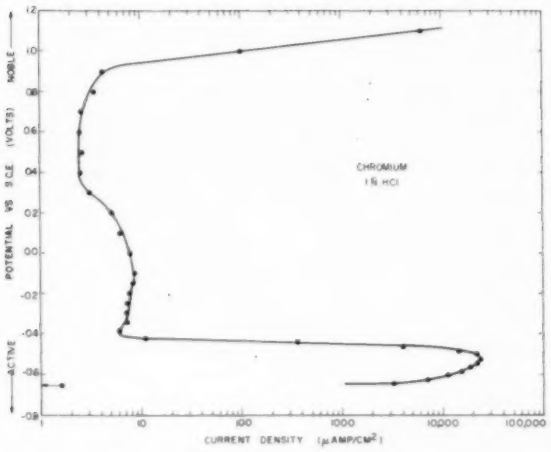

Fig. 1. Anodic polarization of chromium in hydrogen-saturated normal HCl at room temperature.

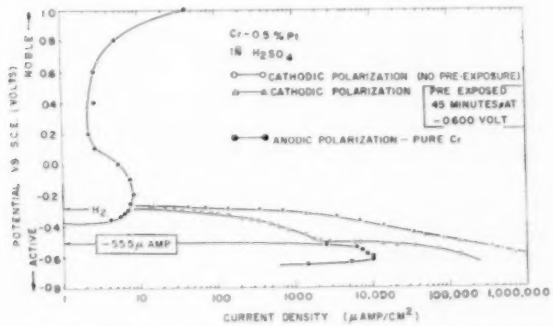

Fig. 2. Cathodic polarization of chromium-0.5% platinum alloy in hydrogen-saturated normal H_2SO_4 at room temperature.

values of chromium in normal HCl and H_2SO_4 (E_{pp} = −0.600 v; I_c = 10.5 ma/cm²) shows that it is passivated more readily in H_2SO_4. The critical anodic current density is smaller, and the primary passive potential occurs at a more active potential. This difference becomes more pronounced at acid concentrations of 5*N* (H_2SO_4: E_{pp} = −0.650 v, I_c = 58 ma/cm²; HCl: E_{pp} = −0.480,[5] I_c = 900 ma/cm²).[5] No evidence of pitting or localized attack was observed on the specimens after anodic polarization in HCl solutions.

Although experimental evidence supporting surface enrichment has been shown for titanium-noble metal alloys (12), it was desirable to verify this for chromium-noble metal alloys. Figure 2 shows the cathodic polarization of chromium-0.5% platinum in normal H_2SO_4. Measurements were made with a constant current source, and potentials were measured after a 2-min interval. Reversible hydrogen potential, measured with platinized platinum, is indicated on the ordinate. An anodic polarization curve of unalloyed chromium is included for illustrative purposes. Open circles show cathodic polarization of a specimen immediately after immersion. Note the change in slope at −0.500 v, indicating a decrease in hydrogen overvoltage. This corresponds closely to the potential at which the dissolution rate of chromium increases markedly. In this region, potentials become time-dependent at each current setting, shifting rapidly to more noble values. These observations are consistent with the view that platinum is accumulating on the specimen surface during dissolution of the matrix metal.

As a further check on surface enrichment, another cathodic polarization measurement was performed with a specimen which had been held for 45 min at −0.600 v. Considering the anodic behavior of pure chromium, this treatment should produce pronounced surface enrichment of platinum. Results are shown in Fig. 2, and it is obvious that this specimen demonstrates less hydrogen overvoltage than the untreated specimen. The curve demonstrates a Tafel constant, β, of approximately 0.1 v and an exchange current, i_o, of 5 x 10^{-4} amp/cm². These parameters differ considerably from those of unalloyed chromium: β = 0.125 v, $i_o = 10^{-6}$ amp/cm² (25, 26).

These experiments, and those reported elsewhere (12), definitely establish that noble metals accumulate on alloy surfaces and alter their cathodic process kinetics. However, there have been no experimental measurements to determine whether noble metal alloying also affects anodic dissolution kinetics. Since the presence of noble metals prevents direct measurement of anodic dissolution current in the active-passive transition region, it was necessary to employ controlled-potential weight loss tests for this purpose. Weight losses were measured in normal H_2SO_4 after 3 hr at −0.600 v, the primary passive potential of chromium. Critical anodic currents were calculated from Faraday's law assuming: $Cr \rightarrow Cr^{+3} + 3e$. Calculated I_c values for various chromium alloys are shown in Table III. Also shown are the applied cathodic currents necessary to maintain the electrodes at −0.600 v. It should be emphasized that these I_c values are averages as indicated by the time

Table III. Critical anodic current densities (I_c) of chromium alloys in normal sulfuric acid at room temperature potential held at −0.600 v for 3 hr

Alloy	Calculated critical anodic current (I_c), ma/cm²	Applied cathodic current, ma/cm²	
		Initial, 5 min	Final, 3 hr
Cr + 0.5% Ir	0.055	132	136
Cr + 0.5% Pd	0.130	40	600
Cr + 0.5% Rh	0.145	600	900
Cr + 0.5% Pt	0.315	115	210
Cr + 0.5% Os	0.380	232	228
Cr + 0.5% Re	10.0	12	86
Cr + 0.5% Ag	12.5	10.4*	2.5*
Cr + 0.5% Au	15.8	20	230

* Anodic current.

Table IV. Effect of time on the critical anodic current density (I_c) of Cr-0.5% Pt in normal H_2SO_4 at room temperature

Test duration, hr	Calculated critical anodic current (I_c), ma/cm²	Applied cathodic current, ma/cm²	
		Initial	Final
1	0.327	187	271
3	0.315	115	210
8	0.233	270	355
48	0.083	163	202

[5] Approximate values, control limit of the potentiostat was exceeded.

effects shown in Table IV. It appears that the critical anodic current densities of chromium-noble metal alloys decrease with time.

Table III demonstrates several interesting aspects. All alloys, except those containing rhenium, silver, and gold, have critical anodic current densities much lower than the 10.5 ma/cm² observed for pure chromium. The observed changes in I_c appear reasonable, since surface accumulation of a noble metal component would be expected to impede anodic dissolution. The variations in I_c cannot be attributed to experimental errors. Reduction of hydrogen ion concentration at the electrode surfaces as a result of concentration polarization is unlikely. Fig. 2 shows no evidence of concentration polarization at cathodic current densities up to 500 ma/cm². Further, there is no indication of an inverse relationship between I_c and cathodic current density in Table III as would be expected if concentration polarization effects were significant. Similarly, weighing errors and the possibility of chromium dissolving in a valence state other than +3 cannot account for the large differences observed. Direct measurements of I_c for pure chromium are generally reproducible to ±3 ma/cm². Therefore, rhenium and silver have no detectable effect. Gold appears to increase I_c, although this is probably not significant. The alloying elements listed in order of decreasing effect on I_c are: iridium, palladium, rhodium, platinum, osmium, rhenium, silver, and gold. Like hydrogen exchange current densities, this order also generally parallels the corrosion rates of the various alloys (Table I).

It is interesting to note that, with the exception of chromium-silver, applied cathodic currents increase with time, a further indication of noble metal surface enrichment. Since the applied cathodic currents were measured at a constant potential, they are a relative measure of hydrogen exchange current density. In this respect, chromium-iridium and chromium-gold are unusual. The cathodic current of chromium-iridium appears too low while that of chromium-gold seems too high, considering the exchange current densities of iridium and gold noted before.

Discussion

Several aspects of the preceding results merit further discussion. In boiling 65% HNO_3, the presence of alloying elements, especially platinum, gold, and ruthenium, is detrimental to corrosion resistance (Table I). This is a direct consequence of the transpassive region exhibited by chromium. The corrosion potential of chromium in boiling 65% HNO_3 is very noble and is probably very close to the beginning of its transpassive region (q.v. Fig. 1 and 2). Alloying with an inert element having a greater exchange current density for the reduction of HNO_3 than chromium shifts the mixed potential in the noble direction, resulting in an increased dissolution rate. This is illustrated schematically in Fig. 3. Here, the anodic dissolution curve of a typical metal demonstrating active, passive, and transpassive behavior is shown. E_o is the redox potential of the medium, and $i_{o,m}$ and $i_{o,a}$ are the exchange current densities of the pure metal and a noble metal alloy, respectively. Provided the alloying element is unattacked and has an exchange current density greater than the base metal, and that the mixed potential of the pure metal is close to the transpassive region, the corrosion rate is increased. The pure metal corrodes at potential M at a rate $i_{corr(M)}$, while the alloy corrodes at A with a rate $i_{corr(A)}$.

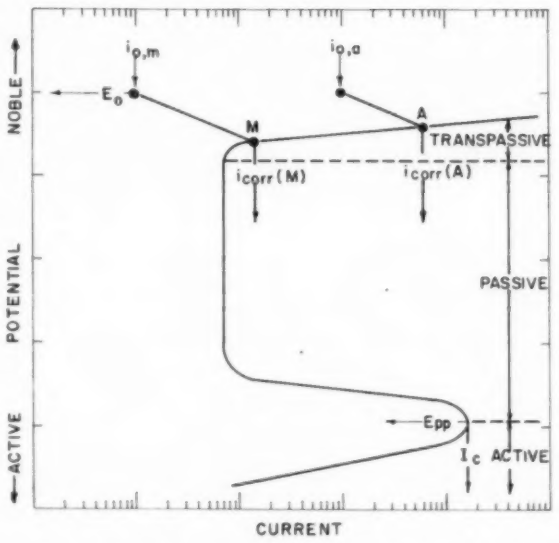

Fig. 3. Effect of exchange current density on corrosion behavior in transpassive region (schematic).

Table I supports the above hypothesis. Small amounts of osmium, palladium, rhenium, and silver, which are rapidly attacked by HNO_3 (27), have a negligible effect on the corrosion resistance of chromium in HNO_3. Due to their high corrosion rates, these elements cannot accumulate appreciably on an alloy surface. However, at higher concentrations, detrimental effects are observed as shown by palladium in Table II. This is probably the reason for the poor HNO_3 resistance of chromium-2% copper. Platinum, iridium, ruthenium, gold, and rhodium are unattacked by hot, concentrated HNO_3 (28). All these elements with the exception of rhodium, markedly reduce the corrosion resistance of chromium. The behavior of rhodium is surprising; possibly it is due to a small exchange current density for HNO_3 reduction.

Corrosion potential measurements in boiling 65% HNO_3 are also consistent with the above hypothesis and Fig. 3. Chromium and chromium-0.5% palladium, which are slightly attacked, have corrosion potentials of approximately 1.00 v. However, chromium-0.5% platinum, which corrodes at 200 mpy, has a mixed potential of 1.10 v.

Titanium, unlike chromium, possesses no transpassive region (17). Hence, noble metal alloy additions are not detrimental to its corrosion resistance in highly oxidizing media (12, 18).

Here it is shown that noble metal alloy additions can affect both anodic and cathodic reaction kinetics. A noble element simultaneously can increase cathodic exchange current density and decrease critical anodic current density when alloyed with a metal. Both these changes increase passivation tendency.

The corrosion resistance of a noble metal alloy is quite likely related to the type and structure of the noble metal deposit on its surface. A loose, porous deposit would have a high surface area and, consequently, a high apparent cathodic exchange current density. Such a deposit would have little effect on anodic dissolution rate. Chromium-gold appears to be an illustration of this effect. Its hydrogen overvoltage is surprisingly low, and its I_c value is similar to pure chromium. A smooth, dense surface deposit of noble metal should markedly affect anodic dissolution while demonstrating a relatively high hydrogen overvoltage. The behavior of chromium-iridium is consistent with this model. Although these ideas are speculative and require additional verification, the nature of the noble metal deposit must affect corrosion resistance.

Summary

1. The corrosion resistance of chromium in H_2SO_4 and HCl is improved markedly by alloying with small amounts of various noble metals. Rhodium, palladium, and osmium improve the corrosion resistance of chromium in nonoxidizing acids without appreciably affecting its corrosion rate in oxidizing media such as nitric acid.

2. The concept of producing passivity by noble metal alloying has been verified and extended for chromium. Noble metals accumulate on an alloy surface during dissolution of the matrix metal. In most cases, the surface enrichment of a noble metal increases cathodic exchange current density and decreases critical anodic current density. Both these effects enhance the passivating tendency.

3. The accelerated dissolution of some chromium alloys in HNO_3 is a direct consequence of the transpassive characteristics of chromium. Alloying elements which are unattacked by HNO_3 and possess large cathodic exchange currents increase the corrosion rate of chromium in this medium. Elements which are rapidly attacked by HNO_3 have little effect on HNO_3 resistance when present in small quantities.

4. Chromium exhibits passivity in HCl and shows no evidence of pitting or localized attack.

Acknowledgments

The authors gratefully appreciate the assistance of Mr. E. A. Tomes and Mr. R. R. Granieri in conducting the experimental measurements.

Manuscript received Feb. 7, 1961. This paper was prepared for delivery before the Detroit Meeting, Oct. 1-5, 1961.

Any discussion of this paper will appear in a Discussion Section to be published in the June 1962 JOURNAL.

REFERENCES

1. C. Edeleanu, *Nature*, **173**, 739 (1954).
2. C. Edeleanu, *J. Iron Steel Inst.*, **188**, 122 (1958).
3. M. Stern, *This Journal*, **105**, 638 (1958).
4. Y. M. Kolotyrkin, *Z. Elektrochem.*, **62**, 664 (1958).
5. U. F. Franck, *ibid.*, p. 642.
6. G. Okamoto and M. Nagayama, *Corrosion Engineers* (Japan), **7**, 1 (1958).
7. C. Edeleanu, *Metallurgia*, **50**, 113 (1954).
8. N. D. Tomashov, R. M. Altovsky, and A. G. Arakelov, *Doklady Akad. Nauk.*, **121**, 885 (1958).
9. N. Y. Bune and Y. M. Kolotyrkin, *ibid.*, **111**, 1050 (1956).
10. N. D. Tomashov and G. P. Chernova, *ibid.*, **89**, 121 (1953).
11. N. D. Tomashov, *Corrosion*, **14**, 229t (1958).
12. M. Stern and H. Wissenberg, *This Journal*, **106**, 759 (1959).
13. G. P. Chernova and R. M. Altovsky, *Doklady Akad. Nauk.*, **110**, 1030 (1956).
14. G. M. Florianovich, Y. M. Kolotyrkin, and N. K. Smirnova, *ibid.*, **120**, 845 (1958).
15. R. Olivier, Dissertation, Leiden, 1955. Polarization data summarized by H. Gerischer, *Angew. Chem.*, **70**, 285 (1958); T. Heumann, *Arch. Eisenhüttenw.*, **29**, 505 (1958).
16. J. B. Cotton, *Chem. & Ind.*, p. 68, Jan. 18, 1958.
17. M. Stern and H. Wissenberg, *This Journal*, **106**, 755 (1959).
18. M. Stern and C. R. Bishop, *Trans. ASM*, **52**, 239 (1960).
19. N. D. Greene, C. R. Bishop, and M. Stern, To be published.
20. N. D. Greene, *Corrosion*, **15**, 369t (1959).
21. B. E. Conway, "Electrochemical Data," p. 335, Elsevier, New York (1952).
22. J. O'M. Bockris, "Modern Aspects of Electrochemistry," p. 198, Butterworths, London, (1954).
23. M. Brieter, C. A. Knorr, and R. Meggle, *Z. Elektrochem.*, **59**, 153 (1955).
24. N. Pentland, J. O'M. Bockris, and E. Sheldon, *This Journal*, **104**, 180 (1957).
25. I. M. Issa, I. A. Ammar, and H. Kalifa, *J. Phys. Chem.*, **59**, 492 (1955).
26. T. Heumann and B. Roschenbleck, *Werkstoffe u. Korrosion*, **9** 383 (1958).
27. "Corrosion Handbook"' H. H. Uhlig Editor, pp. 300, 314, John Wiley & Sons, Inc., New York (1948).
28. *Ibid.*, pp. 112, 300.

Some Observations of Copper Deposits on Single Crystals of Copper

Isaac Giron[1] and Fielding Ogburn

National Bureau of Standards, Washington, D. C.

ABSTRACT

Isolated faces of copper single crystals were plated with copper from copper sulfate-sulfuric acid solutions. Deposits on {100} and {110} faces, despite the presence of grain boundaries, gave x-ray diffraction patterns showing uniform lattice orientation. The grain boundaries were associated with topographic features of the deposits. Over-all metal distribution showed a tendency to deviate from that of polycrystal deposits on polycrystalline bases.

The crystal growth of electrodeposits has been investigated from several different points of view. Usually the approach has been toward the study of the over-all polycrystalline deposit. In a number of investigations, the growth of whiskers and dendrites, which often appear to be isolated single crystals, has received attention. Others have observed the general character of deposits on various faces of single crystal spheres and, recently, the growth of deposits on specific faces of single crystals has been the subject of investigations. A group at the University of Birmingham has used the latter approach (1-3) to investigate the growth of copper crystals, with significant results.

The work to be reported here made use of this same approach and was also confined to copper. Much of it had been completed at the time that the publications of the group at the University of Birmingham became available to the authors. Some of the authors' observations of the topography of the deposits serve to confirm the earlier work. The information on x-ray diffraction measurements and on the structure revealed by microscopic examination of cross sections are complementary to their work.

Plating Conditions

Two acid copper plating solutions were used:

	Solution A	Solution B
Copper sulfate	0.5M	0.5M
Sulfuric acid	0.5M	1.5M
Temperature	Room	75°C
Agitation	None	None

A.C.S. reagent quality chemicals and distilled water were used to make up the solutions. No purification procedures were employed. The anodes were strips cut from sheets of electrolytic copper.

Each of the seed crystals which served as cathodes had been cut from large single crystals grown by the Bridgman method and had been mounted in Lucite. These were: 99.99% copper, free of inclusions, relatively free of strains as indicated by lack of asterisms in x-ray patterns, and relatively free of mosaic structure. The mounting and subsequent polishing were such that one flat surface was exposed, and this surface was parallel or almost parallel to either {100}, {110}, or {111} planes. The exposed surface generally approximated a 1-cm square. Electrical contact was made through a hole in the side of the Lucite mount.

The preparation of the surface prior to plating consisted of polishing with successively finer grades of silicon carbide paper, followed by electropolishing in a solution containing 900 g orthophosphoric acid/l. Electropolishing removed cold-worked metal and polishing scratches. After polishing, samples were washed in a dilute orthophosphoric acid solution, then washed thoroughly with distilled water.

Surface Topography

Many of the features of the surface topography of the deposits observed in this investigation were found to be essentially the same as reported by the Birmingham group (3). Some of the examples observed in the present work are described in the following paragraphs.

Figures 1, 2, and 3 are photomicrographs of deposits on the {100} plane. The surfaces of the platelets are smooth and bright, but the over-all surface

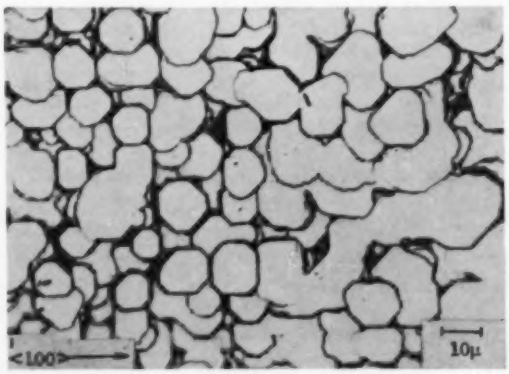

Fig. 1. Surface of copper deposit on {100} face of copper crystal. Plating conditions: solution A, 1 amp/dm², 15 min. Magnification 750X before reduction for publication.

[1] Present address: Cerro de Pasco, La Oroya, Peru. Appointment supported by the International Cooperation Administration under the Visiting Research Scientists Program administered by the National Academy of Sciences of the United States of America.

Fig. 2. Surface of deposit on {100} face. Plating conditions: solution A, 1 amp/dm², 15 min, air agitation. Magnification 1000X before reduction for publication.

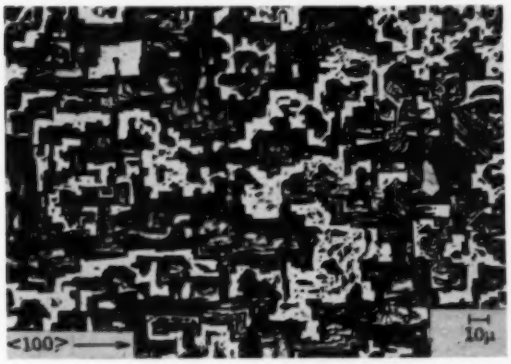

Fig. 3. Surface of deposit on {100} face. Plating conditions: solution B, 1 amp/dm², 4 hr. Magnification 350X before reduction for publication.

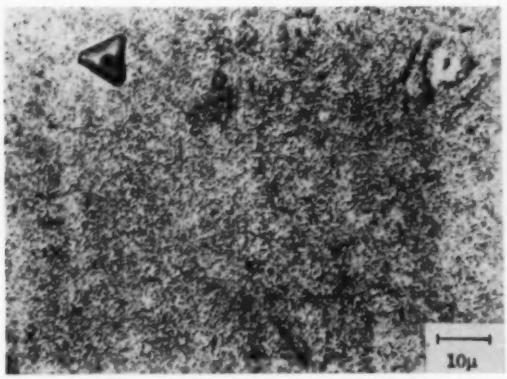

Fig. 4. Surface of deposit on {111} face. Plating conditions: solution B, 1 amp/dm², 15 min. Magnification 1000X before reduction for publication.

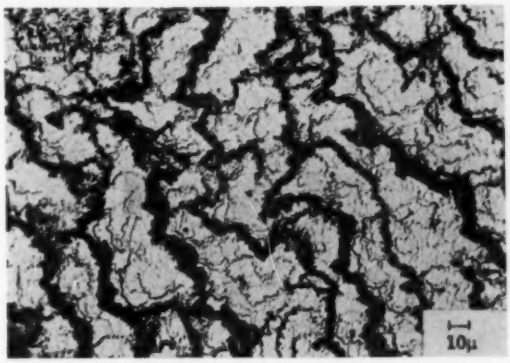

Fig. 5. Surface of deposit on {111} face. Plating conditions: solution B, 1 amp/dm², 4 hr. Magnification 350X before reduction for publication.

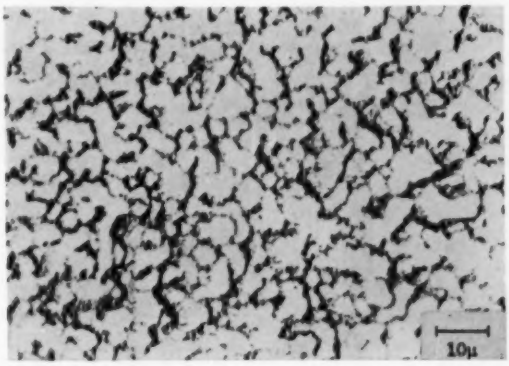

Fig. 6. Surface of deposit on {111} face. Plating conditions: solution A, 1 amp/dm², 15 min. Magnification 1000X before reduction for publication.

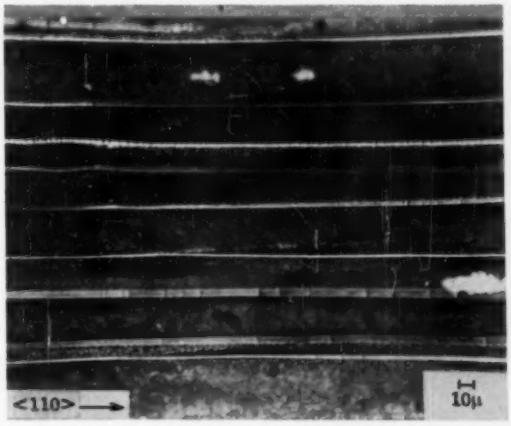

Fig. 7. Surface of deposit on {110} face. Plating conditions: solution A, 1 amp/dm², 19 hr. Magnification 250X before reduction for publication.

is not at all smooth. The platelets have edges which are parallel to the <100> directions, but occasionally some form which are parallel to the <100> and <110> directions. Figures 1 and 2 are much the same as reported previously, while the deposit shown in Fig. 3 was produced at the higher bath temperature and is considerably thicker.

Figures 4, 5, and 6 are photomicrographs of deposits on the {111} plane. The surfaces of the deposits from solution B, Fig. 4 and 5, appear to be continuous; that from solution A, Fig. 6, appears to be made up of islands.

Figures 7, 8, and 9 are photomicrographs of deposits on the {110} plane and illustrate three distinctive topographies. The surface shown in Fig. 7 is made up of ridges that extend in the <110> directions and are bounded by {111} planes as previously reported (3). A cross section of similar

Fig. 8. Surface of deposit on {110} face. Plating conditions: solution A, 0.25 amp/dm², 120 hr. Magnification 350X before reduction for publication.

Fig. 9. Surface of deposit on {110} face. Plating conditions: solution B, 1 amp/dm², 4 hr. Magnification 350X before reduction for publication.

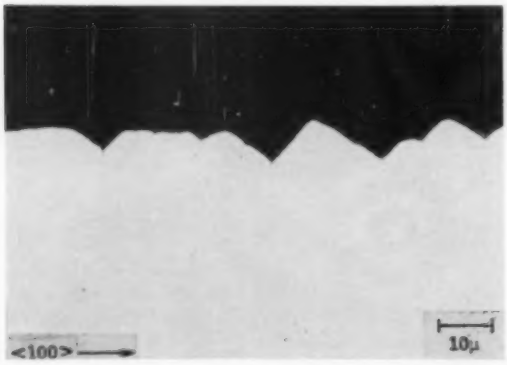

Fig. 10. Cross section of deposit on {110} face. Plating conditions: solution A, 1 amp/dm², 20 hr. Magnification 1000X before reduction for publication.

ridges is shown in Fig. 10. It is interesting to note that the ridges shown in Fig. 7 are much broader than shown by Pick, Storey, and Vaughan (3) since the deposit is substantially thicker. This is a good example of the bunching mechanism discussed by these authors (3). Ridges also appear on the surface shown in Fig. 8, but these extend in the <100> directions and are probably bounded by {100} and {110} planes. The surface shown in Fig. 9 appears to be made up of both types of ridges. If this interpretation is correct, the <100> ridges are

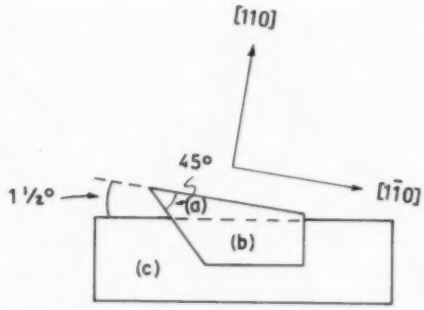

Fig. 11. Diagram of cross section of deposit on {110} face showing realignment of surface plane: Plating conditions: solution A, 0.25 amp/dm², 18 hr. (a) deposit; (b) seed crystal; (c) Lucite.

those extending across the flat tops of the longer and wider <110> ridges.

It seems probable the formation of the two types of ridges is a function of the tilt of the cathode surface with respect to the {110} plane as suggested by the bunching mechanism (3) as well as of other plating variables.

One deposit on a nominal {110} face was found to have a cross-section such as diagramed in Fig. 11. The final surface was tilted about 1½° toward another {110} plane with respect to the original surface. Apparently the original surface was not quite parallel to the {110} plane, and the deposit grew so as to form a surface parallel to that plane. When the same crystal was remounted with the "true" {110} plane flush with the Lucite and plated, the deposit surface remained parallel to the starting surface. Subsequent polishing at about 2° to the "true" {110} plane to reproduce the original surface, again resulted in a deposit parallel to the "true" plane. Here, the bunching mechanism appears to have led to one big bunch, and the metal distribution departed radically from normal metal or primary current distribution.

Of incidental interest is the topography developed when the single crystal is made the anode. In the course of a few exploratory experiments, ridges developed on the {110} face, pyramidal (4 sided) pits developed on the {100} face, and triangular pits developed on the {111} face. These experiments were carried out in solution A at 1 amp/dm².

Microstructures and X-Ray Diffraction Patterns of Deposits

A cross section[2] of a deposit on the {100} surface is shown in Figure 12. The lower horizontal line is the interface between the deposit and the seed crystal. The second is the interface between the deposit and a high current density overplate. Boundaries are evident in this deposit, which was plated at 1 amp/dm² in solution B for 4 hr. On the other hand, x-ray diffraction patterns of a similar deposit gave well-defined Laue spots, suggesting that these are low angle boundaries that divide the deposit into parallel columns which are integral parts of the same over-all crystal. A deposit from solution A showed no evidence of grain boundaries.

[2] All cross sections were etched with Carapella's reagent.

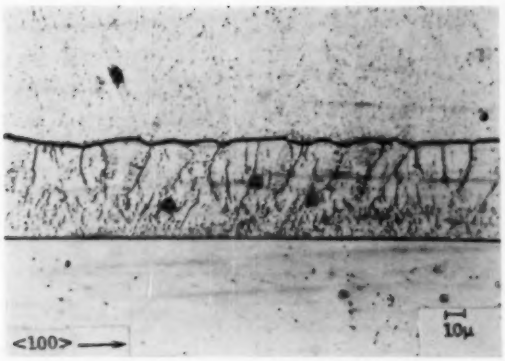

Fig. 12. Cross section of deposit on {100} face. Plating conditions: solution B, 1 amp/dm², 4 hr. Magnification 350X before reduction for publication.

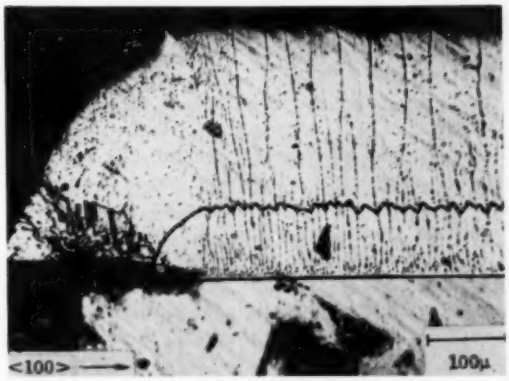

Fig. 13. Cross section of deposit on {110} face. Plating conditions: solution A, 1 amp/dm², 22 hr. Magnification 150X before reduction for publication.

It had been plated ½ hr at 1 amp/dm², cross-sectioned, and etched.

In one series of experiments, copper was plated on the {100} surface from solution B at 1 amp/dm² for 12 hr. At the end of each 4-hr interval, the cathode was removed from the bath, an x-ray diffraction pattern of the deposit surface was obtained, and the cathode was replaced in the bath with no surface preparation. The patterns for the 4- and 8-hr deposits indicated continuation of the single crystal structure or at least uniform orientation. The Laue spots were well defined. At the end of 12 hr, the Laue spots were still well defined, but a complete Debye ring was clearly evident, indicating some polycrystallinity.

Deposits on the {110} face had some interesting features. When a cross section of the specimen was etched to bring out the microstructure, Fig. 13 was obtained. The lower horizontal line is again the interface between the deposit and the seed crystal. The horizontal line within the deposit corresponds to an interruption during plating. It is of interest to note that these interruptions did not seem to alter the over-all growth of the deposit. At the same time, they serve to record permanently the surface contours at the time of interruption. The reader will note the vertical lines passing through the junctures of the ridges. These are evidently the cleavage surfaces or boundaries that form whenever one plates into a sharp corner. These cleavage surfaces must run throughout the deposit and divide it up into grains or branches of the base crystal. If the deposit formed only one set of parallel ridges, each ridge would be the top of a long narrow grain.

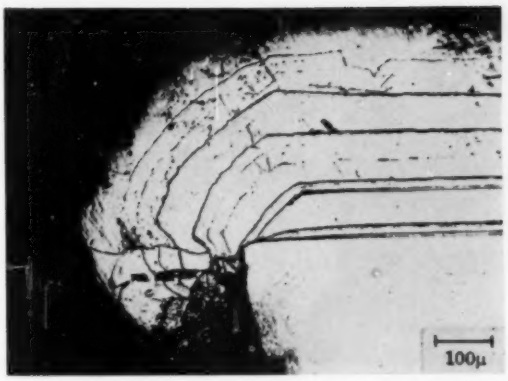

Fig. 14. Cross section of deposit on {111} face. Plating conditions: solution B, 1 amp/dm², 36 hr. Magnification 110X before reduction for publication.

X-ray diffraction patterns were made periodically during the deposition on the {110} face for one specimen. After the first hour of plating, the Laue spots were well defined and about 5° of a Debye ring was superimposed on one Laue spot. With increasing thickness, the Laue spots became more diffuse and larger, but evidences of the Debye ring increased only slightly. After a total of 36 hr of plating at 1 amp/dm² in solution B, the Laue spots apparently maintained the same pattern, but became extremely diffuse and poorly defined. Presumably this change reflected an increasing misalignment of the grains separated by the cleavage surfaces.

The cross section of a deposit on the {111} face is shown in Fig. 14. This was deposited from solution B at 1 amp/dm² for 36 hr. Again the horizontal lines mark interruption of the plating. There is no evidence of other grain boundaries except at the edges of the deposit and on visual examination at the very top of the deposit. Diffraction patterns were well defined. The first pattern, made after 4 hr of plating, contained three segments each about 5° in length, of a Debye ring. These segments, each of which was superimposed on a Laue spot, were only slightly longer after 20 hr of plating, and, after 36 hr, segments of a Debye ring totaling about 90° were evident, although the Laue spot pattern was still well defined. A surface micrograph at this thickness also revealed isolated grains.

A cross section of a deposit on the same face, but from solution A, revealed a multigrain structure which formed after an estimated 1 hr of deposition. The initial deposit appeared to be free of any microstructure.

Growth of Deposits at the Edge of the Crystal

Figure 15 shows the cross section at the edge of a deposit on the {110} face. This was plated in solution A at 1 amp/dm². It will be noted that the de-

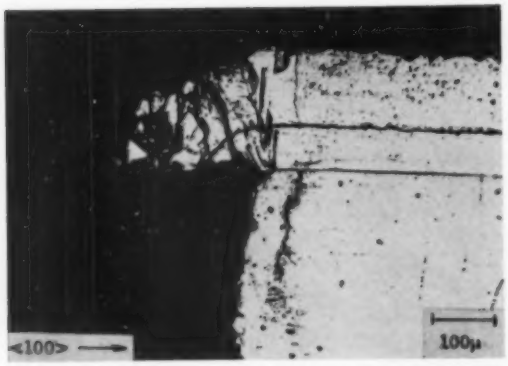

Fig. 15. Cross section of deposit on {110} face. Plating conditions: solution A, 1 amp/dm², 20 hr. Magnification 120X before reduction for publication.

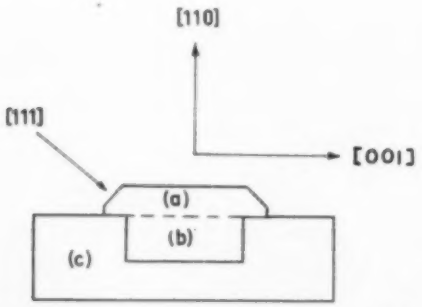

Fig. 16. Diagram of cross section of deposit on {110} face: (a) deposit; (b) seed crystal; (c) Lucite. Plating conditions: solution A, 0.25 amp/dm².

posit in this area is polycrystalline. An x-ray diffraction pattern of the corresponding portion of another deposit also indicated a random orientation. The central portion of these deposits showed the usual ridge structure and virtually uniform orientation.

On the other hand, the shape of the deposit in Fig. 11 at the left-hand edge indicates continuation of the single-crystal structure. Similarly, deposits made on the {110} face in solution A at 0.25 amp/dm² showed evidence of the single crystal structure at one pair of opposite edges. The edges bounded by the {100} planes assumed the shape shown in Fig. 16. The sloping surface was apparently a {111} plane. It was made up of highly reflecting growth layers and formed well-defined angles with the {100} and {110} surfaces.

The cross section at the edge of a deposit on the {111} face is shown in Fig. 14. It is quite clear that the deposit is a single crystal except in and close to the space which opened up between the seed crystal and the Lucite mount. Interesting features of Fig. 14 are the lines produced by interruption of the plating. They indicate that the initial metal distribution ignored the higher current density that normally exists at the edge of a cathode and seem to be correcting a misalignment in the polishing of the seed crystal. At later stages, the deposit seems

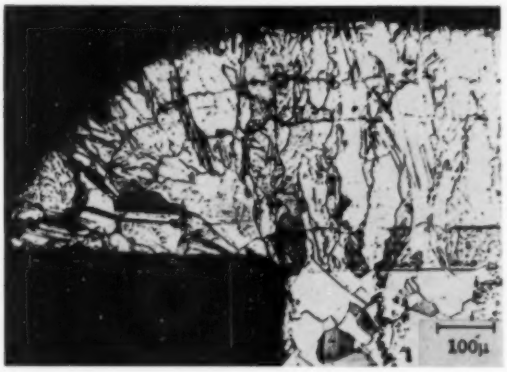

Fig. 17. Cross section of deposit on polycrystal. Plating conditions: solution A, 1 amp/dm², 41 hr. Magnification 110X before reduction for publication.

to establish a new face at the edge which grew at a rate about the same as that of the bulk of the deposit surface.

One interesting aspect of these edge growths is that they do not conform to normal current or metal distribution experienced on polycrystalline cathodes. Normally the deposit would be expected to grow more rapidly at the edge and assume a shape like that shown in Fig. 17. The departure from the usual metal distribution obviously reflects the single crystal structure. It is probably due to differences in the potential gradients required for deposition on the various crystal faces.

Twinning in Deposits

Orem (4) and Barnes (5) each have reported twinning in deposits on the {111} face of copper crystals. This was not observed during this investigation. This may reflect differences in current density or polarization. Orem plated at 3 amp/dm² and Barnes at 1.5 amp/dm² while the authors did not go higher than 1 amp/dm².

Acknowledgment

The authors are indebted to Theodore H. Orem for providing the Bridgman crystals, for the x-ray diffraction patterns, and for his helpful suggestions and encouraging interest.

Manuscript received Feb. 17, 1961. This paper was prepared for delivery before the Houston Meeting, Oct. 9-13, 1960.

Any discussion of this paper will appear in a Discussion Section to be published in the June 1962 JOURNAL.

REFERENCES

1. H. J. Pick and J. Wilcock, *Trans. Inst. Met. Finishing*, **35**, 298 (1958).
2. G. G. Storey and S. C. Barnes, *ibid.*, **37**, 11 (1960).
3. H. J. Pick, G. G. Storey, and T. B. Vaughan, *Electrochim Acta*, **2**, 165 (1960); T. B. Vaughan and H. J. Pick, *ibid.*, p. 179; S. C. Barnes, G. G. Storey, and H. J. Pick, *ibid.*, p. 195.
4. T. H. Orem, *J. Research Natl. Bureau of Standards*, **60**, No. 6, 597 (1958).
5. S. C. Barnes, *Acta Met.*, **7**, 700 (1959).

Studies of Color Centers Produced in Apatite Halophosphates by Shortwave Ultraviolet Radiation

Lawrence Suchow[1]

Research Department, Westinghouse Electric Corporation, Bloomfield, New Jersey

ABSTRACT

An investigation has been made of the effects of shortwave ultraviolet radiation on nonluminescent base materials in which it is possible to isolate other electronic processes from those of luminescence. This radiation has been found to produce color centers in a typical commercial halophosphate base material, in a similar preparation with manganese present in addition, and also in compounds and solid solutions in the systems $Ca_5(PO_4)_3F$-$Ca_5(PO_4)_3Cl$, $Sr_5(PO_4)_3F$-$Sr_5(PO_4)_3Cl$, and $Ba_5(PO_4)_3F$-$Ba_5(PO_4)_3Cl$. All colors may be bleached thermally and some optically as well. In preparations containing strontium, thermal bleaching is accompanied by luminescence, and glow curves have been measured. Optical bleaching is also accompanied by luminescence.

Previous studies (1) have indicated that the luminous efficiency of fluorescent lamp phosphors is decreased as a result of exposure of the phosphors to shortwave ultraviolet radiation. (In a mercury-vapor discharge, the shortwave ultraviolet is an 1849Å line which is emitted along with the more intense 2537Å.) That this is true of halophosphate phosphors has been shown by Beese and Henry (2), by Singleton (2), and by the author. A study has now been made of the effects of such shortwave ultraviolet radiation on nonluminescent base materials, in which it is possible to isolate other electronic processes from those of luminescence.

The term "halophosphate phosphors" is used here to denote phosphors whose base materials are alkaline earth halophosphates with the hexagonal apatite structure. An example of such a compound is the mineral apatite, $Ca_5(PO_4)_3F$. This compound, which crystallizes in space group $C6_3/m$, has 40% of its Ca ions in one crystallographic position (position 1) and 60% in another (position 2). The Ca ions in position 1 have six oxygens as nearest neighbors while those in position 2 have five oxygens and one fluorine. The compound $Ca_5(PO_4)_3Cl$ is isomorphous except that the chlorines are displaced from the fluorine positions along the c-axis by ¼ of the c dimension of the unit cell. This results in the calciums in position 2 having as nearest neighbors five oxygens and two chlorines. The base materials of many halophosphate phosphors are not simple in composition, but rather consist of solid solutions often containing more than one alkaline earth metal or halogen and also usually nonstoichiometric quantities of the various ions.

Experiments and Discussion

A typical commercial halophosphate base material.—The chemical formula (based on quantities in the mix before firing) of the first material studied may be written $Ca_{4.97}Sr_{0.18}(PO_4)_{2.85}(P_2O_7)_{0.59}F_{0.97}Cl_{0.26}$. This is the base material for a typical commercial halophosphate phosphor, which would of course be activated by the addition of small quantities of MnO and Sb_2O_3. Following synthesis by solid-state reaction among proper quantities of $CaHPO_4$, $CaCO_3$, $SrCl_2$, and CaF_2 at 1100°C, analysis by x-ray diffraction indicated that the product was primarily an apatite, but that a small quantity of $Ca_2P_2O_7$ was also present. A number of studies were then made. It was first found that exposure in vacuum or in an argon atmosphere of this nonluminescent material to a quartz low-pressure mercury-vapor discharge lamp resulted in yellowing. With a similar lamp constructed of Vycor, no yellowing occurred. Since quartz transmits the 1849Å line of the mercury spectrum and Vycor does not, this radiation must therefore be responsible for the yellowing. The yellowing takes place in a rather short time, and the intensity of the color appears to be no greater after several thousand hours exposure than after only one hour or even less. The diffuse reflectance spectra of this base material before and after irradiation (see curves 1 and 2 of Fig. 1) were measured *vs.* magnesium carbonate with a Beckman DU Spectrophotometer with diffuse reflectance attachment and, as with all others in this paper, corrected (3) to give absolute reflectance. It was thus found that the yellowing was due to introduction of a pair of absorption bands extending from 3200 to 4100Å and from 4200 to 4800Å, with respective maxima at 3700Å and 4500Å. It was then found that these absorption bands could be removed simultaneously by irradiation with light

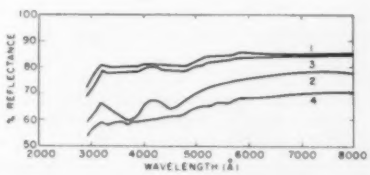

Fig. 1. Diffuse reflectance spectra of typical commercial halophosphate base material: 1, before exposure; 2, after exposure to quartz low pressure mercury-vapor discharge lamp; 3, after bleaching with 3650Å ultraviolet; 4, after heating exposed sample 1 hr at 300°C.

[1] Present address: International Business Machines Corporation Research Center, P. O. Box 218, Yorktown Heights, New York.

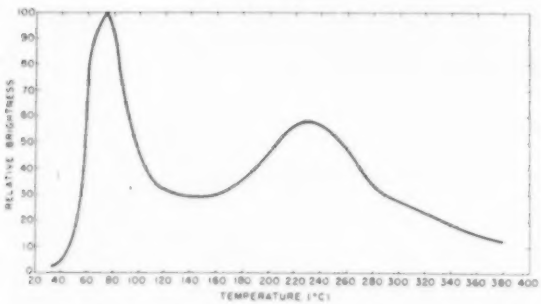

Fig. 2. Glow curve of typical commercial halophosphate base material after irradiation with quartz low-pressure mercury-vapor discharge lamp.

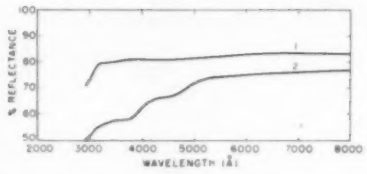

Fig. 3. Diffuse reflectance spectra of material with typical commercial halophosphate formulation except for absence of Sb_2O_3 (that is, base material + MnO): 1, before exposure; 2, after exposure to quartz low-pressure mercury-vapor discharge lamp.

of any wavelength lying in either of the two bands. In other words, the yellow color could be bleached out optically (see curve 3 of Fig. 1). The optical bleaching of the yellowed phosphor base material was observed to be accompanied by red luminescence when the bleaching radiation was, for example, 3650Å.

The absorption bands could also be removed by heating, and here too the bleaching was accompanied by luminescence, that is, thermoluminescence. The diffuse reflectance spectrum after thermal bleaching is given in curve 4 of Fig. 1, in which it will be seen that the absorption bands are removed on heating to 300°C, but that there is also an over-all drop in reflectance. (This drop is seen visually as a tan color which may be removed by heating at 1100°C.) The glow curve plotted in Fig. 2 was obtained by heating an irradiated sample in a small light-shielded box at a rate of approximately 18°C/min; the sample had been exposed at about 35°C to a quartz low-pressure mercury-vapor discharge lamp for 21 hr and then kept in the dark for a half hour before heating. Light emitted was detected by a water-cooled RCA 1P21 photomultiplier whose signal was amplified by a Keithley Electrometer, Model 210, and fed to an Electro-Instruments x-y Recorder which also received a temperature signal from an iron-constantan thermocouple. A light shutter enabled measurement of dark current. It will be seen that peaks occur at 75° and 230°C. If irradiated samples are kept in the dark at room temperature for extended periods, the height of the first peak is found to diminish and finally almost disappear. The thermoluminescence was also observed visually by heating on an open hotplate in a darkroom; it was found to be quite weak with a whitish color.

Color center formation has also been observed in a preparation like that described above, but with Mn (but not Sb) added. This material, which is only very weakly fluorescent, has a formula (based on quantities in the mix before firing) $Ca_{4.97}Sr_{0.13}(PO_4)_{2.59}$-$(P_2O_7)_{0.26}F_{0.97}Cl_{0.28}Mn_{0.17}$. Its diffuse reflectance spectra before and after exposure to radiation from a quartz low-pressure mercury-vapor discharge lamp are given in Fig. 3, where it will be seen that absorption bands introduced are in the same positions as in the preparation without manganese. Glow curve data in Table I indicate that the same thermoluminescent peaks found in the preparation without manganese are probably also present here but that there is a very large additional glow superimposed.

Calcium halophosphates.—It was desired next to study the effect on color center formation of variation of the fluoride to chloride ratio in base materials. To do this, it was decided to simplify the base materials to stoichiometric one-phase apatite compositions and to include in any one preparation either calcium or strontium, but not both. In the case of calcium, this meant compositions of the type $Ca_5(PO_4)_3F_xCl_{1-x}$ (based on composition of the mix before firing), prepared by solid-state reaction

Table I. Thermoluminescence (glow curve) measurements

Sample	Peak temperatures (°C) and relative heights (in parentheses)	
	After exposure to quartz low-pressure Hg-vapor lamp. (1849Å and higher wavelengths)	After exposure to Vycor low-pressure Hg-vapor lamp (2537Å and higher wavelengths)
Typical commercial halophosphate base material $[Ca_{4.97}Sr_{0.13}(PO_4)_{2.59}(P_2O_7)_{0.26}F_{0.97}Cl_{0.28}]$	75° (50) and 230° (29)	None
Typical commercial halophosphate base material + MnO (that is, phosphor less Sb_2O_3) $[Ca_{4.97}Sr_{0.13}(PO_4)_{2.59}(P_2O_7)_{0.26}F_{0.97}Cl_{0.28}Mn_{0.17}]$	Broad emission from about 50° to 400°, fairly constant from about 90° (107) to 340° (125). Maximum at about 240° (135).	None
$Sr_5(PO_4)_3F$	100° (57)	110° (7)
$Sr_5(PO_4)_3F_{0.77}Cl_{0.23}$	165° (106) and a possible shoulder in the vicinity of 230° (28)	None
$Sr_5(PO_4)_3F_{0.5}Cl_{0.5}$	180° (53) and a shoulder at 240° (17)	None
$Sr_5(PO_4)_3F_{0.25}Cl_{0.75}$	160° (56)	None
$Sr_5(PO_4)_3Cl$	120° (3.7)	None

among proper quantities of $CaHPO_4$, $CaCO_3$, CaF_2, and $CaCl_2$ in silica crucibles at 1100°C. X-ray diffraction confirmed earlier reports (4, 5) that there was complete solid-state miscibility in the system $Ca_5(PO_4)_3F$-$Ca_5(PO_4)_3Cl$.

Exposure of these preparations to a quartz low-pressure mercury-vapor discharge lamp resulted in introduction of blue body color in $Ca_5(PO_4)_3Cl$ and others rich in this compound, a yellow color in those rich in $Ca_5(PO_4)_3F$, and no color in $Ca_5(PO_4)_3F$ itself. Although this is the over-all picture, there is some lack of reproducibility in the point at which the yellow gives way to the blue, or rather in the region in which they appear together, since overlap occurs. The exact reasons for lack of reproducibility are not known, but there seems to be a tendency for the yellow color to appear at lower percentages of fluoride when preparations are made in covered crucibles than in open ones. This indicates a possibility of halide volatility or introduction of oxygen as the factor which affects reproducibility. Usually, only the blue color is observed where the solid solution contains 50 mole % or more $Ca_5(PO_4)_3Cl$. At 77 mole % $Ca_5(PO_4)_3F$, the composition corresponding in F:Cl ratio to that in the typical commercial halophosphate phosphor discussed above, the yellow color is often found alone, but this is not always true.

Figure 4 gives the diffuse reflectance spectra of a 77 mole % $Ca_5(PO_4)_3F$ preparation where only yellow was found after exposure. It will be seen that the absorption bands are similar to those in the typical commercial halophosphate base material. Figure 5 gives the diffuse reflectance spectra of $Ca_5(PO_4)_3Cl$ before and after exposure. The blue color formed is seen to be due to broad absorption above about 4700Å, and there is also broad absorption in the ultraviolet below about 3500Å. The shade of the induced blue color (as seen both visually and in the diffuse reflectance spectrum) is apparently the same whether or not $Ca_5(PO_4)_3F$ is present in solid solution with $Ca_5(PO_4)_3Cl$, although the intensity of the color decreases with increasing percentages of the former.

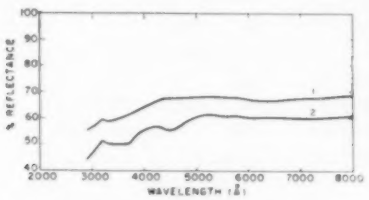

Fig. 4. Diffuse reflectance spectra of unactivated $Ca_5(PO_4)_3F_{0.77}Cl_{0.23}$; 1, before exposure; 2, after exposure to quartz low-pressure mercury-vapor discharge lamp.

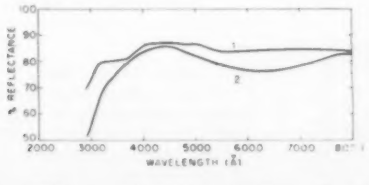

Fig. 5. Diffuse reflectance spectra of unactivated $Ca_5(PO_4)_3Cl$; 1, before exposure; 2, after exposure to quartz low-pressure mercury-vapor discharge lamp.

Unlike the yellow color (which appears to behave in every way, except for the absence of thermoluminescence, like the yellow color formed in the typical commercial halophosphate base material), the blue color cannot be bleached by absorbed light, nor is there any luminescence on exposure to 3650Å radiation. Like the yellow color, the blue color can be bleached out by heating.

Where both yellow and blue occur together, the body color appears green but changes to blue on exposure to 3650Å radiation, which removes only the yellow component (simultaneously producing the expected red luminescence). The superimposition of yellow and blue is also seen in the diffuse reflectance spectrum.

An interesting effect found is that the temperature required to remove the blue color increases with increasing percentages of $Ca_5(PO_4)_3F$, despite the fact that the color itself remains the same over the series. (In the case of those samples where yelow and blue occur together, this statement applies to the blue component which remains after optically bleaching out the yellow). Visually judged bleaching temperatures are given in Fig. 6.

It appears then that the fluoride is capable of stabilizing the blue color without change in the spectral distribution of absorption. At least two explanations for the blue color appear possible. It may be that it is due to a trapped electron. Since light absorbed by the blue material does not bleach out the color, retrapping must occur if this is so. The stabilization of such traps by fluoride could be ascribed to the fluoride raising the temperature at which a radiationless (thermal) transition of an electron back to the ground state occurs. The other possible explanation is that the blue color is due to introduction not of trapped electrons but rather of a new energy level to which electrons can be raised from the ground state, to which they can then return by thermal transition. The new level would in this case probably be a lattice defect, and thermal bleaching could then be ascribed to annealing out the defect.

None of the irradiated preparations in the $Ca_5(PO_4)_3F$-$Ca_5(PO_4)_3Cl$ system has been found to be thermoluminescent. A possible explanation of this finding is given below.

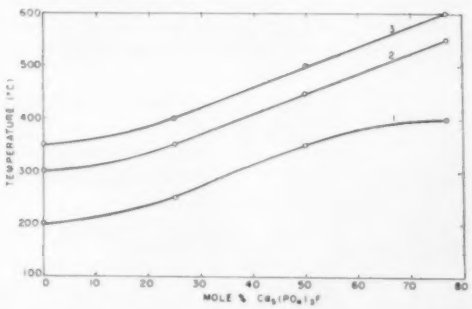

Fig. 6. Thermal bleaching of the blue color induced in calcium halophosphates; 1, temperature at which bleaching appears to start; 2, temperature at which bleaching appears to be nearly complete; 3, temperature at which bleaching is complete.

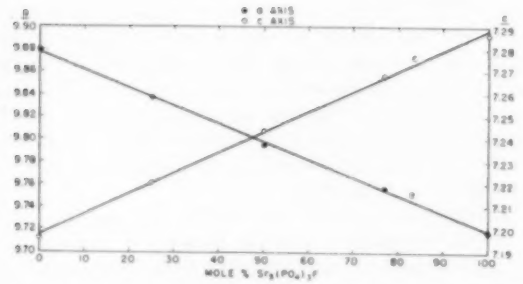

Fig. 7. Lattice constants vs. composition in the system $Sr_5(PO_4)_3F$-$Sr_5(PO_4)_3Cl$.

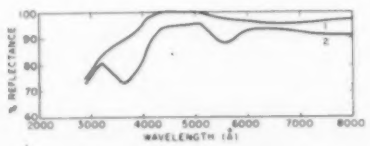

Fig. 8. Diffuse reflectance spectra of unactivated $Sr_5(PO_4)_3F$; 1, before exposure; 2, after exposure to quartz low-pressure mercury-vapor discharge lamp.

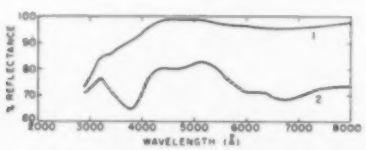

Fig. 9. Diffuse reflectance spectra of unactivated $Sr_5(PO_4)_3F_{0.77}Cl_{0.23}$; 1, before exposure; 2, after exposure to quartz low-pressure mercury-vapor discharge lamp.

Strontium halophosphates.—The system $Sr_5(PO_4)_3F$-$Sr_5(PO_4)_3Cl$ has also been studied. Preparations were made by solid-state reaction among $SrHPO_4$, $SrCO_3$, $SrCl_2$, and SrF_2 in covered silica crucibles at 1100°C. X-ray diffraction studies (see Fig. 7) have shown that there is solid solution formation over the entire composition range and that Vegard's law is followed. Irradiation with a quartz low-pressure mercury-vapor discharge lamp has been observed to produce a variety of colors in this system (see Table II). Figures 8 through 11 give the diffuse reflectance spectra of these preparations before and after irradiation. It will be seen that the slight differences in colors of preparations containing both fluoride and chloride are due not to changes in the major absorption bands but rather to smaller superimposed effects. The difference in color of the

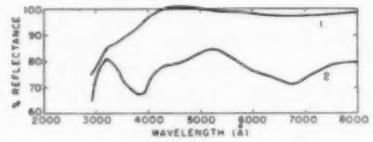

Fig. 10. Diffuse reflectance spectra of unactivated $Sr_5(PO_4)_3F_{0.5}Cl_{0.5}$; 1, before exposure; 2, after exposure to quartz low-pressure mercury-vapor discharge lamp.

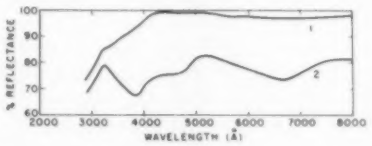

Fig. 11. Diffuse reflectance spectra of unactivated $Sr_5(PO_4)_3F_{0.25}Cl_{0.75}$; 1, before exposure; 2, after exposure to quartz low-pressure mercury-vapor discharge lamp.

$Sr_5(PO_4)_3F$ is however due to development of different absorption bands. No sharp absorption bands are produced in $Sr_5(PO_4)_3Cl$.

All of the irradiated preparations in this system which contained fluoride could be bleached by exposure to 3650Å radiation, and all containing 50 mole % $Sr_5(PO_4)_3F$ or more fluoresced visibly red during this bleaching, with the intensity of fluorescence decreasing with decreasing fluoride content. Bleaching could also be accomplished thermally with accompanying weak whitish thermoluminescence in all cases. Glow curve data are listed in Table I. It is interesting that, of all the many preparations studied in the Ca, Sr, and Ba halophosphate systems, only $Sr_5(PO_4)_3F$ was rendered thermoluminescent by exposure to a Vycor low-pressure mercury-vapor discharge lamp (2537Å, but no 1849Å). These thermoluminescent traps are not however accompanied by color centers observable either visually or spectrophotometrically, although perhaps only because their concentration is too low.

The absence of thermoluminescence in $Ca_5(PO_4)_3F_{0.77}Cl_{0.23}$ after exposure to a quartz low-pressure mercury-vapor discharge lamp is surprising because thermoluminescence is found in the closely related typical commercial halophosphate base material after such irradiation and because the color centers in both of these behave in similar fashion optically (absorption band positions, luminescence upon bleaching). However, the absence of thermal glow has been confirmed visually. This appears to indicate that the

Table II. Color centers in the system $Sr_5(PO_4)_3F$-$Sr_5(PO_4)_3Cl$

Substance	Color after irradiation with quartz low-pressure mercury-vapor lamp	Absorption maxima (reflectance minima) Å	Additional observations
$Sr_5(PO_4)_3F$	Pinkish lavender	3600, 5600	—
$Sr_5(PO_4)_3F_{0.77}Cl_{0.23}$	Blue-green	3800, 6700	These also have some absorption from (*a*) about 4400 to 4900Å, the amount increasing with Cl content, and (*b*) about 6000 to 6250Å, the amount decreasing with increasing Cl content and almost completely absent in $Sr_5(PO_4)_3F_{0.25}Cl_{0.75}$.
$Sr_5(PO_4)_3F_{0.5}Cl_{0.5}$	Green	3800, 6700	
$Sr_5(PO_4)_3F_{0.25}Cl_{0.75}$	Green, but yellower than preceding sample	3800, 6700	
$Sr_5(PO_4)_3Cl$	Very slight color, perhaps yellowish	None	Generally lower reflectance from about 4000 to 6000Å.

whitish-thermoluminescing traps in the typical commercial halophosphate base material are different from the red-photoluminescing traps found in both materials, and that it is the red-photoluminescing traps which are the observed color centers. On the other hand, since glow peaks and thermal bleaching temperatures have been found to coincide where both occur, and since glow curves have been found to be depressed by optical bleaching, it is likely that they are the same traps, although additional glow peaks not connected with absorption in the spectral region studied may also occur. It appears that the presence of strontium is required for thermoluminescence since only preparations containing that element have been found to exhibit this property. It is conceivable that strontium creates an alternate, favored path by which an electron can fall back with light emission on heating, whereas in the absence of strontium the process is nonradiative.

Barium halophosphate.—Barium halophosphates were prepared by solid-state reaction of proper quantities of $BaHPO_4$, $BaCO_3$, $BaCl_2$, and BaF_2 in covered silica crucibles. In this case, it was found that firing at 1100° or 1000°C caused too much sintering, but at 900°C this was not so. Reaction at 900°C was nearly but not quite complete, for x-ray diffraction patterns showed the presence of traces of $Ba_3(PO_4)_2$ along with apatite in products made at that temperature, but only apatite at higher temperatures. There were also slight deviations in lattice constants at different temperatures. Nevertheless, the 900°C preparations were used for color center studies because those prepared at higher temperatures were difficult to grind properly and were rather deeply colored even prior to exposure. In visual tests, $Ba_5(PO_4)_3F$ was found to darken just perceptibly to gray on exposure to a quartz low-pressure mercury-vapor lamp, while all samples containing chloride darkened considerably more to a purplish-pinkish color on exposure. The intensity of this color was found to increase with increasing percentages of chloride, and $Ba_5(PO_4)_3Cl$ turned the darkest of all and perhaps slightly bluer. However, all these colors were very weak and have not shown up as absorption bands on measurement of diffuse reflectance spectra before and after irradiation. The only change noted in each case was a generally slightly lower level of reflectance after irradiation. None of the irradiated barium halophosphates could be bleached optically, but all were susceptible to thermal bleaching without accompanying luminescence.

Concluding Discussion

All of our observations on apatite halophosphates indicate that optically bleachable color centers consist of trapped electrons (or perhaps holes) which can be returned to their original states on proper irradiation or heating. Déjardin, Janin, and Cotton (6) have shown that halophosphate base materials are photoconducting during irradiation with 1849Å ultraviolet. Fitting this together with our observations of color center traps, it appears that 1849Å radiation would raise an electron into the conduction band (or produce a hole in the valence band) from which it would fall into a trap. Therefore it might be expected that emptying the trap with 3650Å radiation would give the reverse process, with photoconductivity occurring again.

There are many parallels between the effect of 1849Å radiation on the base materials studied and on corresponding phosphors, as well as in their behavior following irradiation. It therefore appears quite likely that the color centers and other traps found in the base materials are closely connected with the decrease in luminous efficiency of halophosphate phosphors on exposure to 1849Å radiation in fluorescent lamps. Probably the decrease is due to a competing electronic process or to light absorption by the color centers, but the exact mechanism is not yet clear.

Acknowledgments

The writer wishes to acknowledge the invaluable assistance of Mr. John Minchak as well as very helpful conversations with Dr. Henry F. Ivey, Dr. Claus H. Haake, and Professor Ephraim Banks. Dr. C. K. Lui-Wei was kind enough to provide the x-ray diffraction data.

Manuscript received April 5, 1961. This paper was prepared for delivery before the Indianapolis Meeting, April 30-May 3, 1961.

Any discussion of this paper will appear in a Discussion Section to be published in the June 1962 JOURNAL.

REFERENCES

1. G. Meister and R. Nagy, *J. Opt. Soc. Am.*, **36**, 696 (1946); **37**, 403 (1947).
2. Private communications.
3. F. Benford, G. P. Lloyd, and S. Schwarz, *J. Opt. Soc. Am.*, **38**, 445 (1948); F. Benford, S. Schwarz, and G. P. Lloyd, *ibid.*, 964.
4. P. G. Steward, *Brit. J. Appl. Phys.*, Supplement No. 4, p. S17 (1954).
5. A. Wold, Private communication.
6. G. Déjardin, J. Janin, and L. Cotton, Cahiers phys., No. 106, 217 (1959).

Microsecond Response of Electroluminescent Cells

J. E. Johnson

Research Laboratories, Westinghouse Electric Corporation, Pittsburgh, Pennsylvania

ABSTRACT

Microsecond rise of electroluminescent, EL, output to greater than the steady-state value for a-c sine wave excitation has been achieved in plastic-embedded powder phosphor cells by application of an a-c burst having a d-c component. The decay time for the EL flash, 7 μsec, is considerably longer than the rise time. The EL resulting from a-c bursts of several voltage waveforms has been observed. It has been noted that: (*A*) The EL brightness wave rises in one-half cycle of an a-c voltage burst when a d-c component equal to one-half the a-c peak-to-peak voltage is applied and can exceed the steady-state value, depending on the magnitude of the d-c pulse. (*B*) When there is no d-c component, the EL rises to its equilibrium value in several cycles of the a-c voltage. (*C*) The rate of rise of the EL brightness in (*B*) and the extent of the initial rise in (*A*) have been found to vary with the repetition rate of the a-c burst. (*D*) The application of a square wave having the same peak voltage excursions rather than a sine wave excitation increases the integrated light-output of the cell. The above have been measured, along with the steady-state brightness, at frequencies from 60 cps to 500 kcps. From these measurements it is concluded that device applications of EL cells are feasible where fast rise bursts of light are required.

Square-wave pulses of light having rise and decay times of the order of a microsecond are frequently desired in device and test applications. The purpose of the present investigation is to determine if such pulses could be obtained from EL cells of plastic embedded zinc sulfide powder phosphors. Detailed study of the pulse-excitation behavior of such phosphors also provides a measure of the rate of return to equilibrium of the phosphor after application of a steady a-c voltage.

Haake (1) has earlier found the build-up of EL output to the steady-state value for a zinc sulfide phosphor to require several cycles of applied a-c voltage when the phosphor has first been irradiated with infrared light, or left unexcited in the dark long enough for all filled traps to have been thermally emptied. A smaller number of cycles is required for build-up if the phosphor has been pre-excited. The decay of the EL emission after cessation of the a-c voltage, Haake found, required several milliseconds.

Briggs (2) measured the rise and decay of EL resulting when short square-wave voltage pulses were applied to an EL cell. Rise times of about 1μsec and decay times of about 10 μsec were observed. No indication of the pulse brightness was given.

More recently, Zallen, Eriksen, and Ahlburg (3) studied the emission of an EL cell subjected to pulsed square-wave excitation as a function of pulse repetition rate and duration, and the cell temperature. Their work shows the intensity of the light flash to be dependent on the temperature and the time which has elapsed since the previous voltage excursion. Similar results have been reported by Liamichev and Orlov (4).

The earliest study of pulse-excited EL was that of Waymouth and Bitter(5), Hoffman and Smith (6) recently reviewed EL emission waveforms in some detail.

Experimental

Electroluminescent cells were prepared by spraying a layer, 1.5 mils thick, of ZnS: Cu,Cl(Westinghouse 1658T) small-particle phosphor dispersed in Ucilon polyvinyl chloride acetate plastic onto a glass plate coated with conducting tin oxide. A back electrode of aluminum was then evaporated through a mask onto the phosphor. Electrical contact to the tin oxide was made with a layer of silver paint after the phosphor coating around the aluminum electrode had been scraped away as illustrated in Fig. 1. These cells provide capacitances of 60 pfd/cm^2. For the highest frequency measurements, a cell 0.2 cm^2 in area was used to avoid loading the output of the amplifier supplying the driving waveform.

The output of the EL cell was monitored by an RCA 7102 photomultiplier tube fitted with a cathode follower output. Careful attention was given to the problem of high-frequency response in the construction of the photocell circuit. The voltage and EL waveforms were observed on a Tektronix Model 543 oscilloscope.

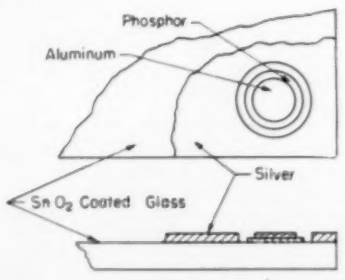

Fig. 1. Electroluminescent cell construction

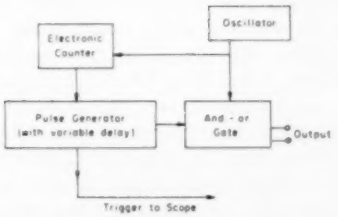

Fig. 2. Voltage waveform generation

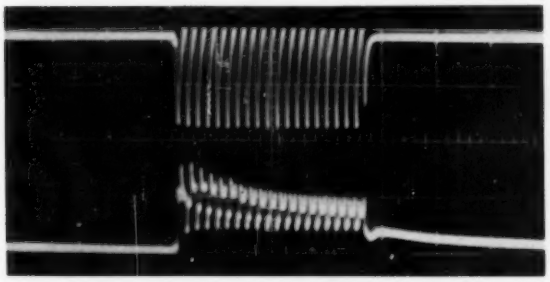

Fig. 3a. Voltage (upper trace) sensitivity, 100 v/cm; brightness (lower trace) sensitivity, arbitrary; sweep speed, 10 μsec/cm.

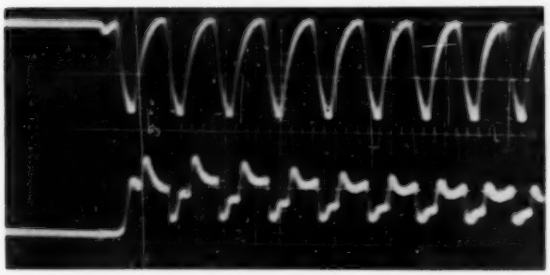

Fig. 3b. Voltage (upper trace) sensitivity, 100 v/cm; brightness (lower trace) sensitivity, arbitrary; sweep speed, 2 μsec/cm.

Measurements of the EL output under steady excitation were made with a Spectra Brightness Meter, Model UB (Photo Research Corporation).

The exciting voltages are generated by the apparatus shown in block diagram in Fig. 2. All components of this circuit are commercially available instruments except the "AND-OR" gate, designed by R. F. Hollandbeck of this laboratory.

In the apparatus of Fig. 2, the oscillator provides an a-c carrier which is fed into both the electronic counter and the "AND-OR" gate. The counter is used as a frequency divider, providing trigger pulses to the pulse generator at 10^{-2}, 10^{-4}, or 10^{-5} times the frequency of the a-c carrier. The output pulse of the pulse generator is fed into the "AND-OR" gate which with suitable adjustment can provide at its output either the a-c carrier, or the d-c pulse, or a combination as illustrated in Fig. 3.

Results and Evaluation

A wide variety of voltage pulse waveforms were applied to the EL cell and the brightness waveforms noted. The voltage pulses may be generally described as a-c bursts superimposed on a d-c component. The exciting waveforms used by other workers (1-6) were easily generated and the earlier results duplicated, with the exception of the brightness decay time which will be discussed later in this paper.

An example of a useful voltage pulse is shown in the upper traces of Figures 3a and 3b. The resulting brightness waveform. seen in the lower traces of Fig. 3a and 3b, shows the EL output rising in less than 1 μsec. The brightness decay to the 1/e point requires about 10 μsec. The decay, however, is definitely not of exponential character, and is voltage-driven in its early stages, that is, the initial decay is faster for higher frequency a. c.

The a-c carrier in Fig. 3a and 3b is a 500 kcps distorted sine wave, and the EL rise time is just the voltage rise time. The distortion affects the brightness within the pulse, but not the rise and decay times of the EL output. Similar rise and decay times can be obtained with lower frequency a-c carriers by phasing the beginning and end of the burst properly. Operation in such a mode is not desirable for systems application, but may provide a useful method for the estimation of the nonequilibrium carrier concentration within the phosphor.

Other distorted sine wave a-c bursts superimposed on a d-c component were generated, and in some particular cases, not illustrated, the brightness wave was very nearly a square wave, with little superimposed a-c ripple.

An attempt was made to estimate the pulse brightness by a mechanical integration of the photocell output-*vs.*-time curves in the last portion of the bursts where the transients have largely decayed. Several factors severely limit the accuracy of the estimate obtained:

1. The color of the EL emission shifts from green, peaking at 5100Å, at low excitation frequencies, to blue, peaking at 4500Å, at higher frequencies. The luminous efficiency of a Gaussian distribution of radiation, typical of ZnS:Cu phosphors and peaking at 4500Å, is only 40% of the luminous efficiency of an equal energy Gaussian distribution peaking at 5100Å. As a consequence, measurements corrected for the standard observer would indicate a decrease in brightness as the excitation frequency is increased. The photocell used was uncorrected and, although its sensitivity varied approximately 40% over this wavelength range for monochromatic radiation, its variation for a Gaussian distribution peaking in this range is negligibly small. (The initial flash shown in Fig. 3a and 3b peaks at 4700Å.)

2. Although the only photographs evaluated for the brightness estimate were those with reasonably good sine wave excitation, it was evident that distortion of the voltage wave could influence the EL output (see below).

3. Calibration of the photocell was made by comparing the brightness as measured with the Spectra Brightness meter to the integrated photocell output for two frequencies, 10 and 20 kcps.

The result indicates the photon output per second is little changed from 20 kcps to 500 kcps, as noted also in ref. (6). The luminous output, however, decreases because of the continuing color change from green to blue.

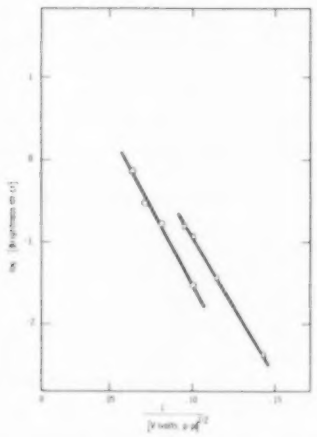

Fig. 4a. Brightness comparison for sine- and square-wave excitation at 60 cps; O, steady sine-wave excitation; □, steady square-wave excitation.

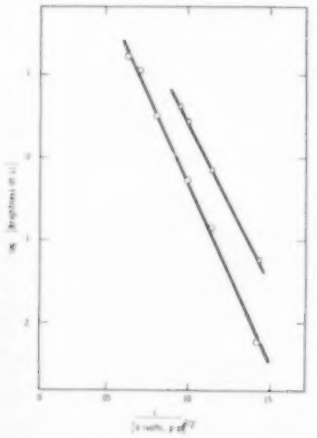

Fig. 4b. Brightness comparison for sine- and square-wave excitation at 20kc; O, steady sine-wave excitation; □, steady square-wave excitation.

The variation of the light output with distortion of the voltage waveform has been investigated quantitatively as follows. An EL cell was subjected to steady a-c (no d-c) excitation of both sine and square waveform for frequencies from 60 cps to 20 kcps over a range of peak-to-peak voltages and the EL output observed with the Spectra meter. Typical results are shown in Fig. 4a and 4b. In all cases the data show a linear relationship between ln (Brightness) and (Applied Voltage)$^{-1/2}$, the EL output being greater for square wave excitation. Similar results were obtained by Briggs (2) in comparing the emission produced by square pulses *vs.* rounded pulses approximately half-sine shape. The difference reaches factors greater than four at low applied voltages and frequencies. At higher voltages and frequencies the output values draw closer together, perhaps because the voltage waveforms become more alike because of distortion.

The emission color shows the same behavior for either square-wave or sine-wave excitation.

The brightness of the initial flash, Fig. 3, was found to depend on the time elapsed since the previous a-c burst. The dependence could be approximated by the relation $L_1 \simeq \ln(K/t)$ used by Liamichev and Orlov (4) with $K \simeq 1$ sec, where L_1 is the peak intensity of the initial flash. After a 1-sec rest, the peak brightness of the initial flash just about equals that of the steady-state flashes. It is evident, therefore, that this a-c plus d-c mode of operation will be useful in high-speed device applications only if a pulse repetition rate greater than one per second is planned. The steady-state brightness, operationally defined above, does not seem to be affected measurably by the d-c component.

When there is no d-c component to the excitation burst, the brightness requires more than one cycle of applied a.c. to reach its steady-state value. In no case were more than five cycles required for the brightness to reach about 90% of the steady-state value. In the first cycle of applied voltage, where $V_{appl} = V_s \sin \theta$, the first light flash is observed at $\theta = 90°$ and is usually quite small. At $\theta = 270°$, the second flash occurs and its intensity was closely examined. In general, the intensity at $\theta = 270°$ is about 80% that of a flash occurring after the steady state is reached. Fluctuations from this value were observed, mostly toward lower intensities, but never to less than about 55% of the steady-state value.

Discussion and Conclusion

Zallen, Eriksen, and Ahlburg have interpreted their results on the basis of the model for Destriau effect electroluminescence which is outlined below.

(*A*) The light output is proportional to the concentration of free carriers. Light is produced by luminescent centers excited when struck by field accelerated carriers.

(*B*) For a given voltage amplitude, a carrier concentration greater than the thermal equilibrium concentration is generated by collisional processes involving hot carriers.

(*C*) The excess carriers require time to decay, the return to equilibrium involving the emptying of traps populated during excitation. The decay time is temperature dependent. This model adequately explains the present results and those of Haake, if it is realized that more than one excursion of an applied sine wave voltage is required before a steady-state carrier concentration is attained.

An alternative explanation for the observed behavior under voltage pulse excitation could be offered were each activated ZnS particle to be considered as a small n-i-p, or n-p block isolated from the electrodes by the dielectric. Such a model has become more plausible recently in the light of work by Ballentyne (7) and Aven and Parodi (8).

In such a model, the injection of carriers could proceed only until the particles became polarized. If traps were present, for which $N_t C_t >> N_L C_L$ where N_t and N_L are the density of traps and luminescent centers, respectively, and C_t and C_L are their capture cross sections, then no light would be observed until sufficient traps were filled that $(N_t - n_t)\, C_t = N_L C_L$, where n_t is the trapped electron concentration. The trapped electrons eventually would be emitted ther-

mally, giving rise to the decay of L_1 with decreasing pulse repetition rate noted above.

One point, as yet uninterpreted, remains. In the present work and in that of Briggs, Liamichev, and Orlov, and Hoffman and Smith, a luminescence decay time of about 10 μsec was observed on removal of the applied field. Haake and Zallen *et al.* have found the decay time to be of millisecond order. The difference could be inherent in the phosphors used, but it is interesting to note that in the published work a definite relation exists between the EL cell thickness and the EL decay time, thicker cells requiring longer decay times. This correlation can be understood if the equivalent circuit for the thin cell is a parallel connected capacitor and resistor. Thicker cells would be series connections of these units. At the end of the excitation pulse, *e.g.*, as in Fig. 3, the amplifier presents a low, *ca.* 1000 ohm, impedance to the decay of charge from the cell. In the series connection of a thicker cell, however, the low generator impedance would not dominate and a much larger RC product would obtain, causing a slower decay of the internal field and of the EL flash. In support of this, Briggs (2), in measuring the charge flow in the cell during pulsing, found that charge continues to flow during the EL decay time, indicating some sort of RC discharge process.

Acknowledgment

This work was supported by the United States Air Force, Wright Air Development Division, through a contract with the Westinghouse Air Arm Division. The author wishes to thank Mr. K. Rumon for preparing the EL cells, and to acknowledge the aid given him in this work by Mr. R. F. Hollandbeck, Dr. E. A. Sack, and Dr. P. N. Wolfe.

Manuscript received March 29, 1961. This paper was presented before the I.R.E. Professional Group on Electron Devices Meeting, Oct. 28, 1960.

Any discussion of this paper will appear in a Discussion Section to be published in the June 1962 JOURNAL.

REFERENCES

1. C. H. Haake, *J. Appl. Phys.*, **28**, 245 (1957).
2. G. R. Briggs, *Bull. Am. Phys. Soc.*, Ser II, **2**, 155 (1957); see also: J. A. Rajchman. G. R. Briggs, and A. W. Lo, *Proc. I. R. E.*, **46**, 1808 (1958).
3. R. Zallen, W. T. Eriksen, and H. Ahlburg, *This Journal*, **107**, 288 (1960).
4. I. Ia. Liamichev and I. N. Orlov, *Optics and Spectroscopy*, **7**, 258 (1959).
5. J. F. Waymouth and F. Bitter, *Phys. Rev.*, **95**, 941 (1954).
6. G. R. Hoffman and D. H. Smith, *J. Elec. Control*, **9**, 161 (1960).
7. D. W. G. Ballentyne, *This Journal*, **107**, 807 (1960).
8. M. Aven and J. A. Parodi, *J. Phys. Chem. Solids*, **13**, 56 (1960).

Germanium Dendrite Studies

I. Studies of Twin Structures and the Seeding Mechanism

J. W. Faust, Jr. and H. F. John

Research Laboratories, Westinghouse Electric Corporation, Pittsburgh, Pennsylvania

ABSTRACT

The importance of suitable seeds in dendritic growth of long ribbons of semiconductors is discussed, and investigations to determine the characteristics of suitable seeds are reported. Studies of growth buttons have yielded information about the initiation of spontaneous and also controlled dendritic growth from buttons. Some information on the growth of the dendrites is presented to suggest that the growth mechanism is more complicated than previously presumed.

The general term dendrite has been used to designate the treelike growth found in ingots of metals and alloys after they have been rapidly cooled from the melt. Dendrites can often be seen in the germanium that is left in the crucible after pulling an ingot when the crucible is allowed to cool rapidly. This type of dendritic growth can be termed spontaneous. Billig and Holmes (1, 2) showed that it is possible to control the dendritic growth of germanium by pulling a seed rapidly from a supercooled melt to give long dendrites which they reported to be single crystals. They showed that the dendrites grew in a <211> direction and showed that, for any {111} plane, three <211> directions allow easier growth than the three directions of opposite sign. Later they found that the dendrites contained a twin lamella (*i.e.*, two twin planes), usually completely enclosed (3). Even-twinned dendrites can grow in any or all of the <211> directions.[1] Bennett and Longini (4) further studied dendritic growth in germanium; their studies resulted in what can truly be called controlled dendritic growth, or preferably ribbon growth. They found that dendrites with an odd number (originally presumed to be one) of twin planes could exhibit growth in only three of the six <211> directions; furthermore, if the seed is vertical with the $[2\bar{1}\bar{1}]$ direction pointing into the melt, ribbon growth will proceed only downward; whereas with

[1] Although even-twinned dendrites that have started to grow in a direction normal to the melt surface may continue to grow in that direction without branching, growth in other directions (i.e. branching) can occur from the dendrite and frequently occurs when seeding.

the seed in the opposite direction (*i.e.*, the $[\bar{2}11]$) growth will proceed at 60° to the downward direction. They put forth a theory to explain their results which was based on nucleation at a single twin plane. Billig (5) had earlier speculated that dendrites grow by an extension of the twin lamella formed initially by two screw dislocations of opposite sign, followed by layered overgrowth. Wagner (6) and Hamilton and Seidensticker (7) showed that ribbons could not be grown with a single twin plane, but required at least two twin planes.

The basic stages in the seeding and growth of dendritic ribbons devised by Bennett are as follows: (i) a suitable seed is introduced into a melt that is not supercooled; (ii) with the seed still in the melt, the temperature is dropped to the desired degree of supercooling and growth on the seed will start in the form of a button; (iii) after the button has grown to a critical size, rapid sideways growth, called "wings," proceeds along the surface of the melt from the twin lamellae in the button; (iv) the seed and the resulting button are pulled rapidly from the melt and ribbon growth takes place from the wings. The top part of a ribbon grown in this manner is shown in Fig. 1. In this paper, the results of studies on the seeds, A, (the letters refer to Fig. 1) and seeding mechanisms, the growth buttons, B, the button wings, C, and the initiation of growth of the dendrite, D, are presented. Paper II of this series will discuss lateral growth, while paper III will involve studies on dislocations in dendrites.

Primitive Dendrites

As mentioned earlier, one of the prime requisites for controlled dendritic growth is a suitable seed. The basic requirements of a suitable seed are: (*a*) it contains at least two twin planes, and (*b*) the crystallographic orientation is that shown in Fig. 2. Seeds with these requirements could be cut from ingots; however, it is extremely difficult to find an ingot with the desired number of closely spaced twins. Dendrites themselves are used as seeds; the initial dendrite seed is obtained by growing primitive dendrites. These can be grown by plunging a single crystal, or even a polycrystalline, seed into a highly supercooled melt and rapidly withdrawing the resulting mass. The relatively cool seed and the highly supercooled melt give the necessary degree of supercooling to force growth to start on the seed by two dimensional nucleation. As the button grows, twin lamellae are produced, generally more or less perpendicular to the growing interface. Some of the twin lamellae grow out from the main mass to give primitive dendrites. Polished and etched cross sections of these primitive buttons were studied to determine which lamellae resulted in primitive dendrites. It was not possible to determine the mechanism by which twin lamellae were produced; all that can be said is that under such drastic conditions the growth rate and the thermal gradient would be in the proper range for the formation of twins as given by Bolling, Tiller, and Rutter (8). Twin lamellae produced in this manner must be composed of an even number of twin planes to satisfy the surrounding orientation relationship. Only seldom will a single twin be generated, and in such cases a grain boundary is found to start at the twin origin to satisfy the orientation relationship. One would expect that only dendrites containing an even number of twin planes would result; however, occasionally two or more lamellae that are close together will lose one twin to give a dendrite with an odd number of twin planes. A twin may be lost by intersecting a grain boundary or another twin boundary along one of the other {111} planes; or, if one lamella is very wide, the "outside" twin plane becomes lost at the surface as the dendritic projection shoots out. At least one example of each has been observed in primitive buttons.

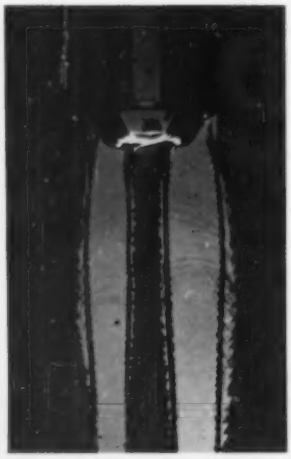

Fig. 1. Germanium dendrite. A, seed; B, growth button; C, wing; D, dendrite.

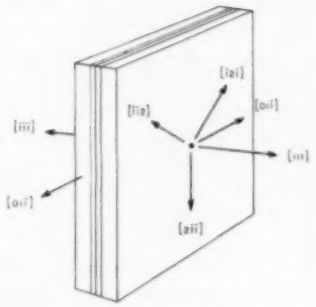

Fig. 2. Orientation relationships in a diamond-like lattice dendrite with three twin planes.

Figure 3 shows a part of one of the sectioned primitive buttons showing the twin lamellae bounded by two twin planes and one lamella (marked A on Fig. 3) that resulted in a primitive dendrite. The thickness of the twin lamellae in the button varied greatly, from approximately ¼ μ to 70 μ. As one can see in the photomicrograph, many more twin lamellae are produced than result in primitive dendritic growth; presumably the growth rate is initially so high as a result of the high degree of supercooling that it is only after the thermal conditions have approached a steady state that the easier nucleation at re-entrant corners is effective.

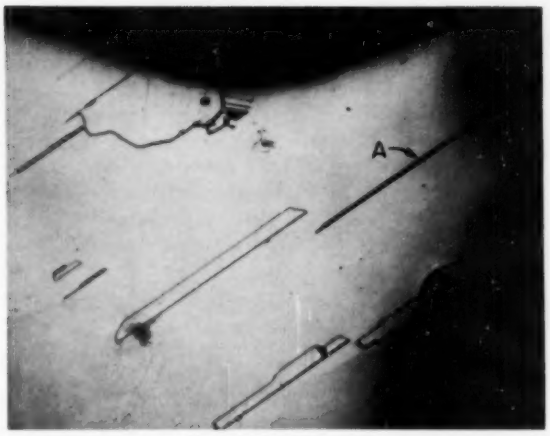

Fig. 3. Cross-section of a primitive growth button. Polished and etched.

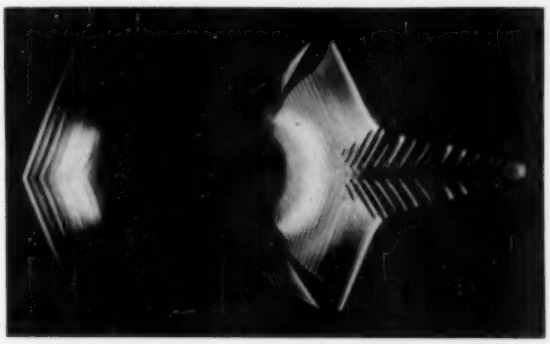

Fig. 4. Unetched top of a growth button showing terraces

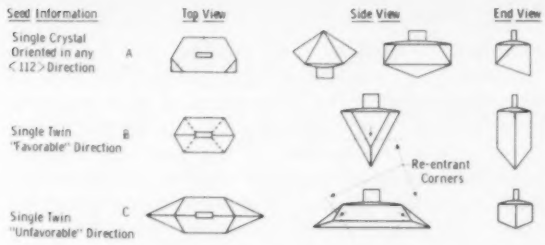

Fig. 5. Drawings of growth buttons

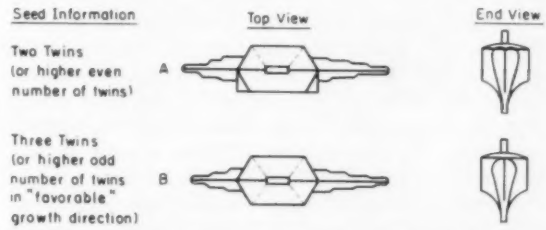
Seed Information
Top View
End View
Two Twins (or higher even number of twins)
A
Three Twins (or higher odd number of twins in "favorable" growth direction)
B

Fig. 6. Drawings of growth buttons which result in ribbon growth.

Furthermore one finds that there appears to be a maximum twin spacing beyond which dendritic growth cannot take place.

To study the twin spacings that actually resulted in primitive dendritic growth, the dendrites, themselves, (approximately 80 primitives) were fractured (9) and examined. Of the particular dendrites grown from normally doped melts, approximately 85% contained two twins, 7.5% three twins, and 7.5% four twins.[2] The twin spacings ranged from $\frac{1}{4}\mu$ to 35μ, with the most probable value being approximately 5μ. Highly doped melts influenced the growth of primitive dendrites by yielding 35% with three twin planes and 65% with two twin planes and by shifting the most probable value of the twin spacing to approximately 11μ.[3] Other requirements for good seed material will be discussed later.

Growth Button Studies

Upon dropping the power input to the crucible to give the desired degree of supercooling, the temperature at the surface of the seed in the melt starts to drop. As soon as the molten material around the seed has become supercooled enough, two dimensional nucleation takes place at the surface of the seed and a button starts to grow. The growth of the button proceeds outward from the seed in all possible <111> directions resulting in a highly faceted button. The top of the button is not a single facet but is terraced by {111} planes, as illustrated in Fig. 4. This terraced structure comes about as a result of the layer growth on the side facets being stopped by the meniscus before it can grow to complete the top {111} surface. As will be shown later, the button growth does not extend very far below the surface of the melt; the full button is not realized until it is pulled from the melt.

The shapes of the buttons are very significant. They fall into three basic classes, shown in Fig. 5, which do not result in dendritic growth and into two classes, shown in Fig. 6, which do result in dendritic growth. Line "A" shows the distorted octahedron that results when a single crystal seed oriented in any of the <211> directions is used. As can be seen the limiting form contains seven of the eight possible {111} planes; the eighth would be the top which is terraced, for reasons given above, rather than smooth like the others.

If the seed contains a single twin plane, the shape of the button depends on the orientation of the seed. Line "B" shows the shape of the button resulting from the seed oriented so that the $[2\bar{1}\bar{1}]$ direction, referred to as the "favorable" direction,[4] points into the melt while line "C" shows the button resulting from the seed oriented in the opposite, or "unfavorable," direction (*i.e.*, $[\bar{2}11]$). The size of the button is determined by the extent to which growth along the surface of the melt is permitted before pulling is started. As the uncompleted button is pulled from the melt, growth continues to fill out the {111} facets already started,

[2] A recent tabulation by A. I. Bennett and J. Meingailis (Westinghouse Research Laboratories) of twin spacings in a larger number of primitive dendrites has also shown that there were more even-twinned primitives than odd-twinned primitives, but the ratio was not nearly so great as quoted here.

[3] We are indebted to Mr. G. R. Booker (Westinghouse Research Laboratories) for permitting us to use his data on the number and the spacing of the twin planes.

[4] The "favorable" and "unfavorable" directions can be found by etching the seed with a preferential etch that reveals {111} planes, such as the WAg (HF:HNO_3:5% aq. soln. $AgNO_3$) or the potassium ferricyanide etch. For these etches, the triangular pits point toward the "unfavorable" direction and away from the "favorable" direction.

and buttons bounded only by planes, ridges, and points result. The dashed lines on the side views of the buttons, Fig. 5, show the position of the re-entrant edges at one stage during growth; the arrows indicate the direction that the re-entrant edges move during growth. It should be noted that the re-entrant edges grow out into points. A more complete discussion of this can be found elsewhere (6, 7). The points, ridges, and faces are all sites of difficult nucleation; since no sites of easy nucleation are perpetuated in any of the three cases, directionally extended (ribbon) growth is impossible.

For a seed containing two or more closely spaced twin planes continuous across its entire cross section, as illustrated in Fig. 2, it is found that the twin configuration is grown into the button. The presence of the additional twin plane, or planes, produces a button that cannot be completely bounded by planes, ridges, and points. Two or more twin planes insure the presence of at least one self-perpetuating re-entrant edge (6, 7). As the button grows, along the surface of the melt the thermal conditions approach a steady state; at this point the easy nucleation at the re-entrant edges predominates and growth in the form of "wings" rapidly proceeds outward in the <110> directions. These wings are in reality <110> dendrites. When pulling is started, the <211> dendrites invariably grow from these wings shown in the button drawings of Fig. 6. The wings on the buttons containing an even number of twin planes have a groove running along the top at the intersection of the twin planes with the top of the wings while wings on buttons containing an odd number of twin planes do not. The buttons, themselves, are characteristic for odd and even number of twin planes. One half of an even-twinned button (line "A", Fig. 6) has the morphology of a single twin button grown in the "favorable" direction and the other half in the "unfavorable" direction. Odd twin buttons have their morphology similar to those with a single twin (compare line "B", Fig. 6 with line "B", Fig. 5). The exact shape of the lower part of these buttons varies considerably depending on the thermal conditions.

Seeding Studies

Even when the basic conditions for seeds are met, not all seeds can be used to grow dendrites. It was found that continuity of the twin structure across the cross section of the seed was important. Figure 7 shows some of the twin structures in seeds used to grow buttons. The fact that wings and dendrites

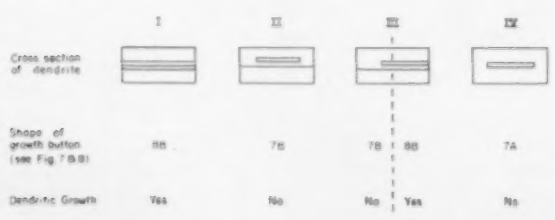

Fig. 7. Summary of the dependence of growth button shape and dendritic growth on twin lamellae continuity (Seed in the "favorable" direction).

can be grown from a seed that has the cross section shown by case I has already been mentioned for both odd and even twin spacings. The twin structures in cases II and IV are termed degenerate and will result in buttons of the single twin and single crystal form, respectively. A seed with the twin structure degenerate on only one side, case III, will yield a button with only one wing and thus one dendrite. The side of the button that has the wing is under the side of the seed that has the twin structure continuous to the edge while the other half of the button has the appropriate form from Fig. 5.

Seeds and growth buttons from these studies were potted and successively polished and etched to follow the course of the twin structures. The twin structure grew into the button in all cases. Where the seed contained a completely degenerate lamella however (II and IV in Fig. 7), the width of the degenerate lamella (but not the spacing between the twin planes) decreased and vanished within the button while the button was being pulled from the melt. Since the degenerate lamella does not vanish when formed while the ribbon is growing, the importance of the re-entrant edges at 60° to the dendritic axis in the growth of the dendrite itself is evident. The presence of these re-entrant edges supports the suggestion by Hamilton and Seidensticker (7) that the growing tip of the dendrite is faceted.

Growth of the Dendrite

The number and spacing of the twin planes in a seed whose twin planes are continuous across the entire cross section (or else degenerate on only one edge) are retained in the button and the resulting ribbon. Furthermore, at the start of the growth of the dendrite, the twin configuration is continuous across its entire cross section. Thereafter the growth conditions may become such that the twin lamellae could degenerate at one or both edges giving cross sections such as II, III, or IV in Fig. 7. The growth conditions that affect the continuity of the twin configuration will be taken up elsewhere (10). Unlike the buttons grown from seeds with such degenerate twin configurations, the dendrite will continue to grow when the twin spacing has become degenerate. Studies of fractured cross sections (9) of many dendrites have shown that: (*A*) the width of the completely enclosed lamellae may be as small as 10μ and still have dendritic growth; (*B*) changes in the width of enclosed lamellae can be quite abrupt, narrowing by an order of magnitude in less than one eighth of an inch of growth; (*C*) for dendrites having a pronounced wide and narrow face and twin structure II in Fig. 9, the single twin plane jogs off toward the narrow face.

These observations cannot be explained satisfactorily by the screw dislocation mechanism of Billig (5), the single twin mechanism of Bennett and Longini (4), nor the growth sequence of Wagner (6). From (*A*) above it is obvious that the twin structure responsible for the downward propagation of the ribbon, is continuous only across the advancing tip of the ribbon. The downward

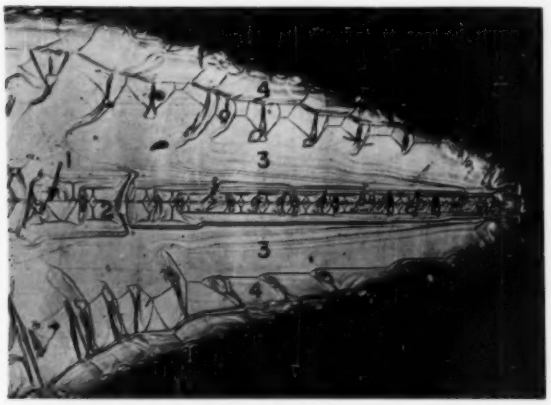

Fig. 8. Etched cross-section of highly doped button

Fig. 9. Etched cross-section of highly doped button showing core of ribbon in the wing. (arrow)

propagation proceeds as a result of the re-entrant edges at these twin planes (6, 7). The lateral growth of the ribbons, however, must proceed independently of the twin planes to account for (*A*), (*B*), and (*C*) above. The mechanism by which this takes place will be discussed in paper (10).

In treating dendritic growth theoretically, one usually assumes that the critical part of the dendrite is already formed. Such an assumption corresponds to a method of seeding whereby dendritic growth takes place directly onto the seed without going through button formation. The problem of how and where the dendrite, or embryonic dendrite, is formed in the button method of seeding is difficult to treat theoretically, but can be explained from studies of the internal structure of buttons containing wings. It has already been pointed out that the wings, in reality <110> dendrites, are the source of ribbon growth. Figure 8, shows a cross section of a highly doped button near the top of the button, *i.e.*, very close to the surface of the melt. The technique of studying highly doped dendrites will be taken up in detail in (10). The similarity of the structure around the twins in the wing to that in a comparable section of a ribbon will be apparent on comparing Fig. 8 to Fig. 2 in paper II. In each, one finds that the twins 1 are confined to a thin layer 2, which is distinct from the layer 3, on either side of 2. Figure 8 has regions 4, which show the faceting on the wings corresponding to the button facets.

When pulling is started, the core[5] of the dendrite forms within region 2 of Fig. 8, and dendritic growth proceeds from this core. It has not been possible to determine the conditions that govern the exact position of core formation on the twin structure along the underside of the wing. By successive polishing and etching of highly doped buttons containing seed, wings, and dendrite, it was possible to follow the core of the dendrite into the wing to determine its origin. It starts close to the surface of the melt, within 10 mils, showing that the button and wing growth before pulling starts does not go much below the surface of the melt. Figure 9 shows part of a section through the wing at a distance of approximately 20 mils below the surface of the melt.

The wing formed at the surface is wider and broader than the resulting dendrite. As pulling commences and the core forms[6] and grows into a dendrite, the thermal conditions are altered drastically. Growth downward from the rest of the wing takes place (this growth surrounds the dendrite core in Fig. 9). The underside of the wing becomes narrower and thinner. At thermal steady state the downward wing growth ceases and the dendrite continues with the width and thickness set by the thermal conditions and pull rate.

Summary

1. Evidence from the growth of buttons and ribbons that have a degenerate twin lamella support the suggestion that the advancing tip is faceted by {111} planes.

2. To insure ribbon growth from the button method of seeding, seeds must have twin lamellae continuous across the entire cross section or else degenerate on only one side.

3. The twin lamellae must be continuous only across the advancing tip for continued ribbon growth.

4. Primitive dendrites grow from growth buttons in a highly supercooled melt by the generation of twin lamellae at the advancing growth front of the button, producing more even-twin groupings than odd-twin groupings.

5. Ribbon growth starts very near the surface of the melt by the formation of a core on the underside of the wing when pulling commences.

6. Dendritic growth takes place in at least two stages: downward propagation which is dependent on the twin planes, followed by lateral growth proceeding independently of the twin planes.

Acknowledgments

The authors are indebted to Drs. A. I. Bennett, W. J. Smith, and S. O'Hara for growing the den-

[5] The significance of the core and cross-section studies of highly doped dendrites will be taken up in paper II (10).

[6] Bolling and Tiller (AIME Symposium, Boston, Aug. 1960) have shown, in a theoretical explanation of dendritic growth, how a dendrite can form from a flat plate containing the necessary closely spaced twin planes normal to it. The core formation on the underside of the wing corresponds closely to their model.

drites used in this study; to W. J. Smith for observational data on the growth of dendrites and for permitting the authors to use a furnace to observe button formation and initial growth. They also wish to acknowledge the able assistance of Mrs. H. Larson and Miss S. A. Warner for the metallographic preparation of specimens. This work was supported in part by the Wright Air Development Division of the Air Force.

Manuscript received Jan. 30, 1961; revised manuscript received May 4, 1961. This paper was prepared for delivery before the Chicago Meeting, May 1-5, 1960.

Any discussion of this paper will appear in a Discussion Section to be published in the June 1962 JOURNAL.

REFERENCES

1. E. Billig, *Proc. Roy. Soc.*, **A229**, 346 (1955).
2. E. Billig and P. J. Holmes, *Acta Cryst.*, **8**, 353 (1955).
3. E. Billig and P. J. Holmes, *Acta Met.*, **5**, 53 (1957).
4. A. I. Bennett and R. L. Longini, *Phys. Rev.*, **116**, 53 (1959).
5. E. Billig, *Acta Met.*, **5**, 54 (1957).
6. R. S. Wagner, *ibid.*, **8**, 57 (1960).
7. D. R. Hamilton and R. G. Seidensticker, *J. Appl. Phys.*, **31**, 1165 (1960).
8. G. F. Bolling, W. A. Tiller, and J. W. Rutter, *Can. J. Phys.*, **34**, 234 (1956).
9. J. W. Faust, Jr. and H. F. John, *This Journal*, **107**, 562 (1960).
10. J. W. Faust, Jr. and H. F. John, *ibid.*, **108**, 860 (1961).

Germanium Dendrite Studies

II. Lateral Growth Processes

J. W. Faust, Jr. and H. F. John

Research Laboratories, Westinghouse Electric Corporation, Pittsburgh, Pennsylvania

ABSTRACT

Growth processes in germanium dendritic ribbons have been studied by metallographic techniques. It is shown that the formation of a ribbon is a complex process involving the lateral extension of arms from the central core to give, at one stage, an H-shaped cross section. Segregation effects between the H-arms can be used to produce p-n junction configurations. Some comparisons are made between dendrites of highly doped and normally doped Ge. The factors which affect the continuity of the twin structure are also discussed.

In the first paper of this series (1) the authors discussed the early stages in the formation of a dendritic ribbon, including seeding mechanisms, growth button formation, and the development of the initial dendritic growth onto the button. The reader is referred to this paper for references to prior work in the field of dendritic growth in diamond lattice and zinc-blende materials. In this paper we will discuss lateral growth processes in dendritic ribbons and show that lateral growth is not dependent on the twin structure.

Experimental

Much of the information presented here was obtained from studies of etched cross-sections and the wide {111} faces of ribbons. Metallographic studies of highly doped Ge and Si dendrites have proven to be particularly informative. The term "highly doped" is used here to refer to concentrations of doping impurities greater than about 10^{18} cm^{-3}. In this concentration range the action of many conventional semiconductor etchants becomes very sensitive to differences in impurity concentration. During the growth of a dendritic ribbon, segregation and pile-up of impurities occur. Since etching reveals these concentration differences, the growth processes can be inferred in a fairly straightforward way from the segregation pattern shown up by etching. Dendrites doped with As, Sb, and B are known to exhibit these etching effects; presumably dendrites containing other dopants in high concentration will do so too.

The cross-sectional samples shown later were prepared for etching by conventional metallographic techniques. The specimen was mounted in a plastic mold, sectioned, and polished with successively smaller abrasives, finishing with a Linde B polish. A 3-10 sec CP4 etch[1] was used most frequently. An etch composed of 3 parts of 48% HF, 1 part conc. HNO_3, and 1 part glacial acetic acid was also used occasionally. Its action is quite similar to, but somewhat slower than, that of the CP4. Segregation traces were revealed on the wide {111} faces of dendrites by a 5-10 sec CP4 or by a 10-45 sec etch with the 3:1:1 solution. The etching attack on the natural {111} faces appears to be somewhat more sensitive to concentration differences than etching attack on polished cross sections. For example, segregation traces can be shown quite easily on the natural {111} faces of normally doped dendrites, whereas heavily doped specimens are necessary to obtain any detailed pattern from a cross section.

Results and Discussion

The photomicrographs shown in Fig. 1 illustrate the type of information which can be obtained from etching highly doped dendrites. These sections, both from the same dendrite, were taken perpendicular

[1] Composition: 25 parts conc. HNO_3, 15 parts glacial acetic acid, 15 parts 48% HF, and 0.3 parts bromine.

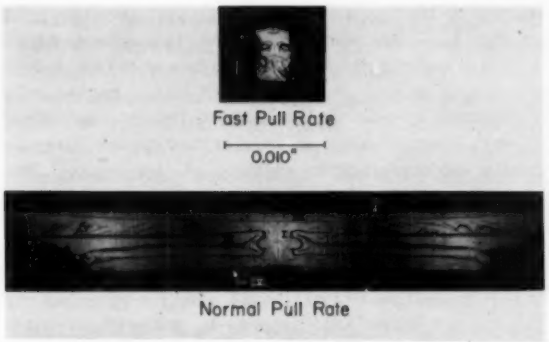

Fig. 1. Etched sections of a Ge dendrite perpendicular to the growth direction and taken from regions of different pull rate.

to the growth axis. The upper section is from a region pulled at about 10 in./min, the lower section is from a region pulled at about 6 in./min. The similarity of the fast-pulled section to the central region of other section suggests that the former did not have time to grow out laterally to any extent because of the relatively fast pull rate. Externally the lower section exhibited a typical, good quality ribbon structure.

Four regions with distinct etching characteristics are present in the lower photomicrograph. Region I, the central core, contains the twin planes which are revealed as two closely spaced lines in the center of the core. This dendrite contains three twin planes, only two of which are revealed by etching. The reasons for this effect have been discussed (2). The functional twin structure in the lower section is confined to the core region. The lines in the core region perpendicular to the twin planes are segregation traces. The configuration of the segregation traces varies with the number and spacing of the twins, as well as on growth conditions (3-5).

Region II is one of four such areas extending in either direction from the top and bottom of the core region in such a way as to form an H-shaped cross section. The rather irregular etching probably indicates an unstable segregation front resulting from the very rapid growth. The arms developed in this particular case to give a cross section which is somewhat concave outward.

Region III froze after the lateral arms were formed. The smoothly etched nature of this region, together with the deeply etched groove along the center line, indicates that this region froze inward in a regular way from the lateral arms, segregating impurities toward the center.

Region IV is composed of surface growth layers, added during the outward growth of, or after, the lateral arms have formed. In cases where the lateral arms do not form perfect {111} faces, these surface growth layers are always present and serve to produce a nearly perfect {111} surface on both wide faces of the dendritic ribbon. In cases where the lateral arms themselves form nearly perfect {111} faces, these surface layers are much less pronounced and may not be present at all.

Figure 2 shows an etched section taken parallel to the growth direction, about half way between the

Fig. 2. Etched section of a Ge dendrite parallel to the growth direction.

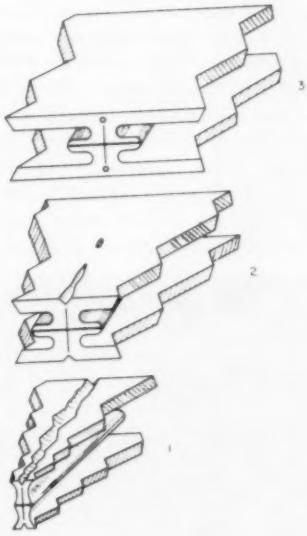

Fig. 3. Schematic views of a Ge dendrite at different stages in its growth.

outer edge and the core. In this dendrite the central twin region grew all the way out to the outer edge, in contrast to the example shown in Fig. 1. Again, externally this dendrite exhibited a good ribbon structure. It can be seen that the twins, 1, are contained in a thin layer, 2, about 0.002 in. thick, which seems to be distinct from a uniformly etched layer, 3, on either side of this central structure. Between region 3 and the lateral arms 5 is a region 4 which froze inward from both the lateral arms and the central core. The last region to freeze is more highly doped and has a more unevenly etched appearance.

From the information available in etched cross sections, as in Fig. 1 and 2, the development of a dendritic ribbon has been reconstructed in the somewhat schematic drawing shown in Fig. 3, which shows three stages in the formation of the ribbon be-

low the surface of the melt. The first sectional view shows the dendrite within a very few thousandths of an inch of the extreme tip. It should be recalled that the dendrite is being propagated rapidly downward by means of the nucleation in the indestructible re-entrant groove produced by the twin planes (6, 7). In this drawing the twins are represented by the heavy line in the center of the cross sections, which are drawn with the general configuration encountered with an odd number of twins. In the first cross-sectional view the dendrite has assumed a somewhat cruciform cross section and has achieved most of its final thickness before appreciable lateral growth has begun. The first sectional view shows small facets developing on the outer edges of the part of the core structure perpendicular to the twins. They are bounded by {111} planes, and the re-entrant corners formed by this series of facets provide nucleation sites. The availability of such nucleation sites allows the outward propagation of arms to give an H-structure as shown in the other two cross sectional views. These arms correspond to region II in Fig. 1 and region 5 in Fig. 2. The heat rejected by the outward growing arms, as well as the rejection of impurities into this region, causes the core to lag behind the H-arms. The presence of the H-arm structure has been confirmed directly by the decanting experiments of Bennett and O'Hara (8).

It is easier to get rid of the heat of crystallization at the outer edges of the facets, which form on the core, than it is in the middle of the face which is formed by these facets. This situation tends to cause the development of an unfilled region down the spine of the dendrite, represented somewhat diagrammatically by the groove in sectional views 1 and 2 of Fig. 3. Under some conditions, the groove which forms is sufficiently deep that layers will freeze over the top of it, trapping pockets of liquid periodically (indicated by the circles in the third cross sectional view). When this liquid freezes, it expands, causing plastic deformation in vicinity of the pocket. The characterization of the dislocation arrays which are sometimes found in dendrites will be covered in the third paper of this series (9).

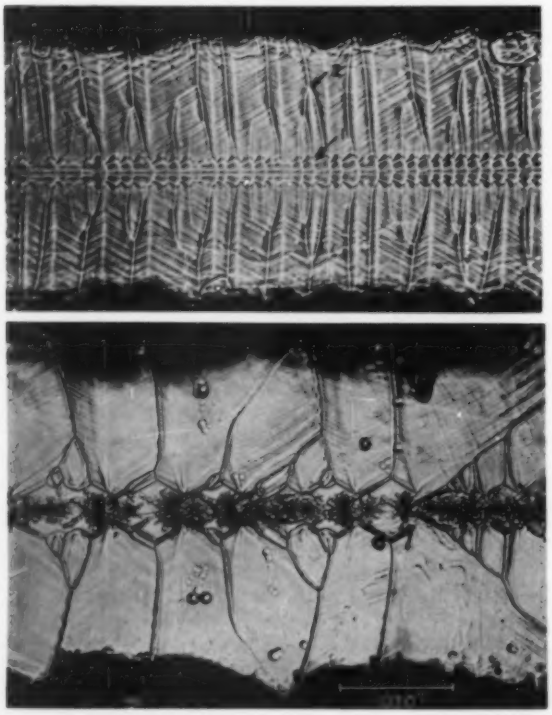

Fig. 4. Etched {111} face of a normally-doped (a) (top) and a highly-doped (b) (bottom) Ge dendrite. Pull direction is to the right.

The way in which the arm structures grow outward from the initial facets can be revealed by etching the wide {111} faces or by pulse electroplating (10). Figure 4a shows an etched {111} face of a normally doped dendrite etched for 15 sec in a CP4 etch. Figure 4b shows an etched {111} face of a highly doped dendrite, also etched for 15 sec in CP4. Both types of dendrites exhibit much the same structure; however details are clearer in the highly doped specimens because of the more selective etching attack. The growth fronts parallel to the original core facets can be discerned clearly. Also the growth front systems originating at some of the re-entrant corners, such as 1 on Fig. 4a, are overwhelmed by neighboring growth front systems, as at 2, to give larger re-entrant corners. Smith (10) has discussed this process in detail and the significance of the segregation traces originating at the peaks and valleys of the core serrations.

In melts with very high impurity content, segregation would be expected to play an important role in the growth processes; however, the structure on the {111} faces of normal and highly doped dendrites show that the main features of growth are the same for both types of ribbons. Other similarities in structure and dislocation arrays support this view. Further evidence has been obtained from studying the surface etch patterns in normally doped dendrites at different distances from the {111} faces.

Surface etch patterns were used to estimate the thickness of the H-arms in normally doped dendrites. A pattern, similar to that shown in Fig. 4a, remained relatively unchanged after 0.0006 in. had been removed from each {111} face of a normally doped dendrite whose initial thickness was 0.0061 in. Some trace of the pattern could still be seen after 0.0016 in. and none after 0.0020 in. had been removed after from each face. Thus the H-arms on each face were no thicker than 0.0020 in.

An example of a third general type of twin structure is shown in Fig. 5. Under these conditions of growth, the twins grew laterally much further than the main body of the dendrite. This structure is in contrast to those shown in Fig. 1 and 2, where the twins were confined to the core region or later grew out to the edge of the H-arms. Conditions which produce thick dendrites with the growth of the H-arms developing relatively far from the twins

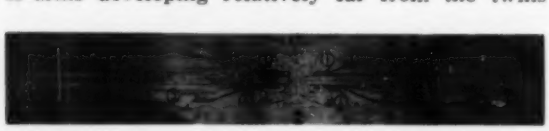

Fig. 5. Etched section of a Ge dendrite showing considerable lateral extension of the twin structure.

would appear to be favorable for this type of growth, since the heat rejected by the initial faceting and subsequent lateral growth is too far away, or too easily removed, to inhibit the lateral extension of layer containing the twin structure. However, it has not been established clearly which is cause and effect. This cross section has basically the same features as Fig. 1; however considerable distortion is noted. The H-arm regions, 1, are poorly developed and extend only a short distance. Pockets, 2, have been trapped along the spine of the dendrite. Four regions of high segregation, 3, are present.

The continuity of the twin structure is worth additional comment. The lateral extension of the twin structure is very sensitive to the conditions under which the dendrite was grown, in extreme cases being limited to the core region itself (Fig. 1) or extending under other conditions well beyond the main body of the dendrite (Fig. 5). In other dendrites the twin structure may extend all the way to the edge of ribbon with no indication of any projection beyond the main body of the dendrite. The whole range between these extremes has been observed in both highly doped and normally doped dendrites, although it is relatively rare to find in normally doped specimens the extreme types shown in Fig. 1 and 5. In dendrites where the twin structure goes all the way, or most of the way, to the edge, it is believed that lateral extension of the twins takes place after the development of the H-arms. For normally doped dendrites, if the temperature gradient is uniform and not too severe in the last stages of freezing, the lateral extension of the twinned region apparently proceeds readily between the H-arms to the edge. On the other hand, if the cooling is too fast or the temperature gradients are asymmetric in the final stages, the twin structure will proceed only part of the way to the edge.

It has been observed that when an odd-twin structure is terminated the boundary so formed (consisting of short segments of single coherent twin planes connected by incoherent twin planes) invariably jogs off toward the narrow face of the dendrite. One face being somewhat wider than the other is indicative of an asymmetric temperature distribution in the melt, the wider side being in a slightly cooler region. Thus when the final freezing-in between the H-arms occurs, solidification takes place somewhat more rapidly from the cooler side; consequently, the original twin structure is pinched off and a single-twin boundary, usually irregular, is formed but is displaced toward the warmer, i.e., narrower, side of the dendrite.

The way in which the dendritic ribbons develop has suggested it should be possible to grow p-n configurations into the ribbons, if a double-doped melt is used which contains one doping impurity which is readily segregated and one doping impurity of the opposite conduction type which is less readily segregated. In such a case, it would be expected that the core and H-arms would have the conductivity type of the less readily segregated impurity and the regions between the H-arms would have the conductivity type of the more readily segregated impurity. Both n-p-n and p-n-p "three-zone" ribbons have been produced in the predicted configuration. "Five-zone" structures have also been produced under conditions where the lateral extension of the twin structure produces a heavily segregated region on both sides of the central twin structure.

The growth features discussed above for Ge dendritic ribbons have been confirmed for Si dendrites through etching studies on highly doped specimens. In the case of dendrites of III-V intermetallic compounds no metallographic studies on highly doped specimens have been made yet; however, it can be inferred from similarities in external features, twin structures, twin terminations, and dislocation arrays that the growth proceeds in the same way for these materials (11, 12).

Summary

The growth of dendritic ribbons of diamond lattice materials is a process which involves the extension of lateral arms parallel to, but independently of, the central twin structure which is instrumental in propagating the dendrite rapidly downward. Many of the characteristic features of dendritic ribbons can be traced to this rather unusual widening process. Certain dislocation arrays are shown to arise from pockets of liquid trapped during the initial faceting which precedes the growth of the lateral arms. It is pointed out how p-n configurations can be grown into the ribbon by using the regions of heavy segregation produced by the outward growth of the lateral arms.

Acknowledgment

The authors wish to thank Dr. A. I. Bennett and Dr. S. O'Hara for supplying them with the dendrites used in this study, as well as Mrs. H. Larson and Miss S. A. Warner for assistance in preparing the sections. This work was supported by Government Contract Number AF33(600) 39378 (Wright Air Development Center).

Manuscript received Jan. 30, 1961; revised manuscript received May 4, 1961. This paper was prepared for delivery before the Chicago Meeting, May 1-5, 1960.

Any discussion of this paper will appear in a Discussion Section to be published in the June 1962 JOURNAL.

REFERENCES

1. J. W. Faust, Jr. and H. F. John, *This Journal*, **108**, 855 (1961).
2. J. W. Faust, Jr. and H. F. John, *ibid.*, **107**, 562 (1960).
3. F. Bolling and W. A. Tiller, AIME Symposium on Properties of Elemental and Compound Semiconductors, Boston, 1960. In press.
4. S. O'Hara, AIME Symposium on Properties of Elemental and Compound Semiconductors, Boston, 1960. In press.
5. J. W. Faust, Jr., H. F. John, and S. O'Hara, Unpublished information.
6. R. S. Wagner, *Acta Met.*, **8**, 57 (1960).
7. D. R. Hamilton and R. G. Seidensticker, *J. Appl. Phys.*, **31**, 1165 (1960).
8. A. I. Bennett and S. O'Hara, *Bull. Am. Phys. Soc., Series II*, **5**, 165 (1960).
9. J. W. Faust, Jr. and H. F. John, *This Journal*, **108**, 864 (1961).
10. R. C. Smith, *ibid.*, **108**, 238 (1961).
11. J. W. Faust, Jr., H. Nicholson, and R. Moss, *ECS Electronics Division Abstracts*, **9**, *No. 1*, p. 165 (1960).
12. R. H. Moss and H. Nicholson, Electrochemical Society Semiconductor Symposium, May 2, 1960 (Recent News Paper).

Germanium Dendrite Studies

III. Dislocations

J. W. Faust, Jr. and H. F. John

Research Laboratories, Westinghouse Electric Corporation, Pittsburgh, Pennsylvania

ABSTRACT

The dislocation arrays in germanium dendritic ribbons are described. It is shown that there are three main areas where dislocations can occur. The sources of these dislocations were found to be entrapped molten germanium which on freezing causes plastic deformation. The arms of the central star patterns were found to consist of dislocation half loops.

In the first two papers (1, 2) of this series, the authors discussed the initiation and propagation of dendritic growth. It was shown how the dislocations are produced during dendritic growth as a consequence of the entrapment of liquid Ge during the development of the dendrite. It is the purpose of this paper to discuss the crystal perfection of the dendrites in more detail and to describe the dislocation arrays which arise when dendritic ribbons are not pulled under carefully controlled conditions.

Billig in his original paper (3) noted that the unetched dendrites contained hillocks and, occasionally, hollows along a line down the center of the faces. The hillocks, some of which were triangular with flat tops, were presumed to be growth platelets. Later (4) it was pointed out that the triangular hillocks were made up of smaller triangles and were associated with slip during growth. Bennett and Longini (5) reported that hillocks were found occasionally, some of which showed faults which they ascribed to slip occurring after growth while the dendrite was cooling.

Upon etching the dendrites, Billig (3) and Bennett and Longini (5) both found a narrow band of dislocations running along the main faces of the dendrites. The central band was often made up of star-like patterns. Billig (3) believed that these patterns were the starting point for the growth hillocks; while Bennett and Longini (5) mentioned that these patterns were suggestive of inclusions of foreign matter. Billig and Holmes (6) examined further the dislocations in their germanium dendrites by etching polished cross sections and dendrites that had been lapped parallel to a face to expose the twin lamella. They reported that the material in the lamella between the twin planes was very perfect, being devoid of etch pits, but the remainder of the dendrite was heavily pitted. They suggested that the central stripe of dislocations starts as small clusters at the twin planes and develop outward, finally assuming a characteristic pattern at the surface. They also postulated that other dislocations originated at the twin planes. These investigators (5, 6) used the WAg etch for revealing dislocations, apparently presuming that this etch acts only on dislocations at a surface.

The authors have shown (2) that dislocations in germanium dendrites are produced when pockets of molten germanium, trapped during growth, freeze while the germanium is still in the plastic deformation range. They showed how the pockets which give the central stripe of dislocations are produced during the initial faceting which precedes the growth of the lateral arms. It was shown further that pockets which produce the dislocations along the edges form between the lateral arms which give an H-shaped cross section at one stage in growth. The CP4 etch on polished cross sections of highly doped dendrites has revealed the frozen droplets, while direct examination of the surfaces near the tip has revealed the groove where the molten germanium could become trapped.

Comments on Etch Pitting

It has been shown (7) that the WAg etch does indeed form pits at dislocations; however, being a preferential etch, pits form at other sites on the surface (8). There is also a lesser attack over the entire surface producing small, shallow, dish-shaped triangles. The latter attack Billig (3) described on the dendrites as giving the appearance of a "crazed" surface.

The reliability of dislocation studies depends on the ability to distinguish between the pits produced by the various causes and in being able to see all of the dislocation pits. The triangular pits produced by the WAg or the ferricyanide etch on {111} surfaces point in the $<\bar{2}11>$ directions as Bennett and Longini (5) correctly show rather than the $<2\bar{1}\bar{1}>$ directions as reported by Billig (3). Pits formed at dislocations by these etchants can be identified easily from others on {111} surfaces since they are completed pyramidal pits; however, it is not possible to distinguish between dislocation pits and other pits on {211} surfaces. Pits, however, that initially formed at dislocations lose their full pyramidal character by becoming truncated when the dislocation has left the confines of the pit, such as happens in the case of dislocation half loops. It is usually not possible to distinguish these pits from the purely crystallographic pits formed from other causes. Billig (3) states that only rarely were the triangular

pits on the etched faces of his dendrites fully developed pyramids; thus for lack of further evidence, it must be assumed that many of the pits reported by Billig and Holmes (6) did not show the presence of dislocations. A further difficulty with this type of etchant is that, for dislocation clusters of at least $10^6/cm^2$, the pits overlap so much that erroneous and often absurdly low dislocation densities are obtained. Holmes (9) states that the side planes on pits produced by these etches are much shallower than {111} planes. This is correct for pits at dislocations, as explained by Faust (8); however, the sides of the truncated pits, formed at places other than dislocations, are {111} planes (7, 10).

Experimental Procedures

In order to obtain as complete a picture as possible of the perfection of dendrites, a piece was removed carefully by the fracturing technique (11) from a large number of dendrites grown under various conditions. These specimens were etched for 30 to 45 sec with the CP4 to reveal the dislocations. Both faces and the fractured ends were examined for dislocations. Detailed studies to determine the extent of the penetration of the dislocations into the bulk and any change in the dislocation pattern included (*a*) successive etching from one side only completely through sections of dendrites and (*b*) etching samples lapped at a slight angle to a main {111} face, the lapped region extending down through the twin planes. The CP4 was used for all of these studies because it is possible to distinguish between dislocations, pits from which the dislocation has left the confines of the pit, and pits from other causes, even after many successive etchings. Using the CP4, it is also possible to count dislocations in areas of relatively high density. Adjacent sections of dendrites were etched with the WAg and the CP4 for comparison.

General Areas of Dislocations

The number and distribution of dislocations in dendrites can have wide extremes. For example, under adverse growing conditions, the faces of the dendrite may be covered uniformly with a high density of dislocations, or under proper growing conditions, the dendrites will be free of dislocations. The amount of doping seems to have no direct effect on the mechanism for the production of dislocations. When dislocations are present in a dendrite, however, one usually finds them in specific areas. Figure 1 gives a schematic representation of these areas (the lines showing area I have no other meaning than to indicate its relative position). Area I is a central stripe composed of clusters of very high dislocation density. These clusters may be widely spaced or so closely spaced that they form an almost continuous stripe. These clusters can go down as far as the first twin plane as shown at the top of the schematic or only part way down as shown on the bottom of the schematic. We have never found any crossing a twin boundary. The central stripe may be absent on both faces, absent on only one face, or present on both faces. Area II is a more or less uniform distribution of dislocations near the edge of the flat face. It may be present on one or both edges of a face. If it is present on an edge of one face, it is usually found on the same edge of the opposite face, although this is not always true. Area III are pipes of dislocations running parallel to the growth axis between the surface and the first twin boundary. They may be absent or in any or all of the four areas shown in the schematic.

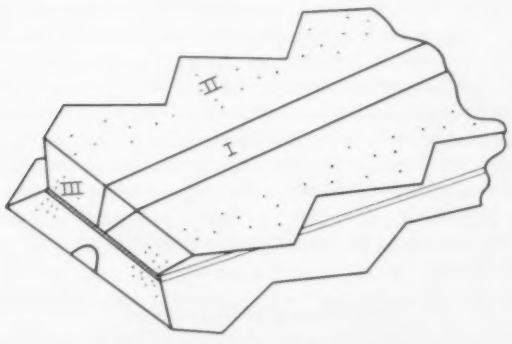

Fig. 1. General areas of dislocations

The Central Stripe

Examination of the unetched surfaces of germanium dendrites often reveals, besides the growth steps (12), hillocks and slip patterns running in a line down the face; in more imperfect growth regions, such as very narrow dendrites, pits instead of hillocks may be found. Figure 2 shows the characteristic shape of the slipped areas and also shows a pronounced hillock (the curved lines running across the photomicrograph are growth steps). This figure also shows that the slipped areas and hillocks are of varying size. The slipped area is made up of many slip lines that cannot be resolved in the photomicro-

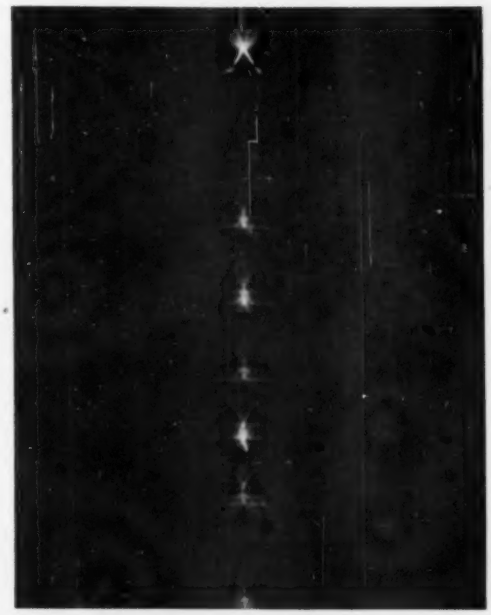

Fig. 2. Slip patterns, hillocks and growth steps on the unetched face of a dendrite.

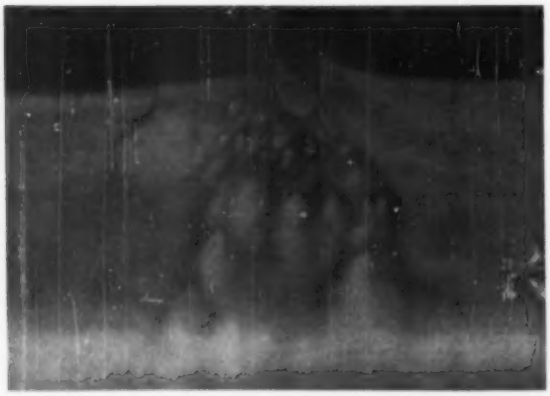

Fig. 3. Part of a fractured and etched cross-section showing the hillock and dislocations. Magnification 500X before reduction for publication.

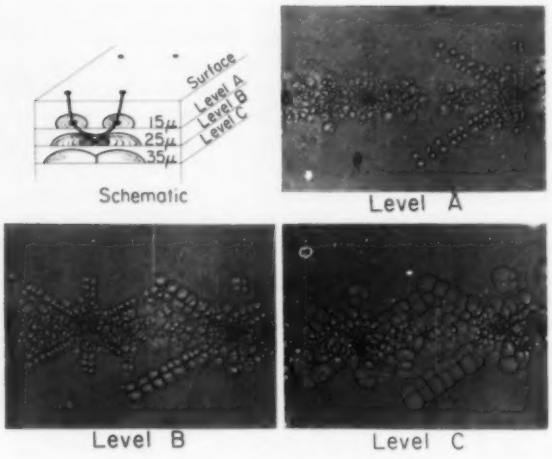

Fig. 4. Evidence for arms of star patterns being made up of dislocation half loops. (A) Schematic with sketches of etch pits at various levels; (B) photomicrograph at level A. Dislocation still in etch pits; (C) photomicrograph at level B. Dislocations in arms have been removed by etching; (D) photomicrograph at level C. Pits in arms beginning to smooth out. Magnification 200X before reduction for publication.

graph. The position of this line relative to the edges of the face depends on the thermal symmetry around the dendrite in the melt. For example, the line will be in the center of the face if the dendrite is pulled vertically from a melt with good thermal symmetry; however, the dendrite will not have good thermal symmetry with respect to the growth direction if pulled at 60° to the vertical, and the line will be closer to one edge.

Upon polishing and etching highly doped cross sections, it is seen that the line of hillocks and slipped areas runs directly over the core and entrapped droplets. On examining numerous cross sections prepared in this manner, one finds various sizes of entrapped droplets which account for various sized hillocks and slip. By repeated polishing and etching of the cross sections one can show that these are, indeed, entrapped droplets and not a continuous "rod." When the dendrites are etched to reveal the dislocations, and photomicrographs of the same area, etched and unetched, are compared, one finds that each hillock and slipped area is the site of a cluster of dislocations, but that there are usually more clusters than there were visible hillocks. Further evidence for the association of entrapped droplets, hillocks, slip, and dislocations was obtained from etching of fractured cross sections. Figure 3 shows part of a cross section that was fractured through one of the more severe hillocks and then etched. The hillock can be seen plainly. The area between the hillock and the twin lamellae (which shows up as a light streak near the bottom of the photomicrograph) contains dislocations from this severe hillock. Studies of numerous fractured and etched cross sections have shown that many of the clusters, in particular the less severe ones, do not extend down to the twin planes. These observations clearly cannot be explained on Billig's mechanism (6), but can be explained by the entrapped droplet mechanism.

The dislocation clusters that make up the central stripe have several different patterns: (i) no apparent symmetry, (ii) a more or less triangular shape, and (iii) a triangular shape with paired rows of etch pits radiating out from it (the star-like pattern). The size of any one of these types of clusters varies from small to large, although generally those of type (i) are small while those of type (iii) are large. The number of the clusters per unit length of dendrite also varies from zero to such a number that they overlap, forming a continuous central stripe. The width of the stripe generally stays constant, even when the dendrite is made to grow narrower, until the central stripe covers the whole narrow face. By simultaneously narrowing the dendrite and decreasing its thickness, it is often possible to eliminate the central stripe; however, the central stripe reappears when the original conditions are restored.

The area covered by the slip pattern of a particular hillock on the unetched surfaces and by the cluster revealed by etching are the same; however, the arms of the star-like patterns extend beyond the slip pattern. The dislocation density in such areas is high, at least $10^6/cm^2$. The density in some clusters was found to be so high that parts of them were outlined by a lineage line. The arms that make up the star pattern radiate out along slip planes from the highly dislocated area. These arms were studied by sequential etching and found to be dislocation half loops extending into the bulk from 6 to 30μ. Figure 4a shows a schematic representation of a dislocation half loop with the shape of the pit formed by the CP4 etch at various levels from the surface. Figures 4b, c, d show photomicrographs at these levels. In Fig. 4b the dislocations are still in the pits as evidenced by the bright dot in the pits. In Fig. 4c the dislocation has just left the confines of the pit, and a flat is forming where the dislocation line had been. It is obvious from the location of the flats on adjacent pits that the dislocations had been looping toward each other. In Fig. 4d the etch has continued to smooth out the pits; continued etching eventually leaves no trace of the pits.

Other Areas of Dislocations

The dislocations in area II are generally confined to the region near the edges of the dendrites, al-

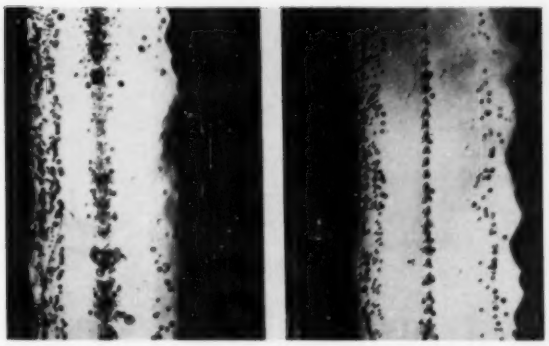

Fig. 5. Opposite faces of highly dislocated dendrite. Etched to reveal dislocations. Magnification 50X before reduction for publication.

though they can also be spread out so that they almost reach the central stripe. Figure 5 shows opposite faces of a dendrite etched to reveal the dislocations; face b has been turned upside down to indicate that the more heavily dislocated edge on face a is also the more heavily dislocated edge on face b. This dendrite is one of the more highly dislocated ones. The dislocation density in this area is more or less uniform; densities range from less than 10 to rarely greater than 10^4 pits/cm^2. It is not uncommon to have dislocations absent in the area II (and III) and still have a central stripe (area I). Billig (13) has reported numerous dislocations arranged along slip planes in the edge areas. We have not found this except in one or two instances; however, this is not surprising when one considers the difference in the control during the growth of our dendrites and Billig's.[1] The existence of these dislocations in the edge region is sometimes associated with an incoherent twin boundary (*i.e.*, the boundary at the edges of a degenerate twin lamella), although this is neither a necessary nor a sufficient condition. Certainly an incoherent twin boundary can be a source of dislocations.

Billig and Holmes (6) have said that the twin lamella is highly perfect and that the rest of the dendrite is full of dislocations. Our studies show also that the material within the twin planes is highly perfect; however, the rest of the dendrite was not found to be as highly dislocated as Billig's. In no case did we find the cross sections so highly dislocated that the twin lamellae were completely outlined by them. The latter may be the difference in the control of growth previously mentioned or in the difficulty of distinguishing dislocation pits from others when the WAg etch is used as opposed to the CP4 etch. Area II and area III dislocations may be found together, but this is not a necessary condition. We have found a number of dendrites which appeared to be dislocation free, but examination of the fractured and etched cross sections revealed area III dislocations.

In addition to the pits formed at line dislocations, the CP4 etch also shows up some shallow cylindrical pits in areas free of dislocations and on dislocation free dendrites. These pits have been noted on dislocation free germanium grown by the Czochralski technique and have been attributed to collapsed vacancy clusters. This may also be the origin of these pits found on dendrites, but we have no experimental evidence to state one way or the other.

Discussion

We have shown that dislocations may be found in three main areas. For areas I and II, the dislocations intersect the two main faces, and thus the source of these dislocations must be continuously generated during growth. Although area III is not necessarily independent of area II, once the dislocations are formed in area III they can be propagated during growth since they run approximately parallel to the growth direction. The problem, then, of the origin of dislocations in dendrites is to find a mechanism that gives a continuous generation of sources. The experimental observations indicate that, although there are three main areas of dislocations, there may actually be as many as six sources (two for area I and as many as four for area III) that may be in operation independently at the same time.

The existence of star patterns in the central stripe indicates a localized pressure. The dislocation half loops are quite similar to the prismatic loops found by Jones and Mitchell (14) who obtained their localized pressure by embedding glass spheres in AgCl. The entire star pattern is similar to that reported in silicon by Dash (15) who used a diamond stylus as an external localized pressure. In the case of dendritic growth, the localized pressure is internal, as we have shown in this paper and in the previous one (2), and does not arise from an inclusion of foreign matter as suggested by Bennett and Longini (5). The various sizes of slipped areas and hillocks reflect the size of the entrapped droplet. How large a droplet is entrapped depends on how deep the groove is [the depth of the groove is shown by the V faceting traces on the etched cross-sections in our previous paper (2)] and the time delay between groove formation and layer overgrowth. These factors will be influenced by minor fluctuations in the thermal conditions during growing. A schematic representation of the formation of the groove during growth is given by Fig. 3 of ref. (2).[2] Faceting traces on even twinned dendrites indicate that the groove begins at the twin plane on the face with the unfavorable growth direction;[3] thus the pockets will be deeper on this face than on faces with a favorable growth direction, making the unfavorable growth face of a two twin dendrite more susceptible to having a worse central stripe than the favorable growth face. For an odd-twin dendrite grown in the unfavorable, $\langle\bar{2}11\rangle$ direction, both sides of the dendrite will have a faceting development which is particularly prone to the entrapment of droplets.

There appears to be two sources of dislocations in area II (and initially for area III); (*a*) an entrap-

[1] Holmes (AIME Semiconductor Symposium, Boston, Aug. 1960. To be published in a Symposium monograph) has briefly described the essence of their procedures.

[2] A more illustrative drawing showing how the various facets grow together from the tip to form pockets in the groove is given for both the favorable and unfavorable growth directions by Bolling and Tiller (G. F. Bolling and W. A. Tiller, AIME Semiconductor Symposium, Boston, Aug. 1960. To be published in a symposium monograph.)

[3] This point has been discussed briefly by John and Faust (AIME Semiconductor Symposium, Boston, Aug. 1960. To be published in a symposium monograph).

ment of molten material between the H-arms (a mechanism not too different from that for the central stripe), and (*b*) incoherent twin boundaries. Source (*a*) is responsible for the dislocations in dendrites that have twin lamellae continuous to both edges. For such dendrites the H-arms and the twin lamellae proceed outward from the core although the H-arms almost always precede the lateral growth of the twin structure. The region between each arm and the twin lamellae then freezes outward. Although we have no direct experimental evidence, it appears from our studies that before the material between the H-arm and the twin lamellae has grown out completely, material freezes bridging their extremities and entrapping molten material. Since growth in this area is outward from the core, inward from the H-arm and twin lamellae, and downward (*i.e.*, in the growth direction) from the dendrite already frozen, the material entrapped here would be in a "rod" rather than a droplet form. This means that as the "rod" freezes, some of the expansion would be relieved at the open downward interface and the dislocation density would not be as severe as in the central stripe. This would also account for the more uniform dislocation density. From our studies it is not possible to say whether source (*a*) or (*b*) is acting singly in a given dendrite that has a degenerate twin lamella. Most probably these two sources work together. In this case, however, the freezing on the degenerate end or ends is between the two H-arms rather than each H-arm and the twin lamellae as in the cases where the twin lamellae are continuous across the entire cross section; thus, one would expect some interaction of the sources on one edge as mentioned in reference to Fig. 5.

Summary

Detailed studies of dislocations in germanium dendrites have shown that they are found in three main areas. The sources of these dislocations have been found to be entrapped droplets in the central stripe, and entrapped "rods" and/or incoherent twin boundaries in degenerate twin lamellae on the edges. It has been possible to change the growth conditions so that dislocation free germanium dendrites are grown routinely.

Acknowledgment

The authors wish to thank W. J. Smith, A. I. Bennett, and S. O'Hara for supplying them with dislocated dendrites, as well as Miss S. A. Warner and Mrs. H. Larson for helping with the etching studies. This was supported in part by the Wright Air Development Division of the Air Force.

Manuscript received March 20, 1961. This paper was presented before the American Physical Society Meeting in Detroit, March 21, 1960.

Any discussion of this paper will appear in a Discussion Section to be published in the June 1962 JOURNAL.

REFERENCES

1. J. W. Faust, Jr. and H. F. John, *This Journal*, **108**, 855 (1961).
2. J. W. Faust, Jr. and H. F. John, *ibid.*, **108**, 860 (1961).
3. E. Billig, *Proc. Roy Soc.*, **A229**, 346 (1955).
4. E. Billig, *Acta Met.*, **5**, 54 (1957).
5. A. I. Bennett and R. L. Longini, *Phys. Rev.*, **116**, 53 (1959).
6. E. Billig and P. J. Holmes, *Acta Met.*, **5**, 53 (1957).
7. J. W. Faust, Jr., "Methods of Experimental Physics," K. Lark-Horovitz and V. Johnson, Editors, Vol. 6A, Academic Press, New York (1959).
8. J. W. Faust, Jr., "The Surface Chemistry of Metals and Semiconductors," H. C. Gatos, Editor, John Wiley & Sons, Inc., New York (1960).
9. P. J. Holmes, *Phys. Rev.*, **119**, 131 (1960).
10. R. H. Wynne and C. Goldberg, *Trans. AIME*, **197**, 436 (1953).
11. J. W. Faust, Jr. and H. F. John, *This Journal*, **107**, 562 (1960).
12. G. R. Booker, *ibid.*, **108**, 564 (1961).
13. E. Billig, *Proc. Roy. Soc.*, **235A**, 37 (1956).
14. D. A. Jones and J. W. Mitchell, *Phil. Mag.*, **3**, 1 (1958).
15. W. C. Dash, "Properties of Elemental and Compound Semiconductors," H. C. Gatos, Editor, Interscience Publishers, New York (1960).

Scribe-Plating and -Etching

W. Rindner and J. M. Lavine

Research Division, Raytheon Company, Waltham, Massachusetts

ABSTRACT

A technique is described which permits the fabrication of miniature and microminiature ohmic and doped contacts in complex configurations on a variety of semiconductor materials. This technique involves the preferential nucleation of chemiplated and electroplated metals on microscopically fine lines scribed on semiconductor surfaces and the preferential etching of similarly scribed lines. Lines of the order of 10^{-4} cm have been plated with a variety of metals including doping elements. Scribe plating has yielded p-n junctions and offers promise of the fabrication of p-n junction devices considerably smaller than those currently available. This technique is also potentially useful in the fabrication of conventionally sized devices, some of which are described. Suggestions are advanced for the use of this technique in both microminiature and other device fabrication.

Efforts to reduce the size of electronic circuits have evolved typically about the size reduction of devices and components and the integration of these into complex assemblies. Solid state devices and components have contributed greatly to this advance. It is the purpose of this paper to describe a simple and versatile preferential plating and etching technique which permits the fabrication of large arrays of unconventionally small active and passive components on a single block of semiconducting material. Another potential of this technique is the fabrication of conventionally sized structures.

The technique to be described is based on the preferential nucleation of both electroplated and chemiplated metals on disturbed regions of a semiconductor surface and on the preferential etching of similarly prepared regions. In this work the disturbances were introduced by scribing.

Plating Techniques

Preferential gold plates were deposited on n-type silicon ranging from 10^{-1} ohm-cm to 300 ohm-cm, on p-type silicon ranging from 1 ohm-cm to 5000 ohm-cm, on germanium, both n- and p-type, ranging from 1 ohm-cm to 40 ohm-cm, and on a limited number of samples of indium antimonide and gallium arsenide.

A variety of tool materials were used for scribing microscopically fine lines. These included diamond, sapphire, silicon, germanium, and steel. The radius of the scribing point was varied from less than 1μ to about 25μ. For most of the experiments reported here the scribing was done with a steel tool having a point with a radius of about 10μ. Figure 1 shows a photomicrograph of two intersecting lines scribed on silicon with such a stylus. At lower magnification (Fig. 2) lateral rupture of the silicon surface is observed. Microscopic examination of many surfaces has indicated that the scribing tool removes material in an amount which depends on the stylus material, the radius of the point, the pressure applied, and the semiconductor surface preparation.

Most of the work with preferential plating was performed on polished silicon and germanium slices. The polished surfaces were prepared using standard semiconductor techniques with a final 1μ particle-size diamond polish. Generally, the polishing

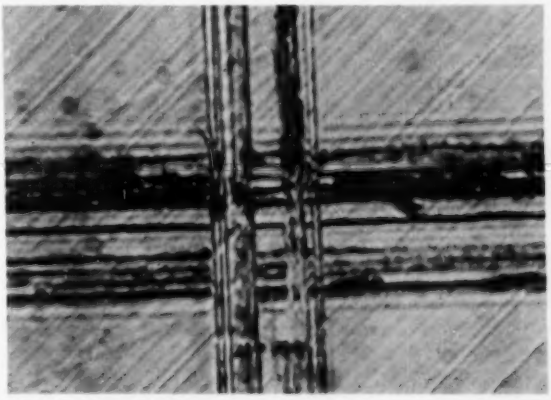

Fig. 1. Two intersecting lines scribed with a steel tool. Magnification approximately 1350X.

Fig. 2. Line scribed with steel tool showing rupture of surface.

Fig. 3. A 1 μ Au plated line. Magnification approximately 650X.

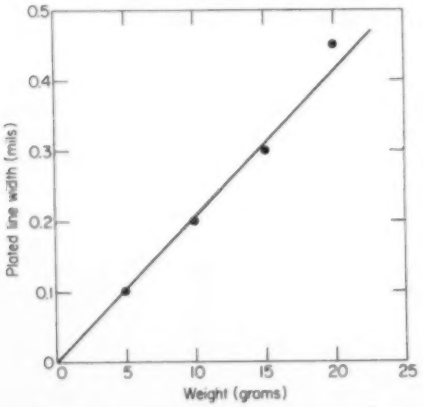

Fig. 4. Plated line width as a function of weight applied to a sapphire stylus.

scratches were much smaller than the scribed line. However, preferential plating has been observed on lapped surfaces as well.

Gold was electroplated from standard sodium-gold cyanide or potassium-gold cyanide solutions. The solution was maintained at 65°C and agitated gently. Electrical contact, even in the case of high-resistivity silicon, was made with a clip lead close to the scribe to be plated. Plating times ranged from several seconds to a few minutes, depending on the desired thickness and extent of the plate. Plating current densities have been estimated at about 100 amp/cm^2, assuming that all the current flows through the preferentially plated region. The total current used in plating short lines was of the order of tens of microamperes. Figure 3 shows a photomicrograph of a silicon sample with a scribed and gold plated line about 1μ wide. A portion of the line which had not plated continuously was chosen in order to show the contrast between plated and unplated portions of the scribed line. Throughout the remainder of this paper somewhat wider lines will be demonstrated because of the greater ease of photographing the details of such lines.

In order to provide wider lines the force applied to the scribing stylus was increased. The extent to which additional force increases the width of the

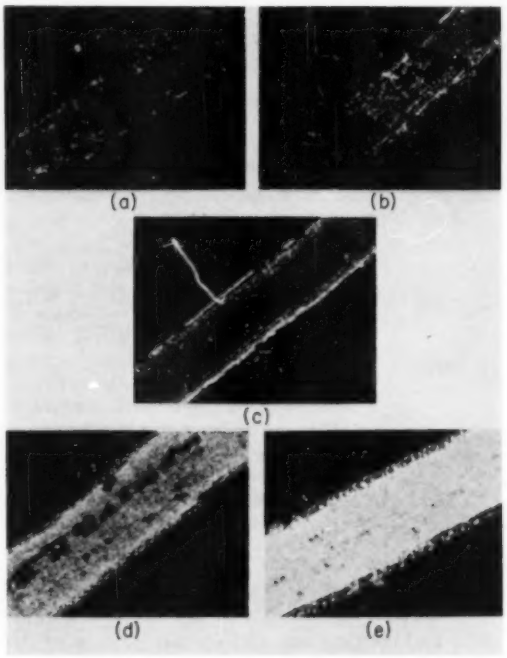

Fig. 5. Photomicrographs demonstrating growth of a preferential Au plate. Magnification approximately 350X.

scribed and hence the plated line is shown in Fig. 4. By varying the weight applied to a sapphire stylus and plating the resulting lines under nearly identical conditions, a plot (Fig. 4) of the width of the plated line as a function of the weight applied to the sapphire stylus was obtained. Estimates of the area of the stylus in contact with the substrate (of the order of 10^{-4} cm^2) suggest that pressures of the order of a few thousand kg/cm^2 were employed.

Within a single scribed line it was possible to follow the growth of the plate by plating portions of the same line for different lengths of time. Figure 5 shows a sequence of photomicrographs of several sections of a line which was step-wise plated for times varying up to 6 min. Initially (Fig. 5a) plating occurred at localized regions predominantly along the edges of the scribe. Continued plating tended to fill in the interior of the scribed region as shown in Fig. 5b. This photomicrograph also shows the transition between two regions plated for different times. Figure 5c shows a fairly uniform distribution of plated areas in the interior of the scribe, a thickening of the plate at the edges, and a visible lateral growth. In Fig. 5d an increase in the width of the line occurs, and Fig. 5e shows the uniformly plated line about 50μ wide.

Indium was plated using a bath consisting of 8.6 g of $In_2(SO_4)_3$ + 4.9 g H_2SO_4/liter. Approximately the same current densities and times were employed for the indium plating as were used for the gold plating. Antimony was electroplated from a solution consisting of 10 g of SbF_3 + 200 cc of ethylene glycol + 5cc of HF + 500 cc of distilled H_2O. Electroless nickel (1) also was deposited preferentially on lines scribed on silicon. Gold was chemically plated from a

standard gold plating solution with the addition of ammonium bifluoride. Preferential deposits of several metals have been plated on one another by this technique.

Etching

The preferential chemical etching of lines scribed on both germanium and silicon has been observed. Although the preferential etching of damaged regions of semiconductors has been known for several years (2), this technique is a natural supplement to preferential plating and thus was explored also. Scribing for preferential etching was tried with a variety of tool materials on germanium and silicon of various resistivities. The results showed some dependence on the resistivity of the substrate and the material of the scribing tool. In most cases a steel scribing tool was used on relatively high-resistivity silicon. The etchant was CP-4. During the first few seconds of etching there was a noticeable increase of both width and depth of the scribed line. During the entire etching process there was uniform but considerably slower attack on the unscribed portions of the sample. Preferential action usually ceased after several seconds. Figure 6 shows three photomicrographs of the same line. Figure 6a shows a section of the scribed but unetched line. The two parallel lines were sometimes visible at low magnification. The transverse rupture lines were visible only at high magnification. Figure 6b shows the same line after etching in CP-4. The attack is seen to have occurred mostly at the rupture lines. Figure 6c shows the line after additional etching. The width of the scribed line after etching is determined by the width of the transverse rupture which occurs on scribing.

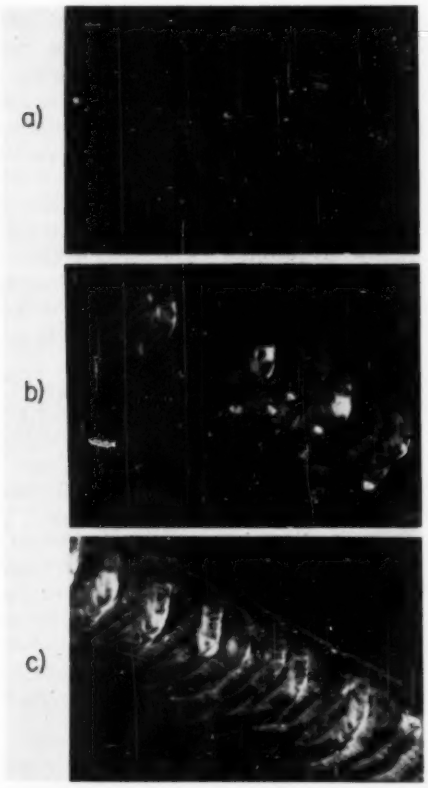

Fig. 6. Photomicrograph of a scribed line (6a), moderately etched in CP-4 (6b), and heavily etched (6c). Magnification approximately 500X.

Devices and Components

Gold plated lines and lines plated with the addition of a doping agent have been alloyed into both n- and p-type silicon and germanium. The usual difficulties attendant with the alloying of very thin films were encountered, particularly on silicon, where wetting can be a problem. However, doped lines preferentially deposited and suitably alloyed into both germanium and silicon substrates have exhibited diode action. Electrolytically sharpened tungsten points were micromanipulated to establish electrical contact with these structures.

Several transistor structures have been fabricated by this technique. In the first, two p-n junctions, closely spaced side-by-side, were plated and alloyed. Although such a structure is undesirable for several reasons, transistor action was observed. Diffused collector, alloyed emitter mesa transistor structures have also been fabricated. For this effort, several samples of germanium and silicon were diffused to different depths. The emitter and the base contacts were then scribed, preferentially plated with appropriate doping materials, and alloyed. This preliminary work suggests that the damage which results from the scribing of even very fine lines probably extends to a depth of several microns. Thus transistor action was observed only on those samples with collector junctions of the order of several microns below the surface.

Resistor elements were fabricated upon a 300 ohm-cm n-type silicon substrate by plating gold on scribed lines about 1 cm in length. The gold was not alloyed into the silicon. Plating times to 5 min were used with about 100 μa of plating current. Figure 7 shows a plot of the total resistance of one such line as a function of plating time. Figure 8 shows a photomicrograph of a portion of a heavily plated line about 70μ wide, which provided about 10 ohms of resistance. Figure 9 shows a photomicrograph of a section of a line plated with gold for about 30 sec at 100 μa. This line was about 65μ wide and yielded 100 kilohms. This plate is seen to consist of several longitudinal lines, the transverse rupture lines, and a random distribution of dots. In some places the longi-

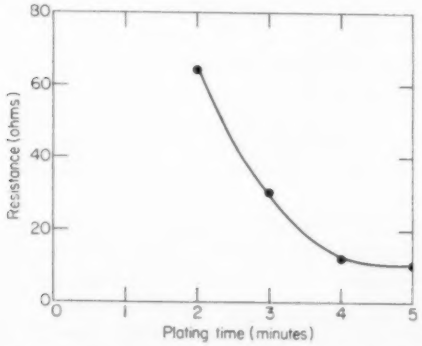

Fig. 7. Resistance of a 1 cm x 70μ Au plated line as a function of plating time.

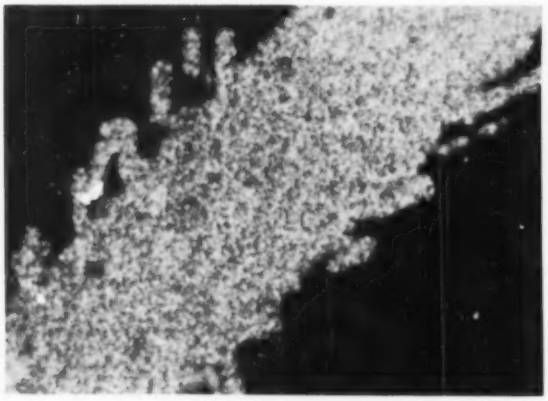

Fig. 8. Photomicrograph of a section of Au plated unalloyed line whch provided 10 ohms of resistance. Magnification approximately 650X.

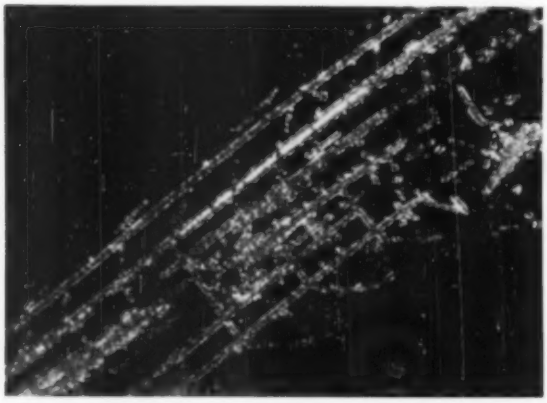

Fig. 9. Photomicrograph of a section of a Au plated unalloyed line which provided 100 kilohms. Magnification approximately 650X.

tudinal lines showed breaks implying that current flowed through the semiconductor. Therefore, large resistances will probably depend on the resistivity of the substrate.

Potentialities

Several techniques are currently available for fabricating very small area junctions. Junctions of the order of 25μ can be fabricated by standard alloying techniques. Larger area junctions can, of course, be reduced by etching to less than 25μ in diameter. Vacuum deposition through a mask has yielded (3) lines as small as 7.5 x 25μ and in principle can be reduced even farther. However, the chief advantage of preferential plating is the simplicity with which lines of the order of a few microns in width may be alloyed into both germanium and silicon. These lines may be reduced in length to about the same dimension.

Figure 3 shows that a single line of the order of 1μ may be plated by these techniques and preliminary work has indicated that an array of such lines scribed with a diffraction grating ruling machine (6000 lines/cm) can also be plated. Assuming that gridding of such assemblies is possible, very large assemblies of p-n junctions can thus be envisioned.

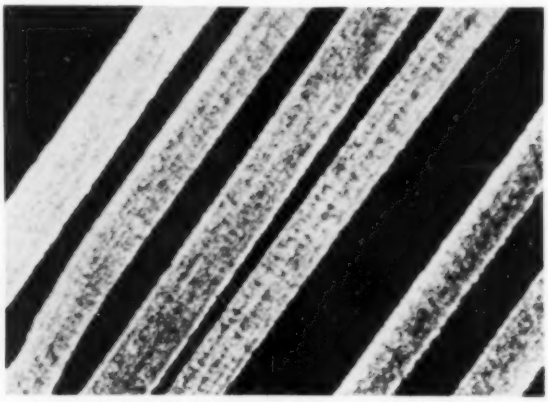

Fig. 10. Photomicrograph of a section of a comb-like structure hand scribed and preferentially Au plated. Magnification approximately 200X.

One micron electrode dimensions also offer the possibility of high-frequency transistor fabrication using double diffused (4), alloy-diffused (5), or post-alloy diffused (6) techniques. The full potentialities of this technique are not clear at present because of the unknown extent of the damage which occurs with scribing. The technique of preferential plating may also be useful in conjunction with other more widely used techniques in the fabrication of conventional low-frequency or high-power transistors. For example, by scribing and plating dots, emitter configurations may be inserted within small alloyed base rings. In the case of power transistors requiring long emitter-base configurations (7), comb-like structures may be scribed and plated as shown in Fig. 10. Scribing in this case was done by hand; consequently the lines are neither parallel nor uniformly spaced. However, results such as this indicate that lines about 25μ wide separated by a few microns may be obtained.

The feasibility of plating lines which measure only a few ohms suggests an interesting application in the fabrication of large area solar cells. A thick plate may be circumscribed around the exterior of the light-sensitive surface which may then be gridded with many narrow lines which cover only a small portion of the active surface.

Resistance elements may also be fabricated using the preferential etching technique. For this purpose a relatively thin conducting layer separated from the bulk by a junction is required. Scribing and preferential etching of two parallel lines will then permit the isolation of a small resistance strip.

Preferential etching may be useful in other areas as well. For example, the isolation of large regions of the diffused layer surrounding each of the active devices in a solid circuit (8) may be readily accomplished by scribing and etching. Preferential etching may also be used to replace masking and etching of mesa transistors.

Discussion

The large electric field which exists at regions of small curvature such as those observed within the scribed region of the semiconductor probably results in a large current density at these points and hence

in an initial metallic deposition. The initial deposit then alters the potential distribution within the sample so as to enhance the preferential action. Under certain conditions, the plating may not be preferential, and plating can occur at other portions of the surface. For example, polishing scratches also act as nucleating centers for plating, and improperly prepared surfaces may plate over the entire surface. Location of the electrical contact far from the scribed line can also result in preferential deposit at the nearby edges and corners of the sample. The current flow through the system depends on the usual parameters involved in plating such as the resistivity and the surface geometry of the semiconducting sample, the location of the electrical contact with respect to the scribed portion of the sample, the electrode configuration within the plating solution, and many properties of the solution.

In the case of electroless plating of nickel which has been widely used in silicon technology, experience indicates that plating occurs more readily on a lapped than on a polished surface. Brenner and Riddell (9), who first developed the electroless nickel technique, have suggested that the reaction is autocatalytic. Therefore once the initial deposit has occurred within the rough portions of the scribed line in preference to the polished surface, the deposited nickel catalyzes the reaction. In the case of electroless gold, the mechanism is not understood. It has been noted, however, that both the electroplating and the electroless plating of metals will not occur if the scribed line has been etched first. This suggests that surface roughness may be required for the initial deposit.

The preferential etching of damaged and dislocated regions has been reported previously (2, 10) and preferential etching has been used to test (11) for the presence of damage. From Fig. 6 it may be observed that the damage extends many diameters beyond the path of the scribing tool. This can readily account for the observed increase in the size of the scribed line with etching. The cessation of the preferential etching action after a short time lends strong support that the origin of the effect is damage.

Conclusion

Scribing has proved to be a feasible method for creating nucleation centers for both electrodeposited and chemically deposited metals as well as for obtaining localized etching. A variety of metals has been deposited which provides both ohmic and rectifying contacts on n- and p-type germanium and silicon when suitably alloyed. Although the technique described here requires additional study, nevertheless it appears feasible for reducing the dimensions of semiconductor devices and components as well as for fabricating conventionally sized structures. Moreover, it may be possible by disturbing the surface by other means, as for example by ion or electron bombardment, to reduce further the size of the nucleating area for preferential plating and the damaged area for etching. The potential of this technique for fabricating transistor-like structures may be restricted ultimately by the damage (12) due to scribing.

Acknowledgments

The authors would like to thank Mrs. J. Norman and D. Davis for assistance in the plating and etching work, and Mrs. F. Huff for polishing many samples.

Manuscript received Feb. 3, 1961; revised manuscript received May 19, 1961.

Any discussion of this paper will appear in a Discussion Section to be published in the June 1962 JOURNAL.

REFERENCES

1. M. V. Sullivan and J. H. Eigler, *This Journal*, **104**, 226 (1957).
2. P. R. Camp, *ibid.*, **102**, 586 (1955).
3. J. M. Early, *Proc. I.R.E.*, **46**, 1924 (1958).
4. C. A. Lee, *Bell Syst. Tech. J.*, **35**, 23 (1956).
5. M. Tanenbaum and D. E. Thomas, *ibid.*, **35**, 1 (1956).
6. J. R. A. Beale, *Proc. Phys. Soc.*, **B70**. 1087 (1957); P. Kaufmann and G. Freedman, "Solid State Physics in Electronics and Telecommunication," Vol. 2, p. 977, M. Desirant and J. L. Michiels Editors, Academic Press, Inc.. London (1960).
7. R. N. Hall, *Proc. I.R.E.*, **40**, 1512 (1952); N. H. Fletcher, *ibid.*, **43**, 551 (1955).
8. J. W. Lathrop, R. E. Lee, and C. H. Phipps, *Electronics*, **33**, No. 20, 69 (1960).
9. A. Brenner and G. Riddell, *Proc. Am. Electroplaters Soc.*, **33**, 23 (1946).
10. J. W. Faust, Jr., "Factors Influencing the Depth of the Damaged Layer Caused by Abrasive Processes," paper presented at the Fall Meeting of The Electrochemical Society, October 1957.
11. E. P. Warekois, M. C. Lavine, and H. C. Gatos, *J. Appl. Phys.*, **31**, 1302 (1960).
12. T. M. Buck and F. S. McKim, *This Journal*, **103**, 593 (1956).

Some Properties of In_2Te_3 and Ga_2Te_3

J. C. Woolley and B. R. Pamplin[1]

Physics Department, University of Nottingham, Nottingham, England

ABSTRACT

This paper summarizes the measurements which have been made to determine various physical parameters for the compounds Ga_2Te_3 and In_2Te_3. The previously described problems of the preparation of stoichiometric In_2Te_3 and Ga_2Te_3 and the associated question of ordering of lattice vacancies in In_2Te_3 are reviewed briefly. Measurements of the thermal coefficient of expansion of the two compounds at liquid air and room temperatures are described. The main section of the work concerns the measurements of electrical conductivity and Hall effect in the compounds. The determination of activation energy values from the electrical measurements and their relation to the energy gap is discussed, and values of activation energies and also of electron mobilities are given for ordered and disordered In_2Te_3. It is shown that the change in activation energy in In_2Te_3 at 470°C is not associated with a change in structure, and an explanation in terms of change in conduction band minimum is considered. Results of preliminary room temperature measurements of thermal conductivity in Ga_2Te_3 and ordered In_2Te_3 are given.

Indium sesquitelluride In_2Te_3 is a semiconductor (1) with either a defect zinc blende or a defect antifluorite structure in which one-third or two-thirds, respectively, of the sites of the indium sublattice are vacant (2). When In_2Te_3 is prepared normally from a stoichiometric melt of indium and tellurium, the lattice vacancies are arranged at random on the indium sublattice. The compounds Ga_2Te_3 and Ga_2Se_3 have similar crystallographic properties. Much of the interest in these compounds stems from the presence of the lattice vacancies, for in the disordered material the concentration of vacancies in the lattice is a factor of 10^6 or so larger than the normal concentration of Frenkel and Shottky defects and of the impurity concentration in good purity materials. This very high concentration of lattice vacancies can be expected to have considerable effect on the electrical and thermal conductivities of the materials concerned. These vacancies, unlike vacant sites in other materials, are not charged however, and so they will not be expected to be as efficient as scattering centers for electrons as normal charged vacancies. However in disordered material there should be a considerable alloy scattering effect due to the randomness of the vacancies in the lattice. It has been shown that the electrical conductivities of these compounds are very low (1). The spacing of these centers is only of the order of the lattice spacing, and hence it is not clear that the conventional plane wave development of band theory to electrical conductivity is applicable in this case, or whether perhaps a hopping process would describe the effect better.

It has been shown that in the case of In_2Te_3 the lattice vacancies can be caused to order (3, 4). Such an ordering is of interest as it can change considerably the conduction properties of the material, for such fundamental parameters as lattice vibration spectrum, Brillouin zone form and energy gap values, mobility values and crystal anisotropy may be affected when ordering occurs.

In a previous paper (2) the authors described a detailed investigation of the ordering which occurs in In_2Te_3. It was found that annealing of specimens as lump ingots or in powder form produced some ordering, but that this was a very slow process. Thus powders annealed at various temperatures below the ordering temperature (620°C) were all found to require several months of annealing before ordering lines could be observed easily in x-ray photographs. Therefore other methods of preparation were considered. It was shown that nonstoichiometry could be a problem in this work, and that the most convenient method of obtaining ordered In_2Te_3 not contaminated with other phases such as Te, InTe, etc., was by the use of a directional freezing technique (see Preparation section). Alloys of composition In_2Te_{13} and In_2Te_{14} (*i.e.*, approximately 1% from stoichiometry on either side) were prepared to investigate the effects of nonstoichiometry. It is to be noted that In_2Te_{13} represents the composition reported by Inuzuka and Sugaike (4) ($In_{2.08}Te_3$) in their work on ordering in In_2Te_3. When quenched, these alloys showed very complex x-ray powder photographs with many lines, among which lines due to In_2Te_3, Te, and InTe could be observed. Obviously this represented a nonequilibrium condition in these samples. They were then further annealed and several months of annealing caused faint In_2Te_3 ordering lines to occur, but lines due to other phases remained, although some were considerably weaker. It is probable that even after this time of annealing, true equilibrium conditions had not been reached, and hence a complete determination of the various phases present was not made. Lattice parameter values were determined from the In_2Te_3 type lines

[1] Present address: Department of Applied Physics, University of Durham, Durham, England.

however and found to be 6.158Å in each case. This lies within the range between the values for disordered and ordered In_2Te_3, *i.e.*, 6.150Å and 6.165Å, respectively. (The value of 6.150Å for disordered In_2Te_3 is somewhat uncertain, probably due to the difficulty in producing a completely disordered sample. The value of 6.150Å would seem reasonable from a consideration of the results of the present authors plus the published data of other workers.) It was found in the case of In_9Te_{11} that this nonstoichiometry reduced the resistivity by a factor of about 1000 compared with stoichiometric In_2Te_3, while the resistivity of In_9Te_{13} was lower still. Mason (5) now reports from thermal analysis data that the optimum ordering composition in this range is In_7Te_9, but that solid solution may extend from this composition to In_2Te_3. A value of ordering temperature of 620° ± 10°C was determined (2), and this has now been confirmed by the work of Gasson *et al.* (6) and Mason (5) although Zhuze *et al.* (7) report a value considerably lower than this.

Initially it was shown that the ordering could be represented by a threefold cubic cell (4), but the present authors (2) showed that the symmetry was lower than cubic, and that the structure could be represented by a smaller cell of lower symmetry. Woolley and Pamplin showed that, if only zinc blende sites are considered, from x-ray intensity considerations the structure must be orthorhombic, space group Imm2, but Holmes showed that, if the enantiomorphous fluorite sites are allowed, a tetragonal structure can give correct x-ray intensities. Holmes (2) assigned his structure to the space group $P4_2mcm$ or $P4_2nm$. On further examination of his structure the present authors and Holmes agree that the true space group for the postulated structure using enantiomorphous sites is I4mm.

The electrical conductivity of In_2Te_3 as a function of temperature has been investigated previously by Appel (1, 8, 9). The results fit a standard exponential variation of the form $\sigma = A \exp\left(-\frac{E_A}{2kT}\right)$, where E_A takes a different value over different ranges of temperature, and E_A, an activation energy, has been interpreted as the energy gap E_g for the material. This is only a valid assumption when the mobility-temperature variation is of a particular form, and thus the use of electrical properties to determine E_g requires measurement of Hall effect. The discontinuities in slope in the log σ v 1/T curves, corresponding to changes in E_A, occurred at temperatures in the range 500°-700°C. Appel suggested that this was due to a structure change from zinc blende to wurtzite. It is shown later that this cannot be true.

Less work has been done on Ga_2Te_3. Although Hahn (3) reported some ordering lines, this has not been confirmed by later workers. Harbeke and Lautz (10) in conductivity measurements as a function of temperature find results similar to those for In_2Te_3 and have determined values of E_A. They have also investigated (11) the effects of copper doping of Ga_2Te_3. They report a lattice parameter increase of 2.7% when up to 10^{-3} at. % of copper is added, after this a second phase appearing. E_A decreases with increased copper concentration until it becomes zero at the limit of solution, conduction then being metallic in character. They define a parameter γ and evaluate it from their experimental data.

$$\gamma = \frac{\text{change in energy gap}}{\text{fractional change in volume}} = -8.5 \text{ ev}$$

Estimates of γ may be made also by measuring pressure effects. These have not been made for $A_2^{III}B_3^{VI}$ compounds, but values comparable with that given above have been obtained for the more conventional semiconductors.

Preparation

The In_2Te_3 was prepared from indium of 99.999% purity and tellurium purified by repeated sublimation, stoichiometric quantities being melted together in vacuum. The Ga_2Te_3 was prepared in a similar way. In each case, zone refining of an ingot sealed under vacuum was attempted, and this was found to cause lines corresponding to other phases to occur in the x-ray photograph, indicating some decomposition of the compound. This was confirmed by holding a quantity of In_2Te_3 in a molten state (at 670°C) at one end of an evacuated tube, while the remote end was kept about 100°C lower in temperature. After one day, it was found that a sublimate had collected at this colder end. The experiment was continued for a month without any noticeable change in quantity of sublimate. X-ray analysis showed that the sublimate was essentially tellurium and the residue InTe. It thus appeared that it was not possible to zone refine In_2Te_3 in vacuum, but Parrott (12) has since shown that zone refining is possible if a tellurium atmosphere is maintained.

When slow directional freezing was used, the specimens gave good single phase x-ray photographs, showing ordering lines in the case of In_2Te_3, but no observable ordering lines with Ga_2Te_3. In the latter case, however, annealing of a directionally frozen ingot was found to increase the lattice parameter to 5.906 Au, the quenched material having a value of 5.901 Au [Hahn (3) quoted 5.874 Au]. A similar effect had been observed with In_2Te_3. This increase in lattice parameter with time of anneal can be explained on the assumption that, on quenching, insufficient lattice vacancies are introduced into the lattice, but, on annealing, more vacancies diffuse into the structure. Measurements of density in In_2Te_3 confirmed that the disordered material is denser than the ordered, *i.e.*, the density of the quenched material is higher than the value calculated from lattice parameter, while that of the ordered material is lower than the calculated value.

Experimental Measurements and Results

Thermal expansion.—These measurements were carried out to obtain a volume coefficient of expansion to be used with the known temperature coefficient of the optical energy gap β to give a value for the parameter, γ, defined earlier. Rod shaped specimens, 5 mm in diameter and about 5 cm long, were cast in evacuated quartz tubes, and for each specimen its change in length relative to a quartz rod was observed as a function of temperature from

Table I. Coefficients of linear expansion (/°C)

	Liquid air temperature	Room temperature
In_2Te_3	$(9.0 \pm 0.5) \times 10^{-6}$	$(9.2 \pm 0.2) \times 10^{-6}$
Ga_2Te_3	$(9.2 \pm 0.3) \times 10^{-6}$	$(8.3 \pm 0.3) \times 10^{-6}$

liquid air up to approximately 60°C. In this measurement, the specimen was mounted in a cylindrical hole in a copper block to provide uniformity of temperature down the specimen, and the relative change in length found by means of a thin roller placed between a brass block supported on a quartz tube and a similar block resting on a quartz rod, which in turn was carried by the specimen. The roller carried a mirror, and its rotation when relative change in length occurred was observed with a lamp and scale at approximately 1 m distance. Measurements were made at various temperatures between liquid air and 60°C, and expansion coefficients calculated at liquid air and room temperatures. Corrections had to be applied for an expansion in the brass head of the apparatus and for the expansion of the quartz tube relative to which measurements were made. These effects were relatively small, and a check of the system by measurement of the linear expansion of copper gave a figure within 1% of the standard value. The results for In_2Te_3 and Ga_2Te_3 are given in Table I.

The available estimate of β for In_2Te_3 and Ga_2Te_3 range from -1.0×10^{-4} to -5.5×10^{-4} ev/°C and -4.8×10^{-4} to 7.7×10^{-4} ev/°C, respectively (13). These values combined with the expansion coefficients of Table I result in a range of values for γ of -3.7 to -20 ev for In_2Te_3 and -18 to -29 ev for Ga_2Te_3. These, although a little higher, are of the same order of magnitude as the value obtained by Harbeke and Lautz. It is to be expected that larger values of γ will be obtained however when the volume change is caused by temperature variation rather than by pressure or solid solution effects, since, in this case, in addition to the change caused by lattice parameter variation, the change in thermal vibration of the atoms will also affect the energy gap value.

Conductivity and Hall effect measurements.—Because of the effects obtained with samples of composition In_9Te_{14} and In_9Te_{13} (equivalent to the $In_{2.00}Te_3$ described by Inuzuka and Sugaike) as described earlier, detailed electrical measurements were confined to specimens of composition In_2Te_3, and no zone refined samples were measured. Specimens of both In_2Te_3 and Ga_2Te_3 were cut from directionally frozen ingots and mounted in a pyrophilite jig. Electrical connections, *viz.* current electrodes and potential and Hall probes, were made by pressure contact. The jig was placed inside a quartz tube which could be evacuated or filled with an inert gas, and it could be heated to temperatures up to 750°C by a furnace wound on the tube. The whole unit was mounted between the poles of an electromagnet so that fields of up to 6K oersteds could be applied.

Initial measurements showed that specimens of both compounds lost their initial high resistivity on being heated above about 300°C, and in a typical

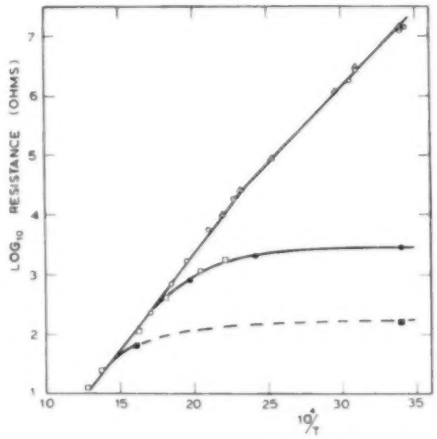

Fig. 1. Variation of resistance with the reciprocal of absolute temperature for a specimen of In_2Te_3. △, First run heating; ○, 2nd run heating; ●, 2nd run cooling; □, 3rd run heating; ■, 3rd run cooling.

specimen the room temperature resistivity dropped from 10 megohm cm to 10 kilohm cm. This loss of resistivity was greater the higher the temperature used. Measurements were repeated using copper, platinum, lead, and iron electrodes, under vacuum and in atmospheres of pure nitrogen and of pure argon at approximately atmospheric pressure. Investigation showed that the effect was independent of the type of electrode used and of the ambient atmosphere. However used specimens recovered their resistivity when polished with emery cloth. Also small deposits of tellurium were observed in the cooler parts of the tube after repeated measurements. It thus appears that these compounds lose tellurium from their surface under these conditions, and that the lower resistance of the specimens which have been heated is due to a surface layer of indium (or gallium) rich material. One Ga_2Te_3 specimen which showed this effect markedly was found to give weak GaTe lines in its x-ray photograph. A typical change in resistance after successive temperature runs for an In_2Te_3 specimen is shown in Fig. 1. Here it is seen that after each heating and cooling the specimen was taken to a higher temperature in the next run and the room temperature resistivity was correspondingly lowered. It is seen however that in each run, despite the previous loss, the initial curve is

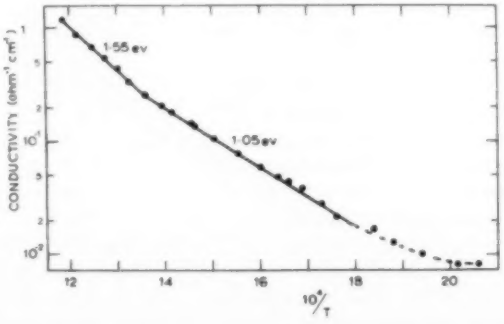

Fig. 2a. Variation of conductivity with reciprocal of absolute temperature for ordered In_2Te_3.

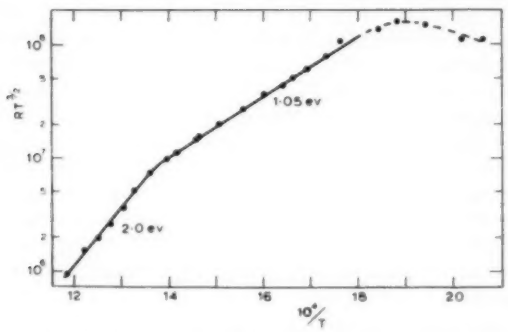

Fig. 2b. Variation of $R_H T^{3/2}$ with reciprocal of absolute temperature for ordered In_2Te_3.

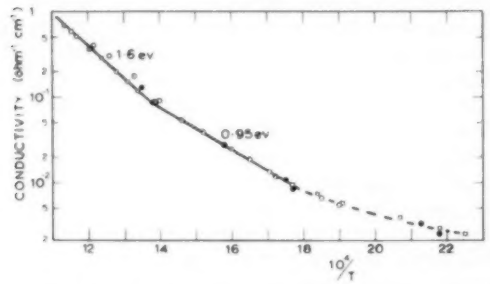

Fig. 3a. Variation of conductivity with reciprocal of absolute temperature for disordered In_2Te_3. ○, 1st run heating; ●, 1st run cooling; □, 2nd run heating.

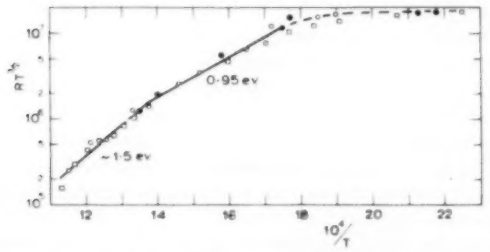

Fig. 3b. Variation of $R_H T^{3/2}$ with reciprocal of absolute temperature for disordered In_2Te_3. ○, 1st run heating; ●, 1st run cooling; □, 2nd run heating.

recovered when higher temperatures are approached. Thus the measurements which were used in all cases were those made during the initial heating run in any temperature range and, although some tellurium loss must have occurred, it was estimated that the effect gave an inaccuracy of less than 5% at the worst and that most results were more accurate than this. Because of this effect however the maximum temperature used in the present electrical measurements was 580°-600°C.

The conductivity and Hall effect results for a typical ordered specimen of In_2Te_3 are presented in Fig. 2 where values of log σ and log $R_H T^{3/2}$ are plotted against 1/T. Similar values for a typical disordered specimen of In_2Te_3 are shown in Fig. 3. The measured values of R_H if interpreted on a single carrier assumption give values of $n \approx 10^{14} - 10^{15}$/cc at 250°C. Occasional good specimens enabled measurements to be made at lower temperatures, and the value of carrier density at room temperature was estimated to be of the order $10^{12} - 10^{13}$/cc. The majority of specimens showed n-type behavior and in Fig. 4 values of electron Hall mobility $\mu (= \sigma R_H)$ are plotted against T for an ordered specimen. The maximum value of μ recorded in the series of measurements was 340 cm²/v sec at 260°C. A few samples appeared to have a p-type Hall effect at the lower end of the temperature range, but the values obtained showed wide fluctuations between successive measurements, giving a maximum value of μ of about 50. It is possible however that this is a spurious surface effect, and the quoted value of μ is suspect. The values of μ obtained for the disordered material were small ($\approx 5 - 10$ for n-type specimens), and the accuracy of measurement was insufficient to show a significant change with temperature.

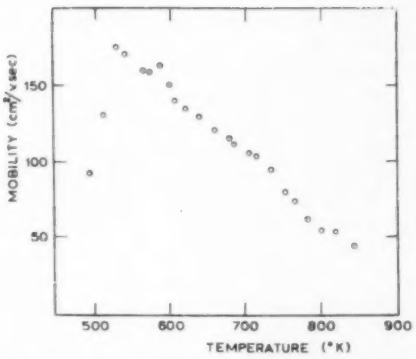

Fig. 4. Variation of electron mobility with absolute temperature for ordered In_2Te_3.

Considering first the conductivity results, it is seen that for temperatures below about 250°C ($10^4/T > 19$) the results are rather indeterminate, possibly due to the surface effect mentioned above. Above this temperature, log σ is found to vary linearly with $1/T$ but with a discontinuity in slope occurring at a temperature of about 470°C for both ordered and disordered material. Below the transition the resulting values of E_A are 1.05 ± 0.05 ev for ordered and 0.95 ± 0.05 ev for disordered material. Above the transition the value of E_A is 1.55 ± 0.1 ev for both materials. Other values of E_A were observed for some samples, *e.g.*, 1.4 ev in the range 250°-550°C and 2.2-2.3 ev at higher temperatures, but it was found that the samples giving these values were very impure. The value of 2.2 ev at high temperatures was reported by Appel (8, 9).

The graphs of log $R_H T^{3/2}$ *V* $1/T$ should give correct values of the band gap extrapolated to absolute zero E_0. These curves again are in the majority of cases indeterminate below 250°C, but above this temperature have two linear sections as in the case of the log σ graphs, and show the same transition temperature. The values of E_0 obtained here for the ordered material are 1.05 ± 0.05 ev below the transition and 2.0 ± 0.05 ev above, while for disordered material the value of E_0 below the transition is 0.95 ± 0.1 ev, the value above the transition, lying in the range 1.3 to 1.8 ev, being less certain because of the difficulties

in measuring Hall coefficients in these high-resistivity materials.

The close agreement between the values of E_A and E_o in the lower temperature range implies that $\mu(=\sigma R_H)$ varies approximately as $T^{-3/2}$, although deviations from the 3/2 power would make only small changes in the apparent value of E_A. The graph of μ v T in Fig. 4 indicates that the relation between μ and T may be nearer to a linear one. The discrepancy between E_A and E_o for ordered In_2Te_3 in the higher temperature range can again be attributed to the temperature variation of μ. However, insufficient data are available in this temperature range to enable the form of the mobility temperature relation to be determined with any accuracy. The results in Fig. 4 would appear to indicate that μ falls rapidly at temperatures below about 260°C. This form of variation would be in qualitative agreement with the results given by Ioffe (14) when reporting the work of Zhuze, but the results of this work (7) are not as yet available, and also, as indicated above, the present data may not be significant at temperatures below 250°C.

The results obtained with Ga_2Te_3 were less satisfactory, for the various specimens did not give a constant value of E_A. In some cases the gradient of the log σ v $1/T$ graph increased with increasing temperature tending to an E_A value of 1.55 ev obtained by Harbeke and Lautz (10). Other specimens gave a linear graph, but the values of E_A differed from specimen to specimen in the range 1.15 to 1.35 ev. Attempts at Hall effect measurement on Ga_2Te_3 were all unsuccessful, and it is estimated from the sensitivity of the apparatus that this sets an upper limit of 2 cm^2/v sec on the value of Hall mobility at 300°C. The conductivity data on the various Ga_2Te_3 samples can be made to agree with the extrapolated optical energy gap value of 1.1 ev by means of an equation of the form $\sigma = AT^x \exp(-1.1/2kT)$ where, for the various cases, x lies between 1 and 2.

As the conductivity of these tellurides is exceedingly small at room temperature and rises exponentially with temperature, it was considered possible in view of the high concentration of lattice vacancies that the conduction might be ionic in character. To check this possibility, measurements were made on a sample of ordered In_2Te_3 in the form of a thin plate. Two small weighed plates of indium were placed on either side of the weighed In_2Te_3 plate and between graphite electrodes, good contact being made by pressure. A current of 6 ma was then passed continuously for three months. After this time no change could be detected in the mass of the indium electrodes or the In_2Te_3 sample. This indicated that any ionic contribution to the conductivity which involved net transport of indium was less than 0.1% of the total. The specimen was x-rayed and was found to have retained its ordering, indicating no interchange of indium atoms and lattice vacancies. It thus appears that the conduction in In_2Te_3 is electronic in character.

Discussion

As indicated above, the σ and R_H measurements made up to a maximum temperature of 600°C show a discontinuity near 470°C in both ordered and disordered specimens. This is lower than the ordering temperature of 620°C, but is in agreement with the results of Appel (8, 9). Appel postulated a change in structure from zinc blende to wurtzite to explain the discontinuity. However, the present authors have made x-ray measurements at temperatures from 600°-670°C and find that the zinc blende (or antifluorite) structure is retained at these temperatures, and hence it would appear that the discontinuity cannot be explained in terms of a crystallographic change.

Another possible explanation of the effect can be that a change of lowest conduction band minimum occurs with change in temperature. If two conduction band minima are at energies E_1 and E_2 above the valence band maximum where E_1 and E_2 are temperature dependent, it is possible for $E_1 < E_2$ at temperatures below 470°C and $E_1 > E_2$ above, 470°C being the transition temperature where $E_1 = E_2$. Since the electrical properties will be mainly determined by the lower minimum, if E_1 and E_2 extrapolate to different values at absolute zero (E_{o1} and E_{o2}), the slope of the log $R_H T^{m/x}$ v $1/T$ curve at temperatures well above 480°C will be different from that at temperatures well below this transition point. Such a change in the conduction band form is found in GaSb (15), and it has been shown (16) that the electrical results for GaSb show a discontinuity which is similar to that described above, and which can be correlated with the conduction band change. If the energy gaps are assumed to vary with temperature in such a way that $E_1 = E_{o1} + \beta_1 T$ and $E_2 = E_{o2} + \beta_2 T$, values of extrapolated energy gaps E_{o1} and E_{o2} can be obtained from Fig. 2 and 3 ($E_{o1} = 1.05$ ev and $E_{o2} = 2.0$ ev for ordered and $E_{o1} = 0.95$ ev and $E_{o2} = 1.6$ ev for disordered material). From these values and the assumption that $E_1 = E_2$ at 470°C, it is possible to calculate the difference between the temperature coefficients of E_1 and E_2 necessary to give these results. Thus this gives $\beta_2 - \beta_1 = -1.4 \times 10^{-3}$ ev/°C for ordered and $\beta_2 - \beta_1 = -0.86 \times 10^{-3}$ ev/°C for disordered material, and these values are not unreasonable.

The values of R_H for ordered and disordered material at the same temperature show a difference of a factor five, and on the single carrier analysis this indicates five times as many carriers in the disordered material as in the ordered. The difference in energy gap of 0.1 ev in 1 ev would account only for a factor of about 2-2.5. The remaining difference could indicate that the effective mass product $m_n m_p$ is smaller in the ordered case which would in turn indicate a change in band form on ordering. Thus the smaller zone of the ordered structure could result in a greater curvature at the conduction band minimum and hence a smaller effective mass value. Alternatively, since the symmetry of the ordered material is lower than that of the disordered, the extra factor in the number of carriers could be due to the fact that the number of equivalent conduction band minima may be different in the two cases, the number being larger for the disordered than for the ordered case.

It is seen that the observed values of mobility for the ordered material are a factor of more than 10 larger than these for disordered material under the same conditions. The major effect producing this change will be scattering of carriers due to the random arrangement of vacancies in the disordered material. Other factors such as the possible difference in effective masses mentioned may also make some contribution.

The above discussion has assumed that the normal interpretation of electrical results to give values of carrier density and mobility is valid. It is worth noting that this need not necessarily be the case, since with the very low mobilities observed in these cases it is not certain that the normal band theory concepts involving plane wave scattering calculations are applicable, although the values of mobility in the ordered structure do attain reasonably large values. This problem has been stressed by Ioffe (14), who suggests that the conduction may be better considered in terms of a hopping mechanism. In such a case the interpretation of Hall data, etc., in terms of carrier density might require some modification. It has been found so far however that the application of normal band theory to results for In_2Te_3 and its alloys (17) has given reasonably consistent results. Ioffe (14) reports an exponential rise in mobility in In_2Te_3 at low temperatures which is unusual, but the complete results of this work (7) are not yet available.

These considerations are important when the very low carrier densities observed in In_2Te_3 are considered. The value of 10^{12}/cc is a reasonable value for intrinsic behavior at room temperature in a material of energy gap of 1 ev, but in the In_2Te_3 used here the impurity contribution might be expected to be considerably greater than this. Various explanations can be postulated for this. Thus it is possible that the impurities can provide carriers for a hopping mechanism, but that the low carrier density observed is due to an invalid interpretation of the Hall data as indicated above. A second possibility is that the impurity donor levels are found at about the center of the energy gap in In_2Te_3, and hence the activation of these is comparable with the intrinsic case. An alternative possibility, mentioned in a consideration of InAs-In_2Te_3 alloys (17) is that, because of the alloying properties of In_2Te_3, whereby a gain or loss of lattice vacancies can compensate for the presence of impurity atoms, the material is effectively self-compensating and hence impurities make practically no contribution to the carrier density and only intrinsic carriers are observed.

Preliminary Thermal Conductivity Measurements

Since the above work was completed, Pamplin and Spencer have used the same samples of In_2Te_3 and Ga_2Te_3 to make preliminary measurements of thermal conductivity (K) at room temperature. The Ioffe method of measurement (18) has been used and the apparatus checked by measurements on quartz. The room temperature value of K obtained for ordered In_2Te_3 is 0.014 watts/cm°C and for samples of directionally frozen Ga_2Te_3 0.013 watts/cm°C with an estimated accuracy of ±3% in each case.

This value of K for In_2Te_3 is to be compared with the values given by Averkin *et al.* (19) of 0.008 watts/cm°C for In_2Te_3 and by Gasson *et al.* (6) of 0.0035 watts/cm°C for disordered and 0.008 watts/cm°C for ordered In_2Te_3. The range of values of K obtained in the various cases reflect the degree of ordering which is present. It is to be noted that the ratio of maximum to minimum measured values of K is considerably less than the corresponding ratio for electrical mobility. Thus it is seen that ordering in these materials improves the thermoelectric figure of merit.

Acknowledgments

The authors are indebted to Professor L. F. Bates and Professor D. A. Wright for the facilities of their laboratories. They wish to thank Mr. P. M. Spencer for making the measurements of thermal conductivity. The crystallographic and electrical work described forms part of an investigation carried out for the Admiralty, and was a section of the thesis submitted by B.R.P. in part fulfilment of the requirements for a Ph.D. at Nottingham University (1960).

Manuscript received Feb. 13, 1961; revised manuscript received May 4, 1961.

Any discussion of this paper will appear in a Discussion Section to be published in the June 1962 JOURNAL.

REFERENCES

1. G. Appel and G. Lautz, *Physica*, **20**, 1110 (1954).
2. J. C. Woolley, B. R. Pamplin, and P. J. Holmes, *J. Less Common Metals*, **1**, 362 (1959).
3. H. Hahn, *Angew. Chem.*, **64**, 203 (1952).
4. H. Inuzuka and S. Sugaike, *Proc. Japan. Acad.*, **30**, 383 (1954).
5. D. R. Mason, International Conference on Semiconductor Physics, Prague, 1960.
6. D. B. Gasson, P. J. Holmes, I. C. Jennings, J. E. Parrott, and A. W. Penn, International Conference on Semiconductor Physics, Prague, 1960.
7. V. P. Zhuze, A I. Zaslavskii, V. A. Petrusevic, V. M. Sergeeva, I. A. Smirnov, and A. I. Shelykh, International Conference on Semiconductor Physics, Prague (1960).
8. J. Appel, Z. *Naturforsch.*, **9a**, 265 (1954).
9. J. Appel, Dissertation, Braunschweig (1955).
10. G. Harbeke and G. Lautz, Z. *Naturforsch.*, **11a**, 1015 (1956).
11. G. Harbeke and G. Lautz, *ibid.*, **13a**, 771 (1958).
12. J. E. Parrott, Private communication.
13. G. Harbeke and G. Lautz, *ibid.*, **13a**, 775 (1958).
14. A. F. Ioffe, *J. Phys. Chem. Solids*, **8**, 6 (1959).
15. A. Sagar, *Phys. Rev.*, **117**, 93 (1960).
16. J. C. Woolley and C. M. Gillett, *J. Phys. Chem. Solids*, **17**, 34 (1960).
17. J. C. Woolley, B. R. Pamplin, and J. A. Evans, In press. (*J. Phys. Chem. Solids*).
18. A. F. Ioffe and A. V. Ioffe, *Sov. Phys.—Tech. Phys.*, **3**, 2163 (1958).
19. A. A. Averkin, V. M. Sergeeva, and A. I. Shelykh, *Sov. Phys. Solid State*, **2**, 319 (1960-61).

Single Crystal Silicon Overgrowths

Albert Mark

U. S. Army Signal Research and Development Laboratory, Fort Monmouth, New Jersey

ABSTRACT

The pyrolytic process for the vapor phase deposition of single crystal silicon overgrowths on parent substrates is described. This method utilizes the dissociation of silicon tetrachloride by hydrogen in an open tube flow process. Free energy and vapor pressure data are plotted for $SiCl_4$, BCl_3, and PCl_3 showing the dissociation relationship between these reacting species for junction formation. Photographs indicate the dependence on temperature of the silicon morphologies that deposit on the substrates, other variables being held constant. Because of the low thermal conductivity of silicon, emphasis is placed on direct contact heating of the silicon substrates to control overgrowth quality. Large temperature gradients were found to exist on the substrate surface with indirect heating by the reactant gases.

Recent developments in the homogeneous deposition of single crystal silicon overgrowths by pyrolysis of silicon halides and hydrides have shown the simultaneous formation of planar junctions at the overgrowth substrate interfaces. Alternate introduction of donor or acceptor impurity atoms at any particular time during the growth process results in multijunction solid-state structures.[1]

This means direct device fabrication from the vapor phase as elemental silicon is deposited on a silicon substrate. Since the conductivity type of the deposit can be changed at any increment of thickness, it becomes possible to fabricate silicon devices with geometries not possible by conventional diffusion techniques. Most important, the direct formation of devices from vapor phase reactions eliminates the complex procedures of device fabrication by chemical and physical processing of bulk ingots.

Electrical evaluations of silicon overgrowth junctions compare favorably with junctions made by diffusion techniques and show promise of improved characteristics as the various vapor phase processes are developed.

The purpose of this paper is to describe the process involved in producing a single crystal overgrowth of silicon on a silicon substrate with the controlled reduction of silicon tetrachloride by hydrogen in an open tube flow process. (Announcement of this was made in the June, 1960 issue of this *Journal*.)

Experimental Procedure

The formation of a single crystal overgrowth of silicon on a like substrate is dependent on providing a source of elemental silicon atoms which, before nucleating into polycrystalline morphologies, will react with the substrate surface and continue the oriented lattice structure without physical boundaries at the growing interfaces.

The choice of a particular silicon halide or hydride for supplying the silicon in elemental form is governed by various considerations: substrate temperature, decomposition temperatures of reactants, physical state of the reactants at room temperatures, optimum yield of silicon over substrate surfaces for proper orientation, final purity of deposited silicon, probable effect of by-products on substrate surfaces, reversibility of the reaction, design of apparatus necessary for handling explosive silicon hydrides or toxic halides, possible formation of oxides at surface interfaces, substrate preparation, and compatibility of decomposition temperatures of dopant compounds as, for example, PCl_3 and BCl_3, with that of the decomposition temperatures of the halides or hydrides.

Silicon tetrachloride met the majority of requirements for possible overgrowths in relation to silicon

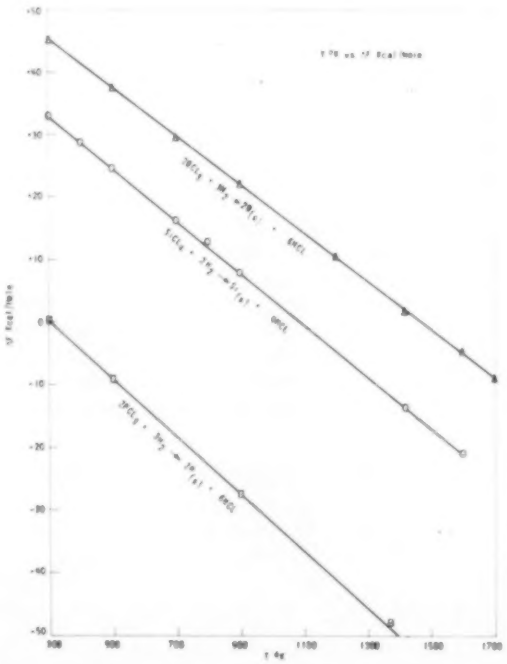

Fig. 1. Free energy vs. temperature of $SiCl_4$ reduction by hydrogen compared with p-dopant BCl_3 and n-dopant PCl_3.

[1] Merck & Co., Rahway, N. J.

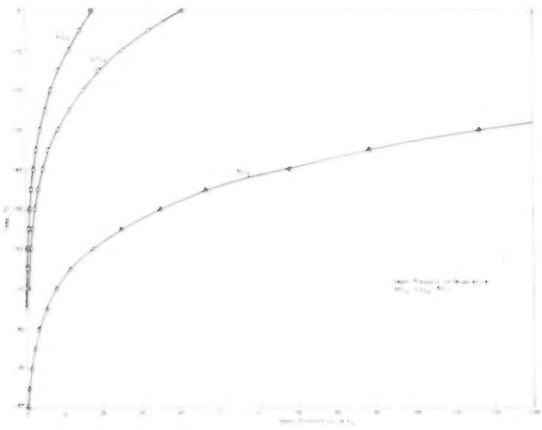

Fig. 2. Comparison of vapor pressures vs. temperature °K for $SiCl_4$, BCl_3, and PCl_3.

hydrides or the other halides and was selected on that basis.

From the calculated thermodynamic data plotted in Fig. 1, it is seen that the negative free energy values for $SiCl_4$ start at 825°C. For the tentative dopant compounds, as BCl_3, it is approximately 375° higher at 1200°C, while for PCl_3 negative free energy values begin at 25°C.

Accordingly, at any particular dissociation temperature of $SiCl_4$, the probability of the dissociation of large concentrations of phosphorus is high and for boron it would be low. These relative differences in concentrations of the reactants depositing out at an optimum epitaxial temperature of the silicon substrate can be compensated by controlling their vapor pressures at the source of entry into the system.

For the dissociation reaction

$$SiCl_4 + 2H_2 \rightarrow Si + 4HCl$$

the concentration of the $SiCl_4$ through the system was controlled by cooling with liquid nitrogen, and maintained at any particular temperature and corresponding vapor pressure by an on-and-off heater arrangement. The vapors were carried through the system by a constant flow of hydrogen bubbled into a measured volume or, alternately, by passing it over the liquid surface.

For an approximate reference, the vapor pressures of the three reacting species are plotted as shown in Fig. 2 from data derived using the Clausius-Clapeyron equation:

$$\log \frac{P}{P_o} = \frac{\lambda}{2.30\,3R}\left(\frac{1}{T_o} - \frac{1}{T}\right)$$

where λ is the latent heat of vaporization, P_o the known vapor pressure at known temperature T_o, and T the known temperature at which vapor pressure P is sought.

The initial epitaxial substrate temperatures and related dissociation temperatures of the $SiCl_4$ were explored initially by aligning twelve wafers in a quartz reactor mounted between two Globars[2] at its midsection. This resulted in diminishing temperature gradients over the substrate wafers on each side of the narrow heat zone. Temperature differences from center wafers to those on the extremities were approximately 350°C. Runs were made using various heat zone temperatures, measured over the center wafer, from 1000° to 1390°C. The hydrogen flow rates were also correspondingly varied from 200 to 4000 ml/min. The $SiCl_4$ was generated through the system at the inlet source from −60°C to room temperatures by hydrogen passing over an exposed area or bubbled through the liquid. The substrate temperatures were varied by changing the distance between the bottom of the reactor tube and the horizontal Globars.

The temperature extremities of the heat zone, in which the substrates were located, approximately corresponded to the minimum dissociation temperature of the $SiCl_4$. These temperature variations would induce many varieties of polycrystalline forms of silicon to deposit out.

Substrate No. 1, at approximately 1000°C, was always covered with gray needle silicon mixed with spiked maces. At lower temperatures the deposit was of a finer cocoon-like texture from yellow-tan to brown in color.

On substrate No. 2 and extending partly on to substrate No. 3, the deposits changed abruptly from gray needle formations to hollow and solid spheres. These again were lustrous gray or dark tan, depending on the temperature. The gray deposits regardless of the morphologies were always associated with temperatures over 1000°C, the yellow-tan deposits with lower temperatures (Fig. 3).

Substrates 4, 5, and 6, located near or in the hot zone, had smooth polycrystalline deposits with evidence of minute single crystal areas. Any previous scratches from lapping that remained on the surfaces tended to induce lineage growth. Dislocation centers induced diamond-shaped nodules to grow at these points (Fig. 4).

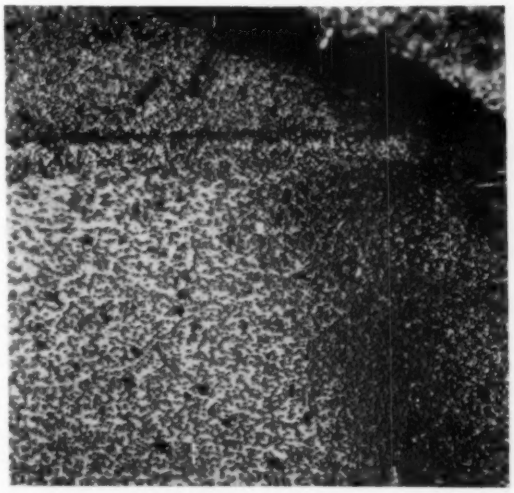

Fig. 3. Spherical silicon deposits on substrate at approximately 975°C. Magnification 30X before reduction for publication.

[2] Trademark of Carborundum Co., Niagara Falls, N. Y.

Fig. 4. Smooth polycrystalline silicon deposit with nodules growing from dislocation centers and lineage following scratch in substrate surface. Magnification 50X before reduction for publication.

Leaving the hot zone, substrate No. 7 was covered with a smooth gray metallic deposit. Approaching the right edge, the deposit changed from gray to yellow. On substrate No. 8, the surface was covered with a heavy canary yellow deposit that became dark orange toward the right edge. The surface of substrate No. 9 was attacked and pockmarked by eroded areas permeating the entire crystal. The balance of the substrates would be covered with a whitish deposit of high molecular weight silicon chlorides.

Increasing the hydrogen flow rate or bubbling it into the $SiCl_4$ resulted in heavier silicon deposits on the substrates and walls of the reactor and also caused a shifting of the deposit zone further to the right in the reactor.

It became apparent that the substrate had little influence on the character of the silicon depositing on its surface unless it was placed directly over the horizontal bottom Globar. In this location, the growth was smooth and planar. If placement was slightly to the right or left of this position, the substrate edge farthest from the Globar was covered with tan-brown amorphous silicon. If the hydrogen flow rate was less than 200 ml/min (H_2 over $SiCl_4$ surface) at 1150°C, the substrate surfaces would erode, or the expression

$$Si + 3HCl \rightarrow SiHCl_3 + H_2$$

would tend to dominate the reaction.

Use of the two-Globar furnace established the general parameters for epitaxial overgrowths from studies of the silicon morphologies that deposited out as a result of temperature gradients and diminishing concentrations of $SiCl_4$ passing over the substrates.

Overgrowth apparatus.—Silicon overgrowths were made in the apparatus shown in Fig. 5. In this system the range of the constant heat zone was increased by

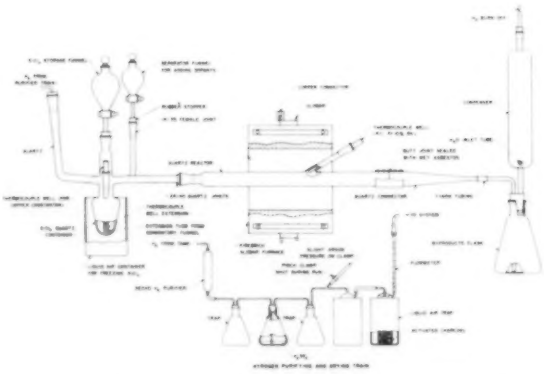

Fig. 5. Diagram of original overgrowth apparatus for silicon.

surrounding the midsection of the reactor by a network of Globars. With the exception of the Pyrex condenser and drying train, the separate components were made of quartz. The drying train can be eliminated if extra dry, high-purity hydrogen is available. It consists of a Deoxo[3] unit, a flask containing H_2SO_4, two liquid nitrogen traps, and a 0-5000 cc/min flowmeter.

The complete apparatus, for descriptive purposes, can be divided into three main sections: Section 1 is the materials inlet source and attaches to Section 2 through a 24/40 male quartz joint. Section 2 is the reactor proper in which the substrates are heated and the dissociating $SiCl_4$ supplies the elemental silicon for epitaxial overgrowths. Section 3 is the posterior unit that collects and dissipates the reaction by-products during a run and connects and seals to section 2 by an asbestos-covered butt joint.

Referring again to Fig. 5 for a more detailed description, the inlet section consists of a transparent quartz bulb and is tapered along its length. In its upper section it terminates in a 24/40 female quartz joint for adapting through a male joint, the storage funnel containing the liquid $SiCl_4$. The long tube extending from the funnel is placed just above the bottom of the bowl. The main stem supports three inlet arms integrated into its body at 90° angles to each other. The hydrogen inlet arm extends out almost horizontally and then bends to an angle slightly over 90°. The extension arm leading to the reactor is almost horizontal and tapers slightly back to the direction of the bowl. It terminates in a male 24/40 quartz joint for connecting to the reactor. The smaller diameter supporting arm is for introducing liquid or gaseous dopants into the system. A thermocouple well is mounted on the shoulder of the bulb and is at an acute angle of approximately 20°. It terminates in a 14/35 quartz joint. Its male counterpart is a tube of quartz that extends down into the bowl, with its upper terminus ending in a male 14/35 quartz joint hermetically sealed during a run. A copper-constantan thermocouple wire rests at the closed end of the tube for controlling and monitoring the temperature of the $SiCl_4$. A 5-amp heater jacket (not shown) immersed in alcohol embraces the bowl which, in turn, is in a Dewar flask containing liquid nitrogen.

[3] Engelhard Industries, Inc., Newark, N. J.

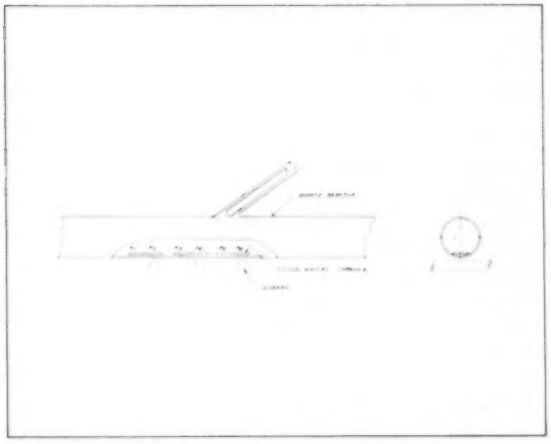

Fig. 6. Positions of silicon substrates in reactor during runs

Section 2 comprises the quartz reactor. The anterior end terminates in a female 24/40 quartz joint and seals to its male counterpart when assembled. The posterior end is left open for sealing, with wet asbestos, to section 3 after substrate placement. A quartz thermocouple well is incorporated into the midsection of the reactor and houses through its male counterpart a platinum-rhodium thermocouple for monitoring the heat source. The thermocouple well is at an approximate angle of 30°.

Section 3 when assembled is comprised of three separate pieces of Pyrex and miscellaneous glass tubing. The wide end of a quartz connector seals to the reactor. The tapered end connects with Tygon tubing to a Pyrex tube which is bent at right angles and is supported in a two-hole stopper mounted in a heavy-walled flask. This, in turn, holds a water-cooled condenser mounted in its neck. A tapered jet tube for burning off exhaust hydrogen is attached to the top of the condenser through a rubber stopper.

The heat source comprises eight pieces of firebrick, housing six horizontal and four vertical Globar heating elements mounted within its body. Three of the horizontal Globars are aligned above the reactor and the other three below the reactor at its midsection. The four vertical Globars are aligned two on each side of the reactor tube at its midsection between and equidistant from the center horizontal Globars. Power is supplied by a 150-amp transformer assembly and monitored by commercial records and controllers.

Run cycle.—Six silicon wafers were used in each experimental run and positioned as shown in Fig. 6. These were sliced from [100] oriented bulk ingots. Resistivities ranged from 0.1 to 10 ohm-cm. Wafers were ½-⅝ in. in diameter and lapped to 10-11 mils thickness. Mechanical polishing of surfaces was done with ¼μ diamond polishing compound. For deposition on a chemically treated surface, the wafers were etched down to 7 mils in a fast etch consisting of 1 part acetic acid, 5 parts nitric acid, and 5 parts hydrofluoric acid. In most instances, increasing the acetic acid content to 3 parts resulted in smoother, more planar surfaces. On some crystals, however, the etched surface acquired a grayish mottled appearance. Mixing small portions of the etches instead of bulk quantities resulted in more uniform, nonreflective surfaces. Etching times varied from 6 to 30 sec to remove 3 mils of silicon. The etching action was stopped by flooding the acid solutions with water. The wafers were held by plastic tweezers and did not come in contact with air while being etched. After washing in deionized water, the etched wafers were rinsed in ethyl alcohol and dried between lint-free paper. Dust particles were removed with a static-free camel's hair brush. The wafers were aligned after etching in the midsection of the reactor and the system sealed off.

Parts of the substrate wafers were masked by placing a polished face of a quarter section of a silicon wafer in contact with the surface of the substrate crystal. This was done as a control to measure the difference in growth before and after an overgrowth deposit.

The system was dried by passing hydrogen at room temperature through the system for 30 min and burned off at the outlet jet. A yellowish flame gradually converts to a blue-green flame when all moisture present in the system is exhausted.

The power is turned on after the drying out period and is operated at no less than 1175°C and maintained at this temperature for 30 min. The hydrogen reducing atmosphere serves to remove contaminants occluded on the substrate surfaces. After substrate treatment, the temperature is lowered to 1150°C at a hydrogen flow rate of 250 ml/min; 75 cc of $SiCl_4$ that has been cooled near its freezing point is introduced into the separatory funnel. The bulb is also reduced in temperature to approximately −100°C by adding liquid nitrogen to the Dewar. The separatory funnel is slowly emptied of $SiCl_4$ that freezes into a white solid mass as it enters the bulb.

The reaction is started by applying a rapid charge of current through the heater jacket, causing instant thawing of the $SiCl_4$. The volatile vapors are carried over the substrate surfaces by the hydrogen. The temperature of the $SiCl_4$ is kept at −30°C during the run which corresponds to an approximate vapor pressure of 6.3 mm Hg. The deposition rate of the silicon overgrowth at these parameters is approximately 6 μ/hr.

Experimental Results

Substrate wafers at positions No. 1 and 2, as in the two Globar furnaces, were always covered with a heavy deposit of polycrystalline, lustrous gray, mixed needle and spherical silicon. There was an abrupt change in the deposit characteristics on substrates at position No. 3 from mixed random parasitic morphologies loosely attached to the substrate surfaces to metallic gray deposits with a grainy texture and firmly bound to the substrate surface.

The single crystal silicon overgrowths grew on the substrate wafers located at position No. 4 in the middle of the heat zone and directly over Globar element No. 2. Silicon overgrowths also occurred on substrates located at position No. 6 over Globar element No. 3, but were thinner and of poor surface quality. The 1150°C temperature was measured on the center of the substrate. Use of a roughly etched

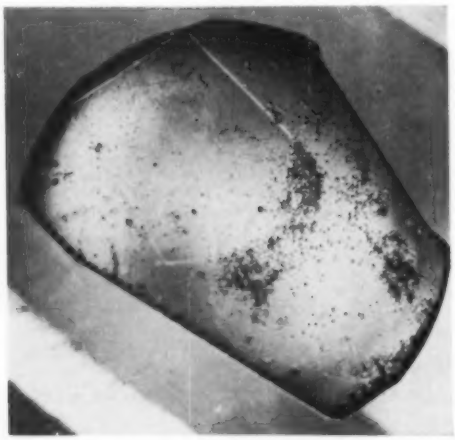

Fig. 7. Silicon overgrowth on polished surface. Masked area averaged from 1-2 μ growth. Note lineage lines extending up into shoulder of heavier deposit and continuing original configuration. Exposed surface approximately 6 μ thick measured along periphery of ridge. Unfilled areas are due to minimum concentrations of $SiCl_4$ over substrate during growth. Magnification 15X before reduction for publication.

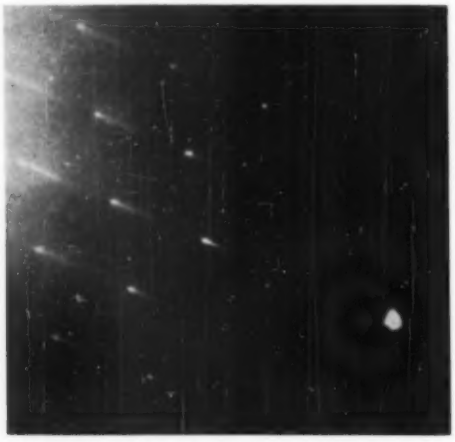

Fig. 8. Electron diffraction pattern of overgrowth surface. Sample rotated during exposure. Photo by H. S. Yearian.

substrate surface for deposition would result in a correspondingly rough overgrowth surface, with the deposit growth imitating the initial substrate configuration exposed after the etch treatment. Depositing on a highly polished silicon substrate surface would result in a corresponding smooth overgrowth surface. Temperature variations and low concentrations of reactants would leave unfilled areas in the surface. Dislocation centers would induce nodule growth (Fig. 7). A typical electron diffraction pattern of the silicon overgrowth is shown in Fig. 8.

For obtaining uniform overgrowth resistivities, the liquid dopants, such as PCl_3 and BBr_3, are added directly to the $SiCl_4$ before the start of the run. The per cent by volumes of the dopant added can be standardized and related to the resulting measured resistivity values of the overgrowth. Optimum volumes can range from 0.001% to over 1%, depending on the particular resistivity requirement.

If the dopant is not mixed initially with the $SiCl_4$ in the liquid state, it is introduced into the system separately in the vapor phase, and its vapor pressure monitored independently during the run. This is necessary with BCl_3 since it exists as a gas at normal pressures and room temperatures. Separate introduction of the dopant into the system enables varying the doping level at the overgrowth-substrate interface or within the increment of overgrowth thickness.

The choice of using liquid or gaseous dopants, or whether a liquid dopant can be mixed with the $SiCl_4$, however, is governed by the degree of diffusion into the substrate that may occur during the deposition run. This is a significant factor to consider if (*a*) the epitaxial substrate temperature is high; (*b*) the growth rate is slow; (*c*) the $SiCl_4$ would be required to contain large concentrations of the dopant; or (*d*) the overgrowth thickness would be held to minute dimensions.

Summary

Single crystal silicon overgrowths were obtained on silicon substrates at temperatures between 1150° and 1200°C with hydrogen flow rates of 250-2000 ml/min. Mole ratio of H_2 to $SiCl_4$ was no less than 60 to 1.

Quality, or surface perfection, depended on keeping substrate temperatures constant during runs and maintaining a constant vapor pressure on the $SiCl_4$ at source of entry.

Substrates would erode at temperatures above 1150°C unless the concentrations of H_2 and $SiCl_4$ were correspondingly increased, i.e., the equilibrium would shift to the left. At 1200°C and a hydrogen flow rate of 2 l/min, a 25μ deposit was obtained in approximately 30 min.

Substrate diameters were found to affect deposit characteristics. The greater their diameters, the farther they lay from the bottom heat source due to the curvature of the reactor, with a resultant decrease in the substrate temperature. Deposits on these cooler surfaces were irregular and polycrystalline.

Parasitic growths would nucleate on the substrates if the $SiCl_4$ concentration was too great for a particular substrate temperature. This occurred when, for example, the $SiCl_4$ was generated into the system at room temperatures.

Unfilled areas in the overgrowth layer would result from low concentrations of $SiCl_4$ passing over the substrates at the 1150°-1200°C substrate temperatures.

Substrate erosion tended to occur on substrates at the posterior end of the reactor where $SiCl_4$ concentrations were approaching a minimum. Substrates located between Globars had little or no growth on their surfaces. The growth that did occur tended to be polycrystalline.

Runs at high substrate temperatures resulted in faster deposits per unit time at the expense of probable diffusion effects.

Overgrowth layers were mirror images of the original substrate surfaces.

Nucleation would occur above 900°C on the reactor walls and compete with the nucleation process on the substrate wafers.

Conclusions

Overgrowths of silicon were obtained in relation to the degree of accuracy that constant temperatures could be maintained over the substrate wafers during runs. It was found that heating the substrates indirectly by the gaseous reactant atmosphere resulted in relatively large temperature gradients at numerous points measured over the entire surface, although the crystal was located in a constant heat zone. At simulated dry run conditions, with thermocouples on various locations from center to edges of the substrate face, variations in temperature averaged over 75°C. Consequently, the temperatures within the bulk of the substrate would also vary by significant proportions.

In this respect, it is not unlikely that many of the anomalous characteristics of solid-state devices are due in part to the temperature gradients existing over the silicon wafers during diffusion processing, since many of the techniques involve indirect heating by the diffusant gases and the inefficient transfer of heat from the quartz surfaces supporting and in direct contact with the wafers.

Since the morphology of the deposit is related to temperature, direct or contact heating of the substrate is the key for the occurrence of high quality oriented homogeneous overgrowths and the manifestation of inherent and stable electronic responses.

Acknowledgment

The author is indebted to Professor H. J. Yearian of Purdue University for the electron diffraction evaluations of the original samples, and to the following individuals from the U. S. Army Signal Research and Development Laboratory: Miss Marie Micale, S. Sokoloff, and C. Marlett for their technical assistance, and W. Pharo and Mrs. P. Palmateer for the preparation of the silicon wafers.

Manuscript received March 2, 1961; revised manuscript received May 19, 1961.

Any discussion of this paper will appear in a Discussion Section to be published in the June 1962 JOURNAL.

REFERENCES

1. F. D. Rossini, "Selected Values of Chemical Thermodynamic Properties," National Bureau of Standards, Washington, D. C.
2. O. A. Hougen and K. M. Watson, "Chemical Process Principles," Chap. III and VIII, Part I; Chapter XVI, Part II, John Wiley & Sons, Inc., New York (1949).
3. W. E. Garner, "Chemistry of the Solid State," Chap. 6, Academic Press, New York (1955).

Oxidation-Resistant Silicide Coatings for Columbium and Tantalum Alloys by Vapor Phase Reaction

R. H. Lorenz and A. B. Michael

Research Division, Fansteel Metallurgical Corporation, North Chicago, Illinois

ABSTRACT

Two oxidation-resistant silicide coatings on substrates of columbium, tantalum, and three of their alloys were investigated. For the "conversion" coating, a thin layer of the substrate was converted to its silicides. The "duplex" and more oxidation-resistant coating was produced by depositing a molybdenum-rich layer on the substrate and converting this to molybdenum disilicide. The silicides were formed by vapor phase reaction with silicon tetrachloride and hydrogen. The coating techniques are described, and the structures and oxidation mechanisms of the coatings are discussed. On columbium alloys, the "conversion" and "duplex" coatings gave excellent protection in air at 1260°C for up to 40 and 70 hr, respectively, under cyclic conditions. These coatings were less effective for protecting tantalum and the tantalum alloy.

Columbium-base and tantalum-base alloys which possess a combination of high-temperature strength, low-temperature ductility, ease of fabrication, and good weldability have been developed. However, the alloys exhibiting these desirable properties oxidize at high rates in air at the anticipated service temperatures of 1100°C and higher. It is generally recognized that protective coatings will be required if the high-temperature potentialities of these alloys are to be realized (1-3).

The physical properties required of protective coatings on these materials vary considerably with the intended application. However, the primary requirements for an ideal coating are: it should be a thin, adherent, self-healing, oxidation-resistant layer which will block the diffusion of oxygen and nitrogen into the base metal and be capable of cold and hot deformation and thermal cycling without failure. The method of applying the coating should produce a uniform and smooth layer on irregular shapes and have a high reliability without sacrificing the desirable properties of the base material.

A consideration of the various possible protective coating systems indicated that one coating probably would not meet all of the requirements. In the work reported here, oxidation-resistant silicide coatings,

applied by vapor-phase-deposition techniques, were selected since, to a fairly large degree, they satisfied the primary requirements of an ideal coating with the exceptions that they were neither markedly self-healing nor capable of cold deformation. The silicides have high melting points and preliminary studies showed that the oxidation resistances of silicides of some columbium and tantalum alloys were promising although inferior to the highly oxidation-resistant molybdenum disilicide. The vapor-phase-deposition technique was selected because it was well suited to the formation of silicide coatings on refractory metal substrates. The reaction of silicon tetrachloride and hydrogen with the substrates studied was found capable of producing a uniform, smooth, and thin coating on irregular surfaces without impairing the properties of the base materials.

Two types of coatings were investigated. In one case, the metal or alloy substrate was reacted with silicon tetrachloride and hydrogen to convert a surface layer to its silicides. This coating will be referred to as the "conversion" coating. The compositions and oxidation resistances of the silicide layers formed by the "conversion" technique were, of course, dependent on the compositions of the substrates. The other coating, referred to as the "duplex" coating, was produced by depositing a molybdenum-rich layer on the substrate and then reacting it with silicon tetrachloride and hydrogen to form a molybdenum disilicide layer. Molybdenum disilicide was selected because of its exceptionally high resistance to oxidation, high melting point, and the compatibility of its coefficient of thermal expansion with those of columbium, tantalum, and the alloys investigated.

The vapor deposition of molybdenum disilicide on molybdenum has been investigated in considerable detail. This coating was reported to have a lifetime of 1000 hr in air at 1700°C (4). Data for the properties of vapor-deposited silicides on columbium and tantalum are meager, although it has been reported that silicide coatings on these metals are protective in air at 1000°C (5). There are no published data for the properties of vapor-deposited silicides on columbium and tantalum alloys or molybdenum disilicide on substrates of columbium, tantalum, and their alloys.

Experimental Procedures

Materials and tests.—Conversion and duplex coatings were investigated on sheet prepared from cast columbium, tantalum, two columbium-base alloys, and a tantalum-base alloy. The compositions of these materials are given in Table I.

Oxidation tests, bend ductility measurements, and metallographic and x-ray studies were made on coated specimens, 1.5 x 0.5 x 0.10 in. The edges of the specimens were ground to a radius of about 0.02 in. and then etched in an aqueous solution containing 7 wt% HF, 16 wt% HNO_3, and 61 wt% H_2SO_4, prior to coating. Oxidation tests were in air using zirconia boats and Globar or platinum wound furnaces in which the flow of air was maintained to give one volume change per minute. Weight changes during oxidation testing were obtained by periodically removing the specimens from the furnace and, after cooling to room temperature, weighing them to the nearest 0.2 mg on an analytical balance. This resulted in cyclic testing of the specimens, ranging up to 11 cycles for the more oxidation-resistant coatings. Microhardness traverses were used to measure the extent of oxygen diffusion after testing. Bend ductility tests were made over a radius of about 0.05 in. at room temperature.

Conversion coating.—The conversion-type coating was formed by the vapor-phase reaction of the substrate materials with commercial $SiCl_4$ and hydrogen having a dew point below −40°C.

A line drawing of the apparatus is shown in Fig. 1. A molybdenum wire basket was used for supporting the specimen, S, in a 1 in. diameter Vycor tube, V. When a spot welded molybdenum wire was used to support the specimen, defects traceable to the welding were observed. Heating was by means of an external induction coil, C, using a frequency of 450 kc. The optimum coating temperature for the materials studied was 1450°C.

After the system was purged with hydrogen, the specimen was heated to 1450°C. Silicon tetrachloride then was introduced by passing hydrogen through liquid $SiCl_4$ contained in the flask, W, at room temperature. The resulting vapor contained from 25 to 30 mole % $SiCl_4$, as determined by the vapor pressure of $SiCl_4$. Alternatively, liquid $SiCl_4$ was introduced into the evaporation flask, E, where it was vaporized and mixed with hydrogen. The reaction was continued for 20 min producing a well-defined, 0.002 in. silicide layer. At lower temperatures and higher $SiCl_4$ concentrations, silicon was deposited at a higher rate than was required for silicide formation, and a sur-

Table I. Compositions of substrates

Material	Composition (wt %)										
	Cb	Ta	W	Zr	Ti	Fe	Ni	Si	N	O	C
Columbium	Bal.	0.05	0.01	0.01	0.005	0.007	0.007	0.01	0.015	0.03	0.015
Tantalum	0.06	Bal.	0.01	—	0.01	0.005	0.005	0.01	0.002	0.003	0.005
Cb-Ta-Zr alloy (82 Alloy)*	Bal.	32	0.02	0.7	0.02	0.007	0.007	0.001	0.018	0.07	0.015
Cb-Ta-W-Zr alloy	Bal.	28	4.5	0.6	—	—	—	—	0.012	0.051	0.036
Ta-W alloy (Tantaloy)*	0.04	Bal.	10	—	0.02	0.008	—	0.02	0.004	0.004	0.006

* Trade designations.

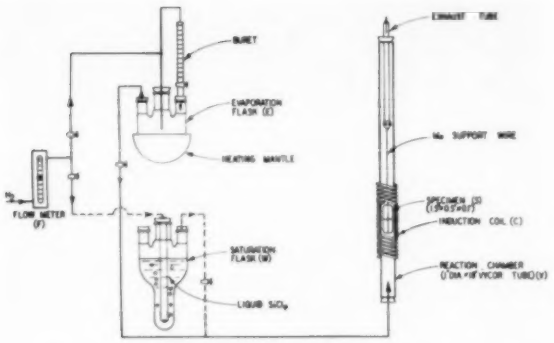

Fig. 1. Schematic diagram of siliciding apparatus

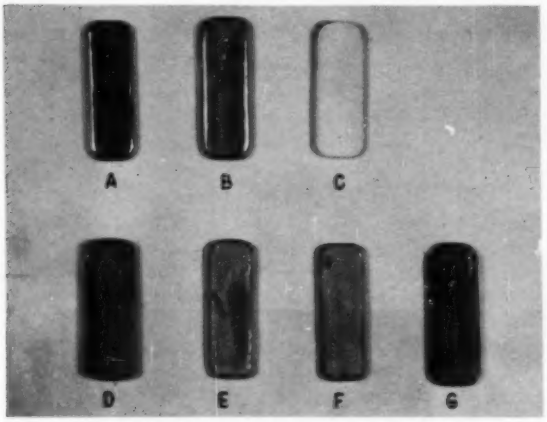

Fig. 2. Cb-Ta-Zr alloy at various stages of coating and after testing: (A) uncoated, (B) conversion coated, (C) conversion coated after 20 hr in air at 1260°C, (D) after immersion in liquid MoO_3, (E) after hydrogen reduction of MoO_3, (F) duplex coated after siliciding, (G) duplex coated after 20 hr in air at 1260°C.

face layer of silicon was formed. This silicon layer could be removed by maintaining the specimen at 1450°C in the absence of $SiCl_4$ to permit diffusion and conversion of the excess silicon to the silicides. A specimen, at the various stages of the conversion coating process and after exposure to air at 1260°C for 20 hr, is shown in Fig. 2A through 2C.

A zone coating technique was used for the siliciding of large and irregularly shaped specimens, in which case the specimen was moved through the induction coil, limiting the coating reaction to the hot zone. For specimens having irregular shapes, the hot zone was maintained at a constant temperature by varying the power input to the induction coil.

During the coating process, columbium, tantalum, and their alloys pass through the temperature range where the solubility of hydrogen in them is high. This gives rise to the possibility of hydrogen embrittlement. In the work reported here the rates of heating and cooling were high, and hydrogen pickup was not significant. This was based on the observation that on heating and cooling in pure hydrogen, in the same manner used during the coating process, the hardnesses and ductilities of uncoated columbium and tantalum specimens were not affected. However, with massive sections the rates of heating and cooling may

Table II. Methods of deposition of molybdenum-rich-layer for duplex coating

Method	Remarks
1. Flame spraying of Mo powder	Poor adherence.
2. Vapor plating with $Mo(CO)_6$	Poor reproducibility.
3. Vapor deposition of MoO_3	Easily done; good results.
4. Immersion in liquid MoO_3	Easily done; good results.
5. Deposition of $MoSi_2$ from $MoCl_5$-$SiCl_4$-H_2 vapor.*	Initial attempts not encouraging. Not extensively investigated.

* Saturated solution of $MoCl_5$ in $SiCl_4$ introduced into evaporation flask at 100°C.

be low enough to permit hydrogen embrittlement. In this case it would be necessary to carry out the heating and cooling in an inert atmosphere or vacuum.

Duplex molybdenum disilicide coating.—The techniques surveyed for preparing the duplex coating are summarized in Table II. With the exception of the formation of $MoSi_2$ by codeposition from a $SiCl_4$-$MoCl_5$-H_2 vapor, these techniques required the deposition of molybdenum metal or a molybdenum compound on the substrate. This was followed by the conversion of the molybdenum-rich layer to $MoSi_2$ by reaction with $SiCl_4$ and hydrogen, as described in the previous section. The selection of the duplex coating techniques used in this work was based on the degree and reliability of the oxidation and contamination resistances of the coatings produced by the various methods given in Table II.

For columbium and columbium alloys the best duplex coatings were obtained by: (*a*) deposition of MoO_3 from the liquid phase, (*b*) reduction in hydrogen at 800°C, and (*c*) conversion to molybdenum disilicide by reaction with $SiCl_4$ and hydrogen for approximately 20 min. This resulted in a 0.002-0.003 in. outer layer of $MoSi_2$ and a 0.002 in. layer of the substrate silicides. The deposition of molybdenum oxide from the liquid phase was accomplished by immersion in liquid MoO_3 at 800°C. The molybdenum oxide layer was adherent and was identified as a mixture of MoO_3 and Mo_nO_{3n}. Attempts to apply a molybdenum oxide layer on a conversion coating by liquid phase immersion were not successful because the silicide surfaces were not wet by molybdenum oxide. A specimen at the various stages of the duplex coating process and after exposure to air at 1260°C for 20 hr is shown in Fig. 2D through 2G.

For tantalum and the tantalum alloy the best results were obtained by producing a 0.001 in. conversion coating on the substrate followed by the deposition of MoO_3 from the vapor phase. After reducing the molybdenum oxide in hydrogen at 800°C and then siliciding the resulting Mo layer to $MoSi_2$ by reaction with $SiCl_4$ and hydrogen, a 0.002 in. silicide layer containing only a small amount of $MoSi_2$ was produced. The deposition of MoO_3 from the vapor phase was carried out by supporting the specimen in molybdenum oxide vapor above a bath of MoO_3 maintained at 800°C. This treatment was also suc-

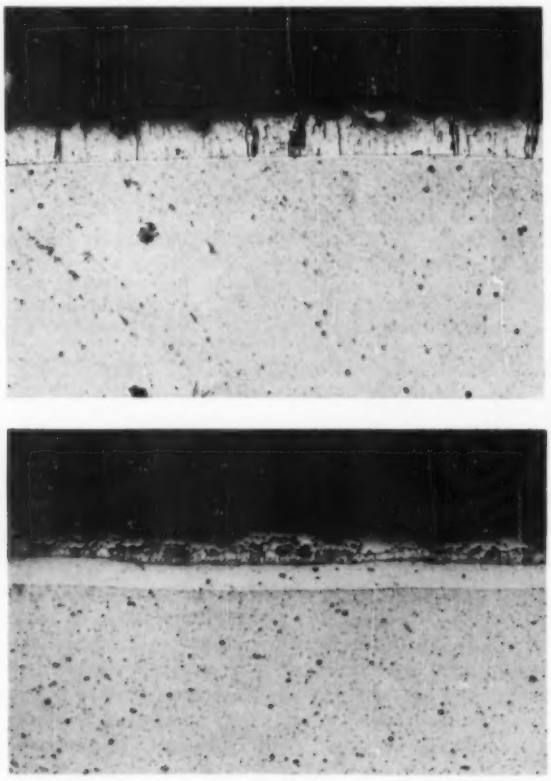

Fig. 3. Silicide layers of a conversion coating on Cb-Ta-Zr alloy before and after heating in vacuum at 1260°C. (A) (top) As coated, (B) (bottom) after 64 hr. Magnification 300X before reduction for publication.

cessfully applied to columbium and columbium alloys.

The application of MoO_3 from the liquid phase to tantalum and the tantalum alloy resulted in embrittlement of the base metal after formation of the silicide layers. Up to the final siliciding step, however, the base material remained ductile. The reasons for this occurring with tantalum and not columbium were not established.

Results

Coating structures.—Conversion coatings.—As-silicided conversion coatings on columbium, tantalum, and their alloys consisted of two distinct silicide layers, as shown in Fig. 3A for a coating on the Cb-Ta-Zr alloy. The outer columnar silicide was identified as $CbSi_2$ on columbium and as $TaSi_2$ on tantalum. On the two columbium alloys the predominant structure was $CbSi_2$. The outer layer of the conversion coating on the tantalum-tungsten alloy contained principally $TaSi_2$ with some WSi_2. The inner zone on the Cb-Ta-Zr alloy had the $M_{4.5}Si$ structure where M is either Cb or Ta. In order to obtain an x-ray diffraction pattern from the inner zone, the as-silicided Cb-Ta-Zr specimen was heated in vacuum for 200 hr at 1260°C to permit the inner zone to grow at the expense of the outer disilicide layer. This resulted in an inner zone of $M_{4.5}Si$, which was the major phase, and an outer zone of M_5Si_3. A comparison of Fig. 3A and 3B shows the growth of the inner zone during this diffusion treatment. A decrease in weight was also observed after diffusion, and some of the porosity evident in Fig. 3B is attributed to the evaporation of silicon during heating in vacuum. No attempt was made to identify the inner zone for the other materials. The similarity of the columbium-silicon and tantalum-silicon systems and the almost ideal solid solutions in binary columbium-tantalum alloys suggests that this zone would have the same structure in all the materials investigated, with the possible exception of the alloys containing tungsten (6, 7).

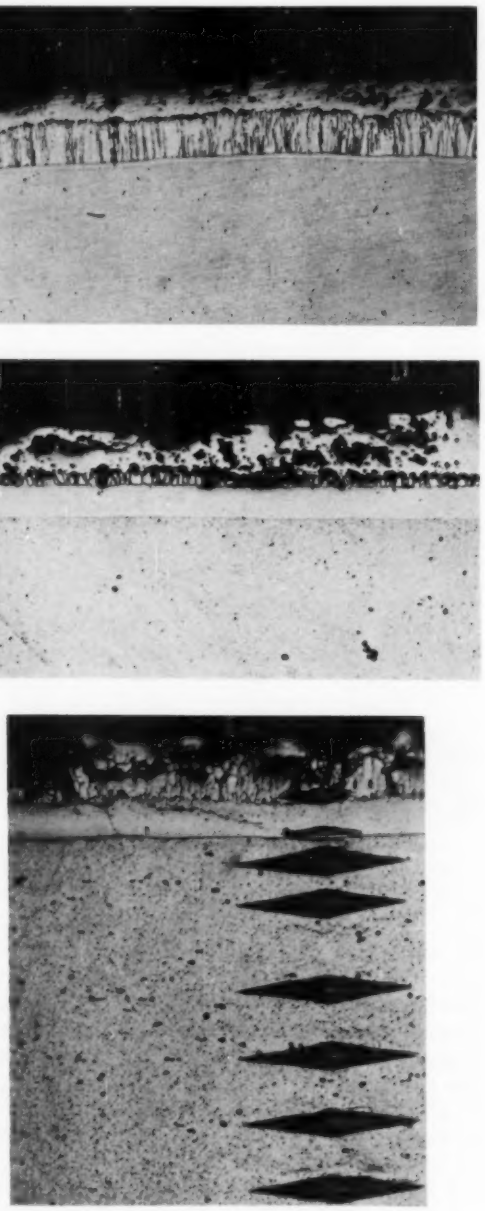

Fig. 4. Silicide layers of a duplex coating on Cb before and after heating in vacuum and in air at 1260°C. (A) (top) As coated, (B) (center) after 64 hr in vacuum, (C) (bottom) after 64 hr in air. Magnification 300X before reduction for publication.

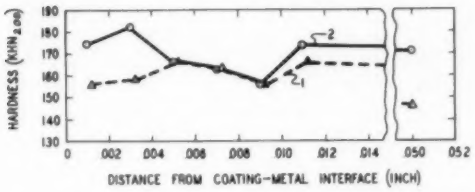

Fig. 5. Substrate hardnesses after oxidation testing of coatings on a Cb-Ta-Zr alloy. [1] Conversion coated after 20 hr in air at 1260°C, [2] duplex coated (MoO_3 liquid dip) after 64 hr in air at 1260°C.

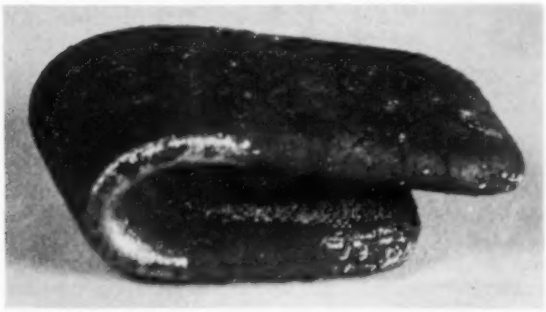

Fig. 6. Duplex coated (MoO_3 liquid dip) Cb-Ta-Zr alloy specimen bent 180° at room temperature after 71 hr in air at 1260°C.

Duplex coating.—The as-silicided duplex coatings consisted of three distinct layers, as shown in Fig. 4A, for a duplex coating on columbium. The outer layer was identified as molybdenum disilicide, and the inner layers were the same as the layers of the conversion coating. On heating in vacuum the innermost layer grew at the expense of the other layers, as shown in Fig. 4B for the duplex coating after a diffusion treatment of 64 hr at 1260°C in vacuum. However, even after 200 hr, $MoSi_2$ was still present. As in the case of the conversion coating, some of the porosity evident in Fig. 4B is attributed to the evaporation of silicon during heating in vacuum.

Oxidation behavior.—Contamination resistance.—The elevated temperature contamination of columbium, tantalum, and their alloys, due to the solution and diffusion of oxygen and nitrogen, results in embrittlement and an increase in hardness. One of the primary requirements of a protective coating is to block or retard this inward diffusion. The effectiveness of the conversion and duplex coatings in preventing contamination of the substrate materials was evaluated by microhardness traverses and room temperature bend tests before and after oxidation testing.

Microhardness traverses showed that the conversion and duplex coatings were very effective in preventing oxygen and nitrogen contamination of all of the materials investigated. After exposure to air at 1260°C, there was no measurable increase in hardness of the substrate at 0.002 in. under the coating after 64 hr for the duplex coating and after 20 hr for the conversion coating, Fig. 5. Room temperature bend tests demonstrated that there was no embrittlement of the parent substrate materials after exposure to air at 1260°C for up to 71 hr, as shown in Fig. 6.

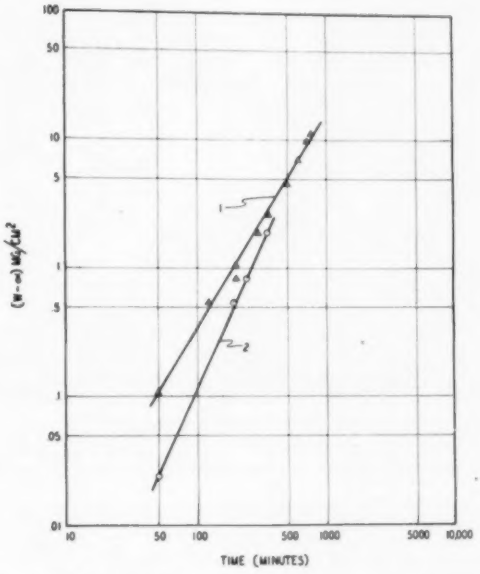

Fig. 7. Weight gain vs. time of exposure to air at 1260°C. [1] Conversion coated Cb, [2] Duplex coated (MoO_3 vapor treated) Cb.

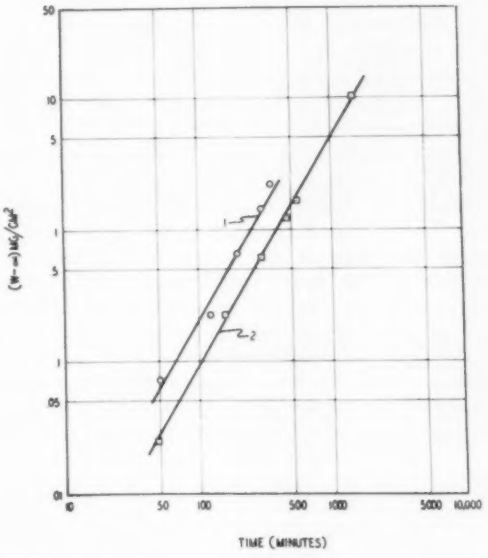

Fig. 8. Weight gain vs. time of exposure to air at 1260°C. [1] Conversion coated Ta-W alloy, [2] duplex coated (MoO_3 vapor treated) Ta.

Although the deformation during bending resulted in cracking and spalling of the coating there was no evidence of failure in the substrate.

Oxidation rates.—The weight increases prior to "failure" of the conversion and duplex coatings on exposure to air at 1260°C are summarized in Fig. 7 through 10. Note that in these figures, data from an individual specimen is plotted with a common symbol. Thus, curve No. 1 in Fig. 10 is based on data from 3 separate specimens. These data can be expressed as $(w - \alpha) = kt^n$, where w is the weight increase in

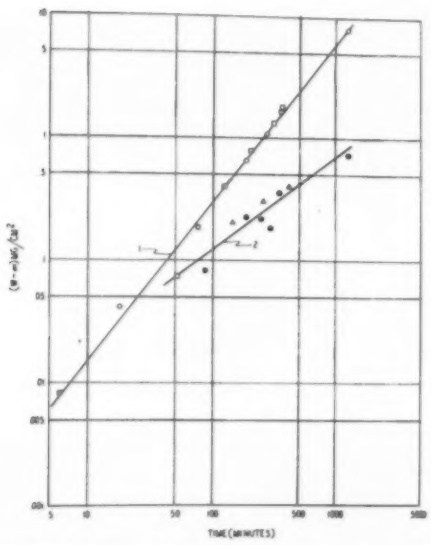

Fig. 9. Weight gain vs. time of exposure to air at 1260°C. [1] Conversion coated Cb-Ta-Zr alloy, [2] duplex coated (MoO_3 liquid dip) Cb-Ta-Zr alloy.

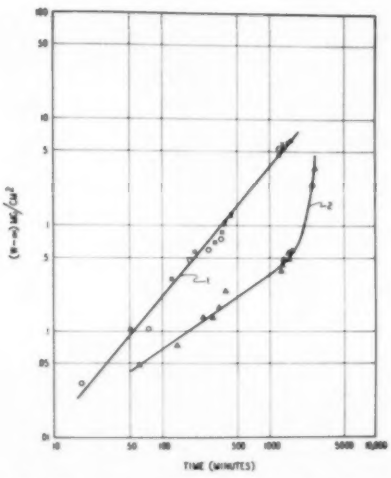

Fig. 10. Weight gain vs. time of exposure to air at 1260°C. [1] Conversion coated Cb-Ta-W-Zr alloy, [2] duplex coated (MoO_3 liquid dip) Cb-Ta-W-Zr alloy.

g/cm² at constant temperature, t is the time in minutes, and α, k, and n are constants. Since there was no contamination of the substrate materials, the measured increase in weight was attributed solely to oxide formation on the coating. For the purposes of this work, the inception of coating "failure" was taken as the point at which there was a rapid increase in the rates of oxidation as indicated by an abrupt change in slope of the weight gained *vs.* time curve, as shown by Curve 2 of Fig. 10.

The constants α, k, and n are summarized in Table III in the order of increasing values of n which also corresponds more or less to the order of decreasing lifetimes. Thus, the lowest rate of oxidation was observed for the duplex coating on the Cb-Ta-Zr alloy and the highest rate of oxidation for the conversion coating on tantalum.

Coating lifetimes.—Two modes of coating breakdown were observed for the conversion and duplex coatings: premature breakdown in isolated areas due to imperfections and uniform breakdown. The coating "lifetime" referred to in Fig. 11 is the time for the inception of coating "failure," as characterized by a uniform scaling of the entire specimen. The figure shows a plot of the logarithm of the lifetime of the conversion coating on a Cb-Ta-Zr alloy as a function of the absolute temperature. If the slope of the curve is interpreted as an activation energy, a value of 114 kcal/mole is obtained for the over-all oxidation process. The lifetimes at 1260°C for all the coatings and substrates investigated are summarized in column 4 of Table III. The lifetimes given in the table are to break down in isolated areas.

Discussion

Failure due to coating imperfections resulted in excessively high rates of oxidation in isolated areas. A typical failure of this type due to a pinhole is shown in Fig. 12 for a conversion coating on the Cb-Ta-Zr alloy. Premature failure occurred after 20 hr at 1260°C, whereas a similar coating, free of imperfections, had a life of 40 hr at this temperature.

Table III. Values of α, k, and n, and lifetimes of conversion and duplex coatings on various substrates

Substrate	Coating	Constants			Lifetimes* at 1260°C (hr)			
		α, mg/cm²	k, mg/cm²-min^n	n	max	min	average	Estimated standard deviation
Cb-Ta-W-Zr alloy	Duplex (MoO_3 liquid treated)	0	2.68×10^{-6}	0.704	44	17	31	±13
Cb-Ta-Zr alloy	Duplex (MoO_3 liquid treated)	0	3.72×10^{-6}	0.758	71	17	34	±23
Cb-Ta-W-Zr alloy	Conversion	0.0163	7.68×10^{-4}	1.22	28	19	23	±4
Cb-Ta-Zr alloy	Conversion	0.0163	7.41×10^{-4}	1.30	42	6	24	±10
Ta-W alloy	Conversion	0.106	1.47×10^{-4}	1.68	21	6	12	±6
Columbium	Duplex (MoO_3 vapor treated)	0.106	2.96×10^{-5}	1.74	—	—	25**	—
Columbium	Conversion	0.204	6.55×10^{-5}	1.74	17	6	10	±6
Tantalum	Duplex (MoO_3 vapor treated)	0.416	3.96×10^{-6}	2.23	15	6	12	±5
Tantalum	Conversion	—	—	—	2.4	0.05	0.6	±0.9

* To occurrence of first failure, usually in localized area observed as a pinhole.
** One test.

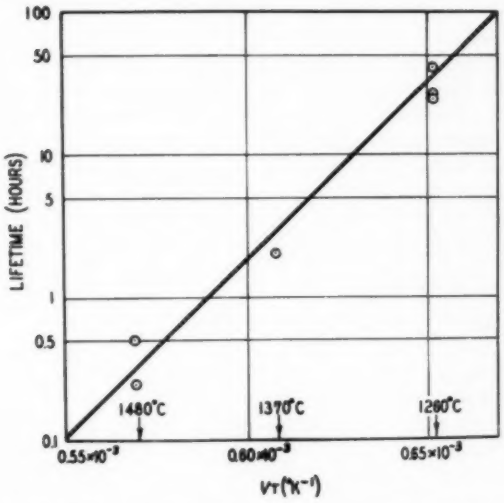

Fig. 11. Lifetime of the conversion coating on a Cb-Ta-Zr alloy vs. temperature. $(\text{Lifetime})^{-1} = 4.77 \times 10^{14} \exp(-114 \times 10^3/RT)$.

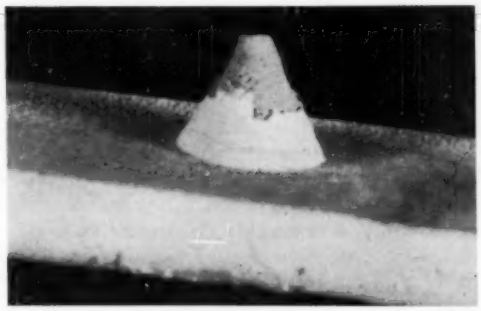

Fig. 12. Typical pinhole failure in a conversion coating on the Cb-Ta-Zr alloy after 20 hr exposure to air at 1260°C.

Pinhole failure was reduced by vapor deposition of MoO_3 as well as by thorough surface cleaning and careful handling to avoid sources for the formation of these defects. Premature failure also was found to occur at sharp edges and corners. An examination of the coating in these areas showed a plane of weakness in the growth pattern, which acted as a "pipe" and resulted in excessively high rates of oxidation. This was reduced by providing a generous radius at the edges and corners. The increased lifetimes, obtained by the vapor deposition of MoO_3 on the conversion coating and then conversion to $MoSi_2$, apparently resulted from the sealing of imperfections by this treatment.

Diffusion controlled oxidation, which determined the lifetimes of the conversion and duplex coatings, was characterized by a continuous growth of the oxide layer according to the equation, $(w - \alpha) = kt^n$. This oxidation process commenced by the formation of a lineal oxide network, as shown in Fig. 13, for a coating after 10 min in air at 1260°C. The interior of the network showed only the interference colors characteristic of thin oxide films, although oxide nodules were beginning to form. No change in the thicknesses or structures of the disilicide and inner silicide layers was apparent in this short time. With

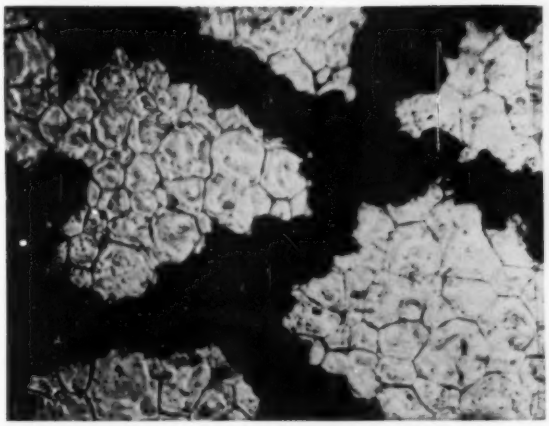

Fig. 13. Initial oxide formation on the surface of a conversion coating on the Cb-Ta-Zr alloy after 10 min in air at 1260°C. Magnification 750X before reduction for publication.

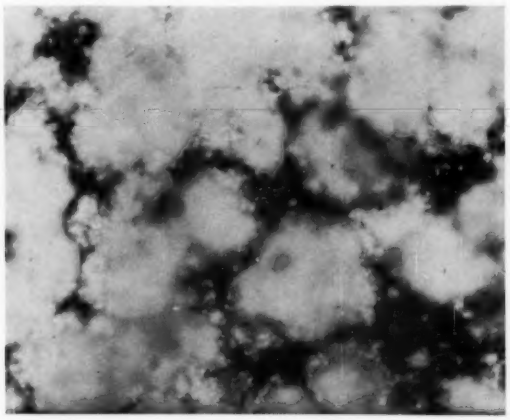

Fig. 14. Oxide formation on the surface of a conversion coating on the Cb-Ta-Zr alloy after 16 hr exposure to air at 1260°C. Note whisker growth. Magnification 250X before reduction for publication.

increasing times the oxide network was more pronounced, as shown in Fig. 14 for a coating after 16 hr in air at 1260°C. There was also a significant increase in the thickness of the inner silicide layer which had grown at the expense of the outer disilicide layer. After 20 hr in air at 1260°C a continuous white oxide layer had developed on the conversion coating, Fig. 2C and 15, whereas only a thin blue oxide layer had developed on the duplex coating, Fig. 2G. After 64 hr in air at 1260°C the duplex coating had developed a lineal oxide network, as shown in Fig. 16. X-ray diffraction showed that the oxidation products formed on the conversion coatings contained the H form of Ta_2O_5 and/or Cb_2O_5, depending on the substrate, and only a small amount of α-cristabolite. However, emission spectrography showed the presence of considerable silicon, from which it is inferred that silicon is present in a glassy phase. The oxidation products formed on the duplex coating were not identified.

In the preceding discussion it has been shown that the inner silicide layer grows at the expense of the disilicide layer, in vacuum or air at elevated temperatures, until the disilicide layer is consumed.

Fig. 15. Cross section of a conversion coated Cb-Ta-Zr alloy showing the continuous white oxide layer, after 20 hr in air at 1260°C. Polarized light. Magnification 300X before reduction for publication.

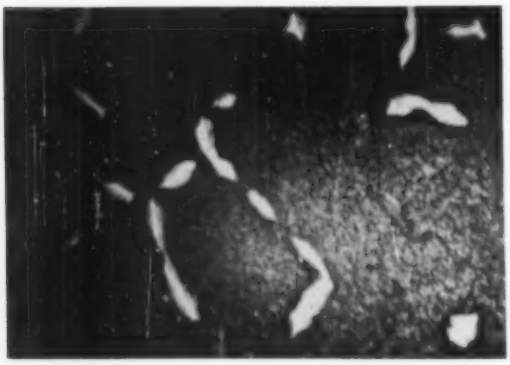

Fig. 16. Formation of the oxide network on the surface of a duplex coated (MoO_3 liquid dip) Cb-Ta-Zr after 64 hr in air at 1260°C. Magnification 10X before reduction for publication.

Growth of the inner zone can result from the diffusion of silicon inward to the substrate interface and/or the diffusion of substrate atoms to the disilicide interface. On the basis of the data obtained, however, it was not possible to establish unequivocally the predominate mechanism. Inert marker diffusion experiments would be necessary to do this. Oxidation tests on specimens which had only the M_5Si_3 and $M_{5-x}Si$ layers, prepared by vacuum diffusion of the conversion coated Cb-Ta-Zr alloy as described previously, had a very high oxidation rate with a coating lifetime of only 2 hr in air at 1260°C.

These observations indicate that the lifetimes of the conversion and duplex coatings are determined by the rate of decrease in thickness of the disilicide layer, which is dependent on the rate at which it is oxidized and the rate of increase in the thickness of the inner lower silicide zones which grow at the expense of the disilicide layer. These inner zones have a low resistance to oxidation, and coating failure occurs with the disappearance of the disilicide layer.

It is proposed that the rates of oxidation of these coatings are lower on columbium than on tantalum due to lower diffusion rates of silicon and/or metal atoms through the lower silicide layers on columbium. Also, the rate of oxidation of the duplex coating is lower than for the conversion coating. This may be due mainly to the higher oxidation resistance of molybdenum disilicide as compared to columbium and tantalum disilicides. A higher oxidation resistance would lower the rate at which the thickness of the disilicide layer is decreased. Lower rates of oxidation and longer lifetimes were observed for coated Cb-Ta-Zr and Cb-Ta-W-Zr alloys than for unalloyed columbium and tantalum. This latter observation suggests that the addition of specific alloying elements to reduce the rates of diffusion of silicon and substrate atoms would decrease the rates of oxidation and increase the lifetimes of these coatings.

On the basis of the preceding discussion, the interpretation proposed for the constants in the rate equation, $(w - \alpha) = kt^n$, is that, α relates to minute imperfections in the coating which result in an initially high oxidation rate until the imperfections are healed by the oxide formed, k is dependent on the diffusion coefficients of the components of the oxide layer, coating and substrate and n is dependent on the rate at which the thickness of the disilicide layer is reduced and depleted of silicon. In diffusion-limited oxidation, for which the mechanism is by the diffusion of defects through the oxide, the parabolic rate law applies and n is ½ and α is zero. The parabolic law assumes equilibrium concentrations at the oxide-substrate interface and infinite sources. Deviations from the parabolic rate law which were observed for the conversion and duplex coatings, Table III, are attributed in part to the finite silicon source. This results in varying boundary conditions as oxidation proceeds; that is, the composition of the disilicide layer changes while the diffusion path through the disilicide layer decreases due to growth of the lower silicide layers at the expense of the disilicide layer as well as by oxidation of the disilicide layer.

Summary and Conclusions

1. Conversion silicide coatings were formed by converting a layer of the substrate to its silicides. These coatings provided excellent contamination and oxidation protection in air at 1260°C for up to 40 hr on the Cb-Ta-Zr alloy, 20 hr on a Ta-W alloy, 15 hr on columbium and for less than 1 hr on tantalum.

2. The lifetime in hours of the conversion coating on the Cb-Ta-Zr alloy can be expressed as: $(\text{Lifetime})^{-1} = 4.77 \times 10^{14} \exp(-114 \times 10^3/RT)$, giving an activation energy of 114 kcal/mole for the overall oxidation process.

3. In one case, duplex silicide coatings were prepared by the vapor deposition of MoO_3 on conversion coated specimens, followed by reaction with $SiCl_4$ and hydrogen to form $MoSi_2$. This technique improved the oxidation resistance and reliability of conversion coatings.

4. A second duplex silicide coating was prepared by immersing an uncoated specimen in liquid MoO_3 followed by reacting wtih $SiCl_4$ and hydrogen to form $MoSi_2$. This coating provided contamination and oxi-

dation protection in air at 1260°C for up to 70 hr on a Cb-Ta-Zr alloy.

5. In all cases, oxidation protection depended on the presence of a disilicide layer, and coating failure occurred with the disappearance of this layer.

6. The oxidation of the conversion and duplex coatings can be expressed as: $(w - \alpha) = kt^n$ where w is the gain in weight, t is the time, and α, k, and n are constants. The proposed interpretation of these constants is: α relates to minute imperfections which result in an initially high oxidation rate until the imperfections are healed by the oxide formed, k is dependent on the diffusion coefficients in the oxide layer, coating, and substrate, and n, which varied from 0.7 to 2.2, is dependent on the rate at which the thickness of the disilicide layer is reduced by oxidation and by growth of the lower silicide layers at the expense of the disilicide layer. The deviations from the parabolic rate law were attributed in part to the finite source and also, in the case of the conversion coatings, to a porous, nonprotecting oxide formation. This resulted in varying boundary conditions as oxidation proceeded; that is, the composition of the disilicide layer changed and the diffusion path through the disilicide layer decreased.

7. The observed differences in the rates of oxidation of the conversion coatings on the substrates investigated were attributed to differences in rates of diffusion. This suggests that the rate of oxidation of silicide coatings could be reduced by the addition of specific elements to reduce the rates of diffusion of silicon and/or substrate atoms in the silicide layers and possibly the substrate.

Acknowledgment

The authors wish to acknowledge the assistance of R. C. Parker and F. H. Tulley who contributed to the experimental portions of this study.

Manuscript received Jan. 26, 1961. This paper was prepared for delivery before the Houston Meeting, Oct. 9-13, 1961.

Any discussion of this paper will appear in a Discussion Section to be published in the June 1962 JOURNAL.

REFERENCES

1. "Physical and Mechanical Properties of Columbium and Columbium-Base Alloys," DMIC Report 125, Feb. 22, 1960, Defense Materials Center, Battelle Memorial Institute, Columbus, Ohio.
2. A. B. Michael, "Oxidation of Columbium-Base and Tantalum-Base Alloys," in "Reactive Metals," Vol. 2, p. 487, AIME Metallurgical Society Conference, 1959. Interscience Publishers, Inc., New York.
3. A. B. Michael, "Tantalum and Tantalum-Base Alloys," AIME Symposium on Refractory Metals, Detroit, Michigan, May 1960. To be published.
4. C. F. Powell, I. E. Campbell, and B. W. Gonser, "Vapor Plating," p. 133, John Wiley & Sons, Inc., New York (1955).
5. *Ibid.*, p. 134.
6. M. Hansen, "Constitution of Binary Alloys," pp. 1018 and 1195, McGraw-Hill Book Co., Inc., New York (1958).
7. D. E. Williams and W. H. Pechin, *Trans. ASM*, **50**, 1081 (1958).
8. C. Wagner, "Diffusion and High Temperature Oxidation of Metals" in "Atom Movements," p. 153, ASM, Cleveland (1951).

Influence of Some Factors on Cathodic Formation of Hydrogen in the Mercury Cell

J. H. Entwisle and W. E. Cowley

*Research and Development Department, The Associated Octel Company, Limited, Ellesmere Port, Cheshire, England**

ABSTRACT

The influence of variations in brine pH and concentration, cathodic current density, sodium concentration in the amalgam, and movement of the cathode on cathodic hydrogen formation in the mercury cell have been studied in a laboratory cell and by polarographic methods. The kinetics of the process have also been investigated. The results indicate that the small proportion of hydrogen normally formed in the cell is determined essentially by the rate of transfer of hydrogen ions to the cathode surface. If the cathode surface should become saturated with sodium, however, the over-all rate of sodium amalgam formation can become limited by the rate of transfer of dissolved sodium from the cathode surface into its bulk. Hydrogen formation can then increase by the process

$$H_2O + e \rightarrow \tfrac{1}{2}H_2 + OH^-$$

In recent years considerable attention has been given to the study of the effect of impurities on the amount of hydrogen formed at the cathode of a mercury cell during the electrolysis of a sodium chloride brine (1-8). In contrast, little has been published of the effect of factors such as the design and the operating conditions of such a cell on the amount of hydrogen formed in the absence of impurities. In addition, the reason why this amount is normally so small is incompletely understood (9).

The effect of varying operating conditions on the current efficiencies for two of the cathodic processes in the cell, *i.e.*, sodium amalgam and hydrogen for-

* Formerly The Associated Ethyl Co. Ltd.

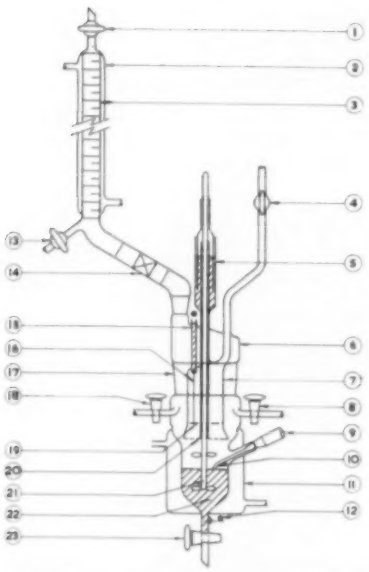

Fig. 1. Schematic diagram of laboratory cell: 1, hydrogen outlet; 2, water jacket; 3, gas buret; 4, chlorine (or chlorine and brine) outlet; 5, mercury seal; 6, cathode compartment; 7, anode compartment; 8, brine outlet; 9, salt bridge connecting to calomel electrode; 10, Luggin capillary; 11, water jacket; 12, cathode contact (Pt wire); 13, connection to pressure levelling bottle; 14, clip on flexible tube to isolate gas buret from the cell; 15, anode contact (mercury well); 16, anode contact (Pt wire); 17, B.100 joint; 18, brine inlet; 19, Pt anode; 20, sintered glass filter; 21, stirrer; 22, mercury cathode; 23, mercury outlet.

mation, has been studied in a laboratory cell in which pure mercury was used as the cathode and a pure sodium chloride brine as the electrolyte. The kinetics of the hydrogen formation process have also been studied by polarographic methods.

The results obtained indicate some of the possible rate-determining steps in the hydrogen formation process, and they permit an explanation to be given of the effect of some operating conditions on the amount of hydrogen formed. The implications of the results in terms of industrial mercury cell operation are discussed.

Current Efficiency Studies

Description of the laboratory cell.—The cell used, shown schematically in Fig. 1, was a modification of a type (10) often used in voltammetric studies at a mercury cathode under constant current conditions where a uniform current density is required. The modifications made include the provision of: (*a*) a gas buret, 3, in which any hydrogen formed at the cathode could be collected and measured; (*b*) a stirrer, 21, which could be used to stir the mercury cathode and the catholyte at constant speed, so that there was no rippling of the cathode surface; and (*c*) an inlet, 18, and outlets, 4 and 8, which could be used to feed brine through the cell at a concentration and rate sufficient to maintain a constant average sodium chloride (NaCl) content of the brine in the cell during electrolysis.

An important feature of the cell, and one which differs from designs of cell used industrially, was the diaphragm, 20. The diaphragm was made of sintered glass and separated the hydrogen and chlorine released at the cathode and anode, respectively, and enabled the hydrogen to be collected separately. The diaphragm also prevented diffusion of dissolved anodic products to the cathode.

Another feature of the cell was the water jacket, 11, which enabled the cell to be operated at any desired constant temperature by circulating water from a constant temperature bath through the jacket.

The cell was also equipped with a salt bridge, 9, and Luggin capillary, 10, to enable the cathode potential of the cell to be measured if required.

The anode of the cell consisted of a platinum disk, 19, supported by a platinum wire, 16, sealed through the mercury well, 15. Chlorine produced at the anode left the anode compartment, 7, through the outlet, 4.

The cathode consisted of 128 ml (at 20°C) of ANALAR[1] grade redistilled mercury and had an apparent area of 43 cm^2. Samples of the cathode could be taken through 23 if required. The brine used was prepared from ANALAR NaCl, and distilled water, ANALAR hydrochloric acid (HCl) being added to give the desired initial acidity.

A constant, direct current was supplied to the cell, either from a full wave a-c rectification unit or from batteries. The current passing through the cell was calculated from measurements of the voltage drop across a standard 0.1 ohm resistance placed in series with the cell.

Experimental Procedure and Treatment of the Results

It will have been noted that the design of the cell was such that it could be operated under constant known conditions, namely, temperature, cell current, stirrer speed, average NaCl content of brine, and that the initial hydrogen ion content of the brine was determined by the initial amount of HCl added to the brine with which the cell was filled.

In the first experiments the quantities of both the hydrogen and the sodium amalgam formed were measured at known times after starting the electrolysis. As the current was kept constant, the times corresponded to the passage of known quantities of electricity through the cell. The current efficiencies for both hydrogen formation (C.E. for hydrogen) and for sodium amalgam formation [C.E. for amalgam] could therefore be calculated by Faraday's laws. The time increments chosen generally corresponded to the passage of 7,353 coulombs, this being the theoretical quantity of electricity required to increase the sodium content of the cathode by 0.1 g per 100 g of Hg, assuming formation of sodium amalgam occurred with 100% current efficiency. This procedure simplified the calculation of C.E. for amalgam. It was found that the sum of the two efficiencies totalled 100% within the error of measurement of the quantities of electricity,[2] and it was concluded that no cathodic processes were occurring other than those of hydrogen and sodium amalgam formation.

[1] The term "ANALAR" is a registered trade mark, and chemicals of this grade have specified limits of impurities (11).

[2] This error amounted to $\pm 0.05\ t$ coulombs, where t is time in seconds after the commencement of electrolysis.

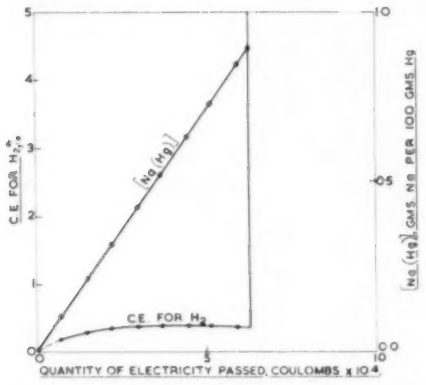

Fig. 2. Results of a typical run on the laboratory cell (stirred conditions). [NaCl], 5M; initial [HCl], 0.002M; cell temperature 70°C; apparent cathodic C.D., 0.25 amp/cm²; S.S., 95 rpm.

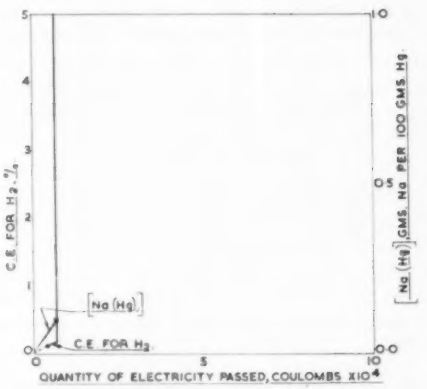

Fig. 3. Results of a typical run on the laboratory cell (unstirred conditions). [NaCl], 5M; initial [HCl], 0.002M; cell temperature, 70°C; apparent cathodic C.D., 0.25 amp/cm²; S.S., zero.

In the later experiments, therefore, only the quantities of hydrogen formed were measured, and the corresponding values of C.E. for hydrogen calculated. The value of C.E. for amalgam was obtained by difference and the corresponding average sodium content of the amalgam, [Na(Hg)] calculated. The values of C.E. for hydrogen and [Na(Hg)] were plotted against the quantity of electricity passed to give graphs of which Fig. 2 is a typical example.

The reproducibility of the current efficiency measurements was checked by repeats of runs under the same conditions: for example, Table I gives the mean value, standard deviation, and 90% confidence limit of six runs made under the conditions of the run shown in Fig 2.

Table I shows that the reproducibility was found to be best in the middle of the runs. For this reason, values of C.E. for hydrogen corresponding to the passage of 29,412 coulombs (*i.e.*, four standard time increments) through the cell were obtained from the graphs of the various runs for the study of the effects of changing such parameters as average NaCl content and initial HCl content of the brine, and the current density. It may also be mentioned that the range of values given to these parameters was such as to be most relevant to industrial mercury cell operation. The poor reproducibility in the initial stages of a run is probably due to different amounts of hydrogen adhering to the walls of the cell and not entering the gas buret. It is also considered that the initial rise in the value for C.E. for hydrogen shown in Fig. 2 is due to this kind of loss of hydrogen which becomes proportionately less as the run proceeds. These views are confirmed by the fact that the reproducibility was best, and the initial rise of current efficiency least, for runs made with high HCl contents of the brine when larger quantities of hydrogen were formed. As the runs progressed, it became more difficult to detach bubbles of hydrogen trapped under the diaphragm, and the fall in reproducibility shown in Table I is attributed to this difficulty.

Table I. Reproducibility of the run shown in Fig. 2

Coulombs passed at time of measurement	Arithmetic mean of C.E. for hydrogen (6 determinations)	Standard deviation as % of the arithmetic mean	90% confidence limit as % of the arithmetic mean
7,353	0.211	±22.03	±44.3
14,706	0.315	±14.51	±29.2
22,059	0.345	±5.02	±10.1
29,412	0.355	±3.88	±7.8
36,765	0.364	±3.70	±7.4
44,118	0.370	±6.34	±12.7
51,471	0.372	±6.21	±12.5
58,824	0.373	±6.61	±13.3

The slight fall in the second part of the current efficiency curve shown in Fig. 2, which was observed in most runs, is attributed to a depletion of the HCl content of the brine as the electrolysis proceeds.

A further source of error, which became important when the electrolysis was carried out at low initial HCl concentrations, was the catalytic decomposition of the sodium amalgam at the glass walls of the cell. The small amount of hydrogen formed by this process could be observed visually.

Results

Effect of the sodium content of the amalgam on the current efficiency for hydrogen formation under stirred and unstirred conditions.—Figures 2 and 3 show the curves obtained by plotting values of C.E. for hydrogen and [Na(Hg)] as a function of the quantity of electricity passed through the cell for two runs carried out under identical conditions, except that the cathode was stirred in the case of Fig. 2, and unstirred in the other run.

The rapid rise in the current efficiency, corresponding to a sudden increase in the rate of hydrogen formation, is a feature of both runs, and this point coincided with the formation of a brownish gray film on the cathode surface. Under stirred conditions, the point corresponded to a concentration of sodium in amalgam approaching that of the solubility of sodium in mercury at the temperature of the cell (1.0% by weight) (12). For unstirred conditions, the same phenomenon occurred at a much lower concentration of sodium in the amalgam, and it is probable that, as shown by Dodero *et al.* (13), this point corresponds with the saturation of the cathode surface with sodium.

Table II. Effect of stirring and current density on the rate of saturation of the cathode surface with sodium

Current density amp/cm²	Quantity of electricity passed at time of saturation (coulombs)		Calculated [Na (Hg)] at time of saturation, g Na/100 g Hg	
	Stirred	Unstirred	Stirred	Unstirred
0.30	64,242	5,612	0.873	0.076
0.25	66,177	5,913	0.900	0.080
0.20	66,177	6,020	0.900	0.082
0.15	67,467	10,320	0.918	0.140
0.10	—	18,000	—	0.246

[NaCl], 5M; temperature, 70°C; S.S., 0 and 95 rpm.
[HCl], zero.

It was further observed that the sodium concentration of an unstirred cathode at the point of saturation was higher the lower the current density used, and, with the stirred cathode, the nearer the concentration approached the solubility limit. This is shown by the data given in Table II.

It is probable, therefore, that the point at which the rate of formation of hydrogen will suddenly increase depends on the solubility of sodium in mercury, which will be a function of the temperature of operation, and of the relative rates of amalgam formation and transfer of dissolved sodium from the surface into the bulk of the cathode by diffusion and convection.

Effect of the initial acid concentration on the current efficiency for hydrogen formation.—Figure 4 shows the effect of varying the initial HCl content of brine on the C.E. for hydrogen measured after 29,412 coulombs had passed through the cell, i.e., at a point where the reproducibility of the measurements was best and where the surface of the cathode was not saturated with sodium.

It will be noted that, except at low values, the current efficiency is directly proportional to the initial concentration of HCl. This means that the rate of hydrogen formation is kinetically of the first order with respect to the HCl content of brine, i.e, $(\partial H_2/\partial t) = k[HCl]$. The deviation from the straight line relationship at low initial concentrations of HCl is thought to be due to the error already mentioned, caused by the decomposition of a small amount of the sodium amalgam catalyzed by the glass wall of the cell, leading to an apparent rate of hydrogen formation greater than would be expected from the electrolysis alone.

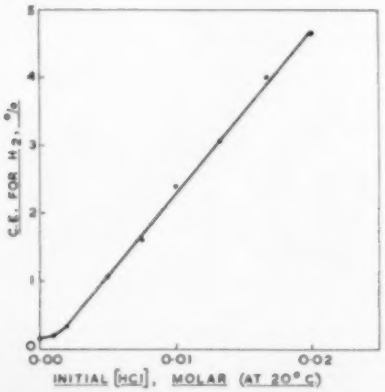

Fig. 4. Influence of varying the initial HCl content of brine. [NaCl], 5M; cell temperature, 70°C; apparent cathodic C.D., 0.25 amp/cm²; S.S., 95 rpm.

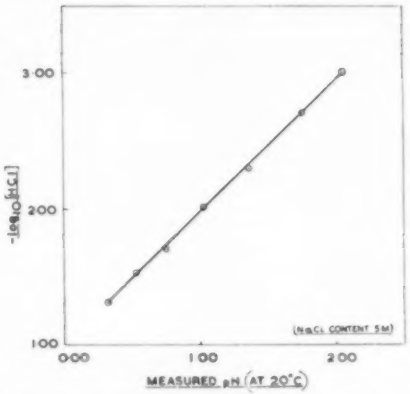

Fig. 5. Measured pH of brines 5M in NaCl as a function of the negative logarithm of their HCl content.

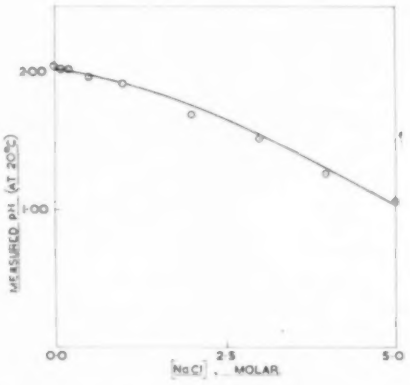

Fig. 6. Measured pH of brines 0.01M in HCl as a function of their NaCl content.

Relationship between HCl *concentration in brine and hydrogen ion activity in brine.*—For reasons which will be apparent later, it would have been preferable to interpret the C.E. for hydrogen as a function of the hydrogen ion activity in brine rather than the HCl content. To this end, attempts were made to measure the pH of the brines. A Cambridge pH meter and a glass-saturated calomel electrode pair were used. Results of such measurements are shown in Fig. 5 and 6.

Figure 5 shows the measured pH of brines 5M in NaCl as a function of the negative decadic logarithm of their HCl content. The straight line relationship indicates that the hydrogen ion activity in brine is directly proportional to the HCl content, for a fixed NaCl content and in this range of HCl concentrations. However, it will be noted that the hydrogen ion activity is apparently ten times greater than the HCl concentration. It appears difficult to explain this large difference by a change in the activity coefficient of hydrogen ions; it might arise from sodium ions influencing the potential of the glass electrode (14). The difference is a function of the NaCl content of brine, as is shown by the results of Fig. 6. This plot

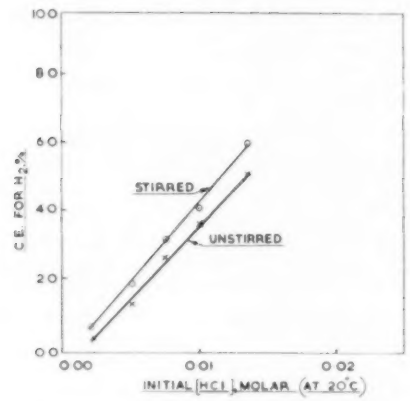

Fig. 7. Effect of stirring of the catholyte. [NaCl], 5M; temperature, 70°C; apparent cathodic C.D., 0.1 amp/cm²; S.S., zero and 95 rpm.

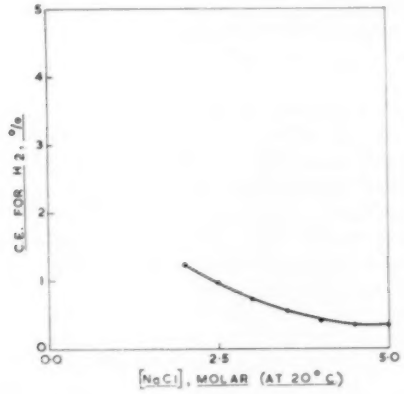

Fig. 8. Influence of varying the average sodium chloride content of brine. Initial [HCl], 0.002M; cell temperature, 70°C; apparent cathodic C.D., 0.25 amp/cm²; S.S., 95 rpm.

shows the measured pH of brines 0.01M in HCl as a function of their NaCl content. However, the difference was thought to be too large to be real, and for this reason the results were not interpreted in terms of hydrogen ion activities.

The effect of stirring the catholyte on the relationship between the initial acid concentration and the current efficiency for hydrogen formation.—Figure 7 shows the influence of stirring on the relationship between the C.E. for hydrogen and the initial HCl content of brine. The runs were carried out at a lower current density and correspond to the passage of a smaller quantity of electricity (11,765 coulombs) in order to ensure that comparison would be made when the cathode surface was not saturated with sodium.

It is to be noted that the C.E. for hydrogen is always greater for stirred than for unstirred conditions.

Effect of the sodium chloride concentration on the current efficiency for hydrogen formation.—Figure 8 shows the effect of the average NaCl content on the C.E. for hydrogen, measured after 29,412 coulombs had passed through the cell, and corresponding to conditions where the cathode surface was not saturated with sodium. The increase in hydrogen formation as the brine is diluted is referred to in the theoretical discussion and is considered to be due to the effect of the NaCl concentration on the diffusion coefficient and the activity of the hydrogen ions, and on the thickness of the diffusion layer in the brine.

Polarographic Studies

For conditions where the cathode surface is not saturated with sodium, the dependence of the C.E. for hydrogen on the initial concentration of HCl and the fact that higher values of C.E. for hydrogen were obtained under stirred than under unstirred conditions suggested that hydrogen was formed by the process

$$H_3O + e \rightarrow \frac{1}{2}H_2 + H_2O$$

and that the over-all rate of this process was dependent on the availability of hydrogen ions at the cathode, i.e. on the rate of transfer of hydrogen ions to the cathode surface. Any current in excess of this rate would then be consumed by the next possible electrode process, namely, that resulting in the formation of sodium amalgam.

$$Na^+ + Hg + e \rightarrow Na(Hg)$$

If the cathode surface becomes saturated with sodium, however, then the latter process will be limited by the rate of transfer of dissolved sodium into the bulk of the cathode. Any excess current will now be used up in a third electrode process, viz.

$$H_2O + e \rightarrow OH^- + \frac{1}{2}H_2$$

the nature of which has been confirmed (15). This will account for the rapid evolution of hydrogen observed at the saturation point.

The nature and order of occurrence of the first two electrode processes was confirmed by polarographic studies. The existence of the suggested rate-limiting step for the first process was also demonstrated. The studies were carried out at room temperature on air-free brines 5M in NaCl to which small amounts of HCl had been added. A Tinsley automatic polarograph was used with a dropping mercury cathode and a mercury pool as reference electrode and anode.

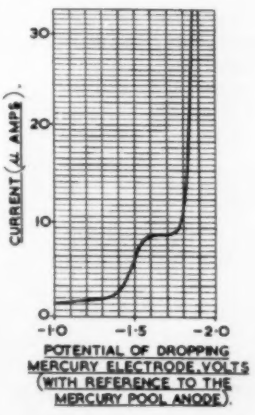

Fig. 9. Part of typical polarogram

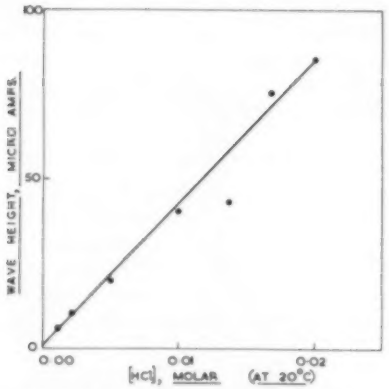

Fig. 10. Wave heights (limiting current values) as a function of the initial HCl content of brine.

The mercury drop time was 2.0 sec and the average weight per drop 4.16 mg.

Part of a typical polarogram, obtained with such a brine 0.001M in HCl, is shown in Fig. 9. This shows a process attaining a limiting current value at the mercury cathode with a half-wave potential of −1.5 v,[2] followed by a further process having an estimated half-wave potential of −1.9 to −2.0v. The wave height (limiting current value) for the first of these two processes was found to be approximately proportional to the HCl content of the brine, as is shown in Fig. 10. The similarity of this relationship with that shown in Fig. 4 for the dependence of the C.E. for hydrogen on the initial HCl concentration will be apparent.

The values found for the half-wave potentials of the two processes, and also the relationship of Fig. 10, confirm that the nature and order of these processes is as suggested. It is also evident that the first process becomes limited by the rate of transfer of hydrogen ions to the cathode surface. A further point of interest, which can be deduced by examination of Fig. 9, is that the brine nearest to the cathode surface must be alkaline when the second process, *i.e.*, sodium ion discharge, commences.

Theoretical Discussion

Both the current efficiency and the polarographic studies show that for brines of composition similar to those used in industrial mercury cell operation, and for the range of values of current densities normally employed, the rate of hydrogen ion discharge is given by a relationship such as

$$\frac{\partial H_2}{\partial t} = k\,[HCl] \qquad [1]$$

The results of the pH measurements show that this relationship may be written

$$\frac{\partial H_2}{\partial t} = k^1\, a_{H_3O^+} \qquad [2]$$

This equation is of the same form as the general equation (16) describing the rate of an electrode process under control by diffusion and convection. For steady-state conditions, and in the absence of fluid turbulence, this general equation may be written

$$\frac{I_{H_3O^+}}{F} = \frac{D_{H_3O^+}}{\delta}\,(a_{H_3O^+} - a^s{}_{H_3O^+}) \qquad [3]$$

where $I_{H_3O^+}$ = C.D. applying to hydrogen ion discharge; $D_{H_3O^+}$ diffusion coefficient for hydrogen ions in brine; δ thickness of "diffusion layer" or "equivalent film thickness" in brine; $a_{H_3O^+}$ activity of hydrogen ions in the bulk of the brine; and $a^s{}_{H_3O^+}$ activity of the hydrogen ions in the brine at the cathode surface.

At the limiting current value, $a^s{}_{H_3O^+} \to 0$ and the equation becomes

$$I^L{}_{H_3O^+} = \frac{F.D._{H_3O^+}\, a_{H_3O^+}}{\delta} \qquad [4]$$

which is identical in form to Eq. [2].

The current efficiency for hydrogen formation resulting from hydrogen ion discharge is determined by the ratio

$$I_{H_3O^+} \Big/ I_T$$

where I_T is the total applied C.D.

When the cathode surface is not saturated with sodium, $I_T = I_{H_3O^+} + I_{Na^+}$ where I_{Na^+} is the C.D. applying to sodium ion discharge.

Examination of these relationships shows why changes in certain of the operating conditions will influence the proportion of hydrogen normally formed in a mercury cell. Changes in current density will only change I_{Na^+} (as is seen from Fig. 9) and the proportion of hydrogen formed will be less as current density increases. Changes in the NaCl content of brines will influence the ratio $\frac{D_{H_3O^+} \cdot a_{H_3O^+}}{\delta}$ in a complex manner, but it would be expected that this ratio, and hence the rate of hydrogen formation, will increase as the NaCl content falls. This is observed in the results of Fig. 8. The design of cell and the rates of brine and mercury flow will influence the thickness of the diffusion layer δ.

When the cathode surface becomes saturated with sodium, the over-all rate of sodium ion discharge becomes limited by the rate at which dissolved sodium is transferred into the bulk of the cathode. Hydrogen formation by a new mechanism can now occur, *viz.*

$$H_2O + e \to OH^- + \frac{1}{2}H_2$$

and the C.E. for hydrogen will be determined by the ratio

$$\frac{I_{H_3O^+} + I_{H_2O}}{I_{H_3O^+} + I_{H_2O} + I_{Na^+}}$$

where I_{H_2O} = C.D. applying to hydrogen formation by the new mechanism.

Application of Results to Industrial Mercury Cell Operation

The results of the laboratory studies show that in the absence of impurities, three mechanisms are possible for hydrogen formation in industrially operated mercury cells, *viz.*

[2] Against the mercury pool anode. The equivalent potential against a standard hydrogen electrode is about −1.3 v.

$$H_{ads} + e \rightarrow \tfrac{1}{2}H_2 + H_2O$$

$$Na(Hg) + H_2O \rightarrow NaOH + \tfrac{1}{2}H_2$$

$$H_2O + e \rightarrow \tfrac{1}{2}H_2 + OH^-$$

Hydrogen formation by the second mechanism is likely to be slight and confined to the walls of the cell in contact with the mercury cathode. Under normal conditions of operation, where the cathode surface is not saturated with sodium, the majority of hydrogen forms by the first mechanism. The rate of hydrogen ion discharge was found to be independent of the sodium content of the amalgam, and for this reason, higher sodium contents than are normally allowed may be possible in industrial practice. Under certain abnormal conditions, the cathode surface of an industrially operated cell may become saturated with sodium. This could occur if the cathode flow rate or the amalgam decomposition rate became inadequate. Impermissably high values of hydrogen in chlorine[4] might then be found, due to the onset of hydrogen formation by the third mechanism.

The studies also indicate that the values of hydrogen in chlorine normally found in industrially operated mercury cells should be proportional to the hydrogen ion activity in brine.

In order to apply the results obtained in the laboratory cell to a more usual design of cell, *i.e.*, one with no "diaphragm," it is necessary to consider the processes which determine the hydrogen ion activity in brine in such a cell. These are complex, as Baar (17) has shown, but in a normally operated cell, the most important process is probably

$$Cl_2 + 2H_2O \rightleftharpoons H_3O^+ + Cl^- + HOCl$$

In general, secondary processes at the anode produce hydrogen ions (or remove hydroxyl ions), which will tend to displace this equilibrium backwards, while those at the cathode remove hydrogen ions (or produce hydroxyl ions) which will tend to displace it forward, *i.e.*, the presence of chlorine in the cell gives rise to a buffering effect. Thus, providing large quantities of hydrogen and/or hydroxyl ions are not introduced into or removed from the brine, the hydrogen ion activity in brine may be taken to be approximately constant. It would, therefore, be expected that, for given conditions, the rate of hydrogen formation in the mercury cell would be constant. Further, this argument would imply that some hydrogen would be formed in the cell even under the most ideal conditions.

An experiment was carried out to determine the quantity of HCl a brine must contain in order for it to have the same measured pH value as when saturated with chlorine. Thus, at 70°C, it was found that an initially neutral brine 5M in NaCl had, after saturation with chlorine, the same measured pH value as a brine 5M in NaCl, 0.0014M in HCl. If the brine was initially 0.001M in HCl, then after chlorine saturation, it had the same measured pH value as a brine 5M in NaCl, 0.002M in HCl. This experiment demonstrates a slight buffering effect due to the presence of chlorine and indicates that mercury cells operating with an acid feed brine would show greater values of hydrogen in chlorine than those operating with a neutral feed brine. It is of interest to note that for the laboratory cell operating under the conditions shown in Fig. 4, the value of C.E. for hydrogen corresponding to an HCl content of 0.0014M is approximately 0.3% This is close to the values of hydrogen in chlorine normally found in the best industrial mercury cell operation.

The effect of varying the average NaCl content of brine on the C.E. for hydrogen in the laboratory cell (Fig. 8), indicates that considerable dilution of the brine is possible without the hydrogen in chlorine rising to dangerous levels. Thus, in the laboratory cell, a change in the average NaCl content of brine from 292.5 to 117 g/liter only increased the value of C.E. for hydrogen from 0.36% to 1.44%

[4] In comparing the results obtained with the laboratory cell with industrially operated mercury cells, it will be useful to note that the C.E. for hydrogen is numerically almost equal to the hydrogen content of chlorine.

Acknowledgments

The authors wish to express their gratitude to their colleagues for assistance and helpful advice and to the Associated Ethyl Company Limited for permission to publish the paper.

Manuscript received April 10, 1961. This paper was prepared for delivery before the Indianapolis Meeting, April 30-May 3, 1961.

Any discussion of this paper will appear in a Discussion Section to be published in the June 1962 JOURNAL.

REFERENCES

1. G. Angel and T. Lundén, *This Journal*, **99**, 435 (1952).
2. G. Angel and R. Brännland, *ibid.*, **100**, 39 (1953).
3. G. Angel, T. Lundén, and R. Brännland, *ibid.*, **102**, 124 (1955).
4. G. Angel, T. Lundén, S. Dahlerus, and R. Brännland, *ibid.*, **102**, 246 (1955).
5. G. Angel, T. Lundén, S. Dahlerus, and R. Brännland, *ibid.*, **104**, 67 (1957).
6. G. I. Volkov, *J. Appl. Chem. U.S.S.R.*, **27**, 643 (1954).
7. A. Czernotzky, *Acta Chim. Hung.*, **18**, 167 (1959).
8. S. Okada. S. Yoshizawa and O. Shiragami, *J. Electrochem. Soc. Japan*, **24**, 265 (1956).
9. "Mellor's Comprehensive Treatise on Inorganic and Theoretical Chemistry," Supplement II, part 1, p. 300. Longmans, Green and Co. London, New York, and Toronto (1956).
10. P. Delahay. "New Instrumental methods in Electrochemistry," p. 358. Interscience Publishers, New York (1954).
11. "Analar" standards for Laboratory Chemicals. Fifth ed., 1957, issued jointly by The British Drug Houses Ltd., and Hopkin & Williams Ltd.
12. M. Hansen, "Constitution of Binary Alloys," p. 827, McGraw-Hill Book Co., Inc., New York, Toronto, London (1958).
13. M. Dodero, C. Deportes, and R. Mayoud. *Proc. 6th Meeting C.I.T.C.E.* (1954). p. 290, Butterworth's, London (1955).
14. J. J. Lingane, "Electroanalytical Chemistry," p. 66, Interscience Publishers, New York (1953).
15. Ref. (10), p. 99.
16. C. W. Tobias, M. Eisenberg, and C. R. Wilke, *This Journal*, **99**, 360C (1952).
17. L. Baar, *ibid.*, **101**, 497 (1954).

"Electrocapillary" Studies on Solid Metals

D. N. Staicopolus

Engineering Research Laboratory, Engineering Department, E. I. du Pont de Nemours & Company, Incorporated, Wilmington, Delaware

ABSTRACT

The use of a revolving-cup friction-measuring apparatus has made possible a study of the adsorption/desorption of ionic species on solid metal/solution interfaces, as a function of applied electrical potential. The results of this study reveal similarities between the friction characteristics at solid metal surfaces and the surface tension of liquid metals under the influence of an applied electrical potential. Specific adsorption and chemisorption of ionic species onto solid metal surfaces can thus be detected from the specific changes in the friction/potential characteristics.

The classical work of Lippmann (1) on the capillary electrometer, the application of the Gibbs' adsorption equation for the interface (σ), i.e.,

$$d\gamma = \tau dP - S\sigma dT - \Sigma\Gamma_i d\mu_i \qquad [1]$$

and the development of the Lippmann equation

$$q = -\left(\frac{\partial\gamma}{\partial E}\right)_{T,P,\mu} \qquad [2]$$

expressing the effect of an applied electrical potential on the interfacial properties of mercury/solution interfaces have prompted extended studies of electrocapillary phenomena (2-9). As a result, a better understanding of the mechanism of adsorption/desorption processes of polar entities at charged mercury/solution interfaces has become possible.

However, in view, of the expected specific interaction between the adsorbed species and the metal at the interface, the electrocapillary characteristics of a particular adsorbate will depend on the nature of the metal as well. Since the standard electrocapillary technique is restricted to liquid metals only, other methods are employed in the study of solid metal/solution interfacial properties.

"Electrocapillary" work on solid metals.—No experimental method for measuring the absolute value of the interfacial tension between a solid metal and a solution has been reported yet, but an indication that such measurements might be possible is given by the work of Udin *et al.* (10-12) on the surface tension of solid copper, silver, and gold, and on the effect of oxygen absorbed on silver.

Measurement of the contact angle θ between a gas bubble and a metal surface immersed in an electrolyte provides a method of observing changes in interfacial tension. This angle is related to the tension of the interfaces gas/liquid (g_{gl}), gas/solid (g_{gs}), and liquid/solid (g_{ls}) by the equation

$$\cos\theta = (\gamma_{gs} - \gamma_{ls})/\gamma_{gl}$$

Frumkin *et al.* (13) have extended the work of Möller (14), using Pt, Zn, Ag, Ca, and Hg as well as amalgams of Tl. They have shown that the value of the potential at the electrocapillary maximum ($E^{e.c.m.}$) for mercury agrees with that obtained from electrocapillary curves; however, the contact angle method is not as accurate as the electrocapillary method. This is attributed by Frumkin to the presence of a film of moisture between the metal and the gas bubble.

Rehbinder and Wenström (15) have suggested the existence of a relation between the interfacial tension of the metal/electrolyte and the hardness of the metal surface. The hardness of the metal surface is considered by them to be responsible for the logarithmic decrement of the oscillations of a Herbert pendulum whose suspension is a small glass sphere, about 0.5 mm in diameter, resting on the surface of the metal covered with electrolyte. The experimental curves have a marked similarity to capillary curves, but no theoretical basis for such a relation is proposed. Bockris and Parry-Jones (16) repeated the work and showed that the $E^{e.c.m.}$ thus obtained for amalgamated copper is identical with that obtained from electrocapillary curves on liquid mercury in the same solution. They concluded, however, that the property thus measured is not the hardness of the metal, but more probably it is related to friction between the glass sphere and the metal surface. Bowden and Young (17) have considered the effect of potential on friction and have concluded that it is due to two cooperating circumstances arising, (i) from the presence of an adsorbed gas, and (ii) from the particular distribution of charges in the double layer.

The present study is based on the assumption that the frictional properties of a metal/solution interface can be altered by selective adsorption or desorption and by chemisorption of polar entities at the interface. Since the state of adsorption of charged species depends on the potential at the electrical double layer, a study of friction as a function of potential could reveal phenomena of "electrocapillary" nature. However, it should be pointed out that the phenomena expected and experimentally observed are based only on the above mentioned intuitive deductions and that at present there exists no theoretical basis for the coincidence of the friction maximum with the electrocapillary maximum.

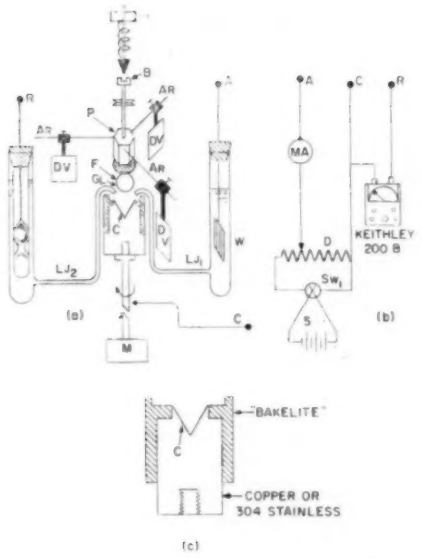

Fig. 1. Friction apparatus (schematic)

Experimental

Apparatus.—The apparatus hereinafter described (Fig. 1a) consists of a pendulum-like structure, P, which is provided with a fulcrum, F, shaped in the form of a sphere. The fulcrum is replaceable and can be a solid organic polymer, a metal, or glass. It rests in a conical cavity of the test electrode, (C), which is filled with the solution of the electrolyte under study. The conical surface constitutes the metal/solution interface. During a measurement, the test electrode is rotated about a vertical axis by a constant-speed motor, M. As the electrode rotates, it causes the pendulum to rotate until the frictional drag on the fulcrum is counterbalanced by gravity acting on a suitable lever arm arrangement.

The polarization at the interface is accomplished by passing a current obtained from an external source, S, via a potential divider, D, as shown schematically in Fig. 1b. The negative lead is normally connected to the test electrode, C, while the positive lead, A, is connected to a "working electrode," W, which is a platinized platinum foil having an apparent surface area of 0.5 in.^{2}. The circuit between W and C is completed through a liquid junction LJ_1. The polarizing current is monitored on a variable-range microammeter, MA. The current at the test electrode is kept below 10^{-5} amp. This insures a negligible error in the measurement of the potential by the introduction of a very small and insignificant IR-drop.

The potential at the test interface is measured against a saturated calomel reference electrode with a high-input impedance voltmeter (Keithley Type 200B). The reference electrode is placed in a separate compartment, R, containing the main electrolyte, *e.g.*, 1*N* Na_2SO_4 or NaCl, as the case may be, without surface-active additives. A liquid junction, LJ_2 provides the necessary current path between R and C.

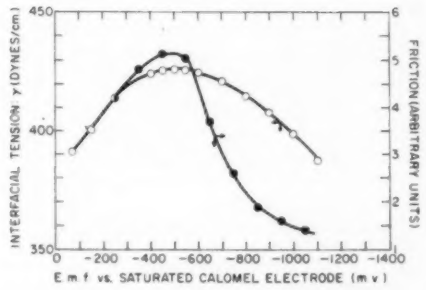

Fig. 2. Electrocapillary curve of mercury (○) and ERL friction data on amalgamated copper (●) in 0.1N KCl.

Preparation of test electrodes.—Preliminary experiments were carried out on amalgamated copper cavities. It was shown that the apparatus responds to an applied potential as expected and that the friction maximum is at the same potential as the maximum in surface tension of liquid mercury ($E^{\gamma_{max}}$) in the same solution, Fig. 2. Subsequent work was confined to copper and Type 304 austenitic stainless steel test electrodes, machined to a shape as shown in Fig. 1c.

A clean and reproducible surface was obtained by etching each test electrode in 35% nitric acid (for copper) or in concentrated HCl (for the stainless alloy) until a uniform gas evolution was observed. It was then rinsed in running ion-exchanged distilled water and finally rinsed and filled with the test solution before mounting on the motor shaft.

Solutions.—The main (or supporting) electrolyte for most of the experiments was a 1*N* solution of sodium sulfate. For some experiments on stainless steel test electrodes sodium chloride containing sodium chromate was used so as to study the relative adsorption of chloride and of chromate ions. To study the behavior of the nitrates of such metals as Ca, Pb, Ce, Ba, a 1*N* solution of $NaNO_3$ was used, in which the desired amount of the metal nitrate was added. Salts of C.P. quality were used. Solutions were prepared with ion-exchanged distilled water.

Surface-active electrolytes were added to the appropriate supporting electrolyte so as to give a 0.1*N* solution. Tests were made with the following electrolytes:

1. Inorganic electrolytes (*e.g.*, salts) of: (*a*) simple cation/simple anion type, (*b*) simple cation/complex anion types, *e.g.*, Na_3PO_4, $Na_2Cr_2O_7$, $Pb(NO_3)_2$, etc.
2. Mixed organo-inorganic electrolytes such as $(NR_4)_2{}^+SO_4{}^=$ and the two electrolytes: glycine and aminophenol.

Procedure.—Following assembly of the apparatus, the test electrode was rotated at a constant speed of 10 rpm. The lever arm served as the indicator of the frictional force (drag) which was induced on the pendulum. This force was followed as a function of test electrode potential which was incrementally increased by 100 mv. The potential after reaching −1.2 to −1.4 v was brought back to the original value in steps of 100 mv as the value of friction was recorded.

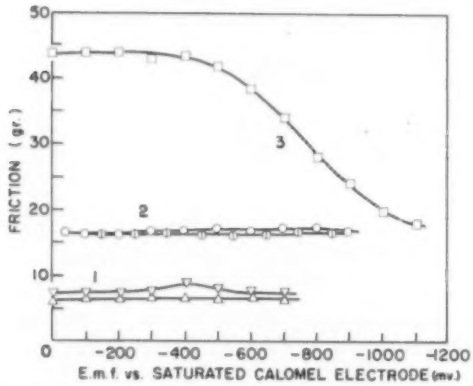

Fig. 3. Effect of applied potential on friction: copper against glass. Open triangle, 1N Na_2SO_4 + 10^{-2}N p-amino phenol; open inverted triangle, 1N Na_2SO_4 + 10^{-2}N o-amino phenol; open circle, 1N Na_2SO_4 + 10^{-1}N glycine (increasing polarization); open circle with a line through the center, 1N Na_2SO_4 + 10^{-1}N glycine (decreasing polarization); open square, 1N Na_2SO_4 + 10^{-1}N o-amino phenol (Na-salt).

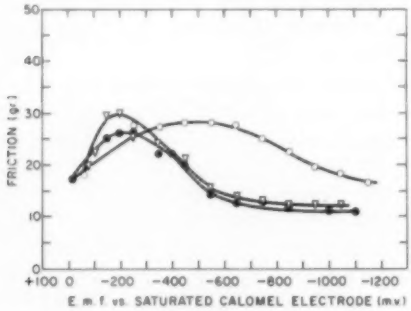

Fig. 4. Effect of applied potential on friction: copper against glass. ○, 1N Na_2SO_4; ●, 1N Na_2SO_4 + 2.10^{-1}N $(n\text{-}BuNH_3)_2SO_4$; ▽, 1N Na_2SO_4 + 2.10^{-1}N $(isoBuNH_3)_2SO_4$.

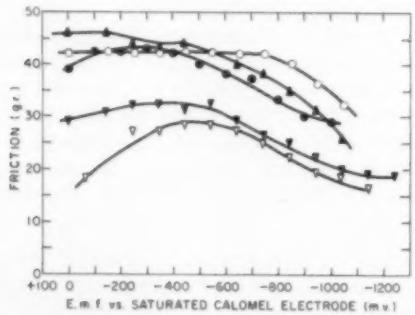

Fig. 5. Effect of applied potential on friction: copper against glass. Open circle, 1N Na_2SO_4 + 1/10N $NaNO_3$; open triangle, 1N Na_2SO_4; solid triangle pointing down, 1N Na_2SO_4 + 1/10N Na_2WO_4; solid triangle, 1N Na_2SO_4 + 1/10N Na_3PO_4; solid circle, 1N Na_2SO_4 + 1/10N Na_2SiO_3.

Analysis of Results

Typical results for Group 1 electrolytes are shown in Fig. 5-8 and for Group 2 electrolytes in Fig. 3 and 4.

There is unquestionable evidence that the friction between a metal and another substance immersed in an electrolytic solution is altered as the applied potential across the metal/solution interface is

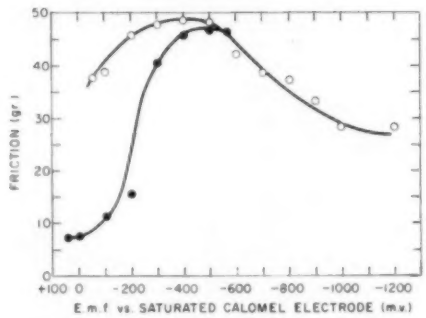

Fig. 6. Effect of applied potential on friction: copper against glass. ○, 1N Na_2SO_4 + 10^{-2} $NaClO_3$; ●, 1N Na_2SO_4 + 10^{-2}N $NaBrO_3$.

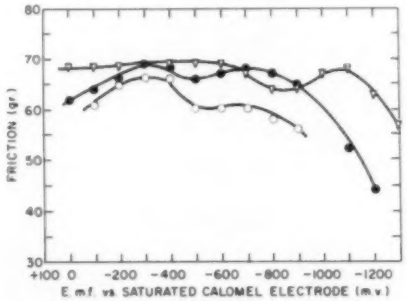

Fig. 7. Effect of applied potential on friction: 304 stainless steel against glass. ●, 1N Na_2SO_4 + 10^{-1}N Na_2CrO_4; ○, 1N Na_2SO_4 + 10^{-1}N $Na_2Cr_2O_7$; ▽, 1N Na_2SO_4 + 10^{-1}N Na_3PO_4.

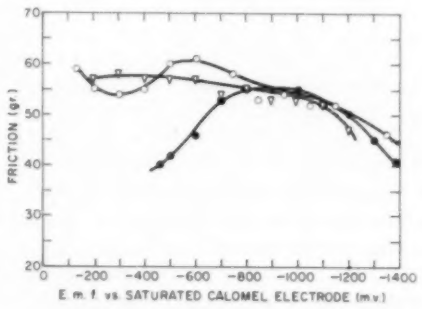

Fig. 8. Effect of applied potential on friction: 304 stainless steel against glass. ●, 5% NaCl; ○, 5% NaCl + 0.2% Na_2CrO_4; ▽, 5% NaCl + 2% Na_2CrO_4.

altered. In general, the trend in the effect of potential on friction shows similarities to the electrocapillary phenomena on liquid mercury. Therefore, it is reasonable to conclude that factors affecting surface tension of liquid mercury, such as the adsorption or the desorption of polar components in electrolytic solutions, are similarly factors affecting the frictional properties of a solid metal.

A qualitative picture of the mechanism by which such effects on solid metals are possible follows.

Ions (or polar components in general) that are attracted to the metal/solution interface, either by selective adsorption or by electrostatic attraction (*e.g.*, due to an externally applied electric field), are held more or less tightly at the interface. The ions that are normally hydrated retain a portion of

their hydration sheath as they become adsorbed. It is postulated that these adsorbed ions, with their associated water, form a "lubricating" layer which separates the two solid surfaces during their relative motion. The effect on friction obviously will be greater the number of ions that are adsorbed and the greater their hydration and their polarizability.[1]

As the potential across the interface is changed, a gradual desorption and/or additional adsorption of other species will occur. If, for example, the potential acquires a value sufficient to cause the desorption of the anions but not sufficient to cause the adsorption of the cations, no selective adsorption prevails and the lubricating layer vanishes, allowing an intimate interaction between the two solid surfaces. This leads to a maximum friction.

The observed behavior in various electrolytes agrees with the above qualitative mechanism (Fig. 2, 4, 6, 8). Additional effects, which for the moment will be considered as "exceptions" to the above mechanism are, however, observed with certain complex anions such as $Cr_2O_7^=$, $WO_4^=$, $PO_4^{\equiv}$, and others in the region of the positive branch of the friction maximum. That is, instead of observing a decrease in friction when such anions are adsorbed at potentials less negative than the friction maximum, as is normally the case with Na_2SO_4, $NaClO_3$, $NaBrO_3$, and NaCl (Fig. 2, 4, 6, 8) a high friction is maintained.

A possible mechanistic interpretation of this effect is as follows: As a surface-active anion of the type $MO_4^=$ or $M_2O_7^=$ approaches the interface, it becomes more or less chemisorbed on the metal surface or possibly undergoes a partial reduction. In either case, a reaction product, such as an insoluble metal salt of the type M′ (MO_4) or M′ (M_2O_7) or even a metal oxide or suboxide, is formed.

The insoluble product remains at the interface and mechanically interacts with the rubbing surfaces, which causes high friction. Had there been adsorption of the anion without chemisorption, the effect would have been a reduction in friction, as is observed with such ions as Cl^-, $SO_4^=$, ClO_3^-, and BrO_3^- (Fig. 2, 4, 6, 8).

It is interesting to note that electrolytes which tend to maintain the high value of friction in the positive branch of the friction-*vs.*-potential curve are among the substances which are considered effective corrosion inhibitors for steel. The indication that a chemisorbed (difficultly soluble) layer of a reaction product forms between the metal surface and selected electrolyte enhances the adsorption theory of corrosion inhibition.

Competition between anions for an adsorption or a chemisorption site on the surface of the metal is revealed by the curves in Fig. 8. Here a bell-shaped friction/potential curve (curve I) is obtained on Type 304 stainless steel in a 5% sodium chloride solution. Addition of a small amount (0.2%) of Na_2CrO_4 to this solution raises the positive branch of the curve to higher friction values (curve II), indicating some preferential adsorption of $CrO_4^=$ over Cl^- in spite of the higher concentration of the Cl^-. Greater additions of Na_2CrO_4 (up to 2%) cause a definite displacement of the adsorbed chloride ion by chemisorption of $CrO_4^=$, and as a result the high friction at the "friction maximum" is maintained even in the region of the positive branch of the curve (curve III). The negative branch of the friction/potential curve is practically unaffected by such additions, as is expected.

The unusual behavior of glycine and of ortho- and para-amino phenol (Fig. 3) can be explained by the fact that each compound would tend to ionize in a neutral solution and from a "zwitter-ion" as is represented in the following equations:

$$H_2N{-}CH_2{-}COOH \xrightarrow{H_2O} H_3N^+{-}CH_2{-}COO^-$$

and

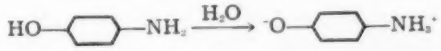

A zwitter-ion, in turn, can adsorb equally well at positively charged interfaces by pointing its negative end toward the metal, and at negatively charged interfaces by pointing its positive end toward the metal. If, however, the zwitter-ion character is suppressed as is the case in the presence of a strong acid or base, *e.g.*, when the sodium salt (or the H_2SO_4 salt) of the aminophenol is used, a friction maximum is observed. If, furthermore, chemisorption is possible between the highly charged $\bar{O}$-R-NH_2 anion and the metal surface (curve III, Fig. 3) a high friction prevails through the positive branch of the friction/potential curve.

Summary and Conclusions

The present study has revealed that the frictional characteristics of a solid metal/solution interface are influenced by the electrical potential existing across this interface.

When no specific interaction between ions and the metal surface is expected, the frictional properties of a solid metal/solution interface change, as does surface tension of liquid metals, with applied electrical potential. Specific interactions, however, not as a rule obtainable from electrocapillary studies on mercury, have been detected from friction-*vs.*-potential studies on solid metals.

From these studies it has become possible to characterize the state of adsorption of polar species at a solid metal/solution interface as follows:[2]

Surface-inactive components.—In this group, metal cations (*e.g.*, those tested except cerium ion which is active) and sulfate anions are included. These are not adsorbed spontaneously at the interface. Their concentration at the interface is equal to that in the bulk of the solution.

Surface-active components.—(Quaternary ammonium and cerium cations, and anions such as Cl^-, ClO_3^-, and BrO_3^-). These are selectively adsorbed on and reversibly desorbed from a metal/solution interface (for those metals tested). They retain

[1] This viewpoint is implied in the paper by Bockris and Parry-Jones (16).

[2] The terms "surface active" or "surface inactive" are intended to express the preference or nonpreference, respectively, of a particular component to collect at the metal/solution interface. A measure of surface activity is the excess concentration of the component at the interface above its bulk concentration.

portions of their water of hydration and act as a lubricating layer at the metal/solution interface.

Reactive surface-active components.—(Ions of the type $MO_4^=$ or $M_2O_7^=$ (except $SO_4^=$), NO_3^- and $^-O—<\!\!\bigcirc\!\!>—R$). These are selectively adsorbed on (and partially reversibly desorbed from) a metal/solution interface. They are characterized specifically by the degree of interaction with the substrate to form a chemisorbed layer. This layer can be the result of the direct interaction of the metal atoms in the surface of the metal with the surface-active component. The reaction product, if it is an insoluble solid salt, will cover the surface of the metal. Alternatively, the surface-active component could be subject to a partial decomposition (reduction by the metal atoms), which can be brought about by excessive polarization during the adsorption step. As a result, a metal oxide (or suboxide) may form at the surface. The extent of this oxide formation will control the irreversibility of the process.

Surface-active "zwitter"-ions.—(Glycine and ortho- and para-amino phenol). These ions behave as "surface-active ions" or as "reactive surface-active ions" (see above), but with the additional characteristic that they can adsorb (or chemisorb) on positively and on negatively charged interfaces. In essence, therefore, such components will more or less be permanently attracted to the interface, irrespective of state of polarization.

The friction-*vs.*-potential method of study of adsorption of polar entities on solid metal/solution interfaces has provided evidence supporting the adsorption theory of corrosion inhibition. It has provided further support of the concept that corrosion inhibitors, of those compounds tested, might behave in that manner because of their ability to form more or less adherent chemisorbed layers on the solid metal for which corrosion protection is desired.

Manuscript received May 12, 1960; revised manuscript received June 6, 1961. Part of this paper was prepared for delivery before the Chicago Meeting, May 1-5, 1960.

Any discussion of this paper will appear in a Discussion Section to be published in the June 1962 JOURNAL.

REFERENCES

1. G. Lippmann, *Pogg. Ann.*, **149**, 547 (1873); *Ann. Chim. Phys.*, (5) **5**, 494 (1875).
2. W. Palmaer, *Z. Phys. Chem.*, **59**, 187 (1907).
3. G. Gouy, *Ann. Phys.*, (Paris), (9) **6**, 5 (1916).
4. A. Frumkin, *Ergeb. exakt. Naturw.*, **7**, 258 (1928).
5. F. O. Koenig, *Z. Phys. Chem.*, **A154**, 454 (1931).
6. L. A. Hansen and J. W. Williams, *J. Phys. Chem.*, **39**, 439 (1935).
7. R. Parsons and M. A. V. Devanathan, *Trans. Faraday Soc.*, **49**, 673 (1953).
8. D. C. Grahame and B. A. Soderberg, *J. Chem. Phys.*, **22**, 449 (1954).
9. E. Blomgren and J. O'M. Bockris, *ibid.*, **63**, 1475 (1959).
10. H. Udin, A. J. Shaler, and J. Wulff, *Trans. Amer. Inst. Mining Met. Engrs.* **185**, 186 (1949).
11. E. R. Funk, H. Udin, and J. Wulff, *J. Metals*, **3**, 1206 (1951).
12. F. H Buttner. E R. Funk, and H. Udin, *J. Phys. Chem.*, **56**, 657 (1952).
13. A. Frumkin, A. Gorodetzkaya, D. Kabanov, and N. Nekrassov, *Phys. Z. Sowjet*, **1**, 255 (1932).
14. H. G. Möller, *Z. Phys. Chem.*, **65**, 226 (1908).
15. P. Rehbinder and E. Wenström, *Acta Physicochim.*, **19**, 36 (1944).
16. J. O'M. Bockris and R. Parry-Jones, *Nature*, **171**, 930 (1953).
17. F. P. Bowden and L. Young, *Research*, **3**, 235 (1950).

Technical Notes

Investigation on the Silver-Zinc Storage Battery with Radioactive Ag^{110} Isotope

Tivadar Z. Palágyi

Central Research Institute for Chemistry, Hungarian Academy of Sciences, Budapest, Hungary

The results of experiments carried out with Zn^{65} isotope on the silver-zinc storage batteries were presented before (1). Here the results of investigations performed with Ag^{110} isotope are described.

Experimental

The experiments were carried out with cells of 10 amp-hr nominal capacity. Some of the cells were manufactured in the Institute for Inorganic Chemical Technology of the Technical University at Budapest and the others produced by the Silberkraft Leichtakkumulatoren GmbH. The former cells contained 4 positive and 5 negative electrodes wrapped in cellophane separators and mounted parallel to the longer base-edge of the casing while the latter cells contained 7 positive and 8 negative electrodes wrapped in cellophane and glass-fabric separators and were mounted parallel to the shorter base-edge of the casing. The dimensions of the plates in the former cells were 83 x 35 x 1 mm while those in the

Table I. Ag^{110} contamination of nonlabeled electrodes as a function of cycling in loosely assembled cells. Positive electrode No. 4 labeled with Ag^{110}

Cell	Cycles	Activity of electrodes corrected for background, mr/hr					
		Pos., No.		Neg., No.			
		2	6	1	3	5	7
21	40	—	—	—	0.05	0.02	—
	60	0.05	0.02	—	0.1	0.05	—
	64	0.1	0.05	—	0.15	0.05	—
24	76	0.05	0.1	—	0.1	0.15	—

* Electrodes 8-15 showed no activity. Cells 22 and 23 in test similar to that of 21 and cells 25 and 26 in test similar to that of 24 showed no contamination.

latter cells were 62 x 16 x 2 mm. As in the experiments described previously (1), the electrodes were mounted in a casing made of Lucite plates. Thus, the opening and resealing of the casings was possible.

The Ag^{110} isotope was deposited electrolytically on the electrodes. Electrolyses were carried out in 50 ml of solution containing 4 g AgCN, 85 g KCN, and several drops of turkey red oil per liter with a specific activity of 1.5 μC/ml. A Pt anode and a plastic electrolyzing vessel were employed with a current density of 0.167 amp/dm^2, an electrode distance of 4 cm, and a cathode surface of 60 cm^2. The electrolyses were continued until the activity of the deposited Ag^{110} isotope was 60 μC which corresponded to deposition of 0.1 g Ag, requiring 15 min. The quantity of the deposited isotope and the activity of the electrodes were measured by the methods described before (2).

After electrolysis the silver plates were wrapped in separators and built into cells as middle electrodes. Each cell contained only one labeled electrode. As in the experiments with the Zn^{65} isotope (1), the cells were assembled in three ways. The number of normally and loosely assembled cells was six each, while that of the tightly assembled ones was eight.

The sealing, filling with electrolyte, and formation of the cells with current, the cycling and the discharges were carried out as before.

The cells were considered deteriorated when their power of intake of current came to an end, or when the current given during discharge decreased below 80% of the nominal capacity.

Results and Discussion

After the initial 20 cycles, three loosely and three normally assembled cells were opened and the plate activities measured. Then the electrodes were replaced and the cycling continued. After each additional 20 cycles this procedure was repeated. The electrodes of the tightly assembled cells were not replaced in the casing.

The activity of electrodes in the cells opened while cycling was measured and the electrodes were replaced in the same way as the experiments with labeled negative electrodes.

Results obtained with the loosely assembled cells are shown in Table I. Activity could be detected on the nonlabeled electrodes (at first on the two negative plates next the labeled one) only in one of the cells opened while cycling. For the cells opened only at the end of cycling, results were similar: nonlabeled electrodes were contaminated with isotope

Table II. Ag^{110} contamination of nonlabeled electrodes as a function of cycle life in normally assembled cells with one positive electrode labeled with Ag^{110}

Cell No.	Time of measurement	Activity of electrodes mr/hr corrected for background on the														
		Positive							Negative							
		Electrode No.														
		2	4	6	8	10	12	14	1	3	5	7	9	11	13	15
27	After 20 cycles	—		—	—				—	—	—	—	—			
	After 40 cycles	—		—	—				—	—	—	—	—			
	After 60 cycles	—		—	—				—	—	—	—	—			
	After 80 cycles	0.04		0.02	—				—	0.05	0.04	—	—			
	After 100 cycles	0.06		0.05	—				0.04	0.15	0.12	0.06	0.02			
	After 106 cycles	0.10		0.06	—				0.04	0.20	0.15	0.06	0.02			
28	After 20 cycles	—		—	—				—	—	—	—	—			
	After 40 cycles	—		—	—				—	—	—	—	—			
	After 60 cycles	—		—	—				—	—	—	—	—			
	After 80 cycles	—		—	—				—	—	—	—	—			
	After 82 cycles	—		—	—				—	—	—	—	—			
29	After 20 cycles	—	—	—		—	—	—	—	—	—	—	—	—	—	—
	After 40 cycles	—	—	—		—	—	—	—	—	—	—	—	—	—	—
	After 60 cycles	—	—	—		—	—	—	—	—	—	—	—	—	—	—
	After 80 cycles	—	—	—		—	—	—	—	—	—	—	—	—	—	—
	After 100 cycles	—	—	0.06		0.02	—	—	—	—	—	0.04	0.1	—	—	—
	After 102 cycles	—	—	0.06		0.04	—	—	—	—		0.04	0.1	—	—	—
30	After 118 cycles	0.02	0.05	0.1		0.08	0.04	0.02	0.02	0.06	0.1	0.15	0.20	0.08	0.04	0.02
31	After 135 cycles	0.06	0.04	0.08		0.06	0.04	0.04	—	0.04	0.06	0.1	0.12	0.1	0.04	—
32	After 142 cycles	0.02	0.06	0.08		0.1	0.05	0.04	—	0.04	0.05	0.1	0.1	0.08	0.02	—

* In cells 27 and 28 electrode No. 4 and in cells 29-32 electrode No. 8 were labeled with Ag^{110}.

Table III. Ag^{110} contamination of nonlabeled electrodes as a function of cycle life in tightly assembled cells with one positive electrode labeled with Ag^{110}

Cell No.	Time of measurement	Activity of electrodes mr/hr corrected for background on the Positive Electrode No. 2	4	6	8	10	12	14	Negative Electrode No. 1	3	5	7	9	11	13	15
33	After 80 cycles	—		0.04	—				—	0.05	0.04	—	—			
34	After 100 cycles	—		—	—				—	0.08	0.1	—	—			
35	After 100 cycles	0.04		0.06	0.02				—	0.06	0.1	0.05	—			
36	After 110 cycles	0.15		0.20	0.10				—	0.12	0.2	0.15	—			
37	After 117 cycles	0.15		0.35	0.10				0.15	0.4	0.3	0.15	—			
38	After 120 cycles	0.05		0.25	0.15				0.05	0.1	0.25	0.35	0.20			
39	After 142 cycles	0.04	0.15	0.3		0.2	0.12	0.05	—	0.08	0.1	0.3	0.25	0.2	0.1	—
40	After 166 cycles	0.06	0.1	0.2		0.25	0.1	0.06	—	0.05	0.1	0.15	0.2	0.15	0.15	—

* In cells 33-38 electrode No. 4 and in cells 39 and 40 electrode No. 8 were labeled with Ag^{110}.

only in one of the cells. The deterioration of the cells was caused by short-circuit by zinc sponge or zinc crystals.

Results for the normally assembled cells are summarized in Table II. The nonlabeled plates of cells 28 and 29 showed no isotope contamination. In the other cells, the degree of contamination with isotope of the nonlabeled electrodes was higher than in the loosely assembled cells. The cause of failure of all except cell 30 was the disintegration of the separators of the positive electrodes, while cell 30 deteriorated by short-circuit caused by acicular zinc crystals.

Results for the tightly assembled cells are shown in Table III. In cell 38 all the nonlabeled electrodes became contaminated with isotope. In each cell two negative plates next to the labeled positive one showed radioactivity. The failure of these cells was caused by the separators, which in most cases lost their insulating properties. In cells 37, 39, and 40 silver "trees" could be observed.

The nonlabeled electrodes of the cells were contaminated by the Ag^{110} ions to a smaller degree than in the former experiments by the Zn^{65} ions. The radioactive silver ions reached all the nonlabeled plates in only one cell.

In the tightly assembled cells the degree of contamination of the negative electrodes with isotope was larger than in the normally or loosely assembled cells. The tight assembling method is disadvantageous since it results in the disintegration of the separators of the positive electrodes, in consequence of which the electrochemically active material of the positive plates dissolves and reaches the negative electrodes. In some cases the reduced silver ions form a crystal aggregate on the zinc plate, causing direct short-circuit. The breakdown of the loosely assembled cells generally resulted from the crumbling and shedding of the zinc electrodes and formation of acicular zinc crystals. Consequently, it can be stated that both the excessively tight and the loose method of assembling are disadvantageous.

Acknowledgment

The author takes pleasure in acknowledging the help of Mr. Rezsö Kerepes during the course of the work.

Manuscript received April 3, 1961.

Any discussion of this paper will appear in a Discussion Section to be published in the June 1962 JOURNAL.

REFERENCES

1. T. Z. Palágyi, *This Journal*, **108**, 201 (1961).
2. T. Z. Palágyi, *ibid.*, **106**, 846 (1959).

Variation of Composition with Thickness in Thin Electrodeposited Films of Nickel-Iron Alloys

G. H. Cockett and E. S. Spencer-Timms

Armament Research and Development Establishment, Fort Halstead, England

Electrodeposition is a potentially advantageous method of preparing the thin films (500-2000Å) of magnetic alloys, particularly of the Permalloy type (80% Ni-20% Fe), that have been proposed for use as memory elements or other rapid switching devices (1, 2).

However, the time necessary to establish a steady state in the cathode film may be a substantial proportion of the total deposition time of such thin films even at low current densities. It is to be expected therefore that a composition gradient will exist in thin metal films and that, for given conditions of plating, the average composition will differ from that of electroplated coatings of conventional thickness.

Since no information appears to be available on

the extent of such composition gradients, the variation of composition with thickness has been determined experimentally.

All the deposits were plated from a mixed sulfate bath containing 200 g/l $NiSO_4 \cdot 7H_2O$, 8 g/l $FeSO_4 \cdot 7H_2O$, 5 g/l $NiCl_2 \cdot 6H_2O$, 25 g/l H_3BO_3, all of A.R. quality; 3 g/l pure saccharin was added as a stress reducer. The bath was operated without agitation at room temperature (21° ± 2°C), at a constant current density of 0.8 amp/dm² and at pH 2.3. A pure nickel anode and a copper foil cathode were used in these experiments, both 13 x 13 cm, and were held parallel to each other at a distance of 20 cm in a simple Perspex jig which just comfortably fitted into a rectangular glass tank. The tank was filled with plating solution to a depth of 13 cm. This setup was established as giving a uniform thickness of deposit over the cathode area.

Both steady and pulsed d-c plating were used in the series of experiments and deposits up to 10,000Å nominal thickness were prepared with total plating times up to 10 min.

In order to investigate the variation in composition across the deposit it was necessary to examine small areas about 2 mm square, weighing as little as 5 μg, which were too small for chemical analysis, *e.g.*, by spectrophotometry. The x-ray method developed for this purpose and subsequently also used for determining the variation of composition with thickness was as follows.

Areas about 1 cm square were cut from each specimen, accurately measured, and the alloy films freed by dissolution of the copper base in a 20% NH_4OH solution containing 10% $(NH_4)_2S_2O_8$ for about 45 min. After thorough washing and drying, the stripped films were weighed on a precision microbalance. The film thickness was calculated using a value for the density as subsequently determined.

X-ray diffraction patterns from all films as deposited were very diffuse and, in order to obtain a precision value for the lattice parameter and hence composition, it was necessary to anneal the deposits. Small portions, about 2 mm square were cut from each stripped film and in turn vacuum annealed in a miniature furnace made out of 8 x 0.1 mm platinum strip. The lower strip on which the foil rested was connected to a 12 v/20 amp supply while the upper strip, hinged to the lower at one side, was slightly bowed to prevent contact with the specimen. Furnace temperature was obtained from a Pt/Pt-Rh thermocouple spot welded to the underside of the lower strip. This was unlikely to give the true temperature of the foil, but it enabled reproducible annealing conditions to be obtained. Annealing for 4 min at 880°C in a vacuum better than 10^{-5} torr was sufficient to yield a material giving a sharp x-ray diffraction pattern. This was the lowest annealing temperature which yielded a constant lattice parameter from any one foil. It was not necessary to cool foils slowly if they contained 74% or less nickel as is the case with bulk material (3).

In mounting the foils in a 114 mm diameter Debye-Scherrer x-ray camera precautions were taken to prevent any bending of the specimens as the resultant strain caused a diffuse diffraction pattern. Unfiltered CuK radiation was used to record these patterns with aluminum foil interposed between specimen and film to reduce the intensity of the fluorescent FeK radiation generated in the specimen. The lattice parameter was determined using the Nelson-Riley extrapolation method, the values being corrected to a standard temperature. On comparing with those found by Owen (4) on bulk alloys, the nickel content and hence the foil density were deduced. The standard deviation of the nickel figures was 0.15%. Good agreement was obtained with the values of composition and thickness found by conventional spectrophotometric analysis on samples of larger area than required by this method.

The variation of the average iron content $\% \overline{y}$, with deposit thickness t is shown in Fig. 1 for two series of deposits, namely steady d.c. and pulsed d-c plating, 1 sec on/2 sec off. The curves for these deposits can be represented by $\overline{y} = \frac{10.3}{t}(1 - e^{-5.0t}) + 13.5$, where t is in 1000Å units and $\overline{y} = \frac{8.8}{t}(1 - e^{-1.6t}) + 24.3$, respectively. If y is the instantaneous iron composition at a deposit thickness t, then $y = \overline{y} + t \cdot \frac{d\overline{y}}{dt}$. From these equations the

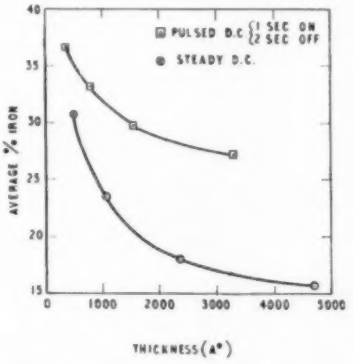

Fig. 1. Variation of average composition with film thickness

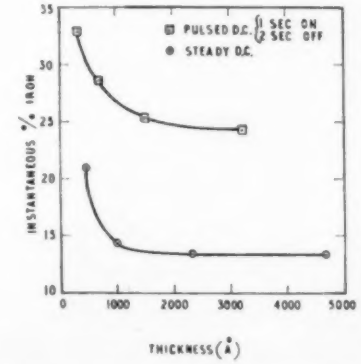

Fig. 2. Variation of instantaneous compositon with film thickness.

instantaneous composition/thickness curves of Fig. 2 were deduced. For "steady" deposits a constant value of y of 13.5% is not found until t exceeds 1500Å while the corresponding quantities for the pulsed deposits of Fig. 2 are 24.3% and 2500Å respectively.

For deposits produced by other ratios of pulsed d-c plating, no appreciable diminution in the composition gradient was observed, but there was still an increase in the over-all iron content and a reduction in cathode efficiency particularly with increase in the ON : OFF plating ratio.

It seems unlikely that a film of uniform composition less than 1500Å thick can be prepared by simple electrodeposition at constant current density from the sulfate bath. Other techniques such as plating at constant cathode potential (5) may be required to achieve the required uniformity of deposit composition.

Acknowledgment

The authors acknowledge the assistance of their colleagues.

Manuscript received May 5, 1961.

Any discussion of this paper will appear in a Discussion Section to be published in the June 1962 JOURNAL.

REFERENCES

1. M. S. Blois, *J. Appl. Phys.*, **26**, 975 (1955).
2. I. Wolf, *Proc. Am. Electroplaters' Soc.*, **44**, 121 (1957).
3. E. A. Owen and E. L. Yates, *Proc. Phys. Soc.*, **49**, 17 (1937).
4. E. A. Owen, E. L. Yates, and A. H. Sully, *ibid.*, **49**, 315 (1937).
5. T. Banerjee and A. J. Allmand. *Trans. Faraday Soc.*, **44**, 819 (1948).

FUTURE MEETINGS OF
The Electrochemical Society

Detroit, Mich., October 1, 2, 3, 4, and 5, 1961
Headquarters at the Statler Hilton Hotel
Sessions will be scheduled on
Batteries, Corrosion (including a Symposium on Surface Structure vs. Corrosion Behavior), Battery–Corrosion Joint Symposium on Fused Salt Corrosion, Electrodeposition (including symposia on Addition Agents and on Electrodeposited Magnetic Films), Electronics (Semiconductors), Electro-Organics, and Electrothermics and Metallurgy
(*See* pp. 155C-186C of August issue for complete program)

★ ★ ★

Los Angeles, Calif., May 6, 7, 8, 9, and 10, 1962
Headquarters at the Statler Hilton Hotel
Sessions probably will be scheduled on
Electric Insulation, Electronics (including Luminescence and Semiconductors), Electrothermics and Metallurgy, Industrial Electrolytics, and Theoretical Electrochemistry

★ ★ ★

Boston, Mass., September 16, 17, 18, 19, and 20, 1962
Headquarters at the Statler Hilton Hotel

★ ★ ★

Pittsburgh, Pa., April 14, 15, 16, 17, and 18, 1963
Headquarters at the Penn Sheraton Hotel

★ ★ ★

New York, N. Y., September 29, 30, and October 1, 2, and 3, 1963
Headquarters at the New Yorker Hotel

★ ★ ★

Toronto, Ont., Canada, May 3, 4, 5, 6, and 7, 1964
Headquarters at the Royal York Hotel

Papers are now being solicited for the meeting to be held in Los Angeles, Calif., May 6-10, 1962. Triplicate copies of each abstract (*not exceeding 75 words in length*) are due at Society Headquarters, 1860 Broadway, New York 23, N. Y., *not later than December 15, 1961* in order to be included in the program. *Please indicate on abstract for which Division's symposium the paper is to be scheduled, and underline the name of the author who will present the paper.* No paper will be placed on the program unless one of the authors, or a qualified person designated by the authors, has agreed to present it in person. An author who wishes his paper considered for publication in the JOURNAL should send triplicate copies of the manuscript to the Managing Editor of the JOURNAL, 1860 Broadway, New York 23, N. Y.

Presentation of a paper at a technical meeting of the Society does not guarantee publication in the JOURNAL. However, all papers so presented become the property of The Electrochemical Society, and may not be published elsewhere, either in whole or in part, unless permission for release is requested of and granted by the Editor. Papers already published elsewhere, or submitted for publication elsewhere, are not acceptable for oral presentation except on invitation by a Divisional program Chairman.

Current Affairs

Herbert H. Uhlig to Receive 1961 ECS Palladium Medal Award

Herbert H. Uhlig has been selected by The Electrochemical Society as its 1961 Palladium Medalist, and will receive the sixth impression of the medal on October 3, 1961 during the Fall Meeting of the Society to be held in Detroit, Mich.

Professor Uhlig's work in the field of corrosion began in 1936 when he became research associate at the Massachusetts Institute of Technology, Cambridge, in charge of the Corrosion Laboratory established to investigate pitting corrosion of stainless steels. In 1940 he joined the staff of the General Electric Research Laboratory at Schenectady, where he continued work in corrosion and related fields. He returned to M.I.T. in 1946 where he currently is professor of metallurgy in charge of the Corrosion Laboratory.

Professor Uhlig's principal researches have been in corrosion and electrochemistry, with particular emphasis on fundamental studies of passivity, and the chemical and metallurgical behavior of corrosion-resistant alloys. He is one of the few men who has extensively used basic scientific principles from many fields in an effort to understand corrosion, and has been involved in such related areas as electronic structure of metals and alloys, adsorption, catalysis, work function, electric field theory, complex ion formation, and free radical reactions.

To scientists, he has tried, through articles and lectures, to point out specific challenges, both applied and theoretical, lying in numerous corrosion and electrochemical problems; to industrial and government administrators, he has shown the staggering financial losses resulting from metallic corrosion, and has pointed up the need for long-range fundamental research.

© Fabian Bachrach

Herbert H. Uhlig

In his courses on corrosion and electrochemistry at M.I.T., he continuously points out principles and existing challenges. This is opposed to the usual technique of supplying students with empirical facts and empirical remedies for corrosion. His students tend to remain active in these fields.

Since joining The Electrochemical Society in 1937, Professor Uhlig has participated actively in its affairs. He has been a Vice-President, and served as President in 1955-1956. He is a Past Chairman of the Corrosion Division, of which he was one of the founders, and of the Theoretical Electrochemistry Division, as well as of the Gordon Research Conferences on Corrosion, and the Intersociety Corrosion Committee. He helped organize, and served as the Society's representative at, the first International Conference on Passivity held at Jugenheim, West Germany, in September 1957. He has written more than 100 papers, and holds five patents, in the field; and is Editor of the "Corrosion Handbook," sponsored by the Corrosion Division of the Society. He is a Past Editor of the JOURNAL; it was during his period of responsibility that the JOURNAL changed to its present format. From 1958 to 1960, he served as Chairman of the Publication Committee.

He is a member of the Advisory Committee for the Prevention of Deterioration Center of the National Research Council, and of the Corrosion Research Council established in 1955 by the Engineering Foundation. He is also a member of the American Academy of Arts and Sciences, and of several other scientific and technical societies.

In 1951 he received the highest honor of the National Association of Corrosion Engineers, the Willis R. Whitney Award, which is given in recognition of contributions to the science of corrosion.

Brief Communications

The JOURNAL accepts short technical reports having unusual importance or timely interest, where speed of publication is a consideration. The communication may summarize results of important research justifying announcement before such time as a more detailed manuscript can be published. Consideration also will be given to reports of significant unfinished research which the author cannot pursue further, but the results of which are of potential use to others. Comments on papers already published in the JOURNAL should be reserved for the Discussion Section published biannually.

Submit communications in triplicate, typewritten double-spaced, to the Editor, Journal of The Electrochemical Society, 1860 Broadway, New York 23, N. Y.

Plans Completed for the Detroit Meeting, October 1-5, 1961

Arrangements have been concluded for the Fall Meeting of The Electrochemical Society to be held in Detroit, Mich., from October 1 through October 5, 1961, at the Statler-Hilton and Tuller Hotels. The complete program, general information, and 75-word abstracts of the papers to be presented appeared in the August JOURNAL, pp. 155*C*-186*C*. Any changes in this program will appear in the program booklet which will be available at the Detroit Meeting.

Local Committee

The members of the Detroit Local Committee are: Manuel Ben, General Chairman; Seward Beacom, Vice-General Chairman; Mrs. Ann Piken, Ladies' Committee; John Griffin, Registration; Sidney Selis, Finance; Sam Piken, Entertainment; Frank Passal, Plant Tours and Transportation; James Hoare, Publicity; and Robert Trees, Hotel Arrangements.

One of the high lights of the convention will be the Palladium Medal Award Lecture by Herbert H. Uhlig on Tuesday at 5:00 P.M. in the Wayne Room of the Statler-Hilton Hotel. Members of the Detroit Symphony Orchestra will entertain the guests at the Tuesday Evening Banquet to be held in honor of the Palladium Medalist.

For the Ladies

Because Detroit is a notable fashion center with fine specialty shops and department stores carrying many imports and originals, plenty of time will be set aside for the ladies' national pastime, shopping. As noted in the general program in the August JOURNAL, a schedule of exciting trips has been arranged for the ladies' pleasure by Mrs. Piken.

It has been said that Northland and Eastland Centers, at the city's outskirts, are the world's largest and most beautiful shopping centers, featuring striking architecture, modern sculptures and fountains, landscaped malls and terraces, and the world's largest branch store. Many excellent restaurants are near the major stores or in the stores themselves.

For the Sportsmen

Having major-league teams in all four of the major professional sports of baseball, football, hockey, and basketball certainly qualifies Detroit as a sports capital. Supporting this claim, Detroit offers excellent facilities for those who enjoy bowling, boating, golf, fishing, and horse racing, among others. Some of the best amateur sports talent is available to those in the Detroit area through colleges of the Big Ten Conference, Wayne State University and the University of Detroit. For those so inclined, some of these sports events may be enjoyed around the time of the Detroit Meeting as noted in the July JOURNAL, pg. 141C.

For the Men of Industry

Detroit, "The City of Cars," is a world capital of mass production and industrial know-how. It is a giant not only in the field of automobile production but also in the fields of steel, chemicals, drugs, business machines, tires, foundry products, machines, tools, and electrical equipment.

The Rouge plant of the Ford Motor Co. is the world's greatest industrial concentration of factories, foundries, docks, and private railroad lines. The world's longest assembly line is that of the Detroit Plymouth plant. Detroit is the nerve center for the greatest industrial corporation in the world, the world-wide General Motors Corp. Parke-Davis & Co. is a giant among the pharmaceutical industries, and the Burroughs Corp. is one of the largest business machine producers. Salt is mined under the very streets of Detroit. Other large

Detroit skyline with Cobo Hall-Convention Arena in foreground

Manuel Ben

Seward Beacom

Mrs. Ann Piken

John Griffin

industries in the area are the Great Lakes Steel Division of the National Steel Corp. and Wyandotte Chemicals Corp. The Detroit Ordnance District holds up to one-fourth of all United States ordnance contracts. Now that the St. Lawrence Seaway is completed, Detroit is an important world trade port even though it is 1000 miles inland. As a natural consequence of the desire for decorative trim on automobiles, Detroit is the center for electroplating activities.

For the Culturally Minded

Two miles from downtown is located what is known as Detroit's Culture Center. The Detroit Institute of Art, containing an excellent collection of art treasures, faces the main Public Library on Woodward Ave., Detroit's main artery. These are flanked by the Detroit Historical Museum; the Horace H. Rackham Educational Memorial Building, Detroit seat of more than 40 engineering and scientific societies and of the Detroit Extension Service of the University of Michigan; and the International Institute, a center for folk art and folk culture. Adjacent to all this is the campus of Wayne State University. In Bloomfield Hills is Cranbrook, a strikingly landscaped park in which are set six outstanding cultural institutions. Greenfield Village in Dearborn is not only a collection of objects but also a collection of landmarks such as the courthouse where Abe Lincoln practiced law, the laboratory in which Edison invented the electric light, the house in which Webster compiled the first American dictionary, and, of course, the shed where Ford built his first car, to name a few. The Henry Ford Museum at the entrance of Greenfield Village is the world's greatest collection of industrial Americana. Space is too short to list all the galleries and institutes available to those interested in the fine arts.

The outstanding Broadway stage plays and shows are presented at several legitimate theaters in Detroit. The Detroit Symphony Orchestra presents concerts at the Ford Auditorium in the Civic Center on the waterfront. Ballets and opera at the Masonic Temple auditorium, ice shows at Olympia Stadium, and industrial exhibits at Cobo Hall give a variety of enjoyment to those who appreciate fine entertainment.

Belle Isle, the island park in the Detroit River, features lovely gardens, an unusual aquarium, and a children's zoo of baby animals. The Detroit Zoo has over 600 animals in nature-like outdoor settings guarded only by deep moats.

For the Evening Adventurers

Detroit is also a city of bright lights where the evening revelers may dine and dance at sophisticated night clubs, such as the Roostertail, or at the mysterious Middle East show places, such as the Cedars and the Harem. Excellent eating places provide a variety of menus and atmospheres to suit any taste.

Across the Detroit River our Canadian neighbors in Windsor, Ont., have provided many excellent restaurants and show places to delight the night-clubber.

It may be seen that Detroit offers entertainment and cultural attractions designed for persons of every bent. The Local Committee cordially welcomes you to Detroit and will make every effort to insure that your stay in Detroit will be one filled with pleasant memories.

J. P. Hoare, *Publicity Chairman*
ECS Detroit Meeting

Sidney Selis

Sam Piken

James Hoare

© Paul Gach
Robert Trees

Abstracts of "Recent News" Papers

Presented at Electronics Division Semiconductor Symposia

Indianapolis Meeting May 1-3, 1961

The Generation and Distribution of Dislocations by Solute Diffusion

S. Prussin, Pacific Semiconductors Inc., Culver City, Calif.

The stress introduced by solute lattice contraction of boron and phosphorus in silicon is shown to be sufficient to generate dislocations in silicon wafers. Such dislocations were observed. Expressions for the density distribution and for the total number of dislocations generated are derived and a mechanism of dislocation generation and distribution during the diffusion process is postulated. The dislocation distribution is shown to be highly dependent on the nature of the diffusion process.

Epitaxial Films of Gallium Arsenide

A. Hagenlocher, General Telephone & Electronics Labs., Inc., Bayside 60, N. Y.

The growth of epitaxial GaAs is discussed. Films were grown by an iodide vapor-phase disproportionation in a sealed-off evacuated tube using GaAs as the source material. A small amount of H_2 aided the reaction by keeping the surface clean. The temperature of the substrate is critical for crystal growth. Growth was investigated in the 111 and 110 directions and found to occur on the 111 As face but not on the 111 Ga face. As expected, growth in the 110 orientation occurred equally on both sides of the crystal slab. Electrical measurements on these layers also are discussed.

Vapor Growth of Gallium Arsenide*

R. L. Newman and N. Goldsmith, Semiconductor and Materials Div., Radio Corp. of America, Somerville, N. J.

Epitaxial layers of gallium arsenide, on a gallium arsenide substrate, have been grown from the vapor. An open system is used, with hydrogen chloride as the transporting agent. The gallium arsenide is transported from a hot region (*ca.* 1000°C) to a cooler region (*ca.* 900°C).

Layers up to 6-7 mils in thickness have been grown. The interfaces between substrate and growth are quite good. Substrate orientation appears to be critical, controlling both amount of growth and crystalline perfection of the deposit. Some electrical properties of the junctions formed are discussed.

* This work was partially supported by the Electronic Technology Lab., Wright Air Development Div., Air Research and Development Command, U.S. Air Force.

An Explanation of the Superior Radiation Resistance of P-Type Base Si Solar Cells

S. V. Babcock, Materials Labs., Westinghouse Electric Corp., East Pittsburgh, Pa.

Recent studies have shown p-type base Si solar cells to be more than five times as resistant to electron damage as n-type base cells. In this paper, the effects of electron flux on solar cell efficiency, current voltage characteristics, and spectral response are predicted on the assumption of a single damage mechanism: decrease in minority carrier lifetime in the base region. The calculations agree well with the reported electron damage effects.

Surface Protection of Silicon during Diffusions in Nonoxidizing Atmospheres

D. de Nobel, Philips Research Labs., Eindhoven, The Netherlands.

During a diffusion into silicon in a nonoxidizing atmosphere, *e.g.*, hydrogen, argon, etc., it is possible to protect the surface of silicon samples by applying a silicon vapor pressure. The silicon vapor pressure can be built up by embedding the silicon sample into silicon powder. Applying this method, a very simple method for aluminum diffusion into silicon is made possible. Then the silicon powder also has the function to reduce Al_2O_3 powder, which is used as a source for diffusion.

High-Speed Germanium Tunnel Diodes

R. M. Minton and R. Glicksman, Semiconductor and Materials Div., Radio Corp. of America, Somerville, N. J.

The preparation of germanium tunnel diodes using the technique of solution regrowth to form the highly doped p-n junction is discussed. Data are presented showing the effect of p-layer concentration on the peak to valley current ratio, series resistance, capacitance, and peak, valley, and forward voltages.

Using the solution growth technique, diodes, with a peak current of 50 ma $\pm$ 5% Ip/IV of 10:1, capacitance of 15 $\mu\mu$f, and a switching speed of 0.15 nanoseconds have been prepared. Temperature coefficient and life data for these units also are presented.

Cadmium-Electrode Micro-Alloyed Transistors

G. L. Schnable and J. A. Hastings, Lansdale Div., Philco Corp., Lansdale, Pa.

Cadmium-electrode micro-alloyed transistors are fabricated by shallow alloying of Sn-Cd-Zn-Ga emitter and Sn-Cd collector alloys to jet-plated cadmium emitter and collector dots on precision-etched n-type Ge structures. Resulting transistors are similar to the previous indium MAT's and MADT's in structure and geometry but have improved physical and life characteristics. Cadmium MADT's are similar to corresponding indium devices in terms of electrical characteristics but are significantly improved in terms of reliability, maximum dissipation, overload capabilities, and maximum survival temperature.

Controlled Chemical Etching in the Production of Semiconductor Dice

P. J. A. McKeown, Transistor Div., Standard Telephone & Cables, Ltd., Footscray, Kent, England.

The production of germanium dice of specified thickness by chemical etching is described. A machine featuring accurate temperature control and an automatic sequence of operations has been developed. The reproducibility attained permits accurate measurements of the effects of temperature, etchant composition, and semiconductor quality on etching rate. In industrial practice, etched wafers have uniform dimensions and surface texture and require no further grading.

Additional factors influencing the controlled etching of slices have been investigated and a practical apparatus giving etched slices of uniform thickness is described.

The Selective Delineation of P-P$^+$, N-N$^+$, and P-N Interfaces in Epitaxial Germanium and Silicon

H. M. Robertson and J. E. McNamara, Materials Research Dept., Motorola Semiconductor Products Div., Phoenix, Ariz.

Chemical methods are described for the delineation of multiple-conductivity type structures in epitaxial silicon and germanium. Illustrations are given of representative structures delineated by these methods.

Contact Etching

W. Rindner and J. M. Lavine, Research Div., Raytheon Co., Waltham, Mass.

The preferential chemical etching of semiconductors has been observed to occur when any one of a variety of materials is placed in contact with the semiconductor and both are immersed in the etchant. Several mechanisms have been considered, but none are completely satisfactory in explaining the observed phenomena. Contact etching offers a potentially useful technique for drilling and machining semiconductor materials.

Colin Garfield Fink Fellowship Fund Established

The Board of Directors of the Society, at its meeting in Indianapolis, May 1961, authorized the establishment of the Colin Garfield Fink Fellowship to perpetuate the memory of the one individual most responsible for the welfare of The Electrochemical Society through two very trying periods in history, namely, the depression of the 1930's and World War II. It was through Dr. Fink's devotion and loyalty that the continued existence of The Electrochemical Society was made possible; for this reason, there is no individual more worthy of commemoration.

The original contribution for the establishment of the Fellowship was made by Dr. and Mrs. Henry B. Linford. Further contributions to the fund should be made payable to The Electrochemical Society, Inc., and sent to Robert K. Shannon, Executive Secretary, 1860 Broadway, New York 23, N. Y.

The October issue of the JOURNAL will include a Feature article on Dr. Fink.

Colin Garfield Fink
1881-1953

President of The Electrochemical Society, 1918-1919; Secretary of the Society and Editor of its TRANSACTIONS, 1921-1947; elected to Honorary Membership in 1946, and elected Secretary Emeritus in 1947. Received the Acheson Medal in 1933, and the Perkin Medal in 1934.

Division News

Theoretical Division, Spring Meeting, Los Angeles

Special Sessions on Adsorption and Electrochemical Kinetics of Hydrogen, Hydrocarbons, Oxygen, and Hydrogen Peroxides

As part of the Spring Meeting of The Electrochemical Society, to be held at the Statler-Hilton Hotel in Los Angeles, Calif., May 6-10, 1962, the Theoretical Electrochemistry Division is planning to organize, in addition to general sessions, a number of special sessions concentrating on the specific topic, "Adsorption and Electrochemical Kinetics."

Adsorption phenomena are highly important for all electrode reactions. Because of the great current interest in electrochemical oxidation of hydrogen and hydrocarbons and electrochemical reduction of oxygen and hydrogen peroxide, the special sessions will concentrate, in particular, on the mechanism of adsorption and reaction of these species. If possible, three special sessions will be arranged as follows:

(*A*) Adsorption and electrochemical catalysis in general;

(*B*) Adsorption and mechanism of electrochemical oxidation of hydrogen and hydrocarbons;

(*C*) Adsorption and mechanism of electrochemical reduction of oxygen and hydrogen peroxide.

The selection of this topic is particularly appropriate considering that it is five years since adsorption at electrochemical interfaces has been the subject of special consideration at one of our meetings. The last symposium on this subject was held in the Spring of 1956 in San Francisco, with the late Professor K. F. Bonhoeffer of the Max Planck Institute in Göttingen giving the lecture. Back on the West Coast after five years, we hope to have equally interesting sessions in Los Angeles. The Theoretical Division is inviting contributions to this meeting.

P. Rüetschi, *Chairman*

Section News

Boston Section

During the 1960-1961 season, the Boston Section held five meetings as follows.

The first meeting was held on September 29, 1960 at the M.I.T. Graduate House. Ernest Yeager from Western Reserve University, the guest speaker, gave a lucid and complete review of the state of the art and science in the development of fuel cells. In his discussion of the theoretical aspects, construction, engineering, and applications of the fuel cell systems that are showing promise, Dr. Yeager stated that military applications are now being explored, that special industrial uses will be common in five to ten years, and that it will be at least ten years before fuel-cell-powered passenger cars will be practical.

The second meeting held on November 15, 1960 was a departure from the normal program. The group met at Avco R and D, Wilmington, Mass., in the afternoon for a talk on "Early Nose Cone Fabrication and Testing" and a showing of two motion pictures on missiles and arc jet applications. There was a tour of Avco's materials and ballistics laboratory, electroplating development laboratory, solar furnace, and arc plasma facilities. A dinner and business meeting held in Avco's dining room concluded the activities.

The third meeting on December 21, 1960 was held jointly with the National Association of Corrosion Engineers and Institute of Plant Engineers at the Beaconsfield Hotel, Brookline. The speaker was Melvin Romanoff, chemist in the Corrosion Section of the Metals Div. of the National Bureau of Standards. Mr. Romanoff spoke on "Underground Cor-

rosion of Metallic Structures," presenting a comprehensive review of the results of over 25 years of research into the corrosion behavior of ferrous and nonferrous metals buried in six different types of soil. His more recent work on the corrosion of steel piles also was discussed.

The fourth meeting was held on February 23, 1961 at the M.I.T. Graduate House. T. Laszlo of Avco R and D, Wilmington, Mass., gave a talk on "Image Furnaces for High-Temperature Research." Dr. Laszlo discussed the design and operation of solar furnaces and accessories that are useful in high-temperature research, pointing out the advantages and disadvantages of the solar furnace and presenting the results of recent experiments carried out at Avco in the solar furnace on refracting oxides.

The fifth and last meeting of the season was held on April 25, 1961 at the M.I.T. Graduate House. In his talk, "Transport of Uncharged Particles," Peter Debye of Cornell University described the results of his current work on defining the behavior of uncharged molecules subjected to the influence of high electrical fields. Most of Dr. Debye's experiments were carried out with polystyrene resins of various molecular weights dissolved in cyclohexane. A mathematical expression was derived from the experimental values which allowed the calculation of the molecular weight of the polymer being studied.

At the annual business meeting of the Section, preceding Dr. Debye's lecture, the following officers were unanimously elected by voice vote for the 1961-1962 season:

Chairman—Paul T. Woodberry, Materials Dept., Avco R and D, 201 Lowell St., Wilmington, Mass.

Vice-Chairman—Charles W. Jerome, Sylvania Electric Products Inc., 60 Boston St., Salem, Mass.

Secretary—Emerson H. Newton, R & D Div., Arthur D. Little, Inc., 15 Acorn Park, Cambridge, Mass.

Treasurer—Walter W. Harvey, Lincoln Lab., Massachusetts Institute of Technology, P. O. Box 73, Lexington 73, Mass.

Local Section Councilor (1961-1963)—Horace H. Homer, Research Labs., Sylvania Electric Products Inc., 60 Boston St., Salem, Mass.

Five meetings of the Executive Committee and the 1962 Fall Convention Committee of the Section were held during the 1960-1961 season.

E. H. Newton, *Secretary*

New York Metropolitan Section

The following are the newly elected officers of the New York Metropolitan Section for the 1961-1962 season:

Chairman — Richard Glicksman, Semiconductor Div., Radio Corp. of America, Somerville, N. J.

Vice-Chairman — John Everhart, International Nickel Co., Inc., 67 Wall St., New York 5, N. Y.

Secretary-Treasurer—Philip Crispino, Foster D. Snell, Inc., 29 W. 15 St., New York 11, N. Y.

Local Section Councilor (1961-1962) — Gunnar D. Stendahl, American Smelting and Refining Co., South Plainfield, N. J.

Local Section Councilor (1961-1963)—Paul Howard, Technical Operations Dept., Yardney Electric Corp., New York, N. Y.

Representative on Membership Committee—Alvin Salkind, Carl F. Norberg Research Center, Electric Storage Battery Co., Yardley, Pa.

Philip Crispino, *Secretary-Treasurer*

Pittsburgh Section

The Pittsburgh Section held its annual Spring Symposium at Mellon Institute on May 19, 1961. Five papers were presented during the day, following which the group toured the Mellon Institute Research Labs.

At this meeting, E. G. Coleman, a graduate student at Carnegie Institute of Technology, delivered a paper entitled "Some Aspects of Stress Corrosion Cracking." This paper won for Mr. Coleman the Pittsburgh Section's Graduate Student Research Award for 1961.

Notice to Members and Subscribers

(Re Changes of Address)

To insure receipt of each issue of the JOURNAL, please be sure to give us your old address, as well as your new one, when you move. Our records are filed by states and cities, not by individual names. The Post Office does not forward magazines.

We should have this information *by the 16th of the month* to avoid delays in receipt of the next issue.

In the business meeting that followed, J. W. Faust, Chairman, announced that Stanley Guski, Jr., representing McKeesport High School, had received the Pittsburgh Section's School Science Fair Award. His exhibit was a plasma jet. Mr. John A. Sabol was his high school science teacher.

The following officers of the Section for 1961-1962 were elected during the business meeting:

Chairman—Warren E. Haupin, Research Labs., Aluminum Co. of America, New Kensington, Pa.

Vice-Chairman—Edwin J. Smith, Research & Development, National Steel Corp., Weirton, W. Va.

Secretary-Treasurer — Robert P. Frankenthal, Applied Research, U. S. Steel Corp., Monroeville, Pa.

Local Section Councilor (1961-1962)—E. H. Phelps, Applied Research, U. S. Steel Corp., Monroeville, Pa.

Local Section Councilor (1961-1963)—John W. Faust, Jr., Westinghouse Electric Corp., Beulah Rd., Churchill Boro., Pittsburgh 35, Pa.

E. J. Smith, *Vice-Chairman*

San Francisco Section

The May 24 meeting of the San Francisco Section, held at the Men's Faculty Club of the University of California at Berkeley, included the annual business meeting. Reports from the National Meeting in Indianapolis were given, and the following were announced as the newly elected officers of the Section for the year 1961-1962:

Chairman—Worden Waring, Fairchild Semiconductor Corp., Palo Alto, Calif.

Vice-Chairman—F. J. Bowen, Kaiser Aluminum & Chemical Corp., Permanente, Calif.

Secretary—H. F. Bauman, Lockheed Missiles & Space Div., Sunnyvale, Calif.

Treasurer—J. Kinoshita, Varian Associates, Palo Alto, Calif.

Local Section Councilor (1961-1963)—R. A. Zimmerly, Columbia-Geneva Steel Corp., Pittsburg, Calif.

R. A. Lewis continues as Local Section Councilor (1960-1962).

After the business meeting a very interesting and enjoyable talk, to which wives and other guests had been especially invited, was given by Professor Eric Hutchinson of Stanford University. He described, with

the help of color slides, some experiences during his year at Yokohama University as a Fulbright professor.

The usual Planning Committee meeting was held in June; the next Section meeting will be in September.

Worden Waring, *Chairman*

Southern California-Nevada Section

The Southern California-Nevada Section held its fifth technical meeting of the season on Tuesday, June 6, at the Roger Young Auditorium in Los Angeles. The speaker was Milton J. Allen, director of the Chemical Research Dept. of Electro-Optical Systems, Inc. His topic was "The Application of Electrochemical Techniques to Synthetic Organic Chemistry."

Dr. Allen pointed out that it is only within recent years, because of a more fundamental understanding of the various electrode processes involved, that electrochemical methods in this area have been looked on as a practical working tool. The instrumentation and cells used to prepare pinacol by the cathodic reduction of 3-acetylpyridine were described in detail.

The following were elected officers of the Section for the 1961-1962 season:

Chairman—George A. Larchian, Semiconductor Div., Hughes Aircraft Co., P. O. Box 278, Newport Beach, Calif.

Vice-Chairman — Lahmer Lynds, Atomics International, 8900 De-Soto Blvd., Canoga Park, Calif.

Secretary-Treasurer — Martin Prieto, American Potash & Chemical Corp., 201 W. Washington Blvd., Whittier, Calif.

Local Section Councilor (1961-1963)—Birke M. Luckenbill, Morris P. Kirk and Son, Inc., 2700 S. Indiana Blvd., Los Angeles, Calif.

G. A. Larchian, *Chairman*

Personals

John V. N. Dorr has resigned from the Board of Directors of Dorr-Oliver Inc., Stamford, Conn. After acceptance of the resignation, the Board elected him "director emeritus." Dr. Dorr was the founder of The Dorr Co., one of the two principal predecessors of Dorr-Oliver Inc. His personal inventions include sedimentation and classification devices now accepted as basic processing tools throughout the metallurgical and chemical industries, and the water and waste treatment fields. He

ECS Membership Statistics

The following three tables give breakdown of membership as of July 1, 1961. The Secretary's Office feels that a regular accounting of membership will be very stimulating to membership committee activities. In Table I it should be noted that the totals appearing in the right-hand column are *not* the sums of the figures in that line since members belong to more than one Division and, also, because Sustaining Members are not assigned to Divisions. But the totals listed are the total membership in each Section. In Table I, Sustaining Members have been credited to the various Sections.

Table I. *ECS Membership by Sections and Divisions*

Section	Division: Battery	Corrosion	Electric Insulation	Electro-deposition	Electronics	Electro-Organic	Electrothermics & Met.	Industrial Electrolytic	Theoretical Electrochem.	No Division	Total as of 1/1/61	Total as of 7/1/61	Net Change
Boston	21	34	13	36	90	5	25	11	27	6	177	182	+ 5
Chicago	27	35	11	37	34	17	21	15	33	5	148	152	+ 4
Cleveland	53	27	2	41	43	8	32	25	38	7	192	187	— 5
Columbus, Ohio	5	13	3	15	18	2	31	4	9	2	60	67	+ 7
Detroit	24	20	5	51	20	9	11	9	40	6	104	114	+10
India	9	11	2	22	7	6	6	9	16	3	42	40	— 2
Indianapolis	36	14	14	14	31	9	14	7	20	3	69	85	+16
Midland	10	15	2	5	6	3	10	18	10	—	43	48	+ 5
Mohawk-Hudson	16	28	15	11	22	1	13	4	28	5	76	84	+ 8
New York	115	114	35	173	194	36	107	77	129	35	618	638	+20
Niagara Falls	13	17	2	22	26	6	59	55	10	10	168	155	—13
Ontario-Quebec	5	19	2	13	7	1	37	26	12	3	92	85	— 7
Pacific Northwest	6	9	1	9	2	0	7	9	14	3	38	37	— 1
Philadelphia	44	22	7	43	81	10	28	24	49	16	210	224	+14
Pittsburgh	5	44	4	30	47	6	35	19	35	1	133	136	+ 3
San Francisco	18	14	2	29	35	5	20	18	28	2	98	104	+ 6
S. Calif.-Nevada	27	28	4	45	82	7	30	22	47	5	150	175	+25
Texas	7	24	2	14	46	4	7	25	31	1	103	105	+ 2
Washington-Baltimore	38	33	8	35	26	5	13	7	24	3	144	139	— 5
U. S. Non-Section	55	67	14	74	72	32	62	44	78	22	349	332	—17
Foreign Non-Section	66	68	17	71	44	35	49	67	87	87	302	319	+17
Total as of Jan. 1, 1961	558	660	153	790	855	197	633	506	743	220	3316		
Total as of July 1, 1961	600	656	165	790	933	207	617	495	770	225		3408	
Net Change	+42	—4	+12	0	+78	+10	—16	—11	+27	+5			+92

Table II. *ECS Membership by Grade*

	Total as of 1/1/61	Total as of 7/1/61	Net Change
Active	2895	2865	— 30
Faraday (Active)	33	37	+ 4
Deutsche Bunsen Gesellschaft (Active)	17	21	+ 4
Delinquent	84	189	+105
Active Representative Patron Members	10	10	0
Active Representative Sustaining Members	107	99	— 8
Total Active Memebers	3132	3197	+ 65
Life	16	16	0
Emeritus	65	78	+ 13
Associate	39	48	+ 9
Student	43	38	— 5
Honorary	7	7	0
Total	3316	3408	+ 92

The figures pertaining to Patron and Sustaining Member Representatives, and Faraday and Deutsche Bunsen Gesellschaft members subscribing to the JOURNAL, have been added to reflect reclassifications and changes in membership status.

Table III. *ECS Patron and Sustaining Membership*

	Total as of 1/1/61	Total as of 7/1/61	Net Change
Patron Member Companies	5	5	0
Sustaining Member Companies	157	144	— 13

added the words "thickener" and "classifier" to the engineer's vocabulary. Now 89, Dr. Dorr is still active in the affairs of The Dorr Foundation and Dorr Associates, Inc., and is a director of American Synthanite Corp.

Christopher J. B. Fincham has been appointed technical director of the Metals Div., National Research Corp., Cambridge, Mass. Dr. Fincham has specialized in the physical chemistry of metallurgical systems. Before joining NRC in 1956, he served as scientific officer with the British Iron and Steel Research Association, research associate at Columbia University, and lecturer at the University of Toronto. At NRC, Dr. Fincham has managed the development of tantalum products for electronic capacitors.

Curry E. Ford has been named director of development for National Carbon Co., Div. of Union Carbide Corp., New York City. He joined National Carbon in 1937, and was active in the development of carbon and graphite chemical process equipment. Since February 1960, Mr. Ford had been director of marketing.

Bernard A. Gruber, research specialist, has been transferred from Monsanto Chemical Co.'s Research and Enginering Div. Labs. at Dayton, Ohio, to Monsanto Research Corp.'s Boston Labs. at Everett, Mass.

Carl Horowitz has been appointed chief of chemical laboratories for Yardney Chemical Inc., New York City. Mr. Horowitz has been with the company, a wholly owned subsidiary of Yardney Electric Corp., since 1951, first as a chemical engineer, then as assistant to the chief chemist.

Micheal J. Joncich has left his position as associate program director for chemistry at the National Science Foundation, Washington, D. C., to accept a position as professor and head of the Dept. of Chemistry at Northern Illinois University in DeKalb, Ill.

Joseph B. Kushner, professor of engineering at Evansville College, Evansville, Ind., and author and conductor of "Electroplating Know How," a correspondence course in electroplating, has been awarded a National Science Foundation grant to conduct research on electrodeposition. The sum of $8300 was given to Evansville College to enable Dr. Kushner to carry on research on "The Theory of Stress in Electrodeposits" in the metallurgy laboratory of the college. The project will continue previous work done by Dr. Kushner in the field of stressed electrodeposits. The grant is believed to be the first National Science Foundation grant awarded for basic research in electroplating.

Ernest R. Ramirez recently was appointed senior research supervisor of Special Metals, Inc., New Hartford, N. Y. Dr. Ramirez will be responsible for research and development in new areas of products and processes which are as yet undisclosed. Prior to his new position, he was a senior research scientist at General Electric's Metallurgical Products Dept., Detroit, where he directed electrochemistry research related to powder metallurgy.

Joseph S. Russo, formerly a chemist with the Sperry Gyroscope Co.'s Materials Lab. in Great Neck, N. Y., has taken a new position as electrochemical section head at the Solid State Physics Lab. of Lear Inc., Santa Monica, Calif.

Reginald S. Dean

Reginald S. Dean, president of the Chicago Development Corp., Riverdale, Md., died on May 26, 1961 at the age of 64.

Dr. Dean was born in Rolla, Mo., where he studied at the University of Missouri School of Mines, receiving his B.S. and Met. E. degrees in 1915 and 1922, respectively. His Ph.D. degree in physical chemistry was earned in 1936 from the University of Maryland.

Dr. Dean was a member of The Electrochemical Society, American Society for Metals, American Chemical Society, and American Institute of Mining and Metallurgical Engineers.

William M. MacNevin

William M. MacNevin, professor of chemistry at Ohio State University, Columbus, died on July 5, 1961. He was 54 years old. At the time of his death, he was serving as visiting professor at the University of Colorado, Boulder, Colo.

Dr. MacNevin, who was head of the division of analytical chemistry at Ohio State, was the co-author of three textbooks in the field.

In addition to The Electrochemical Society, he was a member of the Columbus Chapter of the American Analytical Society, of which he was a past chairman, the Canadian Chemistry Society, and many other professional chemistry societies

Manuscripts and Abstracts for Spring 1962 Meeting

Papers are now being solicited for the Spring Meeting of the Society, to be held at the Statler Hilton Hotel in Los Angeles, Calif., May 6, 7, 8, 9, and 10, 1962. Technical Sessions probably will be scheduled on Electric Insulation, Electronics (including Luminescence and Semiconductors), Electrothermics and Metallurgy, Industrial Electrolytics, and Theoretical Electrochemistry.

To be considered for this meeting, triplicate copies of abstracts (*not exceeding 75 words in length*) must be received at Society Headquarters, 1860 Broadway, New York 23, N. Y., *not later than December 15, 1961. Please indicate on abstract for which Division's symposium the paper is to be scheduled and underline the name of the author who will present the paper.* No paper will be placed on the program unless one of the authors, or a qualified person designated by the authors, has agreed to present it in person. An author who wishes his paper considered for publication in the JOURNAL should send triplicate copies of the manuscript to the Managing Editor of the JOURNAL, 1860 Broadway, New York 23, N. Y.

Presentation of a paper at a technical meeting of the Society does not guarantee publication in the JOURNAL. However, all papers so presented become the property of The Electrochemical Society, and may not be published elsewhere, either in whole or in part, unless permission for release is requested of and granted by the Editor. Papers already published elsewhere, or submitted for publication elsewhere, are not acceptable for oral presentation except on invitation by a Divisional program Chairman.

Officers of Local Sections of The Electrochemical Society

Council of Local Sections (1961-1962)

J. C. White, Chairman
4205 Woodberry St., University Park, Hyattsville, Md.
R. F. Bechtold, Vice-Chairman
S. W. Scott, Secretary
N. C. Cahoon† (1960-1962)
A. J. Cornish† (1961-1963)

Boston (Spring 1961-1962)

P. T. Woodberry, Chairman
Materials Dept., Avco R and D, 201 Lowell St., Wilmington, Mass.
C. W. Jerome, Vice-Chairman
E. H. Newton, Secretary
W. W. Harvey, Treasurer
H. C. Gatos* (1960-1962)
Charles Levy* (1960-1962)
H. H. Homer* (1961-1963)

Chicago (Spring 1961-1962)

Ralph Wehrmann, Chairman
Fansteel Metallurgical Corp., 2200 Sheridan Rd., North Chicago, Ill.
R. D. Chelton, Vice-Chairman
G. H. Timmings, Secretary
J. J. Daly, Jr., Treasurer
C. A. Hampel* (1960-1962)
E. L. Koehler* (1961-1964)

Cleveland (Fall 1961-1962)

J. F. Yeager, Chairman
Union Carbide Consumer Products Co., Box 6116, Cleveland 1, Ohio
F. C. Keller, Vice-Chairman
W. E. Ishler, Secretary
R. A. Specker, Treasurer
N. C. Cahoon* (1961-1962)
A. E. Middleton* (1961-1962)

Columbus (Fall 1960 to present)

L. D. McGraw, Chairman
Battelle Memorial Institute, Columbus 1, Ohio
R. W. Hale, Vice-Chairman
J. G. Beach, Secretary-Treasurer
J. M. Blocher, Jr.*
F. W. Fink*

Detroit (Spring 1961-1962)

S. E. Beacom, Chairman
Research Labs., General Motors Corp., 12 Mile & Mound Rds., Warren, Mich.
A. A. Johnson, 1st Vice-Chairman (Program)
L. M. Morse, 2nd Vice-Chairman (Membership)
A. G. Piken, Secretary-Treasurer
Frank Passal* (1960-1962)
A. E. Remick* (1961-1963)

† Council Representative on Board of Directors.

* Representative on Council of Local Sections.

India (Fall 1960 to present)

M. S. Thacker, Chairman
Council of Scientific & Industrial Research, Old Mill Rd., New Delhi 2, India
A. Joga Rao, Vice-Chairman
S. Ramaswamy, Vice-Chairman
S. Krishnamurthy, Secretary-Treasurer
H. V. K. Udupa*
J. Balachandra*

Indianapolis (Spring 1961-1962)

R. R. Haberecht, Chairman
Corporate Research Lab., P. R. Mallory & Co., Inc., 3029 E. Washington St., Indianapolis, Ind.
T. C. O'Nan, Vice-Chairman
Marshall Whitehurst, Secretary-Treasurer
Ernest Paskell* (1961-1962)
Maurice Indig* (1961-1963)

Midland (Spring 1961-1962)

Don Chapin, Chairman
Dow Chemical Co., 302 Bldg., Midland, Mich.
C. K. Bon, Vice-Chairman
Jack Robinson, Secretary-Trasurer
R. S. Karpiuk* (1960-1962)
Marvin Bothwell* (1961-1962)

Mohawk-Hudson (Spring 1961-1962)

Cornelius Groot, Chairman
2512 Whamer Lane, Schenectady, N. Y.
W. E. Tragert, Vice-Chairman
E. C. Pitzer, Secretary-Treasurer

New York Metropolitan (Spring 1961-1962)

Richard Glicksman, Chairman
Semiconductor Div., Radio Corp. of America, Somerville, N. J.
John Everhart, Vice-Chairman
Philip Crispino, Secretary-Treasurer
G. D. Stendahl* (1961-1962)
Paul Howard* (1961-1963)

Niagara Falls (Spring 1961-1962)

D. J. Hansen, Chairman
Union Carbide Metals Co., P. O. Box 580, Niagara Falls, N. Y.
J. A. Peterson, Vice-Chairman
W. W. Trainor, Secretary-Treasurer
S. W. Scott* (1961-1962)
W. E. Kuhn* (1961-1963)

Ontario-Quebec (Spring 1961-1962)

R. A. Ritchie, Chairman
Electric Reduction Co. of Canada Ltd., Toronto, Ont., Canada
R. A. Campbell, Vice-Chairman (Programs)
Andre Hone, Vice-Chairman (Membership)
Tom Pezzack, Secretary-Treasurer
Tom Pezzack* (1961-1962)
L. G. Henry* (1961-1962)

Pacific Northwest (Spring 1961-1962)

H. J. Wittrock, Chairman
Dept. of Metallurgical Research, Kaiser Aluminum & Chemical Corp., Spokane 69, Wash.
G. C. Ware, Vice-Chairman
J. A. Ayres, Secretary-Treasurer

Philadelphia (Spring 1961-1962)

H. C. Mandell, Jr., Chairman
Pennsalt Chemicals Corp., P. O. Box 4388, Philadelphia 18, Pa.
E. C. Evers, Vice-Chairman
A. A. Ware, Treasurer
H. C. Miller, Secretary
G. F. Temple*
G. W. Bodamer*

Pittsburgh (Spring 1961-1962)

W. E. Haupin, Chairman
Research Labs., Aluminum Co. of America, New Kensington, Pa.
E. J. Smith, Vice-Chairman
R. P. Frankenthal, Secretary-Treasurer
E. H. Phelps* (1961-1962)
J. W. Faust, Jr.* (1961-1963)

San Francisco (Spring 1961-1962)

G. W. Waring, Chairman
844 Charleston Rd., Palo Alto, Calif.
F. J. Bowen, Vice-Chairman
H. F. Bauman, Secretary
Joshyo Kinoshita, Treasurer
R. A. Lewis* (1960-1962)
R. A. Zimmerly* (1961-1963)

Southern California-Nevada (Spring 1961-1962)

G. A. Larchian, Chairman
11100 Chimineas Ave., Northridge, Calif.
Lahmer Lynds, Vice-Chairman
Martin Prieto, Secretary-Treasurer
W. F. Seyer* (1960-1962)
Birke Luckenbill* (1961-1963)

Texas (Spring 1961-1962)

L. G. Dean, Chairman
Dow Chemical Co., Freeport, Texas
J. J. Banewicz, Vice-Chairman
R. M. Hurd, Secretary-Treasurer
C. C. Templeton* (1959-1961)
T. C. Franklin* (1961-1962)

Washington-Baltimore (Spring 1961-1962)

R. J. Brodd, Chairman
National Bureau of Standards, 1-8, Washington 25, D. C.
Sigmund Schuldiner, Vice-Chairman
V. A. Lamb, Secretary
G. W. Castellan, Treasurer
David Schlain* (1960-1962)
J. C. White* (1961-1963)

Officers of Divisions of The Electrochemical Society

Battery (Fall 1960-1962)
E. J. Ritchie, Chairman
Research Labs., Eagle-Picher Co., Joplin, Mo.
Arthur Fleischer, Vice-Chairman
C. H. Clark, Sec.-Treas.

Corrosion (Fall 1960-1962)
R. T. Foley, Chairman
General Engrg. Lab., Bldg. 37, General Electric Co., Schenectady, N. Y.
H. C. Gatos, Vice-Chairman
E. L. Koehler, Sec.-Treas.

Electric Insulation (Spring 1961-1963)
T. D. Callinan, Chairman
IBM Research Lab., Yorktown Heights, N. Y.
C. C. Houtz, Vice-Chairman
B. R. Eichbaum, Sec.-Treas.

Electrodeposition (Fall 1960-1962)
D. G. Foulke, Chairman
Sel-Rex Corp., Nutley, N. J.
D. R. Turner, Vice-Chairman
Dan Trivich, Sec.-Treas.

Electronics (Spring 1961-1963)
R. J. Ginther, Chairman
Solid State Div., Naval Research Lab., Washington 25, D. C.
H. F. Ivey, Vice Chairman (Luminescence)
C. P. Marsden, Vice-Chairman (Instrumentative/General)
F. H. Horn, Vice-Chairman (Semiconductors)
A. E. Hardy, Sec.-Treas.

Electro-Organic (Fall 1961-1963)
M. J . Allen, Chairman
Electro-Optical Systems, Inc., 125 N. Vinedo Ave., Pasadena, Calif.
R. A. Day, Jr., Vice-Chairman
E. C. Olson, Sec.-Treas.

Electrothermics and Metallurgy (Spring 1961-1963)
J. H. Westbrook, Chairman
Research Dept., General Electric Co., P. O. Box 1088, Schenectady, N. Y.
W. E. Kuhn, Vice-Chairman
L. H. Juel, Vice-Chairman
L. M. Litz, Sec.-Treas.

Industrial Electrolytic (Spring 1960-1962)
W. D. Sherrow, Chairman
Electrode Div., Great Lakes Carbon Corp., Niagara Falls, N. Y.
R. F. Bechtold, Vice-Chairman
J. E. Currey, Sec.-Treas.

Theoretical Electrochemistry (Spring 1961-1963)
Paul Rüetschi, Chairman
Carl F. Norberg Research Center, Electric Storage Battery Co., Yardley, Pa.
Sidney Barnartt, Vice-Chairman
Sigmund Schuldiner, Sec.-Treas.

Book Reviews

Kinetics of Electrode Processes and Null Points of Metals, by L. I. Antropov. Published by Council of Scientific and Industrial Research, New Delhi, India. 1960. x + 94 pages; price: Rs. 5.00, Sh. 7/6 (about $1.05).

This volume is made up of five chapters based on a series of lectures given by Professor Antropov at the Central Electrochemical Research Institute in Karaikudi in 1958. The dominant theme is that electrode kinetics are very much affected by the electrical double layer structure, especially by the charge on the metal with respect to the solution. The first chapter develops the ϕ-scale of potentials, relative to $\phi = 0$ at the null point where there is no potential gradient across the interface. Null points are estimated from electrocapillary curves, from double layer capacities, and by other methods; some of them are not very accurate but, even so, may be useful.

The subsequent chapters are devoted to hydrogen overvoltage, metal deposition, electroreduction, and electrochemical aspects of corrosion. To illustrate the application of ϕ-potentials, we cite three examples:

1. Metals which have positive ϕ-potentials deposit with low overvoltage and *vice versa*. If ϕ is negative, cations are adsorbed and tend to inhibit deposition, but the deposits tend to be fine grained and smooth. When ϕ is positive, as for silver in acid solution, coarse crystals are deposited.

2. Some organic corrosion retardants, not wholly effective alone, decrease the current necessary for cathodic protection. Whether effective cations or anions are needed depends on whether the metal is positive or negative with respect to its null point, since suitable change in the polarization curves depends on adsorption.

3. Copper may be electroplated on steel without interference by direct displacement if suitable surface active agents are present. The choice is based on the fact that ϕ is initially negative, becomes positive (with respect to both iron and copper) during the plating process.

There are 157 literature references, 60% to Russian publications. This is a well-printed book with hard cover.

C. V. King

Physico-Chemical Measurements at High Temperatures. Edited by J. O'M. Bockris, J. L. White, and J. D. Mackenzie. Published by Academic Press, Inc., New York, and Butterworths Scientific Publications, London, 1959. viii + 394 pages; $13.50.

The editors, formerly all part of a high-temperature physiochemical research group at the Imperial College of Science and Technology, London, have brought together a group of highly diversified chapters on various high-temperature techniques and measurements by some 20 chemists and metallurgists.

The wide scope of the topics covered in this book can best be described by listing the titles and authors of the various chapters which follow a brief general introduction by J. O'M. Bockris. These are: "Temperature Measurement" by J. L. Margrave; "Means of Attaining and Controlling Temperature" by K. Motzfeldt; "The Stability of Refractory Materials" by D. T. Livey and P. Murray; "Phase Equilibria with Particular Reference to Silicate Systems" by J. F. Schairer; "Chemical Equilibria" by F. D. Richardson and C. B. Alcock; "Calorimetry" by O. Kubaschewski and W. A. Dench; "Liquid Densitometry" by J. L. White; "Surface Tension" by P. Kozekevitch; "Vapor Pressure" by J. L. Margrave, "Electrochemical Measurements" by J. W. Tomlinson; "Scattering and Absorption of Visible Light in Fused Salts" by W. Bues; "Ultrasonic Velocity Measurements" by N. E. Richards and H. Bloom; "Measurement of Diffusivity in Liquid Systems" by Ling Yang and M. T. Simnad; and "Viscometry" by J. D. Mackenzie. Several Appendices complete the book: "Container Materials for Melts," "Rapid Testing of Refractory Suitability,"

"The Preparation of Molybdenum and Tungsten Apparatus," all by J. D. Mackenzie; "Thermal Expansion of High Temperature Materials" by J. L. White; "Thermodynamic Calculations at High Temperature Systems," "Melting Points and Vapor Pressures of the Elements," and "Data for Radiation Pyrometry," all by J. L. Margrave.

The main object of the volume is to present "under one cover a presentation, critical discussion and comparison of the various methods available for the measurement of a property." For the research specialist in any given area, the corresponding chapter will usually not be of prime interest, because the chapters do not, in general, constitute comprehensive up-to-date reviews, and they are not intended to do so. On the other hand, the chapters outside of his specialty will make a valuable contribution by bringing together much scattered information in an area in which experimental techniques and materials of construction often represent limiting factors.

The coverage of the European literature appears to be more nearly adequate than that of the American. Perhaps this is a reflection of the relatively recent entry of several groups into high-temperature research in this country, and the inevitable time lag involved in the preparation of a multiauthored work of this type. Literature references more recent than 1956 are sparse, although a few 1957 and 1958 references appear. The author index is lamentably incomplete; not even all of those mentioned by name in the text are included, and apparently none of those to whom reference is made by number alone.

Electrochemists will probably take greatest interest in the chapters on attainment, measurement, and control of high temperatures, the stability of refractory materials and chemical equilibria, and in the appendices on container materials, thermal expansion coefficients, and high-temperature thermodynamic properties and calculations.

For anyone considering an entry into high-temperature experimental work, as well as for those already in it, this book can be recommended as a valuable reference volume.

H. A. Laitinen

Announcements from Publishers

"Boron and Its Compounds." Selective Bibliography SB-456* (Supplement to CTR-303); 10 cents.

"The Permeation of Hydrogen through Hastelloy B," Feb. 1961. AEC Report NAA-SR-4898(Rev.),* 16 pages; 75 cents.

"Ion Nature of Molten Salts," G. J. Janz, Rensselaer Polytechnic Institute, for U. S. Air Force, Dec. 1960. Report PB 171 535,* 14 pages; 50 cents.

"Surface Recombination of Hydrogen Atoms in the Presence of Water Vapor," E. J. Nowak, Chemical Engineering Lab., Princeton University, for Office of Scientific Research, U. S. Air Force. Report PB 171 512,* 19 pages; 50 cents.

"Electrodeposition of Aluminum on Magnesium," E. W. Cooke and S. Kritzer, North American Aviation, Inc., for Wright Air Development Center, U. S. Air Force, Nov. 1959. Report PB 161 892,* 26 pages; 75 cents.

"Electron Microscopy of Etch Pits," 1st Lt. R. E. Pawel, USAF, Materials Lab., for Wright Air Development Center, U. S. Air Force, Oct. 1959. Report PB 161 838,* 23 pages; 75 cents.

"Corrosion Survey of Steel Sheet Piling," U. S. Naval Civil Engineering Lab., Dec. 1960. Report PB 171 501,* 59 pages; $1.75.

"Investigation of the Chemical Reaction between Tungsten and Aluminum Oxide," General Telephone and Electronics Labs., Inc., for Air Research and Development Command, U. S. Air Force, April 1960. Report PB 171 373,* 71 pages; $2.00.

"Researches on Hydrogen Evolution," C. A. Knorr, Wright Air Development Div., U. S. Air Force, April 1960. Report PB 161 880,* 50 pages; $1.25.

"Hydrogen Embrittlement of Titanium Alloys," A. E. Riesen and D. H. Kah, Wright Air Development Div., U. S. Air Force, Oct. 1960. Report PB 171 394,* 49 pages; $1.25.

"Vacuum Melting of Beryllium by Electron Bombardment," H. T. Sumison and C. O. Matthews, Lockheed Aircraft Corp., for Dept. of the Navy, Dec. 1959. Report PB 171 521,* 43 pages; $1.25.

* Order from Office of Technial Services, Business and Defense Services Administration, U.S. Dept. of Commerce, Washington 25, D. C.

News Items

New ECS Sustaining Members

The following recently became Sustaining Members of The Electrochemical Society:

Allison Division, General Motors Corp., Indianapolis, Ind.

Leesona Moos Laboratories, Division of Leesona Corp., Jamaica, N. Y.

Lockheed Aircraft Corp., Missiles and Space Division, Sunnyvale, Calif.

Latest Volume in ECS Series

The Electrochemical Society is pleased to announce the availability of the following new volume in The Electrochemical Society Series:

Transactions of the Symposium on Electrode Processes. Edited by Ernest Yeager. Price: $20.00; 374 pages. (*See* advertisement on page 206C of this issue.)

This volume contains the papers and discussions of the Symposium on Electrode Processes, sponsored jointly by the U. S. Air Force, Office of Scientific Research, and The Elec-

June 1962 Discussion Section

A Discussion Section, covering papers published in the July-December 1961 JOURNALS, is scheduled for publication in the June 1962 issue. Any discussion which did not reach the Editor in time for inclusion in the December 1961 Discussion Section will be included in the June 1962 issue.

Those who plan to contribute remarks for this Discussion Section should submit their comments or questions in triplicate to the Managing Editor of the JOURNAL, 1860 Broadway, New York 23, N. Y., *not later than March 1, 1962.* All discussion will be forwarded to the author(s) for reply before being printed in the JOURNAL.

BOSTON AREA SITE OF NEW LABORATORY FOR PHYSICAL SCIENCE

A modern and well-equipped research facility established by P. R. Mallory & Co., Inc. offers the following research staff openings for scientists in solid state physics, thin films, materials, metallurgy and electrochemistry.

RESEARCH SCIENTISTS—for fundamental investigations of:

Thin Films—Dielectric, magnetic, resistive and semiconductor.

Materials—Thermoelectric, semiconductors, (including organics), metallurgical studies.

Electrochemistry—Fuel cells, general electrochemical phenomena.

Electron Microscopy—Films, solid surfaces.

Expressions of interest may be submitted in confidence to Dr. S. P. Wolsky, Director, Laboratory for Physical Science. *Company representatives will also be available at the Detroit Meeting of The Electrochemical Society in October to interview for above positions.* All qualified applicants will receive consideration regardless of race, creed, color or national origin.

P. R. MALLORY & CO., INC.

118 Main Street

Watertown, Massachusetts

trochemical Society, Inc., held at the Philadelphia Meeting of The Electrochemical Society in May 1959.

Fundamentals are presented fully and past work is reviewed, but the stress is on the newer areas of research: Hydrogen discharge kinetics; Electrodeposition and dissolution of metals; The electrical double layer; Adsorption phenomena; Kinetics of fast electrode processes.

The volume is available from the publisher, John Wiley & Sons, Inc., 440 Park Ave. South, New York 16, N. Y. *A 33 1/3% discount is offered to ECS members only and can be obtained by ordering through Society Headquarters, 1860 Broadway, New York 23, N. Y.*

13th Meeting of C.I.T.C.E.

The 13th Meeting of the International Committee for Electrochemical Thermodynamics and Kinetics (C.I.T.C.E.) will be held in Rome, Italy, September 24-29, 1962. Sessions of the following commissions are scheduled: Electrochemical Nomenclature and Definitions; Experimental Methods in Electrochemistry; Batteries; Corrosion; Electrochemical Kinetics; Electrochemistry of High Temperatures. The general theme of the meeting will be: "Recent experimental methods for the study of electrode kinetics and their applications (for instance, new aspects of the methodology and the applications of oscillographic polarography; of the rotating disc; of potentiostatic and potentiokinetic measurements; of impedance measurements)."

Correspondence regarding attendance or presentation of papers at this meeting should be addressed to N. Ibl, Secretary General of C.I.T.C.E., Dept. of Industrial and Engineering Chemistry, Swiss Federal Institute of Technology, Universitätstrasse 6, Zurich, Switzerland.

Titles of papers should be received before May 1, 1962, summaries before June 1, 1962.

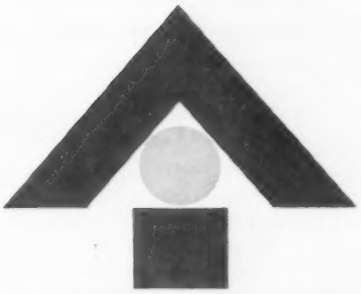

WELCOME ABOARD!

Responsible research positions for

PHYSICAL CHEMISTS
ELECTROCHEMISTS
ELECTROANALYTICAL CHEMISTS

We're seeking men with experience, to research phenomena related to fuel cells and other galvanic systems and investigate electrode kinetics, polarization, catalysis, and electroanalytical techniques.

Astropower is an expanding propulsion R & D firm located in the ideally situated research center at Newport Beach, California, one of the finest recreation areas in the world. Superior employee benefits. Submit resumes to Dr. George Moe, Vice President, Research. Qualified applicants will receive consideration without regard to race, creed or national origin.

ASTROPOWER, INC.

A subsidiary of Douglas Aircraft Co.

2968 Randolph Avenue
Costa Mesa, California

Employment Situations

Please address replies to box shown, c/o The Electrochemical Society, 1860 Broadway, New York 23, N. Y.

Position Wanted

Chemical Engineer, B.S.—Fifteen years' industrial experience—12 years of electrolytic background in development and production work. Supervisory experience. Married, family, 39. *Reply to Box No. 372.*

Positions Available

Solid State Research—Opening for Ph.D. in physical chemistry, physics, or metallurgy. We are producers of highest quality silicon and one of our chief research interests in this field is vapor-deposited single-crystal layers. We are interested in having as accurate and comprehensive information as possible on such structures and on their possible application to devices. We are already engaged in electrical and optical studies and are most desirous of deepening and broadening these studies. A sufficiently qualified applicant would have ample opportunity for choosing and exploiting directions as well as specific problems of interest. Other fields of research in semiconductors are gallium arsenide, germanium, and thermoelectric materials. *Reply in confidence to Box No. A-289.*

Research Chemist for Research Associate position at the National Bureau of Standards to conduct original research on galvanic phenomena associated with atmospheric corrosion. M.S., Ph.D., or equivalent research experience required. *Reply to Fielding Ogburn, Electrolysis and Metal Deposition Section, National Bureau of Standards, Washington 25, D. C.*

Four challenging research positions for experienced surface chemists, in fully-equipped laboratory devoted to research and development on aluminum and copper alloys, involving: A. Electrochemical kinetics, adsorption, and oxide film structure investigations related to finishing processes. B. Studies of interfacial surface reactions between polymeric resins and metal oxide surfaces relating to strength and permanence of joints in the adhesive bonding of metals. C. Mechanisms relating to surface phenomena, associated with liquid metal-solid metal inter-action as applied to soldering and brazing. D. Surface and electrochemical reactions effecting the kinetics of general, localized, and stress corrosion processes. Pleasant living, with access to major university. Send reply to R. H. Endriss, Personnel Manager, Olin Mathieson Chemical Corp., 125 Munson St., New Haven, Conn.

Advertiser's Index

Academic Press, Inc.	204C
American Oil Company	222C
Anaconda American Brass Company	208C
Astropower, Inc., Div. of Douglas Aircraft Co.	221C
Bell Telephone Laboratories, Inc.	207C
Great Lakes Carbon Corp., Electrode Division	Cover 2
ITT Federal Laboratories	222C
P. R. Mallory & Co., Inc.	221C
John Wiley & Sons, Inc.	206C

AMERICAN

ELECTROCHEMIST

Ph.D. or equivalent for program concerned with electrochemical conversion for power and products. Interest in electrode kinetics and catalysis desirable.

A. C. Borg

Research and Development Department
American Oil Company
P.O. Box 431-X
Whiting, Indiana
(near Chicago)

PHYSICAL CHEMIST

A challenging position exists in our Physical Sciences Laboratory for a chemist with accomplishment in the field of solid-state or electro-chemical research. The position will initially be concerned with projects in the field of energy conversion. It also offers an excellent opportunity for an individual interested in developing new ideas in the field of electronic materials and devices. Candidate should have Ph.D. or equivalent.

Send resume to

Mr. K. P. O'Connor
ITT Federal Laboratories
500 Washington Avenue
Nutley 10, New Jersey

All qualified applicants considered without regard to race, creed, color, or national origin.

The Electrochemical Society

Patron Members

Aluminum Co. of Canada, Ltd.,
Montreal, Que., Canada

International Nickel Co., Inc.,
New York, N. Y.

Olin Mathieson Chemical Corp.,
Chemicals Div., Industrial Chemicals
Development Dept., Niagara Falls, N. Y.

Union Carbide Corp.
Divisions:
Union Carbide Metals Co.,
New York, N. Y.
National Carbon Co., New York, N. Y.

Westinghouse Electric Corp., Pittsburgh, Pa.

Sustaining Members

Air Reduction Co., Inc.,
New York, N. Y.

Ajax Electro Metallurgical Corp.,
Philadelphia, Pa.

Allen-Bradley Co., Milwaukee, Wis.

Allied Chemical Corp.
Solvay Process Div., Syracuse, N. Y.
General Chemical Div., Morristown, N. J.

Alloy Steel Products Co., Inc., Linden, N. J.

Aluminum Co. of America,
New Kensington, Pa.

American Metal Climax, Inc.,
New York, N. Y.

American Potash & Chemical Corp.,
Los Angeles, Calif. (2 memberships)

American Smelting and Refining Co.,
South Plainfield, N. J.

American Zinc Co. of Illinois,
East St. Louis, Ill.

American Zinc, Lead & Smelting Co.,
St. Louis, Mo.

American Zinc Oxide Co., Columbus, Ohio

M. Ames Chemical Works, Inc.,
Glens Falls, N. Y.

Armco Steel Corp., Middletown, Ohio

Basic Inc., Maple Grove, Ohio

Bell Telephone Laboratories, Inc.,
New York, N. Y. (2 memberships)

Bethlehem Steel Co., Bethlehem, Pa.
(2 memberships)

Boeing Airplane Co., Seattle, Wash.

Burgess Battery Co., Freeport, Ill.
(4 memberships)

Canadian Industries Ltd., Montreal, Que.,
Canada

Carborundum Co., Niagara Falls, N. Y.

Catalyst Research Corp., Baltimore, Md.

Columbian Carbon Co., New York, N. Y.

Consolidated Mining & Smelting Co. of
Canada, Ltd., Trail, B. C., Canada
(2 memberships)

Continental Can Co., Inc., Chicago, Ill.

Cooper Metallurgical Associates, Cleveland,
Ohio

Corning Glass Works, Corning, N. Y.

Diamond Alkali Co., Painesville, Ohio

Dow Chemical Co., Midland, Mich.

Wilbur B. Driver Co., Newark, N. J.
(2 memberships)

E. I. du Pont de Nemours & Co., Inc.,
Wilmington, Del.

Eagle-Picher Co., Chemical Div., Joplin, Mo.

Eastman Kodak Co., Rochester, N. Y.

Thomas A. Edison Research Laboratory, Div.
of McGraw-Edison Co., West Orange, N. J.

Electric Auto-Lite Co., Toledo, Ohio
C & D Division, Conshohocken, Pa.

Electric Storage Battery Co., Yardley, Pa.

Engelhard Industries, Inc., Newark, N. J.
(2 memberships)

The Eppley Laboratory, Inc., Newport, R. I.
(2 memberships)

Exmet Corp., Tuckahoe, N. Y.

Fairchild Semiconductor Corp., Palo Alto,
Calif.

Food Machinery & Chemical Corp.
Becco Chemical Div., Buffalo, N. Y.
Westvaco Chlor-Alkali Div., South
Charleston, W. Va.

Foote Mineral Co., Paoli, Pa.

Ford Motor Co., Dearborn, Mich.

General Electric Co., Schenectady, N. Y.
Chemistry & Chemical Engineering
Component, General Engineering
Laboratory
Chemistry Research Dept.
General Physics Research Dept.
Metallurgy & Ceramics Research Dept.
Aircraft Accessory Turbine Dept.,
West Lynn, Mass.

General Instrument Corp., Newark, N. J.

General Motors Corp.
Allison Div., Indianapolis, Ind.
Delco-Remy Div., Anderson, Ind.
Guide Lamp Div., Anderson, Ind.
Research Laboratories Div., Warren, Mich.

(Sustaining Members cont'd)

General Telephone & Electronics Laboratories Inc., Bayside, N. Y. (2 memberships)
Gillette Safety Razor Co., Boston, Mass.
Globe-Union, Inc., Milwaukee, Wis.
Gould-National Batteries, Inc., Minneapolis, Minn.
Grace Electronic Chemicals, Inc., Baltimore, Md.
Great Lakes Carbon Corp., New York, N. Y.
Hanson-Van Winkle-Munning Co., Matawan, N. J. (2 memberships)
Harshaw Chemical Co., Cleveland, Ohio (2 memberships)
Hercules Powder Co., Wilmington, Del.
Hewlett-Packard Co., Palo Alto, Calif.
Hill Cross Co., Inc., West New York, N. J.
Hoffman Electronics Corp., Semiconductor Div., El Monte, Calif. (2 memberships)
Hooker Chemical Corp., Niagara Falls, N. Y. (3 memberships)
Hughes Aircraft Co., Culver City, Calif.
International Business Machines Corp., Yorktown Heights, N. Y.
International Minerals & Chemical Corp., Skokie, Ill.
ITT Federal Laboratories, Div. of International Telephone & Telegraph Corp., Nutley, N. J.
Jones & Laughlin Steel Corp., Pittsburgh, Pa.
K. W. Battery Co., Skokie, Ill.
Kaiser Aluminum & Chemical Corp.
Div. of Chemical Research, Permanente, Calif.
Div. of Metallurgical Research, Spokane, Wash.
Kawecki Chemical Co., Boyertown, Pa.
Kennecott Copper Corp., New York, N. Y.
Leesona Moos Laboratories, Div. of Leesona Corp., Jamaica, N. Y.
Libbey-Owens-Ford Glass Co., Toledo, Ohio
Lockheed Aircraft Corp., Missiles & Space Div., Sunnyvale, Calif.
Mallinckrodt Chemical Works, St. Louis, Mo.
P. R. Mallory & Co., Indianapolis, Ind.
Merck & Co., Inc., Rahway, N. J.
Metal & Thermit Corp., Detroit, Mich.
Miles Chemical Co., Div. of Miles Laboratories, Inc., Elkhart, Ind.
Minnesota Mining & Manufacturing Co., St. Paul, Minn.
Monsanto Chemical Co., St. Louis, Mo.
Motorola, Inc., Chicago, Ill.
National Cash Register Co., Dayton, Ohio
National Lead Co., New York, N. Y.
National Research Corp., Cambridge, Mass.
National Steel Corp., Weirton, W. Va.
North American Aviation, Inc., Rocketdyne Div., Canoga Park, Calif.
Northern Electric Co., Montreal, Que., Canada
Norton Co., Worcester, Mass.
Ovitron Corp., Long Island City, N. Y.
Peerless Roll Leaf Co., Inc., Union City, N. J.
Pennsalt Chemicals Corp., Philadelphia, Pa.
Phelps Dodge Refining Corp., Maspeth, N. Y.
Philco Corp., Research Div., Blue Bell, Pa.
Philips Laboratories, Inc., Irvington-on-Hudson, N. Y.
Pittsburgh Plate Glass Co., Chemical Div., Pittsburgh, Pa.
Potash Co. of America, Carlsbad, N. Mex.
Radio Corp. of America
Tube Div., Harrison, N. J.
RCA Victor Record Div., Indianapolis, Ind.
Ray-O-Vac Co., Madison, Wis.
Raytheon Co., Waltham, Mass.
Reynolds Metals Co., Richmond, Va.
Rheem Semiconductor Corp., Mountain View, Calif.
Schering Corporation, Bloomfield, N. J.
Shawinigan Chemicals Ltd., Montreal, Que., Canada
Speer Carbon Co.
International Graphite & Electrode Div., St. Marys, Pa.
Sprague Electric Co., North Adams, Mass.
Stackpole Carbon Co., St. Marys, Pa.
Stauffer Chemical Co., New York, N. Y.
Tennessee Products & Chemical Corp., Nashville, Tenn.
Texas Instruments, Inc., Dallas, Texas
Metals and Controls Corp., Attleboro, Mass.
Three Point One Four Corp., Yonkers, N. Y.
Titanium Metals Corp. of America, Henderson, Nev.
Tung-Sol Electric Inc., Newark, N. J.
Udylite Corp., Detroit, Mich. (4 memberships)
Universal-Cyclops Steel Corp., Bridgeville, Pa.
Upjohn Co., Kalamazoo, Mich.
U. S. Steel Corp., Pittsburgh, Pa.
Victor Chemical Works, Chicago, Ill.
Western Electric Co., Inc., Chicago, Ill.
Wyandotte Chemicals Corp., Wyandotte, Mich.
Yardney Electric Corp., New York, N. Y.